

## Structural Behaviour in Concrete Frame Corners of Civil Defence Shelters

Non-linear Finite Element Analyses and Experiments

MORGAN JOHANSSON

*Division of Concrete Structures  
Department of Structural Engineering  
Chalmers University of Technology  
Göteborg, Sweden 2000*



THESIS FOR THE DEGREE OF DOCTOR OF PHILOSOPHY

**Structural Behaviour in Concrete Frame Corners**

**of Civil Defence Shelters**

Non-linear Finite Element Analyses and Experiments

MORGAN JOHANSSON

Division of Concrete Structures

Department of Structural Engineering

Chalmers University of Technology

Göteborg, Sweden 2000

Structural Behaviour in Concrete Frame Corners of Civil Defence Shelters  
Non-linear Finite Element Analyses and Experiments  
MORGAN JOHANSSON  
ISBN 91-7197-889-5

©MORGAN JOHANSSON, 2000

Doktorsavhandlingar vid Chalmers tekniska högskola  
Ny serie nr 1576  
ISSN 0346-718X

Publication 00:2  
Arb nr: 1106  
Division of Concrete Structures  
Department of Structural Engineering  
Chalmers University of Technology  
SE-41296 Göteborg  
Sweden  
Telephone + 46 (0)31-772 1000

Cover:  
Schematic view of crack pattern obtained in opening (left) and closing (right) frame corners of civil defence shelter subjected to external pressure.

Chalmers Reproservice  
Göteborg, Sweden 2000

Structural Behaviour in Concrete Frame Corners of Civil Defence Shelters  
Non-linear Finite Element Analyses and Experiments  
MORGAN JOHANSSON  
Division of Concrete Structures  
Department of Structural Engineering  
Chalmers University of Technology

#### ABSTRACT

From a safety point of view it is important that a concrete structure, apart from necessary load capacity, also is able to show ductile behaviour that allows redistribution of forces so that a local failure not lead to total collapse of the structure. A structure's ability to exhibit such behaviour is highly dependent on the reinforcement detailing of the joint connections between its independent members. Accordingly, to obtain sound structural behaviour, the joints should ideally be as strong as the structural members connected to them and show ductile behaviour in the ultimate limit state. Even though fulfilling these requirements, the reinforcement detailings in frame corners previously prescribed in the Swedish Shelter Regulations for the design of civil defence shelters were difficult to apply correctly. Therefore, a simpler method, by which all reinforcement bars are spliced within the corner region, was proposed and evaluated.

To examine the effectiveness of the new detailing when subjected to a positive (opening of the corner) or a negative (closing of the corner) moment, a combination of a literature survey, static full-scale tests and static non-linear finite element analyses has been carried out. The main parameters varied were the reinforcement detailing and the reinforcement ratio, and it was found that the new alternative is suitable to use. However, since a civil defence shelter is designed to withstand transient loading, such as blast waves from a nearby explosion or the impact of falling masses from a collapsing building, this also has to be taken into consideration.

When subjected to such loads, the response of a structure may be quite different from that of static loading. The peak load for transient loads is often several times higher than the "equivalent" static load used in the design of the shelter. Further, if the load is applied fast enough, it is possible that part of the structure will still "not be aware" of the loading when another part reaches failure. Therefore, non-linear finite element analyses based on explicit integration were carried out to increase the knowledge of how a structure behaves when subjected to such transient loads. It was found that even though the global structural behaviour may differ widely there are still large similarities in the local behaviour between a static and a transient load case. The results imply that the conclusions made in the previous static studies are valid also for a transient loaded structure.

Keywords: Concrete, frame corners, reinforcement detailing, spliced reinforcement, non-linear finite element analyses, civil defence shelters, blast load, impact load.



## LIST OF PUBLICATIONS

The following papers are included in this thesis:

### **Paper I**

“Reinforcement Detailing in Concrete Frame Corners”

Submitted to *ACI Structural Journal*.

### **Paper II**

“Nonlinear Finite-Element Analyses of Concrete Frame Corners”

Published in *ASCE Journal of Structural Engineering*, Vol. 126, No. 2, February, 2000, pp. 190-199.

### **Paper III**

“FE Analyses of Concrete Civil Defence Shelters Subjected to Transient Loading”

Submitted to *ASCE Journal of Structural Engineering*.





# Preface

This study deals with the reinforcement detailing in concrete frame corners of civil defence shelters and the response of such structures when subjected to transient loads. Experiments and finite element analyses, based on non-linear fracture mechanics, were conducted to evaluate a new design proposal. The work presented in this thesis was carried out from November 1994 to March 2000 at the Division of Concrete Structures, Chalmers University of Technology. The project was financed by the Swedish Rescue Services Agency.

I wish to thank my supervisor, Professor Kent Gylltoft, for his guidance and support. I would also like to thank Björn Ekengren, from the Swedish Rescue Services Agency, for his encouraging engagement in the project, which has resulted in many valuable discussions. Special thanks are due to Mario Plos, who was an invaluable support in my first year as a doctoral student, and after that also has provided valuable advice. For their joyful, never-ending support and encouragement, I thank my fellow colleagues at the Department of Structural Engineering, especially the doctoral students at the Division of Concrete Structures, and in particular my colleague Jonas Magnusson who, despite his peculiar behaviour, has been of great help. Special thanks are also due to my master thesis workers, Mikael Olsson, Mathias Johansson, Stefan Karlsson and Peter Grassl, whom I have had the pleasure to supervise within the project and whose contribution is much appreciated. Thanks also to the staff of the Structural Engineering Laboratory, for their invaluable assistance in the experimental part of this work. Special thanks are due to Lars Wahlström for help with photos and scanned figures. Last, but not least, I would like to express my gratitude to Yvonne Juliusson for her assistance and help.

Göteborg, March 2000

Morgan Johansson



# Contents

Abstract

List of Publications

Preface

Contents

Notations

1	Introduction	1
1.1	Background	1
1.2	Research significance	2
1.3	Aim of the study	5
1.4	Limitations	6
1.5	Outline of contents	7
2	Reinforcement Detailings in Frame Corners	9
2.1	Introduction	9
2.1.1	Requirements	9
2.1.2	Frame corners studied	10
2.1.3	Definition of corner efficiency	12
2.2	Mechanical behaviour of different detailings	14
2.2.1	Opening frame corners	14
2.2.2	Closing frame corners	21
2.2.3	Spalling of the side concrete cover	22
2.3	Corner efficiency	26
2.3.1	Comparison of opening and closing corners	26
2.3.2	Influencing parameters	
2.3.2.1	Inclined bars	29
2.3.2.2	Radial stirrups	34
2.3.2.3	Other important parameters	35
2.3.2.4	Detailings that might attain full efficiency	38
2.3.3	Estimation of corner efficiency in opening corners	39
2.3.3.1	General remarks	39
2.3.3.2	Equilibrium model	40
2.3.3.3	Empirical expressions	42

2.4	Discussion	45
2.4.1	Opening corners	45
2.4.1.1	Choosing detailing	45
2.4.1.2	Expected efficiency	46
2.4.1.3	Use of mechanical reinforcement ratio in the design	50
2.4.2	Closing corners	53
2.5	Concluding remarks	54
3	Non-linear Finite Element Analyses of Concrete Structures	57
3.1	Why use finite element modelling?	57
3.2	Fracture mechanics for concrete	57
3.3	Crack models	59
3.3.1	General	59
3.3.2	Discrete crack models	60
3.3.3	Smearred crack models	60
3.3.4	Embedded crack models	62
3.4	Localisation	63
3.4.1	Tension	63
3.4.2	Compression	67
3.4.3	Possible solution	68
3.5	Numerical approach	69
3.6	Finite element analyses of frame corners	71
3.7	Concluding remarks	76
4	Structural Behaviour at Dynamic Loading	77
4.1	General remarks	77
4.2	Response at transient loading	78
4.3	Blast load	81
4.3.1	Explosive shock in air	81
4.3.2	Reflection of shock waves	83
4.3.3	Diffraction of shock waves	86
4.3.4	Pressure-time relation used in finite element analyses	87
4.4	Impact load	88

5	Strain Rate Effects in Concrete	91
5.1	Introduction	91
5.2	Testing at high strain rates	92
5.3	Strain rate influence of concrete strength	95
5.4	Possible explanations for the increase in concrete strength	96
5.4.1	Characterisation of strain rate effects	96
5.4.2	Viscous effects	97
5.4.3	Structural effects	102
5.5	Effect of concrete strength on strain rate sensitivity	103
5.6	Effect of strain rate on other material parameters	106
5.7	Influence of strain rate on reinforcement	108
5.8	Strain rate mesh dependency in finite element analyses	109
6	Numerical Solution Methods for Dynamic Problems	115
6.1	General	115
6.2	Mode superposition	115
6.3	Direct integration methods	116
6.3.1	General	116
6.3.2	Explicit integration method	117
6.3.3	Implicit integration method	119
6.3.4	Solution of non-linear problems	119
6.3.5	Stability	120
6.3.6	Way of loading	122
6.3.7	Choosing integration method	124
6.3.8	Central difference method in Abaqus/Explicit	125
7	Conclusions	127
7.1	General	127
7.2	Suggestions for future research	129
8	References	131
Appendix A	Summary of Frame Corner Tests	
Appendix B	Simply Supported Beams Reinforced with Spliced Reinforcement Loops	

# Notations

## Roman upper case letters

$A_{element}$	area of element
$A_s$	reinforcement area
$A_s^*$	active reinforcement area when inclined bars are accounted for
$A_{s,i}$	reinforcement area of inclined bars
$A_{s,r}$	reinforcement area of radial stirrups
$A_{s,red}$	reduced reinforcement area of reinforcement loops
$A_\phi$	reinforcement area of one bar
$C$	compressive force, charge, damping matrix
$E$	Young's modulus
$E_B$	energy needed to break one floor slab
$E_c$	Young's modulus of concrete
$E_{impact}$	kinetic energy of falling masses just prior to impact
$E_s$	Young's modulus of reinforcement
$F$	load
$F_c$	compressive force
$F_s$	tensile force, resisting force due to the Stéfan effect
$F_R$	resisting force
$F_{dyn}$	dynamic load capacity
$F_{sta}$	static load capacity
$G_c$	shear modulus of uncracked concrete
$G_{crack}$	shear modulus of cracked concrete
$G_F$	fracture energy
$H$	height of collapsing building
$I$	incident shock wave
$K$	empirical factor, stiffness matrix
$L$	length
$M$	moment, mass matrix
$M_A$	moment in section A
$M_B$	moment in section B
$M_{tot}$	total mass
$M_{uc}$	estimated moment capacity
$M_{uc}^*$	estimated moment capacity when inclined bars are accounted for

$M_{uc,A}$	estimated moment capacity in section A
$M_{uc,B}$	estimated moment capacity in section B
$M_{ue}$	estimated moment capacity using equilibrium model
$M_{ut}$	moment capacity in test
$P$	load vector, load
$P_s^-$	peak underpressure
$P_s^+$	peak overpressure
$R$	tensile force, reflected shock wave
$T$	tensile force
$T^-$	duration of negative phase
$T^+$	duration of positive phase
$U$	velocity of incident wave, displacement vector
$\dot{U}$	velocity vector
$\ddot{U}$	acceleration vector
$V$	volume
$V_I$	velocity of incident wave
$V_R$	velocity of reflected wave

### **Roman lower case letters**

$b$	width
$c$	side concrete cover, stress wave velocity
$d$	effective height
$f_c$	compressive cylinder strength of concrete
$f_c$	characteristic compressive cylinder strength of concrete
$f_{c,cube}$	compressive cube strength of concrete
$f_{su}$	ultimate strength of reinforcement
$f_{sy}$	yield strength of reinforcement
$f_t$	tensile strength of concrete
$f_{t,dyn}$	dynamic tensile strength of concrete
$f_{t,sta}$	static tensile strength of concrete
$f_{yk}$	characteristic yield strength of reinforcement
$f_{sy,r}$	tensile strength of radial stirrups
$f(w)$	softening function
$g$	gravity

$h$	distance between two plates
$\dot{h}$	separation velocity
$h_t$	distance from top of shelter to centre of collapsing building
$i^+$	impulse intensity of positive phase
$i^-$	impulse intensity of negative phase
$h_t$	distance from top of shelter to centre of collapsing building
$k$	stiffness
$l$	lever arm, crack extension
$l_A$	lever arm to section A
$l_B$	lever arm to section B
$l_{crack}, l_{dc}$	effective length in equilibrium model
$l_{element}$	element length
$m$	mass, mass per unit area
$n$	number of floors in collapsing building, number of bars
$p$	pressure
$p_0$	ambient pressure
$q$	distributed load, dynamic pressure
$q_{impact}$	equivalent static impact load
$q_{weapon}$	equivalent static weapon load
$r$	radius of bent bar
$s$	spacing of reinforcement
$s_m$	mean crack spacing
$t$	width of localisation band, time
$t_0$	time constant
$t_a$	time of arrival
$u$	displacement
$v$	velocity
$v_0, v_r, v_s,$	particle velocity
$v_{impact}$	mass velocity at impact
$w$	crack opening
$w/c$	water-cement ratio
$w_u$	ultimate crack opening
$z, z_1, z_2, z^*$	internal lever arm



## Greek letters

$\alpha$	angle, factor controlling decaying overpressure, factor in the Newmark method
$\alpha_I$	angle of incident wave
$\alpha_{I,crit}$	critical angle at which Mach reflection occurs
$\alpha_R$	angle of reflected wave
$\beta$	angle, shear retention
$\gamma$	ratio between tensile forces
$\Delta F$	load increment
$\Delta L$	elongation
$\Delta \dot{L}$	elongation velocity
$\Delta t$	time increment
$\Delta t_{cr}$	critical time step
$\delta$	displacement, numerical damping in the Newmark method
$\dot{\epsilon}$	strain rate
$\epsilon_c$	concrete strain
$\epsilon_{c1}$	strain within localisation band in element using embedded crack model
$\epsilon_{c2}$	strain in element using smeared crack model
$\epsilon_{el}$	elastic strain
$\epsilon_{crack}$	crack strain
$\epsilon_s$	reinforcement strain
$\epsilon_u$	ultimate concrete strain in tension
$\epsilon_{u,1}$	ultimate concrete strain in tension when $l = l_{element}$
$\epsilon_{u,s}$	ultimate concrete strain in tension when $l = s_m$
$\zeta$	amount of extra reinforcement loops
$\eta$	efficiency, liquid viscosity
$\theta$	angle between cracks
$\theta_0, \theta_r, \theta_s$	temperature
$\xi$	damping coefficient
$\rho$	reinforcement ratio, line describing location of triple point, density
$\rho_{crit}$	critical reinforcement ratio
$\rho_i$	reinforcement ratio of inclined bars
$\rho_r$	density in reflected wave
$\rho_s$	density in incident wave
$\sigma$	stress
$\sigma_1, \sigma_2$	principal stresses

$\sigma_c$	concrete stress
$\sigma_s$	reinforcement stress
$\sigma_{sp}$	tensile strength
$\sigma_x$	tensile stress in x-direction
$\sigma_y$	tensile stress in y-direction
$\phi$	bar diameter, eigenvector
$\omega$	angular frequency
$\omega_{crit}$	critical mechanical reinforcement ratio
$\omega_{max}$	maximum angular frequency
$\omega_s$	mechanical reinforcement ratio
$\omega_s^*$	mechanical reinforcement ratio when the presence of inclined bars is considered
$\omega_{shelter}^{max}$	maximum mechanical reinforcement ratio in Swedish civil defence shelters
$\omega_{shelter}^{min}$	minimum mechanical reinforcement ratio in Swedish civil defence shelters

# 1 Introduction

## 1.1 Background

From a safety point of view it is important that a concrete structure, apart from necessary load capacity, also is able to exhibit ductile behaviour that allows redistribution of forces so that a local failure not lead to total collapse of the structure. A concrete frame structure's ability to meet these requirements is highly dependent on the reinforcement detailing of the joint connections between its independent members. Despite this, the discussion and recommendations given in the Swedish building codes and handbooks (e.g. BBK 94, Boverket 1994; Betonghandboken 1990; and BRO 94 1994) about what reinforcement detailing must be used in reinforced concrete joint connections are rather limited. Accordingly, there is a need as well as a demand in Sweden for more knowledge in this field, something that apart from the work presented herein is also made clear by the number of valuable contributions recently made by, for example, Plos (1995), Karlsson (1999) and Lundgren (1999).

The Swedish Rescue Services Agency, though, presents detailed instructions in its Shelter Regulations on how the reinforcement in a civil defence shelter is to be arranged. Nevertheless, the detailings for frame corners prescribed in the previous Shelter Regulations, Swedish Rescue Services Agency (1990, 1994), shown in Figures 1.1a and 1.1b were regarded as time-consuming and rather difficult to carry out correctly. Consequently, the Swedish Rescue Services Agency wanted a simpler corner detailing to be used and a research project was therefore initiated at the Division of Concrete Structures at Chalmers University of Technology; see Plos (1994a, b). The criterion set up was that the new detailing should be able to withstand loading at least as well as the conventional ones but also be easier to assemble at the construction site. With this as a basis the proposal shown in Figure 1.1c, making use of reinforcement loops spliced within the corner, was worked out. This detailing has then been thoroughly evaluated and the results obtained and conclusions drawn are presented in this thesis.

When designing a civil defence shelter according to the present Shelter Regulations, it is for practical reasons regarded as a statically loaded structure. However, in reality a shelter must be able to withstand highly dynamic loading due to, for example, blast waves from a nearby explosion or the impact of falling masses from a collapsing building. When subjected to such loads, the global response of a structure can be considerably different compared to that of static loading. The peak load for transient loads is, for instance, often several times higher

than the “equivalent” static load used in the design of the shelter, but their duration is instead very limited in time. Further, if the load is applied fast enough, it is possible that part of the structure will still not even “be aware” of the external loading when another part reaches failure. Simplified, it can be said that the boundary conditions of the structure change with time. Due to the strain rates obtained in this kind of loading, the material properties of both concrete and reinforcement will also change, making the response of the structure even more complicated to understand. Therefore, the change in material behaviour and change in structural response of a civil defence shelter, when subjected to such loading, were also included in the study.

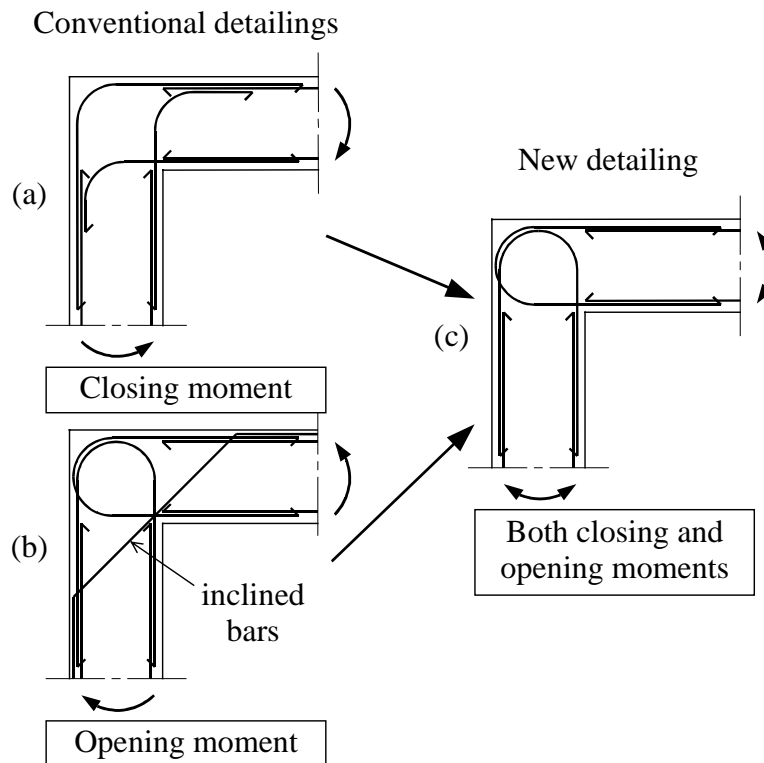


Figure 1.1 Reinforcement detailings previously used in the Swedish Shelter Regulations in (a) closing and (b) opening frame corners. The new reinforcement detailing evaluated herein is shown in (c).

## 1.2 Research significance

When making the design drawing it may seem as easy to use, for instance, the L-shaped reinforcement detailing shown in Figure 1.1a as that of reinforcement loops in Figure 1.1.c. However, there are several occasions when this is not true. A good example is the construction of a civil defence shelter within an existing building. The work is then made

substantially more complicated by the severe lack of space when reinforcing and casting the shelter's concrete members. According to Ekengren (1996) such shelters are approximately three to four times as expensive to build as those in a newly constructed building. An important reason for this considerable increase in cost is the difficulty of carrying out the reinforcement detailings in the structure's joint connections. When for example the shelter roof slab is constructed inside an existing building, it is first cast on the ground and then lifted up to its final position; see Ekengren (1998). After this, the adjoining walls are reinforced, and it is when the connections between the slab and these walls are to be solved that it becomes clearly a significant advantage if the joint detailing can be carried out using reinforcement loops as shown in Figure 1.1c. Accordingly, the advantage of the new proposal is not to decrease the total amount of reinforcement needed; on the contrary, this detailing may even result in an increased amount. Instead, the gain is of practical value. By simplifying the frame corner detailing in this way, the construction work can be carried out in less time and, above all, with a decreased risk of incorrect positioning of the reinforcement. Consequently, the simplification may result in a structure of higher quality that is also less expensive to construct.



Figure 1.2 Casting and lifting of roof slab in civil defence shelter inside an existing building.

Another advantage with this detailing is its potential use in structures made up of prefabricated members. Here, the possibility to produce the structural members at a factory during controlled conditions and then just cast the remaining connections at the construction site seems desirable. When using the conventional detailings, though, this has not been possible. However, since the reinforcement in the new proposal is spliced within the corner region only, such solutions may be considerably easier to use.

Further, when handling very large structural parts, such as the tunnel segments used in the Arlanda Link, between the centre of Stockholm and Arlanda Airport, e.g. Mörnstad (1998), the use of the proposed detailing might be very advantageous. Here, the reinforcement cages for the roof and floor slabs were prefabricated in factory. However, the U-shapes necessary if the wall reinforcement were included, would render difficulties with transportation and handling of the cages. Therefore, it was regarded a better solution to instead add the wall reinforcement at the construction site as shown in Figure 1.3a. The result was that only about 60% of the total reinforcement in the final cages were prefabricated. If reinforcement loops could have been used instead, though, a simplified substructure of the different structural members as shown in Figure 1.3b had also been possible. This had then considerably increased the prefabricated part of the reinforcement cages, and hence made the construction process be more effective, Mörnstad (2000).

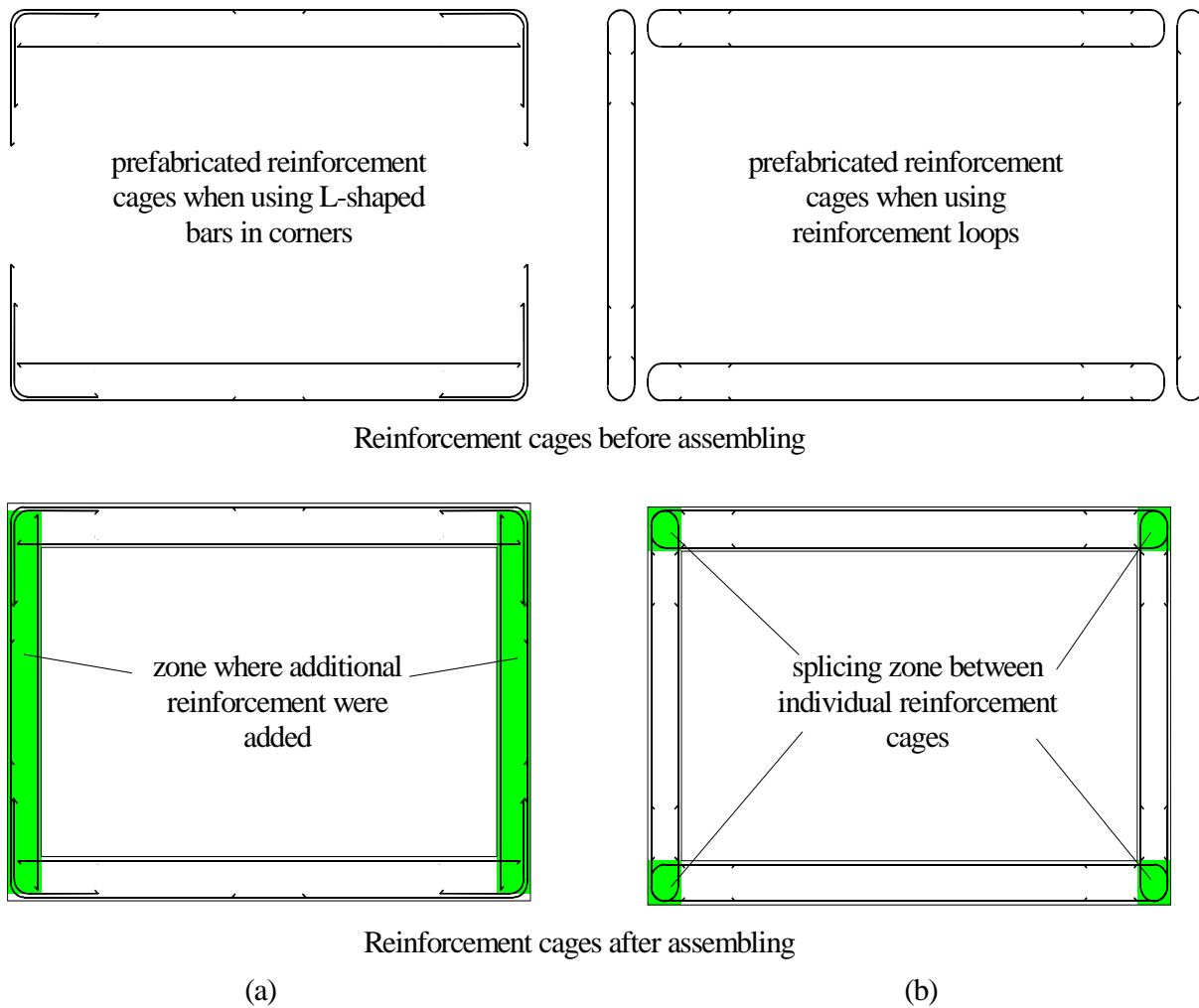


Figure 1.3 Schematic view of reinforcement cages before and after assembling in tunnel segment when using the reinforcement detailings similar to those shown in Figures 1.1a and 1.1c, respectively.

The traditional approach in the study of concrete structures is to carry out experiments. However, to study the structural behaviour more thoroughly, the finite element method may also be used. It has been found that this approach, in which the non-linear behaviour of concrete may be simulated using non-linear fracture mechanics and plasticity, provides an important complement to experiments and that its use may result in further understanding of the concrete response that otherwise would not be possible. Even though the use of non-linear finite element analyses on concrete structures are comparably new in Sweden, there are still quite a few that possess the knowledge necessary to adequately simulate their response when subjected to static loading. Even so, there are still many problems to be solved, of which some are presented and dealt with in this thesis. However, the use of non-linear finite element analyses on concrete structures, subjected to transient loads such as impulse loading from a nearby explosion or impact of falling masses, is still quite modest. Such studies have previously been made mostly by the military, e.g. the Defence Research Establishment, FOA. However, such analyses may also be of substantial interest for civilian purposes, e.g. accidental explosions in the process industry or the impact from a truck colliding at full speed with a concrete column in a bridge. Further, even though Sweden so far has been more or less free from terrorist attacks, one should not forget that important installations, such as nuclear power plants, may still be a potential target. Consequently, the need for further knowledge of how to carry out both static and dynamic analyses must not be underestimated. Hence, it is also important to create a foundation at a university where this kind of knowledge can grow and develop.

### **1.3 Aim of the study**

The main aim of this research project was to evaluate a new design proposal in Swedish civil defence shelters and to determine whether it was appropriate to replace the detailings previously used in closing and opening frame corners with the new alternative. As stated in Section 1.1 the structural service criterion set up by the Swedish Rescue Services Agency was that the new reinforcement detailing must withstand loading at least as well as the conventional detailing so that a safe and ductile structure is obtained. To determine whether this criterion is fulfilled, a better understanding of the behaviour of frame corners under loading to failure and of the structural response in the corner area is required. Therefore, apart from a thorough literature survey, full-scale tests and non-linear finite element analyses were carried out. Experiments provide information on the real behaviour in a structure, while the latter approach makes it possible to simulate the progressive cracking and change in strain and

stress states under increased load, and thus provides the means for further understanding and increased knowledge that otherwise would not be possible. Hence, such a combination may be a very powerful tool and allows a better understanding of the structural behaviour of the frame corner.

The load conditions used in the design of a Swedish civil defence shelter are static equivalents to the dynamic loads expected. However, whether this approximation is appropriate has not been sufficiently examined. Therefore, the main aim of the dynamic study was to increase the knowledge of how a shelter behaves when subjected to such transient loads, which was done by using non-linear finite element analyses. Based on this study, the question whether conclusions gained in static tests and analyses also are valid for structures subjected to transient load cases hoped to be answered. Another aim was to gather knowledge about what influence high strain rate may have on different concrete parameters such as strength and stiffness.

## **1.4 Limitations**

The work presented herein can roughly be divided into two parts: static studies of the behaviour in concrete frame corners and what reinforcement detailing should be used, and dynamic studies of a civil defence shelter subjected to transient loading. Although the work presented in this thesis was originally initiated to improve the reinforcement detailing of civil defence shelters, the results and conclusions reached can of course also be used in other kinds of concrete structures. Nevertheless, the comparisons and discussions of the different detailings made are generally concentrated on their use in civil defence shelters. The corner study was limited to frame corners of 90°. Further, the influence of haunches in the corner, and the possible effect that the corner size may have, were not included. The former, though, are normally not used in a civil defence shelter and the latter is not considered to be a problem since the dimensions examined are similar to those used in such a structure. However, in larger structures, such as a concrete bridge, the dimensions used may be far larger than those studied herein, and consequently a somewhat different behaviour may also be obtained. Some of the finite element analyses presented were unable to accurately simulate the behaviour observed in tests. This was due to the material models used and the approximations chosen in the modelling. As briefly discussed in Section 7.2, though, these shortcomings may be solved, among other things, by the use of better material models now available. The type of transient loads that may act on a civil defence shelter causes high load rates on the structure. This in



turn leads to high strain rates in the material, which is known to affect the properties of both concrete and reinforcement. Nevertheless, the influence of high strain rates on the material properties was not taken into account in the dynamic analyses. This simplification was made mainly for two reasons. First, in the finite element programme used it was not possible to include these effects in the concrete material models. Second, even though it was possible to take these effects into account for the reinforcement it was decided not to do so, since the strain rate obtained here was found to be mesh-dependent; see Section 5.8. Consequently, all dynamic analyses were carried out using non-rate-dependent material models. Further, no experimental tests were performed to verify the dynamic analyses. Nevertheless, it is believed that the knowledge gained will be of significant use.

Another limitation in the dynamic study was that the effects of splinter were neglected in the finite element analyses. To generalise, the influences of splinter essentially mean two things: their impact contribution to the impulse load, and the considerable damage the splinters may cause in both concrete and reinforcement. Further, to complicate matters one cannot be sure whether the splinter or the blast load will reach the structure first since this, among other things, depends on the weight of the exploding device and its distance to the structure. What effect these different cases have on the structure's ability to withstand the explosion, though, is not clear. Consequently, to include this part here would have complicated the study too much and it was thought better to postpone its introduction to a continuing project.

## 1.5 Outline of contents

This thesis is composed of an introductory part and three papers published or submitted for publication in reviewed scientific journals. The introductory part gives a background to the material treated in the papers, but also discusses subjects not included there. Further, some sections in the former stand for themselves, and the introductory part and the three papers should, therefore, be regarded as a whole.

**Chapter 2** presents a literature survey of frame corners subjected to opening or closing moment (static loading). The mechanical behaviour obtained when using different detailings, primarily the three types shown in Figure 1.1, are discussed. Proposals of how to use this knowledge in the design are also given. Non-linear finite element analyses and their use to better understand the mechanical behaviour of frame corners are treated in **Chapter 3**. In **Chapter 4** a discussion about what structural response is obtained when using transient

loading is presented. Further, a brief background for the blast and impact analyses carried out is given. **Chapter 5** deals with the high strain rates obtained when a concrete structure is subjected to such loads, and what effect they may have on the concrete material parameters. Different approaches found in the literature and possible explanations for this phenomenon are presented and discussed. The inclusion of strain rate effects in dynamic finite element analyses is also treated briefly. **Chapter 6** describes the background for different integration methods, and especially the explicit central difference method used in the dynamic finite element analyses carried out herein. Finally, the major conclusions and suggestions for future research are given in **Chapter 7**.

**Papers I and II** deal with the static behaviour of concrete frame corners. The former presents full-scale tests of both opening and closing corners carried out by the author and compares the results with those found in the literature. **Paper II**, though, presents non-linear finite element analyses simulating some of the closing corners in these tests. Finally, dynamic finite element analyses are used in **Paper III** to simulate the structural behaviour of a civil defence shelter subjected to the blast load of a nearby explosion and the impact of falling masses from a collapsing building.

## 2 Reinforcement Detailings in Frame Corners

### 2.1 Introduction

#### 2.1.1 Requirements

In many types of reinforced concrete structures, sectional forces have to be transmitted between adjoining members, as shown in Figure 2.1. From a safety point of view it is important that such structures, apart from necessary load capacity, also exhibit ductile behaviour so that a local failure does not lead to total collapse of the structure. A structure's ability to meet this requirement is highly dependent on the reinforcement detailing used in the joint connections. The positioning of the reinforcing steel in the adjoining members is often obvious; however, this is not the case in corner joints. Compared with the former, the detailing of corners in reinforced concrete frame structures represents a relatively untouched field. Despite important contributions made by, for instance, Nilsson (1973), Mayfield *et al.* (1971, 1972), and Stroband and Kolpa (1981, 1983), for every test made on a corner joint several hundred tests to check the bending and shear capacity of beams have been carried out. Ideally, a joint should resist a moment at least as large as the calculated failure moment of the members framing into it, and ensure ductile behaviour in the ultimate limit state. Nilsson summarises the requirements for a corner subjected to bending as:

- the joint shall be able to withstand a moment of at least the same magnitude as those on the adjoining sections;
- for joints which do not satisfy this design criterion, the ductility shall be sufficient to prevent brittle failure so that redistribution of forces in the structure will be possible;
- crack widths at corners under service load shall be limited to an acceptable magnitude;
- the reinforcement shall be easy to fabricate and position; the risk of incorrect detailing is significantly decreased when a simplified detailing is used.

In the following sections, the structural behaviour of frame corners is presented and different reinforcement detailings are discussed. Since the design criteria in civil defence shelters refer to the ultimate limit state, the requirement of crack widths at service load mentioned as point three above are not further considered; the other three criteria, though, are regarded in the presentation and discussed below.

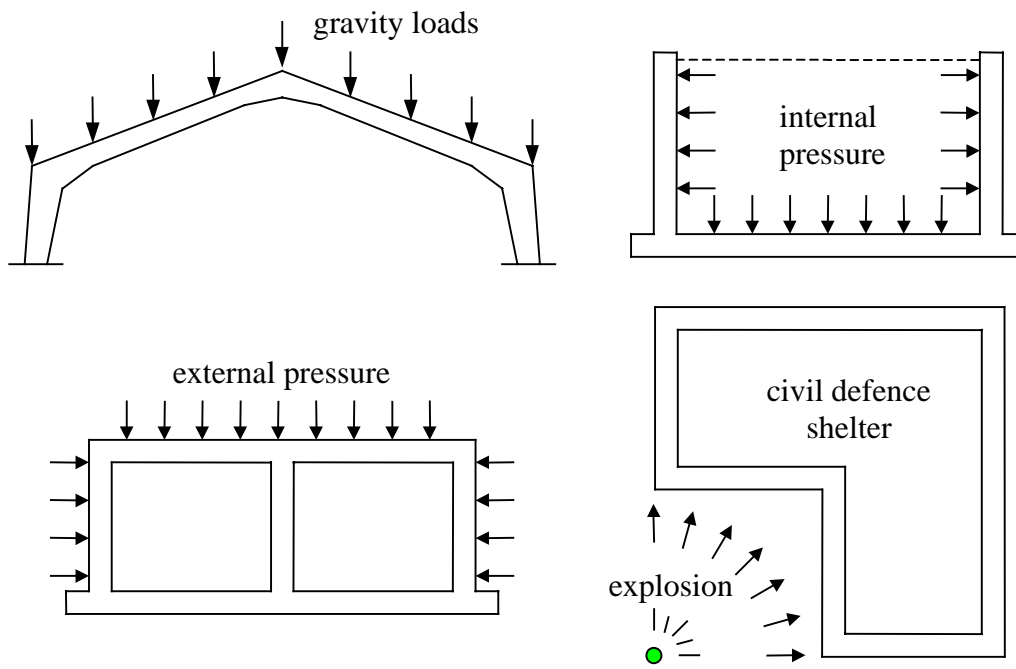


Figure 2.1 Structures with corners subjected to opening or closing moments. Based on Nilson and Winter (1991), and Johansson and Karlsson (1997).

### 2.1.2 Frame corners studied

A concrete frame corner can be separated into two principal types: those that are subjected to a positive moment (opening of the corner) and those subjected to a negative moment (closing of the corner) as shown in Figure 2.2. Generally, the first case is more difficult to detail properly; see Mayfield *et al.* (1971) and Nilsson and Losberg (1976). The reason is schematically shown in Figure 2.3, which shows the difference in the structural behaviour of a frame corner subjected to an opening or a closing moment. By the use of a very simplified strut-and-tie model, it can be shown that an opening of the corner tries to split the corner in two by pushing off the outside concrete portion. This is opposite to what happens when closing the corner; the tensile and compressive forces then instead interact in a way that confines the concrete within the corner. This also means that the two cases will present quite different difficulties in the detailing. However, since the reinforcement detailing in opening corners is more sensitive than that in closing corners, the former is also treated in this thesis more thoroughly. A corner region in a structure may, due to different load combinations, usually be subjected to both opening and closing moments during its service time. This is especially true in structures subjected to dynamic loading, since the structure then might sway back and fourth. For simplicity, though, the following presentation treats only the case of monotonic loading until failure.

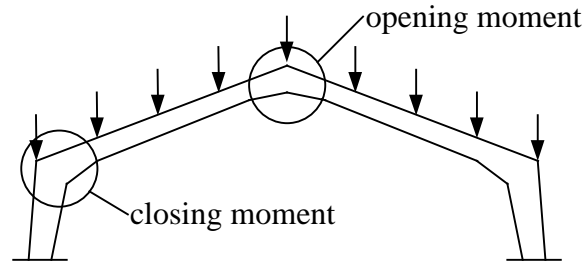


Figure 2.2 Definition of positive (opening) and negative (closing) moment.

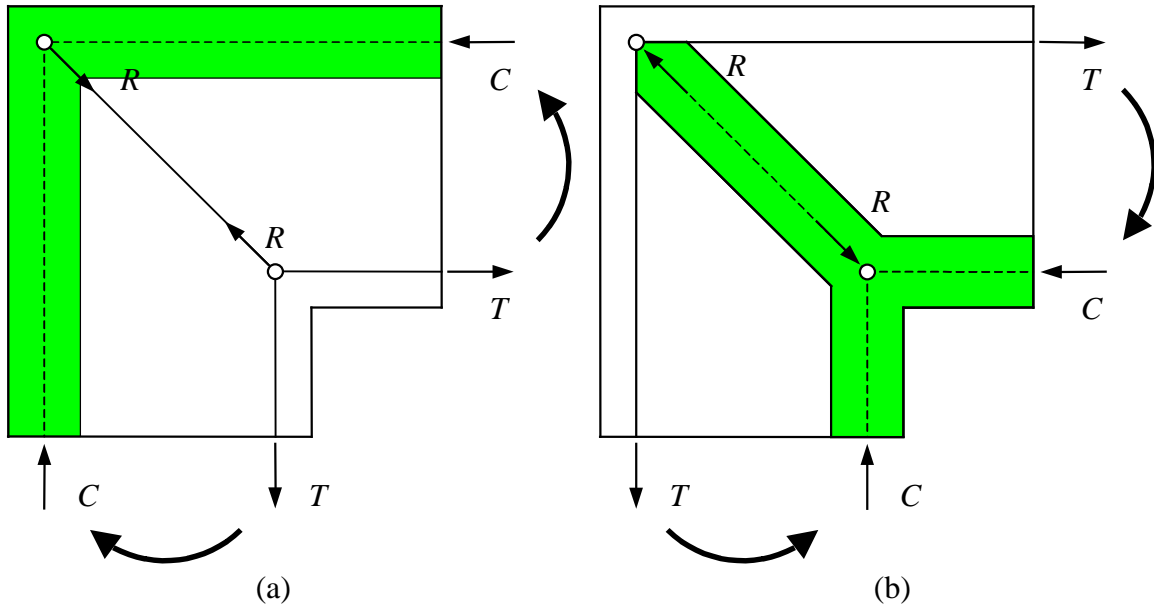


Figure 2.3 Sketch of the principal forces in a corner subjected to (a) positive (opening) moment and (b) negative (closing) moment.

As shown in Figure 2.2 a frame corner may be of any angle; experimental studies of opening corners with other angles than  $90^\circ$  have been reported by Nilsson (1973), Kordina (1984), Abdul-Wahab and Ali (1989), Abdul-Wahab and Al-Roubai (1998), and Abdul-Wahab and Salman (1999). To the author's knowledge no such tests have been carried out on corners subjected to closing moment. Only frame corners at an angle of  $90^\circ$ , though, are treated here. In the following sections the structural behaviour of such frame corners subjected to opening or closing moment is discussed; a thorough summary of the tests treated in this dissertation can be found in Appendix A.

### 2.1.3 Definition of corner efficiency

As stated in the first point in Section 2.1.1, the strength of a corner shall ideally be at least as large as that of its adjoining members. In what degree this requirement is fulfilled, is normally expressed as corner efficiency, and in the following sections this term will also be frequently used in the presentation and discussion of different reinforcement detailings of frame corners.

The corner efficiency is here defined as the ratio between the moment capacity obtained in tests, independent of what final failure mode is obtained, to the theoretically estimated moment capacity of the members (weakest member used) making up the corner. The former was determined as the product of the external force and the lever arm between its acting axis and the critical section as defined in Figure 2.4. These sections mark the border between the corner and its adjoining members, and from this it is clear that somewhat different critical sections are used for opening and closing moments, respectively. The estimated moment capacity was calculated in these sections by a cross-sectional analysis using a rectangular stress block as described in, for example, Betonghandboken (1990) and Eurocode 2, CEN (1991), where the influence of any possible normal force due to the external load and the reinforcement on the compressive side was accounted for (if not stated otherwise, the influence of dead weight was not taken into account).

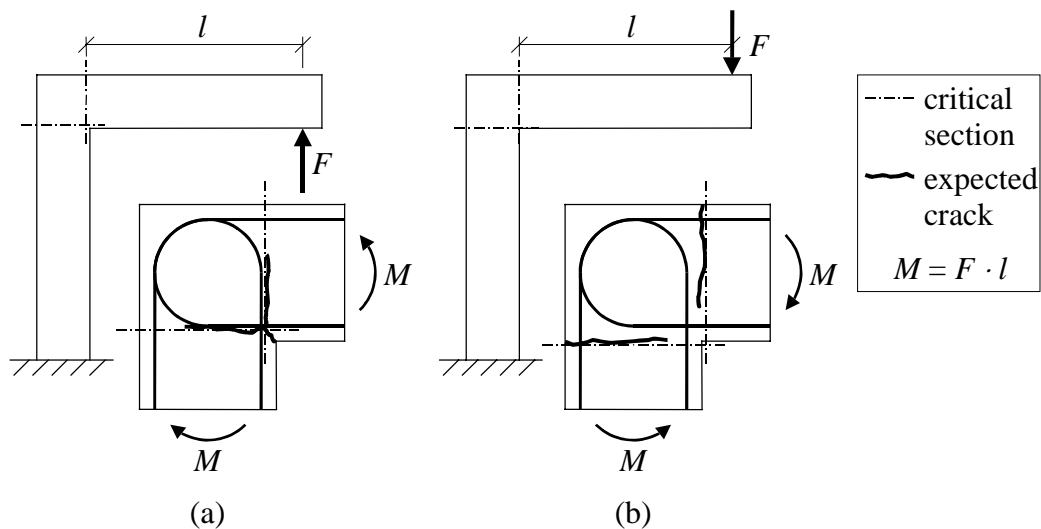


Figure 2.4 Definition of critical sections used when determining moment capacity obtained in tests for: (a) opening moment and (b) closing moment.

The definition made above may appear as clear and simple. However, when additional reinforcement is positioned within the corner in order to strengthen it, the extra reinforcement may also affect the capacity of the adjoining members. This is, for example, the case when inclined bars are added at the inside of a corner subjected to opening moment, as shown in Figure 1.1c. Whether such additional reinforcement should be accounted for, when determining the estimated moment capacity of the adjoining member, can be discussed. In all previous evaluations of opening frame corners referred to in this thesis, the influence of the inclined bars have been neglected when estimating the moment capacity of the weakest adjoining member. Therefore, this approach is herein denoted as *the conventional evaluation method*. However, the presence of such bars would of course not only affect the corner capacity, but also the capacity of the adjoining members. Consequently, it is more correct to take their contribution into account when determining the moment capacity of the member. Rather surprisingly, this approach has, to the author's knowledge, not previously been used in the evaluation of opening frame corners, and it is therefore denoted here as *the new evaluation method*. This approach also makes it possible to consistently compare the efficiency of different reinforcement detailings. It also gives a rather good indication whether a ductile behaviour will be obtained, since 100% efficiency in use of an under-reinforced cross-section will lead to yielding of the reinforcement. Of the detailings compared in the following sections, though, only the one using inclined bars at the inside of the corner will differ in efficiency; for the rest of the detailings, the two evaluation methods are exactly the same.

It can be argued that if the corner capacity reached in a test is equal to or higher than that necessary in the design, all is well. This may be true if only the structure's strength is important, and its ductility is of no interest; i.e. the extra reinforcement has then filled its purpose, and what structural response is obtained at loads higher than the design load is regarded to be of no importance. Hence, it would then be possible to purposely increase the amount of tensile reinforcement at the corner in order to provide the corner strength necessary. However, the magnitude and distribution of the loads that may act on a structure is often not entirely known, and in such cases it is important that a structure shows ductile behaviour that allows redistribution of forces. To obtain this, the structure must be capable of large deformations before final failure. Therefore, an increased moment capacity of the corner joints may not be an adequate solution since ductile behaviour of the corner may be at least as important if the structure is to withstand the external load designed for. Especially in a civil defence shelter, such ductile behaviour is of great importance in enabling the structure to withstand severe impulse loading, in which very large loads act during a limited time period; see Chapter 4 and Paper III. Hence, since the dissipation of energy is considerably larger in

plastic response than in elastic, ductile corner behaviour is more advantageous than that provided by a corner reaching higher load capacity, but fails in brittle manner. Accordingly, it might be more important that the second point given in Section 2.1.1, regarding the joint ductility, is fulfilled than the first point, stating that the joint shall be at least as strong as its weakest adjoining member.

## **2.2 Mechanical behaviour of different detailings**

### **2.2.1 Opening frame corners**

For the opening moment it is quite clear that a crack will form at the inside of the corner. However, it is perhaps not as obvious that there is also risk of a second inclined crack within the corner that has to be taken into account when determining the detailing. Figure 2.5a shows a detailing, denoted *Type 1*, where this has not been done. This solution was common before the extensive experimental studies carried out in the late sixties and early seventies (e.g. Swann 1969; Mayfield *et al.* 1971, 1972; Balint and Taylor 1972; and Nilsson 1973) that showed its substantial shortcoming. It was found that this detailing was far from satisfactory, resulting in efficiencies (i.e. the ratio of the measured capacity divided by the calculated capacity in the adjoining members) as low as 8%. The reason is that there was no diagonal reinforcement to resist the diagonal tensile force in the corner (compare Figure 2.3a) and the compressed concrete outside the tensile reinforcement is therefore pushed off as shown in Figure 2.5b. When this occurs, the compressive zone suddenly disappears and the corner fails in a very brittle manner. The presence of L-shaped reinforcement around the outside of the corner serves little purpose since this reinforcement normally is compressed and, therefore, cannot prevent failure of the corner. Instead, it might even have a negative effect since it may assist in pushing the corner off. A comparison with the strut-and-tie model shown in Figure 2.3 makes it clear that such a corner, without any diagonal reinforcement, depends only on the resistance of the concrete tensile strength to counteract the tensile force  $R$ ; thus, using more reinforcement on either the tensile or compressive sides is of little help.

Nilsson (1973) derived an expression to estimate what bending moment can be applied on an opening corner when the reinforcement detailing matches that of *Type 1*. Based on linear elastic behaviour, he assumed a parabolic stress distribution along an effective length  $l_{dc}$  as



shown in Figure 2.6a, and was thereby able to express what reinforcement ratio  $\rho$  is allowed if the reinforcement is to yield before concrete tensile failure occurs within the corner. That is, if the reinforcement ratio  $\rho$  fulfils the requirement

$$\rho \leq \frac{\sqrt{2}}{3} \cdot \frac{f_t}{f_{sy}} \cdot \frac{l_{dc}}{d} \quad (2.1)$$

where  $f_t$  is the concrete tensile strength,  $f_{sy}$  is the reinforcement yield strength and  $d$  is the effective height, the capacity should be sufficient according to Nilsson. When comparing this expression to test results, Nilsson also found that it rather well predicts the capacity of corners reinforced with *Type 1* detailing. However, for detailings different from this, the expression might underestimate the corner capacity very much. Perhaps the main disadvantage of this expression is that the effective length  $l_{dc}$  is not known in advance but has to be determined from tests or estimated through assumptions. Therefore, a somewhat simplified model, where all geometrical parameters are given from the dimensions of the corner to estimate a lower limit of the frame corner capacity, is presented below.

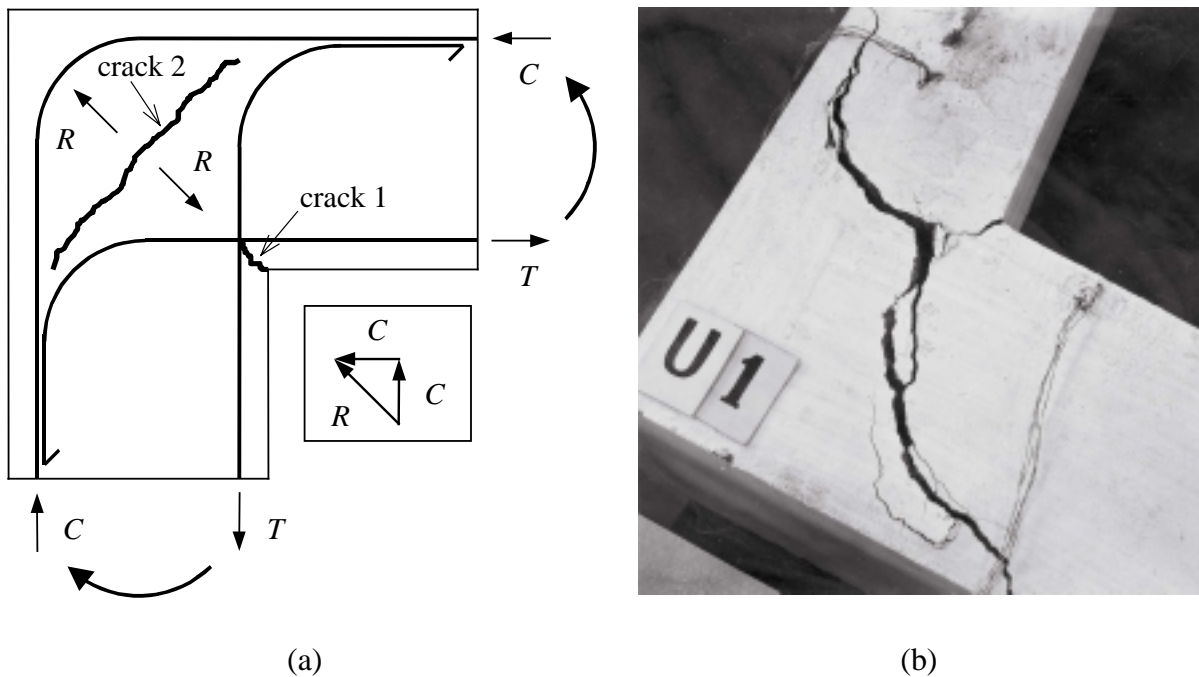


Figure 2.5 (a) Reinforcement detailing in earlier practice (*Type 1*) which is not very successful; (b) typical crack pattern at failure when such a detailing is used (no compressive reinforcement included here, though). From Nilsson (1973).

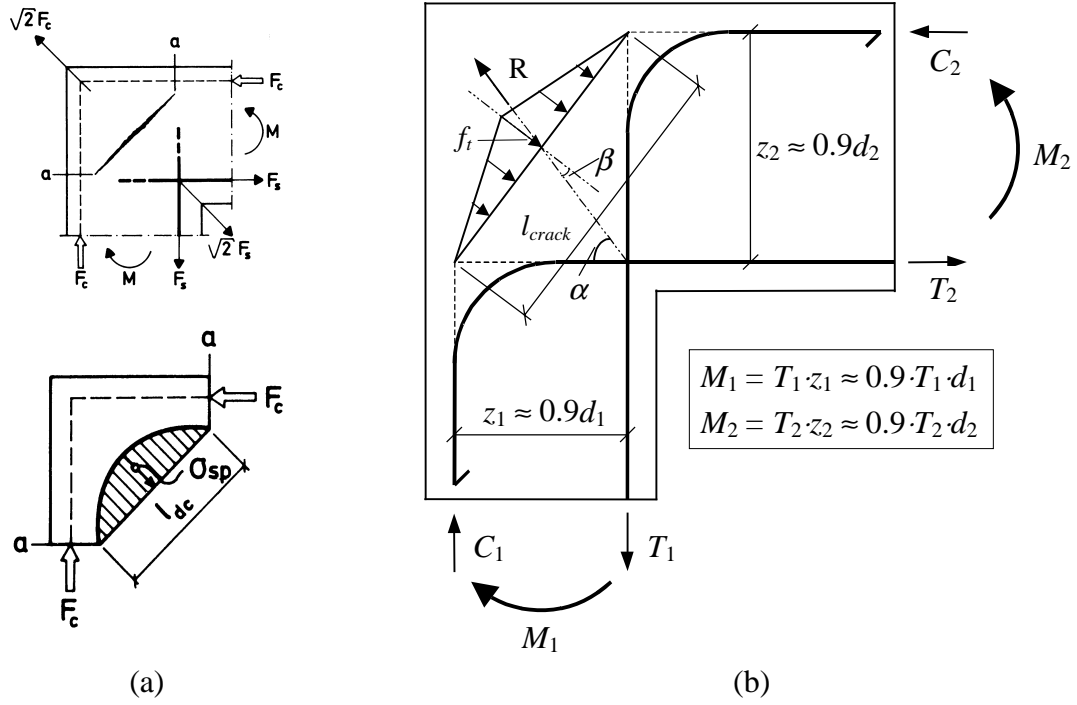


Figure 2.6 (a) Truss idealisation of corner subjected to positive moment, according to Nilsson (1973); (b) stress distribution assumed in the corner for the derivation made by the author.

This derivation is similar to that made by Nilsson, the main difference being that Nilsson used a parabolic stress distribution and that the effective length used was to be determined from tests. Here, however, the effective length is assumed to be  $l_{crack} = \sqrt{z_1^2 + z_2^2}$  as shown in Figure 2.6b, where  $z_1$  and  $z_2$  are the internal lever arms in the adjacent members. To compensate for a larger effective length, a triangular stress distribution is assumed instead of the parabolic one used by Nilsson. In a corner subjected to pure bending, the diagonal force  $R$  acting in the corner can be determined as

$$R = \sqrt{T_1^2 + T_2^2} = T_1 \sqrt{1 + \gamma^2} \quad (2.2)$$

where  $T_1$  and  $T_2$  are the tensile forces in the smaller and larger adjoining members, respectively, and

$$\gamma = \frac{z_1}{z_2} = \frac{T_2}{T_1} \quad (2.3)$$

is a factor obtained from the moment equilibrium  $M_1 = M_2$  shown in Figure 2.6b. Unless using over-reinforced cross-sections, yielding of the tensile reinforcement will be obtained before maximum moment capacity is reached. Hence, the requirement of full efficiency is here approximated to be fulfilled if the tensile reinforcement yields, i.e.

$$R = T_1 \sqrt{1 + \gamma^2} = f_{sy} A_{s,1} \sqrt{1 + \gamma^2} \quad (2.4)$$

where  $f_{sy}$  is the yield strength of the reinforcement and  $A_{s,1}$  is the cross-section area in member 1. If assuming a triangular stress distribution within the corner as shown in Figure 2.6b, the concrete resistance force  $F_R$  offered by the concrete can be estimated as

$$F_R = \frac{f_t b l_{crack}}{2} \cdot \cos \beta \quad (2.5)$$

where  $f_t$  is the concrete tensile strength,  $b$  is the width of the corner,  $l_{crack}$  is the effective length, and  $\beta$  is the angle between the direction of the tensile force  $R$  and the normal to the assumed crack direction. Using the assumption for  $l_{crack}$  given above, expressing

$$\cos \beta = 2 \sin \alpha \cos \alpha = \frac{2z_1 z_2}{z_1^2 + z_2^2} \quad (2.6)$$

and setting  $z_1 \approx 0.9d_1$ , where  $d_1$  is the effective height in the smallest adjacent member, the force  $F_R$  can be written as

$$F_R = \frac{0.9 f_t b d_1}{\sqrt{1 + \gamma^2}} \quad (2.7)$$

Finally, by setting  $R = F_R$  it is possible to estimate a reinforcement ratio  $\rho$  in the smallest adjacent member, below which the reinforcement will yield, as

$$\rho_1 = \frac{A_{s,1}}{b d_1} = \frac{0.9}{1 + \gamma^2} \cdot \frac{f_t}{f_{sy}} \quad (2.8)$$

However, since

$$\gamma = \frac{d_1}{d_2} \leq 1 \quad (2.9)$$

this means that different sizes of the adjoining members result in larger resistance against cracking within the corner. Hence, according to this model the maximum reinforcement ratio that always would be possible to use, while still reaching yielding in the reinforcement, is

$$\rho_{crit} = \frac{0.45f_t}{f_{sy}} \quad (2.10)$$

which corresponds to the case when the two adjoining members are of equal dimensions. Evidently, the efficiency of detailing *Type 1* depends on the concrete tensile strength, the reinforcement ratio and the steel yield strength. This conclusion also holds true for the detailings presented below, even though they are not as critical as this detailing.

A possible solution to balance the tensile force  $R$ , and thus the failure of the corner, would be to position reinforcement bars perpendicular to it as shown in Figure 2.7a. Tests on such detailings, here denoted as *Type 2*, have also been carried out by several researchers (see Appendix A), and it has been shown that the use of such radial reinforcement within the corner substantially improves the structural behaviour of the corner, resulting in a considerable increase of the efficiency. The amount of diagonal reinforcement needed across the crack can be determined by using equation (2.4), making sure that the whole tensile force  $R$  is taken by the reinforcement. Nevertheless, even though this detailing gives considerably improved behaviour, it does still not fulfil the requirement of full efficiency. This is because the radial reinforcement is not anchored at the outside of the corner and the equilibrium requirement of the strut-and-tie model (see Figure 2.3a) can, therefore, not be fulfilled. Instead, a critical crack can therefore form outside the L-shaped reinforcement as shown in Figure 2.7b, and the outer concrete part is pushed off. Further, the detailing does not fulfil the requirement that it should be easy to carry out; see point four in Section 2.1.1. The use of stirrups may be possible in beam-column corners, but in wall-slab corners such a detailing could be quite complicated to carry out. Therefore, another solution is necessary if the demand for an easily fabricated detailing is to be met.

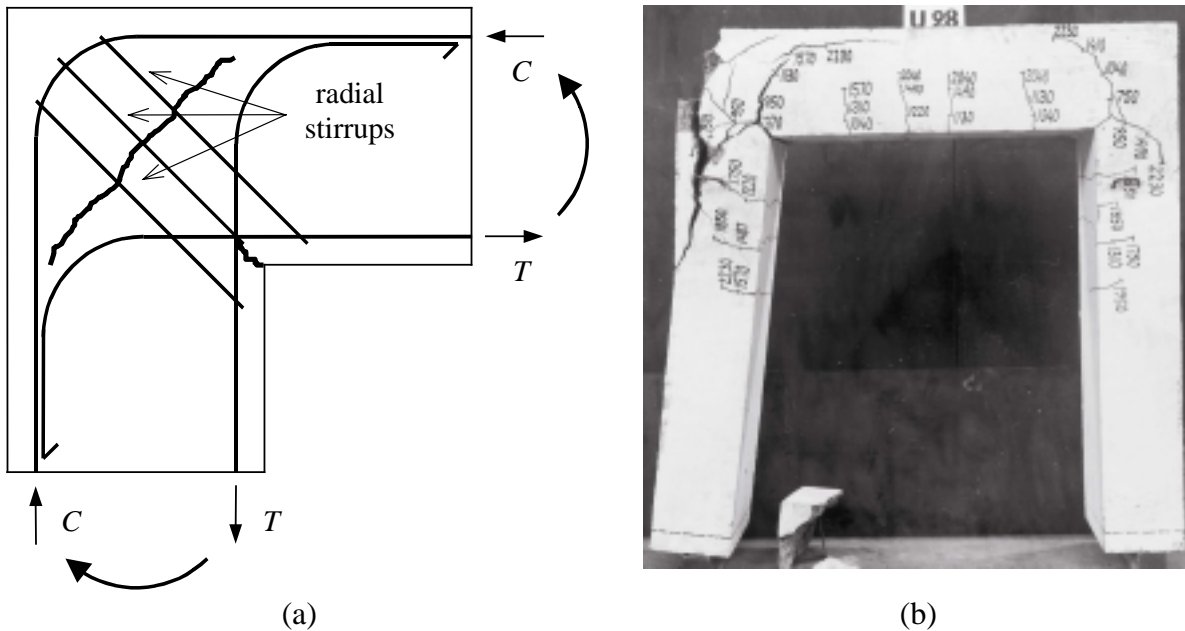


Figure 2.7 (a) Reinforcement detailing of *Type 2* where stirrups are positioned perpendicular to the expected secondary crack. (b) Crack pattern at failure when using this detailing. From Nilsson (1973).

A possible solution that fulfils this requirement, i.e. easy assembly at the construction site is detailing *Type 3* shown in Figure 2.8a. As in the *Type 2* proposal this solution will, due to the  $180^\circ$  bend bars, also present a certain amount of reinforcement perpendicular to crack 2. Further, when the reinforcement is tensioned at the inside, the loops confine the concrete sprint, and hinder the forming of a crack here. Hence, as in the *Type 2* detailing, the reinforcement loops force the diagonal crack (i.e. crack 2 in Figure 2.5a) out in the corner where the tensile stresses are less pronounced. Instead of forming a diagonal crack within the corner, the cracks then follow the loops until close to the compressive reinforcement, at which point they deviate in the direction of the adjoining members. Eventually, the cracks propagate as shown in Figure 2.9 and the concrete outside the reinforcement is pushed off. The anchorage of the loops is then reduced and the load capacity decreases with increasing rotation of the loops. Nevertheless, as shown in Paper I, a rather ductile behaviour may still be obtained.

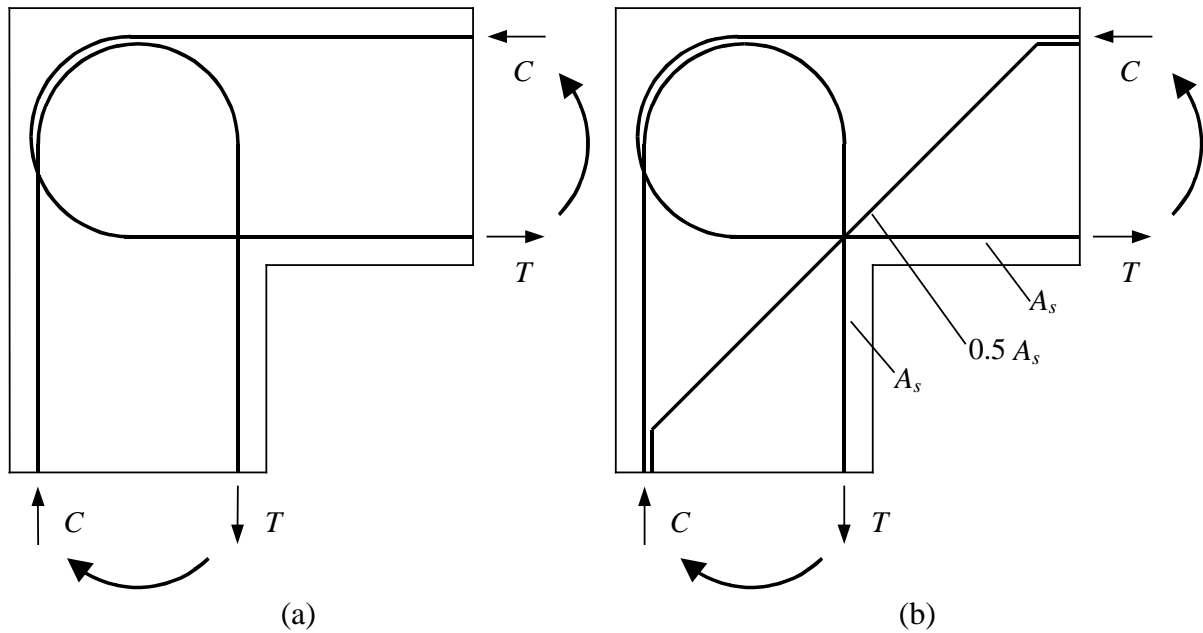


Figure 2.8 Reinforcement detailing of (a) *Type 3* and (b) *Type 4* using reinforcement loops to confine the concrete within the corner. *Type 4* also uses inclined bars to strengthen the corner.

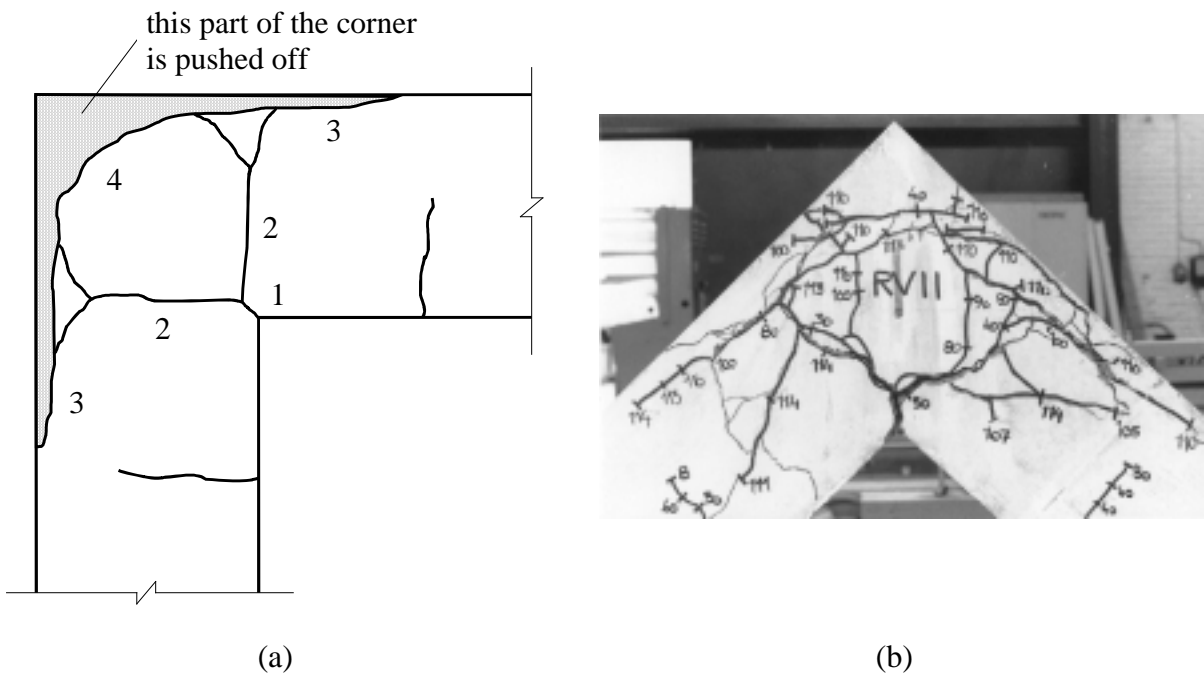


Figure 2.9 Crack pattern in frame corner when using detailing *Type 3* or *Type 4*. The numbers in (a) show the order of appearance of the crack propagation; (b) shows the crack pattern after failure for a frame corner using detailing *Type 3*. Photo from Johansson and Karlsson (1997).

Most researchers working with opening frame corners have tested detailing *Type 3* or similar proposals and it has been shown that the efficiencies of this detailing and that of *Type 2* are comparable. However, full efficiency is not obtained with either detailing and since this, together with an easily fabricated detailing, was the main goal, further studies were carried out. After an extensive experimental test series, Nilsson (1967, 1973) concluded that such a solution is possible (when using the conventional evaluation method, see Section 2.1.3) if the *Type 3* detailing is strengthened by inclined bars positioned at the inside of the corner as shown in Figure 2.8b. Quite naturally, the structural behaviour of this detailing is very similar to that of *Type 3*. The inclined bars, though, delay the growing of the first crack at the inside of the corner and thereby also delay the propagation of the crack outside the compressive reinforcement. Nilsson determined experimentally that the area of the inclined bars should be about one-half that of the main reinforcement; see Figure 2.8b. According to Karlsson (1999) this detailing is nowadays accepted in many countries, possibly in combination with diagonal stirrups positioned similarly to those in *Type 2*.

## 2.2.2 Closing frame corners

As stated in Section 2.1.2, a frame corner subjected to closing moment is not as sensitive as one subjected to an opening moment. This is because it in the former case is considerably easier to attain a reinforcement detailing that may balance the internal forces also after concrete cracking has occurred. For opening corners, though, this is not the case, and it can therefore be said that the behaviour of such corners is characterised by the concrete tensile strength, while closing corners depend more on the concrete compressive strength. Consequently, there also exist several suitable solutions, of which detailing *Type 1* and *Type 3*, shown in Figures 2.4 and 2.7a, respectively, are two good possibilities.

Since the internal lever arm increases within the corner, it might appear that a joint region in a closing corner is always stronger than its adjoining members. Yet it has been shown in tests that the corner in certain cases fails before yielding of the tensile reinforcement, and hence results in capacities lower than that expected. The possible causes of this behaviour are, according to Stroband and Kolpa (1983), the following:

- premature crushing of the concrete at the inside of the corner in the concrete compressive zone;
- crushing failure of the diagonal compressive strut within the corner;
- spalling of the side concrete cover, which causes anchorage failure of the reinforcement.

Further, if the tensile reinforcement is spliced within the corner, the possibility of an anchorage failure exists in the same way, as is the case in an ordinary beam with spliced reinforcement. Of the possible failure types mentioned here, spalling of the side concrete cover is regarded as especially interesting and is therefore treated more thoroughly in Section 2.2.3.

Premature crushing of the concrete at the inside of the corner is possible when the combination of the concrete compressive strength, reinforcement yield strength and reinforcement ratio is such that a high mechanical reinforcement ratio,  $\omega_s$ , is obtained. High compressive stresses are then concentrated in the region of the internal angle; compare the strut-and-tie model in Figure 2.3b. However, in this region there also exists a favourable multiaxial compressive state of stress that wholly or partly compensates for these large stresses and, hence, usually give the corner the strength required to resist concrete crushing. Such a favourable stress state, though, is not necessarily the case in the diagonal compressive strut (it might be if confining stirrups are positioned within the corner) and for large values of  $\omega_s$  there is risk of compressive failure in this part. Stroband and Kolpa derived an expression which suggests that  $\omega_s$  must be limited to 0.240 if such a failure is to be avoided.

### **2.2.3 Spalling of the side concrete cover**

When a bar changes direction, there will be radial compressive stresses as shown in Figure 2.10a. These stresses give rise to tensile stresses that try to split the concrete in the plane of the bend. Tests and theoretical studies of this kind of failure in beams have been carried out by, for instance: Timm (1969), Leonhardt *et al.* (1973), Franz and Timm (1972), Kordina and Fuchs (1972), Dragosavic *et al.* (1975), and Grassl (1999). Wästlund (1935), Östlund (1963), Elinder and Hallhagen (1967), and Stroband and Kolpa (1983) have examined the effect of spalling in frame corners. In this section the effects of this phenomenon and how it can be treated are briefly discussed. For a thorough summary of the behaviour in the concrete around bent reinforcement bars the reader is referred to, for example, Timm (1969) or Grassl (1999).

It has been found that the magnitude of the splitting stresses depends on the bar diameter, their bending radius and the steel yield strength. Further, experimental results indicate that the risk of spalling failure increases when reinforcement loops such as those in detailing *Type 3* are used, compared to the L-shaped bars in detailing *Type 1*; see Stroband and Kolpa and Paper II.



Because of the positive effect of confinement a large side concrete cover has a positive effect on the resistance against spalling. Further, transverse reinforcement bars within the loops or radial stirrups around the loops may help in restraining the tensile stresses perpendicular to the bend. However, although such reinforcement may be easy to assemble in a beam-column joint it might be very difficult to do this in a wall-slab connection at the construction site.

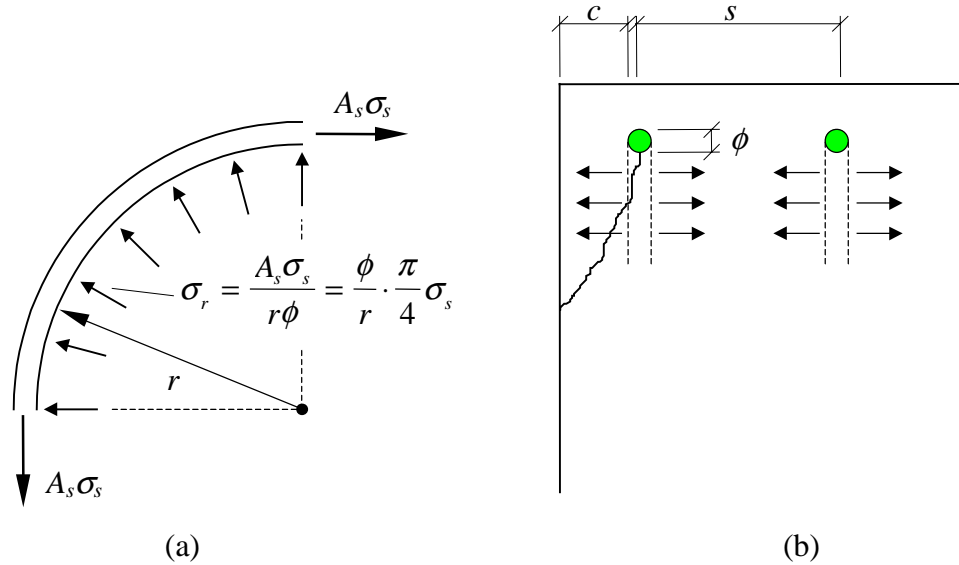


Figure 2.10 Schematic view of (a) radial compressive stresses and (b) possible splitting cracks in the plane of the bent bar. Based on Stroband and Kolpa (1983).

If the splitting stresses reach the tensile strength of the concrete, cracks are formed in the plane of the loops and spalling of the side concrete cover is possible; see Figures 2.10b and 2.11. If this happens, the reinforcement bars close to the free concrete sides lose their anchorage and the load capacity decreases, something that according to Stroband and Kolpa occurs suddenly. However, tests carried out by the author and reported by Grassl show that this is not necessarily the case; see Appendix B. The reason is that even though the outer reinforcement bars are lost, resulting in fewer bars available to transmit the load, the confinement of the interior bars still provides enough anchorage to considerably delay a total failure. Hence, the post-peak response, i.e. the behaviour after maximum load, depends to a large degree on what percentage of the total reinforcement amount is affected. That is, if for instance a beam-column connection reinforced with only a small number of bars (Stroband and Kolpa had two  $\phi 6$  in their tests; see Appendix A) loses the outer bars, there is substantial risk of a brittle behaviour. However, if only a limited number of the total reinforcement bars available are affected, as is the case in a wall-slab joint, the spalling will have little effect on the total load capacity, and ductile behaviour is therefore still possible.

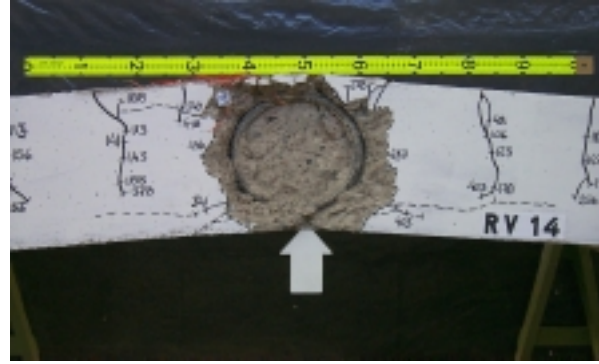


Figure 2.11 Spalling of side concrete cover in frame corner (*Type 3*) when using spliced reinforcement loops. Photos from Johansson (1996) and Grassl (1999), respectively.

Spalling of the side concrete cover may be a problem for both opening and closing frame corners. In the former case, though, failure is often introduced due to other reasons, and side concrete spalling is therefore not regarded as such a large problem for opening corners. For closing corners, though, it is considerably larger risk that this failure mode will cause total corner failure, and then also limit the corner capacity. Nevertheless, tests on opening corners, presented in Paper I, showed that this phenomena might be very important to better understand and interpret the test results of opening corners.

Different proposals of how to take into account the spalling of the side concrete cover can be found in the literature; three of these are compared below. The final expressions are generally derived to give a minimum ratio  $r / \phi$  between the radius of the bend bars and the bar diameter at which the detailing still is able to avoid spalling of the side concrete cover. CEB-FIP Model Code, CEB (1993), presents such an expression based on the concrete response when subjected to splitting forces:

$$\frac{2r}{\phi} \geq 1.6 \cdot \sqrt{\frac{\phi}{2c + \phi}} \cdot \frac{f_{sy}}{f_c} \quad (2.11)$$

where  $c$  is the concrete cover perpendicular to the plane of the bend bars,  $f_{sy}$  is the steel yield strength and  $f_c$  is the compressive strength of the concrete. Using the approximate relation between the compressive stress  $f_c$  and the concrete tensile stress  $f_t$ , given in equation (2.20), it can be rewritten as

$$\frac{r}{\phi} \geq 0.042 \cdot \sqrt{\frac{1}{c/\phi + 0.5}} \cdot \frac{f_{sy}}{f_t} \quad (2.12)$$

which is very similar to that presented in Stroband and Kolpa (1983), i.e.

$$\frac{r}{\phi} \geq 0.050 \cdot \sqrt{\frac{1}{c/\phi + 0.5}} \cdot \frac{f_{sy}}{f_t} \quad (2.13)$$

Neither of the above, though, takes into account at what angle the bars are bent, something that is considered in the Swedish Concrete Code BBK 94, Boverket (1994). Here, an empirical expression

$$\frac{r}{\phi} \geq 0.028 \cdot \frac{f_{sy}}{f_t} - 0.5 - \frac{1}{\sin(\alpha/2)} \cdot \left( \frac{c}{\phi} + 0.5 \right) \quad \text{where } \frac{c}{\phi} \leq 3.5 \quad (2.14)$$

somewhat different from that proposed by CEB and by Stroband and Kolpa is used. Except for the introduction of the bending angle  $\alpha$  ( $\alpha = 180^\circ$  for a reinforcement loop), though, the ratio  $r/\phi$  depends on the same parameters as above. This introduction of the bending angle seems reasonable, since tests by both Stroband and Kolpa and the author indicated that the risk of spalling failure increases when using reinforcement loops, compared to when using L-shaped bars as in the *Type I* detailing. Dragosavic *et al.* (1975) also proposed an empirical expression, in which the influence of transverse bars is taken into account. It is not included here, though, since it requires a large side concrete cover ( $c \geq 4.5\phi$ ) to be valid for use. The results of the other three expressions are compared in Figure 2.12a. From this it can be seen that the minimum value of the ratio  $r/\phi$  varies quite widely for low values of  $f_{sy}/f_t$ . For instance, at a strength ratio of 250, which is quite a reasonable ratio when using mean strengths, the requirement in BBK 94 is only about 60% of that predicted by the CEB-FIP Model Code. A possible reason might be that the expression in the former is based on the characteristic tensile strengths used in BBK 94, which are generally somewhat lower than those given in, for example, the Model Code for concrete of the same compressive strength. Nevertheless, in the tests on frame corners presented in Paper I, spalling of the side concrete cover also occurred despite fulfilling the requirements set by both BBK 94 and the Model Code. Even when more than doubling the side concrete cover in the tests of opening moment,

there were strong indications that splitting stresses caused by the bend bars influenced the response of the outer reinforcement loops. Figure 2.12b compares the ratio  $r/\phi$  in the frame corners, presented in Paper I, using such loops as that required by the Model Code. Here, the ratio between the side concrete cover and the bar diameter varied as  $2 \leq c/\phi \leq 4.5$ , which also has a considerable influence on the predicted ratio  $r/\phi$  allowed. Thus, this very limited comparison suggests that the expressions given in the literature may be inadequate to use for spliced reinforcement loops in frame corners.

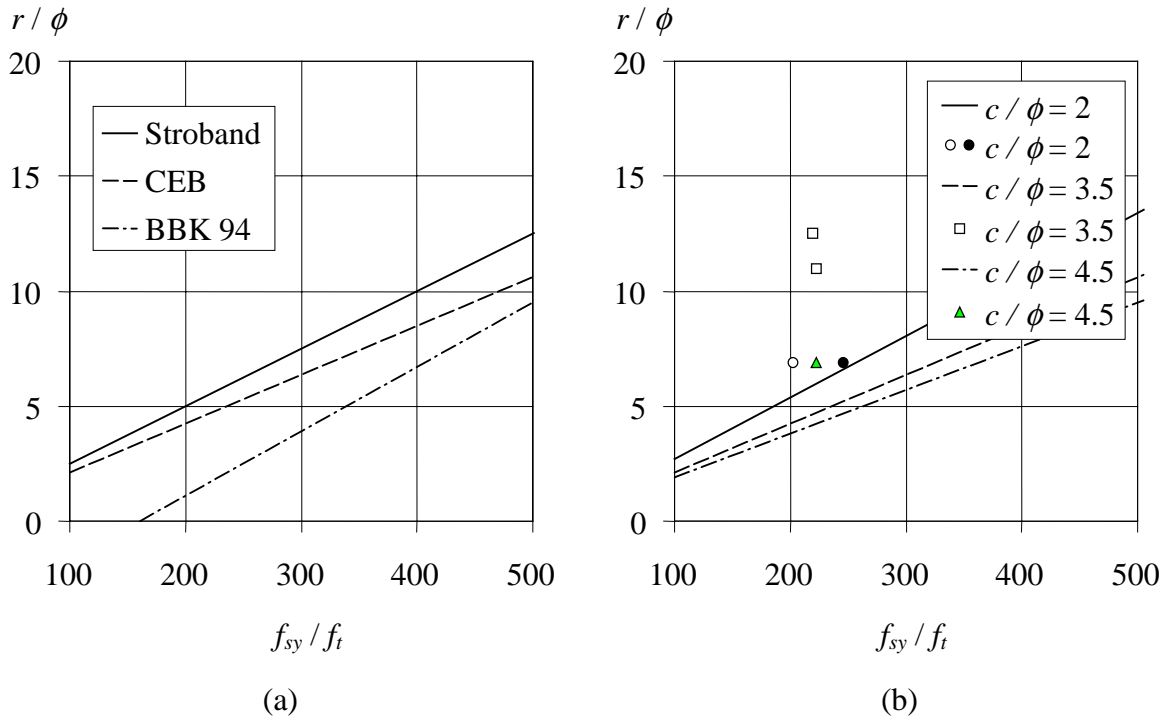


Figure 2.12 (a) Comparison of ratio  $r/\phi$  required in different references to avoid spalling of the side concrete cover when the ratio  $c/\phi = 2$ ; (b) comparison between tests and allowable ratio  $r/\phi$  according to CEB (1993). Black dot means spalling failure, grey means that spalling was initiated, and white means no spalling.

## 2.3 Corner efficiency

### 2.3.1 Comparison of opening and closing corners

When comparing the efficiencies of different corner detailings it is common to plot them as a function of the reinforcement ratio,  $\rho$ . However, since in Section 2.2.1 it was concluded that both the concrete and steel qualities are of high importance, it is better to plot the efficiency as a function of the mechanical reinforcement ratio,  $\omega$ ; i.e.:

$$\omega_s = \rho \frac{f_{sy}}{f_c} = \frac{A_s f_{sy}}{bdf_c} \quad (2.15)$$

where  $f_c$  is the cylinder compressive strength of the concrete.

A comparison of the efficiency obtained in tests of opening frame corners reinforced with the four detailings presented (or similar to those, see Appendix A) is shown in Figure 2.13. To better visualise the background for the conclusions drawn by Nilsson and others, the efficiencies were here determined using the conventional evaluation method, i.e. no account was taken to the extra moment capacity in the adjoining members provide by the inclined bars in the *Type 4* detailing; see Section 2.1.3. Further, of the results containing detailing *Type 2* only those tests where the amount of stirrups were able to counteract the tensile force,  $R$ , are included; all tests of this detailing, though, are compared in Appendix A. The reinforcement ratios used varied between 0.38 and 3.02%, and the approximate concrete cylinder compressive strength ranged from 10 to 52 MPa. From this comparison the considerable inefficiency of the *Type 1* detailing and the apparent advantage of the *Type 4* detailing, respectively, are clear (for a complete summary of these test results, see Appendix A). Further, it can be seen that detailing *Type 3* is rather effective even though not reaching full efficiency; *Type 2*, though, seems to be somewhat less reliable. Therefore, in the following treatment of opening corners only the *Type 3* and *Type 4* detailings are dealt with. A closer look at Figure 2.13 shows that the efficiency of these two detailings seems to drop dramatically when  $\omega_s$  exceeds 0.200, thus suggesting that neither detailing should be particularly appropriate to use for mechanical reinforcement ratios higher than this limit.

The efficiencies of the *Type 1* and *Type 3* detailings in closing frame corners are compared in Figure 2.14. It is found that for mechanical reinforcement ratios  $\omega_s$  below a value of about 0.300 the efficiency is usually in the vicinity of or above 100%. Those results that did not meet this requirement showed for most cases, a different failure mode than the expected flexural failure; see also Paper I and Paper II for further discussion. Nevertheless, since one aim of the work presented in this dissertation was to investigate whether the *Type 1* detailing could be replaced by *Type 3*, it is especially interesting to note that the two detailings, for practical purposes, seem to be quite equivalent. Thus, this indicates that such a change also should be appropriate.

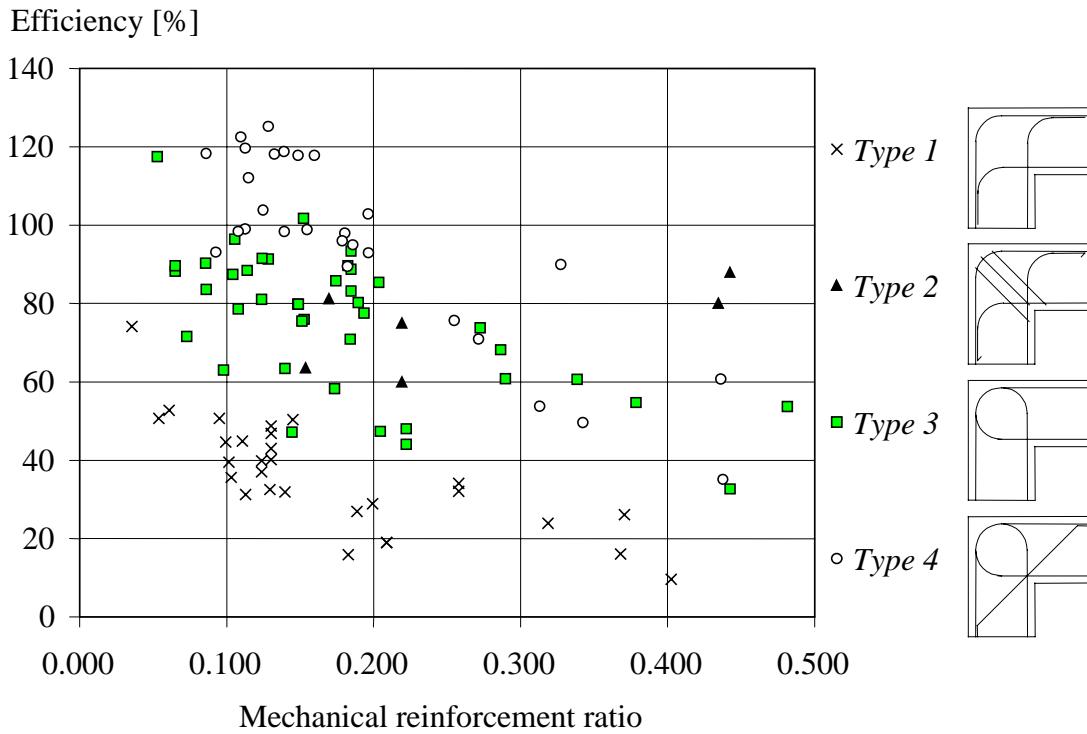


Figure 2.13 Efficiency of reinforcement detailings in frame corner subjecting to opening moment. In the *Type 4* detailing, no account is taken to the inclined bar's contribution to the expected moment capacity; see Section 2.1.3.

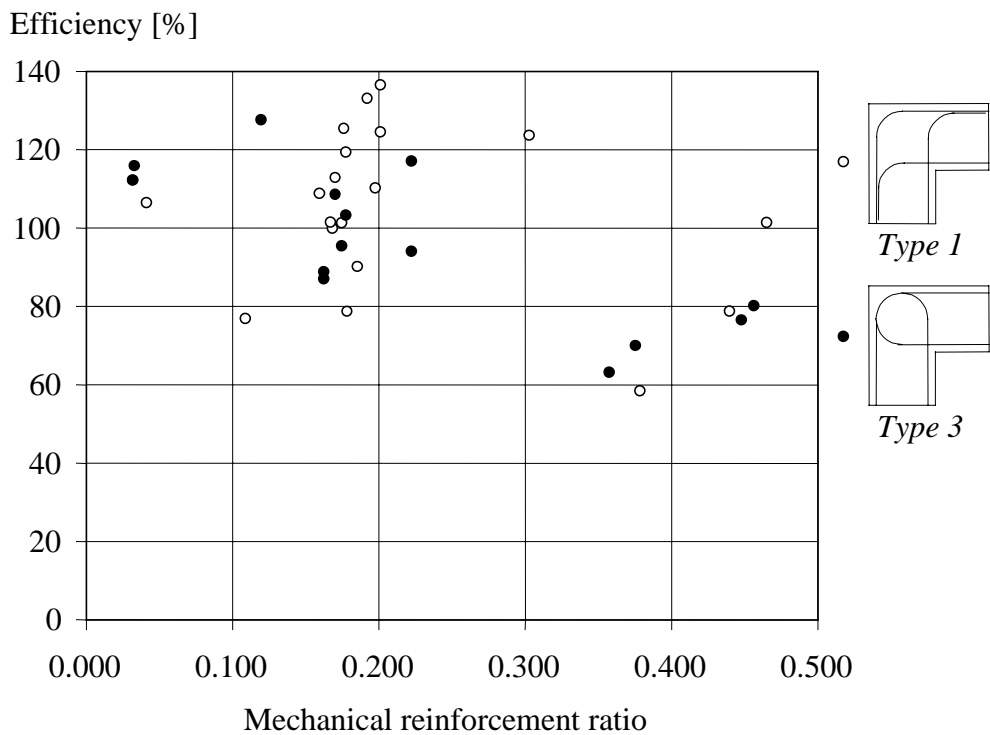


Figure 2.14 Efficiency of different reinforcement detailings in a frame corner subjected to closing moment.

Figure 2.15 compares the efficiencies of detailings *Type 1* and *Type 3* in frame corners subjected to opening and closing moments. From this it is very clear that frame corners subjected to opening moment are considerably more sensitive than frame corners subjected to closing moment. This is especially true for the *Type 1* detailing, which in closing moment generally reaches an efficiency of 100%, while it for opening moment usually is below 50%. The *Type 3* detailing provides a substantial larger resemblance when subjected to opening or closing moment even though the difference in efficiency obtained is still evident. Thus, it can be concluded that the use of reinforcement loops within the corner seems to be a good choice for frame corners that might be subjected to both opening and closing moment. Hence, this detailing is further used in the following section, in which different approaches that might further increase the corner efficiency in opening frame corners is presented and discussed.

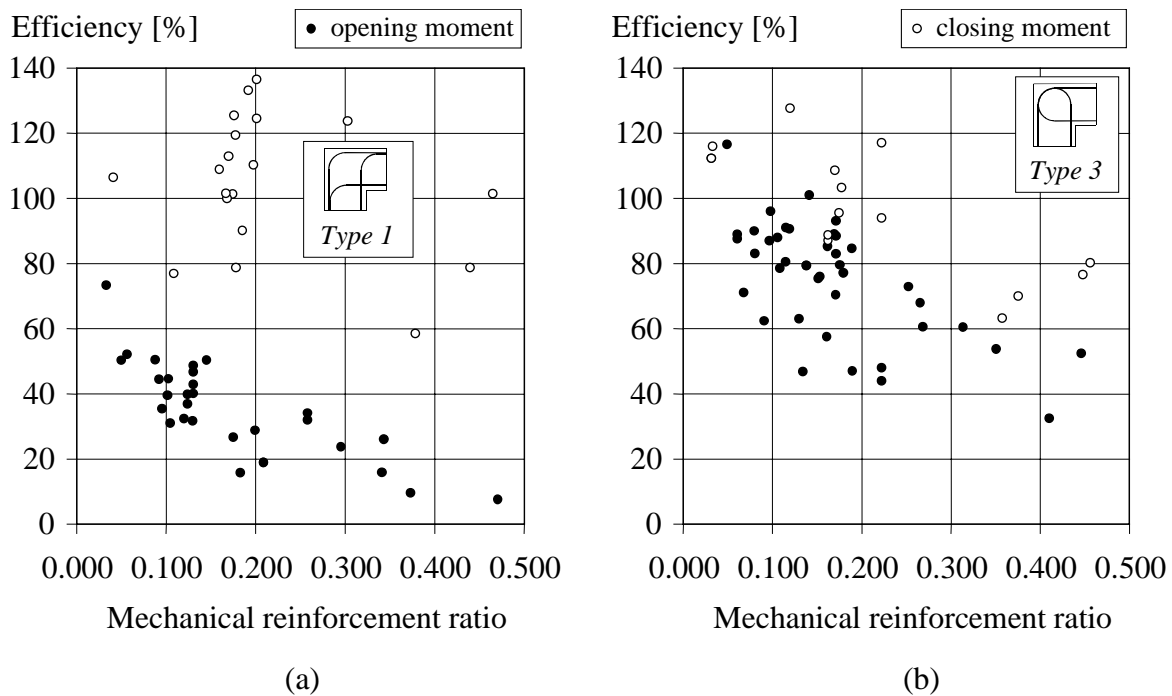


Figure 2.15 Comparison of reinforcement detailings when subjected to opening or closing moment: (a) *Type 1* detailing; (b) *Type 3* detailing.

## 2.3.2 Influencing parameters

### 2.3.2.1 Inclined bars

According to the comparison made in Figure 2.13 the *Type 4* detailing should without doubt be superior to that of *Type 3*. However, a comment on these results should be made before any hasty conclusions are made. As mentioned in Section 2.1.3, when Nilsson and other

researchers determined the efficiency of the Type 4 detailing, they did not include the contribution to the moment capacity in the critical section from the inclined bars. Neither did they take this extra reinforcement into account when determining the reinforcement ratio of the detailing. This approach, the conventional evaluation method, was also used for the results presented in Figure 2.13. Therefore, it is somewhat deceptive to interpret reported test results of opening frame corners that make use of inclined bars positioned at the inside of the corner. However, by using the new evaluation method, described in Section 2.1.3, a consistent comparison of different reinforcement detailings is possible. As shown in Figure 2.16, the active amount of reinforcement  $A_s^*$  counteracting the crack in the critical section can be determined as

$$A_s^* = A_s + \frac{1}{\sqrt{2}} A_{s,i} \quad (2.16)$$

where  $A_s$  and  $A_{s,i}$  are the reinforcement areas of the loops and inclined bars, respectively. Using this area  $A_s^*$  when estimating the corner's moment capacity and mechanical reinforcement ratio, the result will also be quite different; see Figure 2.17. Here, the efficiency of *Type 3* is compared to the modified efficiency of *Type 4*. It is then clear that their efficiencies are rather similar, something that also was confirmed in tests by the author; see Paper I.

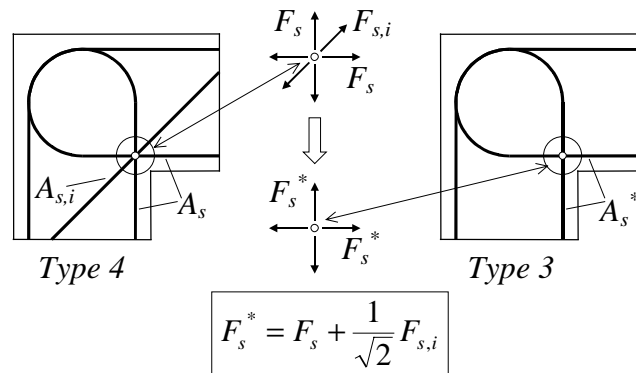


Figure 2.16 How to take into account the contribution of the inclined bars in detailing *Type 4* when transforming it into a *Type 3* detailing.

Consequently, from the author's point of view the *Type 4* detailing does not fulfil the requirement of 100% efficiency. It can be argued that the purpose of adding inclined bars at the inside of an opening corner is not explicitly there to provide full efficiency in the critical section, as defined in the new evaluation method described in Section 2.1.3, but to force the final failure to occur outside the corner. This is also what often happened in tests by Nilsson and others, which led to the detailing being regarded as successful. However, as discussed



below and in Paper I, the appearance of a critical crack outside the corner depends to a large degree on the moment distribution close to the corner and whether the reinforcement loops are spliced to straight bars just outside the corner or not. If the external moment decreases at increasing distance from the corner, as is usually the case, one cannot be sure that a critical crack forms in any of the adjoining members prior to corner failure. Due to the crack distance obtained in reinforced concrete, the moment acting in a potential critical section outside the corner may be considerably lower than that in the corner. If this crack section is positioned too close to the corner, the inclined bars might increase the section's moment capacity, and hence further reduce the chance for the final failure to occur there. Therefore, if the inclined bars are to have a negligible effect on the adjoining member's moment capacity, the critical crack must at least form close to the section where the inclined bars reach the compressive zone.

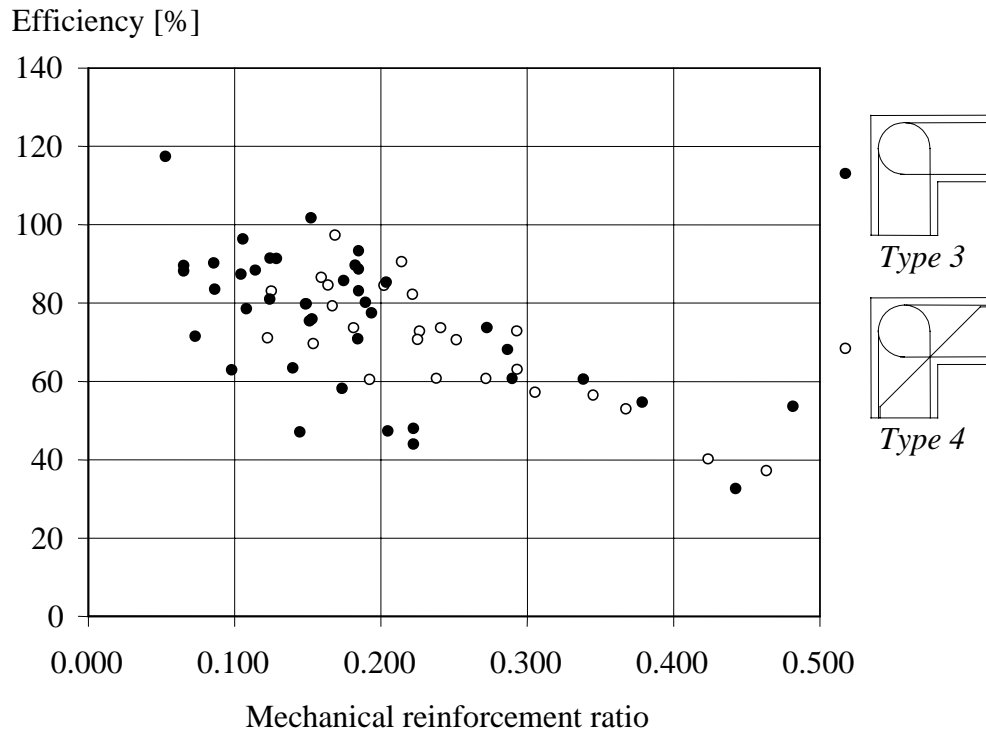


Figure 2.17 Comparison of the efficiencies of detailing *Type 3* and *Type 4* when the inclined bars in *Type 4* are considered in determining the capacity and reinforcement ratio of the detailing, i.e. using the new evaluation method described in Section 2.1.3.

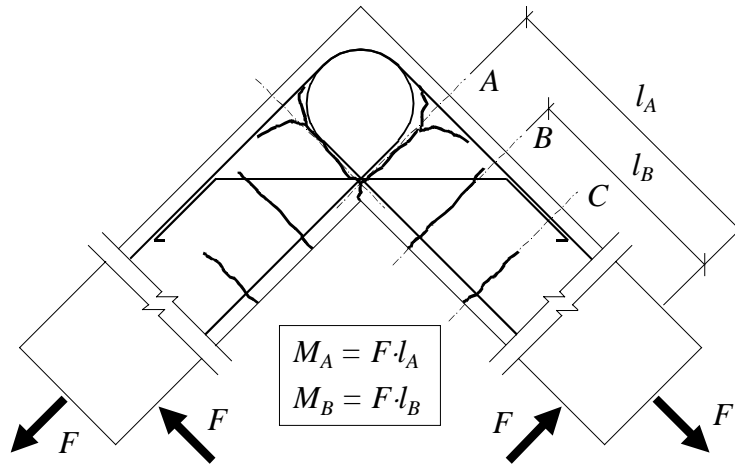


Figure 2.18 Schematic view of potential critical crack sections in an opening corner.

Figure 2.18 shows a schematic case of a corner subjected to opening moment. Here, crack *A* corresponds to the critical defined in Section 2.1.3. Crack *B* is the crack in the adjoining member that is closest to the corner and even though it in this case forms close to the corner, it is assumed here that the inclined bars have a negligible influence on the section's moment capacity. Depending on what effect the inclined bars have on the moment capacity in section *B*, it might instead be crack *C* that has to develop into a critical crack if final failure is to occur outside the corner region. Nevertheless, if failure is to be obtained in section *B*, the moment  $M_B$  has to reach the section's capacity  $M_{uc,B}$  before the moment  $M_A$  reaches the capacity  $M_{uc,A}$  of the corner. The relation between these capacities can be expressed as

$$M_{uc,A} = \eta \cdot M_{uc,B} \quad (2.17)$$

where  $\eta$  represents the efficiency for detailing *Type 4*. According to Figure 2.18 it varies between about 0.90 and 1.25 when  $\omega_s \leq 0.200$ . Thus, if the critical crack is to form outside the corner region, the ratio  $M_A / M_B$  has to be larger than the efficiency  $\eta$ . But since there are an infinite number of possible load cases, it is difficult to give a general statement of whether this will happen or not.

Nevertheless, Figure 2.19 shows some examples of the ratio between these moments that may be obtained for different load cases of an elastic beam with constant stiffness over its length. Here, the critical section in the adjoining member (i.e. crack *B*) is assumed to form at a distance of 0.2 m from crack *A*. Regarding the combined effect of the inclined bars and the mean crack distance in the concrete, this distance is in most cases probably underestimated, which also means that it is an assumption on the safe side. Comparing the moment ratios  $M_A / M_B$ , obtained in the presented load cases, it is clear that they for most cases are higher

than the efficiencies reached when using the *Type 4* detailing. Hence, failure will occur within the corner before any critical cracks are able to form in the adjoining members. The exceptions are the cantilever beams, which for beam lengths of about 4 m and 2 m, respectively, lead to ratios below 1.10, which makes it reasonable to believe that failure in these cases may occur in an adjoining member.

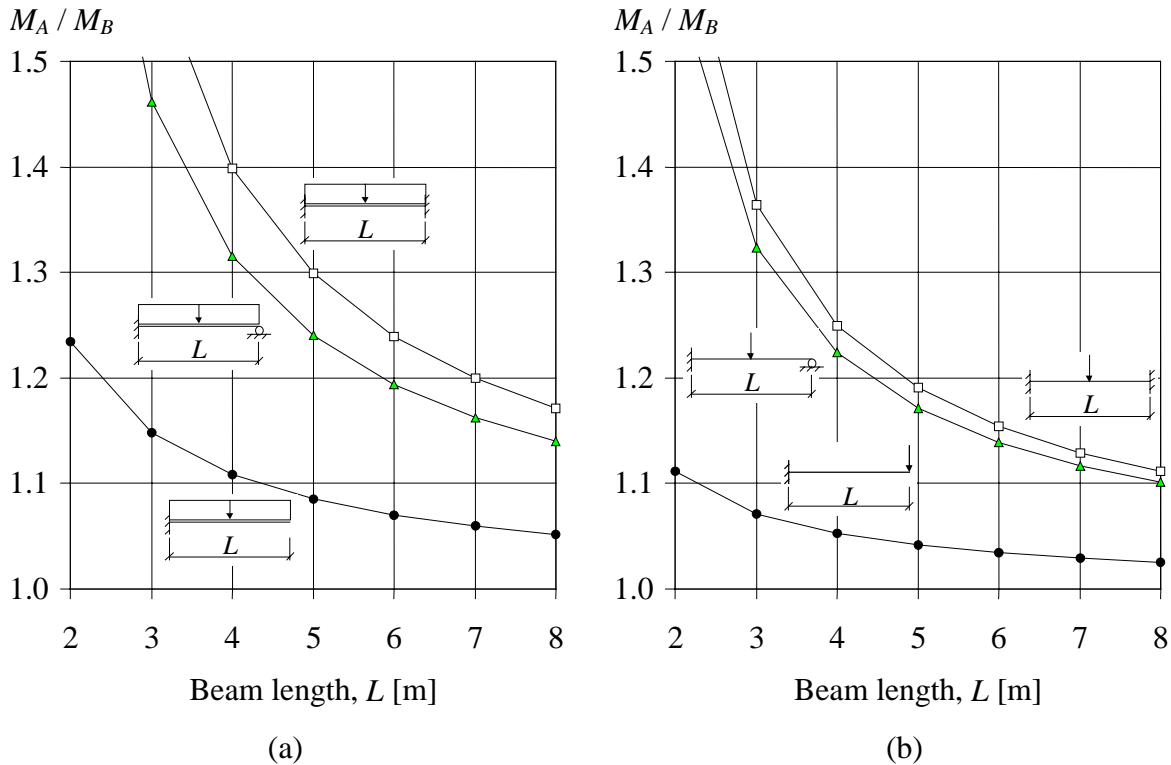


Figure 2.19 Ratio between moment in fixed support and moment at a distance of 0.2 m.

However, if inclined bars are used and the aim to prevent failure within the corner shall be met, one must make sure that the reinforcement loops are not spliced to straight bars just outside the corner region. Under no circumstances shall such splices be positioned closer to the corner than the section where the inclined bars reach the compressive zone; see Figure 2.20. If they are, the presence of extra reinforcement next to the corner will no doubt prevent the forming of a critical crack in this region. When using just reinforcement loops, though, the positioning of the splice probably does not make any difference since the critical cracks then will form within the corner in either case.

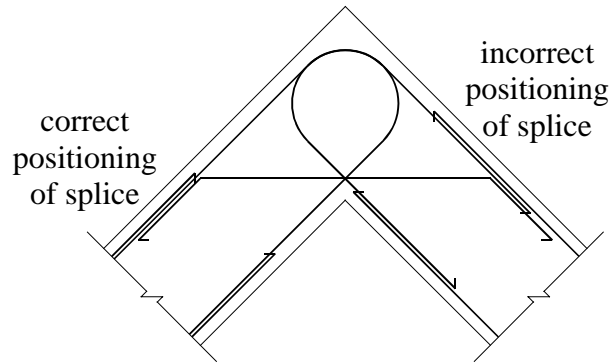


Figure 2.20 Correct and incorrect positioning of splices when using inclined bars.

### 2.3.2.2 Radial stirrups

As shown in Figure 2.13 the addition of radial stirrups within the corner of detail *Type 1*, thus transforming it into detail *Type 2*, has a very positive effect on the corner efficiency. This influence has inspired some researchers (Mayfield *et al.* 1971, 1972; Stroband and Kolpa 1981; and Skettrup *et al.* 1984) to investigate the influence of such radial bars in combination with reinforcement loops, i.e. detailings of *Type 3* and *Type 4*. The results of these tests are summarised in Figure 2.21, and from this it can be seen that the influence of the stirrups (the amount varying between 25% and 141% of that necessary to counteract the tensile force  $R$ ) is not particularly pronounced. In fact it is only for very high mechanical reinforcement ratios ( $\omega_s > 0.300$ ) in the *Type 4* detailing that the stirrups' presence seems to have any particular effect. Hence, this suggests that the adding of such diagonal reinforcement within the corner has a very limited effect if reinforcement loops, such as those in detailing *Type 3* and *Type 4*, are used. This can be interpreted as that the reinforcement loops are sufficient to prevent the forming of a critical crack within the loops. Instead, final failure will be similar to that obtained when no radial stirrups are used, i.e. loss of the concrete part outside the loops and eventually result in an anchorage failure; see Figure 2.9. That additional stirrups within the corner do not have the intended effect is not surprising though. Recalling the strut-and-tie model shown in Figure 2.3a, the tensile force  $R$  still has to be balanced by reinforcement adequately anchored at the outside of the corner. This is still not the case here and full efficiency is therefore not either to be expected.

Thus, the radial stirrups will more or less act as surplus reinforcement and therefore have little effect on the ultimate capacity of the detailing. Nevertheless, the improved efficiencies at high mechanical reinforcement ratio in the *Type 4* detailing indicate that the reinforcement provided still might be of some use. A closer look at those tests without stirrups (carried out

by Swann 1969 and Skettrup *et al.* 1984; see Appendix A) shows that all of them failed due to spalling of the side concrete cover (for a further discussion about this type of failure, see Section 2.2.3 and Paper I). Accordingly, it seems reasonable to believe that the presence of radial stirrups within the corner might strengthen the detailing's resistance against this kind of failure. It can be concluded that the use of stirrups in combination with the *Type 3* and *Type 4* detailings may be effective if there is a risk of concrete spalling. Further, the presence of stirrups may also have a positive effect on the post-peak response; i.e. by confinement the loops are better tied together and the corner ductility may increase.

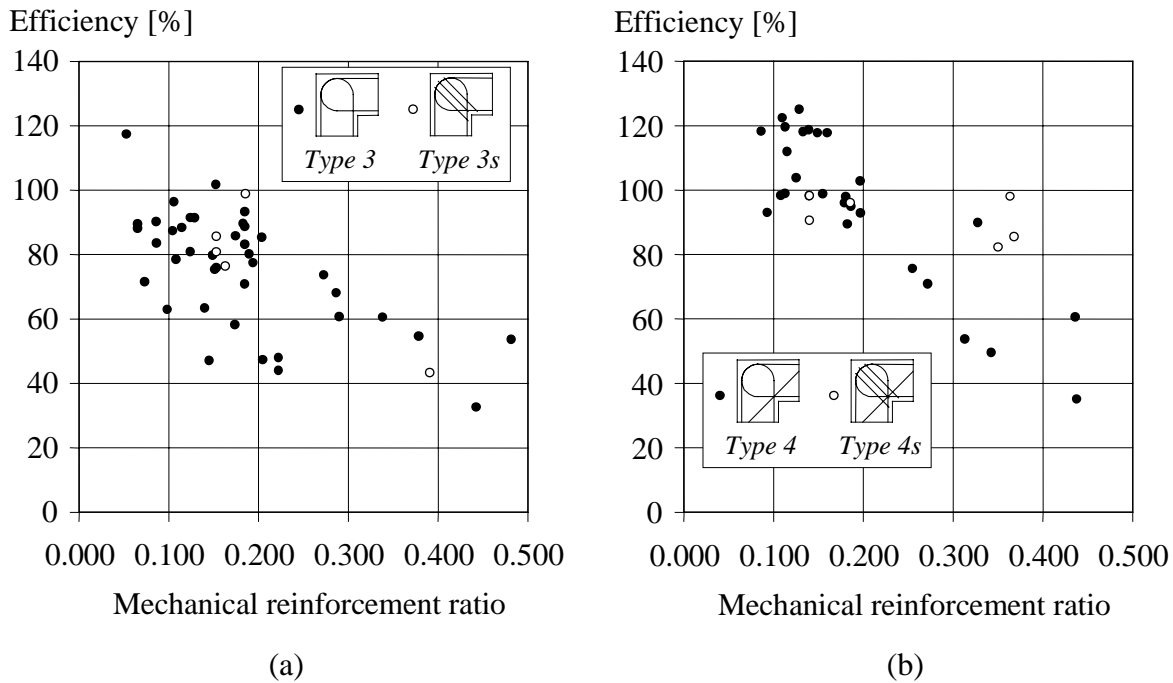


Figure 2.21 Influence of stirrups in detailing (a) *Type 3* and (b) *Type 4*.

### 2.3.2.3 Other important parameters

From Figure 2.13 it is clear that the scatter of the efficiency for detail *Type 3* is quite substantial, and it is therefore of interest to understand better what other factors have a decisive influence on the corner efficiency.

In most works treating opening frame corners, found in the literature, the reinforcement ratio is used when comparing the efficiencies of the detailings examined. In this dissertation, though, the mechanical reinforcement ratio is used to better consider the influence of what reinforcement and concrete strength are used. Nevertheless, it might still be of interest to examine whether the reinforcement ratio itself plays a vital role in what efficiency a detailing

will show. Such a comparison for detailing *Type 3* is shown in Figure 2.22 for various mechanical reinforcement ratios, and from this it can be seen that it is not very obvious whether a low reinforcement ratio has a positive effect or not when the mechanical reinforcement ratio is the same. This indicates that it might just as well be parameters other than the reinforcement ratio that play a vital role in what corner efficiency is obtained.

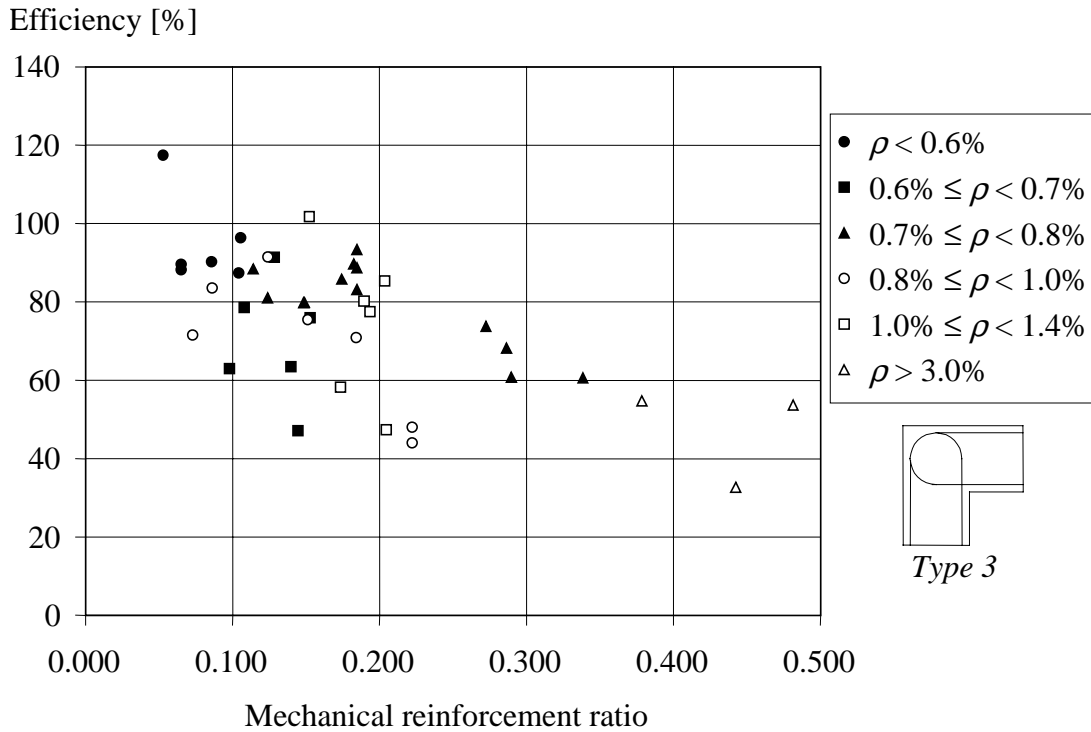


Figure 2.22 Efficiencies of *Type 3* in opening corner when examining the influence of the reinforcement ratio.

Jackson (1995) presents an interesting idea that it is the confining effect that is achieved with the reinforcement loops that is important. Thus, even though a frame corner is made of the same type of concrete and has the same amount of reinforcement, it will still behave very differently depending on the number of bars used, i.e. many small bars are better than a few large ones. Accordingly, Jackson suggests that the corner efficiency depends on the reinforcement bar diameter. This idea also supports the statement made in Section 2.2.2 that the spalling of the side concrete cover is important; see also Paper I. If larger bars are used, there is also an increased risk of transverse spalling failure. Further, if such a failure is initiated its effect is, due to a higher percentage of outermost bars, also larger in a frame corner containing large bars. Figure 2.23a shows the influence of the bar diameter on the corner efficiency. Apart from the two results of Abdul-Wahab and co-workers, the comparison indicates that a smaller bar diameter also results in a higher load capacity, thus supporting the findings of Jackson.

In addition, since in the tests presented in Paper I it was concluded that spalling of the side concrete cover probably affected the maximum load and the risk of spalling depends on the ratio between loop diameter and bar diameter, this relation was also further examined; see Figure 2.23b. The loop diameter was here assumed to be proportional to the effective height, i.e. the ratio shown is  $d/\phi$ . These results suggest that a high value of this ratio also results in higher efficiency. The exception to this is the results reported by Kordina and Fuchs (1970), who obtained rather high efficiencies even though the  $d/\phi$  ratio was relatively low. Their specimens, though, had a width of 700 mm and were reinforced with a total of six bars, which may explain the limited influence of a possible transverse spalling failure. Further, one result from Jackson's test series obtained a low efficiency despite a high value of the ratio  $d/\phi$ . However, the final crack pattern in this specimen strongly indicates that it spalled on at least one of its free sides, thus inevitably also decreasing the final efficiency.

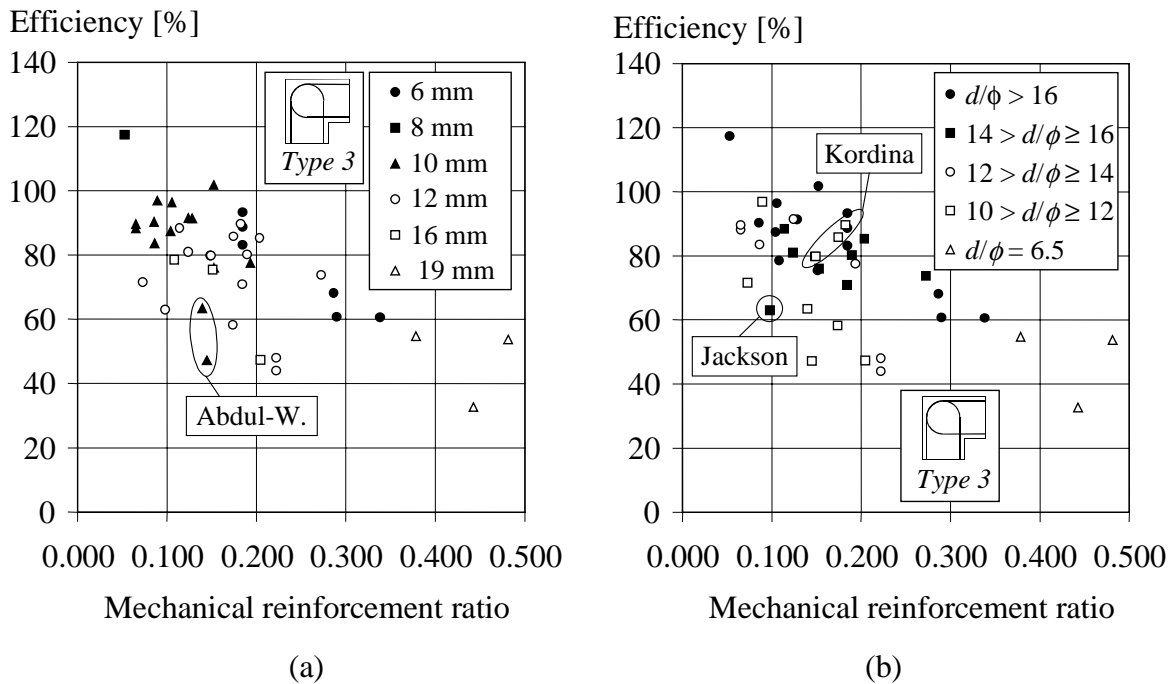


Figure 2.23 Efficiencies of detailing *Type 3* in opening corner when examining the influence of (a) bar diameter, and (b) ratio of effective height and bar diameter.

#### 2.3.2.4 Detailings that might attain full efficiency

From the above it is clear that neither of the detailings previously discussed could guarantee full efficiency when this is defined as in the new evaluation method shown presented in Section 2.1.3. To succeed in this task, it is necessary to ensure that spalling of the outside part of the corner does not occur. As shown in Section 2.3.2.2 the adding of radial stirrups around the reinforcement loops has proven to be insufficient. This is because such reinforcement is unable to prevent the forming of critical cracks at the outside of the corner; instead the cracks evade the reinforcement and propagate behind it. Accordingly, to hinder such cracks the reinforcement bars have to be anchored at the outside of the corner. A detailing that might fulfil this requirement but which is complicated to carry out is shown in Figure 2.24a. Here, the radial stirrups within the corner are connected to an anchorage plate positioned outside the corner, thus enabling the reinforcement to counteract the tensile force  $R$ , shown in Figure 2.3a, once cracking of the concrete has occurred. The amount of stirrups should then be determined to correspond to this force  $R$ . Further, no extra reinforcement loops or inclined bars should be needed since the stirrups and anchorage plate then fill their purpose. Finally, eventual splices of loops and straight bars in the adjoining members should, as discussed in Section 2.3.2.1, be positioned at a certain distance from the corner to enable the forming of critical cracks in the adjoining members. Whether such a solution would behave as intended, though, has to be further examined before used in practice. In any case, it is the author's belief that this detailing, due to its rather high complexity, might not be very desirable. Nevertheless, it is still mentioned here as a possible solution to this complex problem.

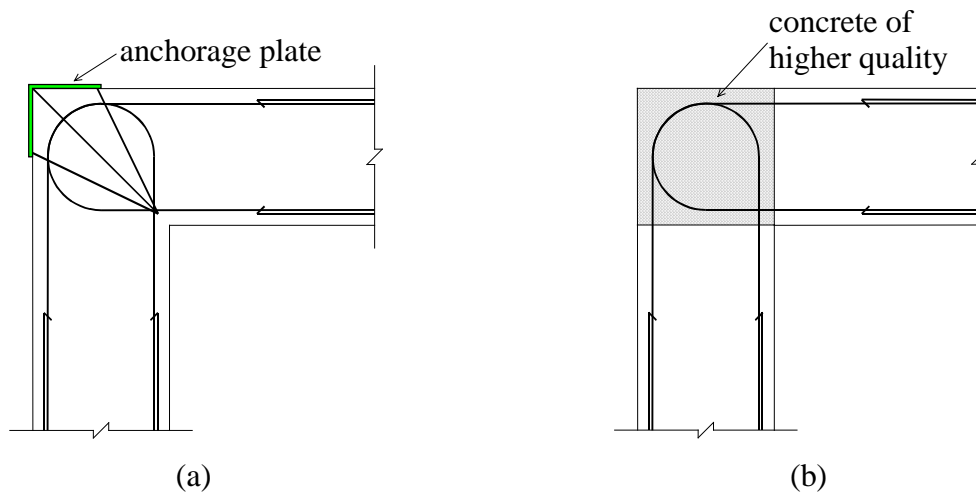


Figure 2.24 Suggestion of possible improvements in the detailings used in opening frame corners.



Another way to achieve full efficiency, when using reinforcement loops only, is to make sure that the mechanical reinforcement ratio  $\omega_s$  does not exceed the limit given in equation (2.18). With sufficiently small reinforcement ratios, this might be possible by using concrete of higher strength in just the corner region; see Figure 2.24b. Hence, the mechanical reinforcement ratio in the corner would be determined based on the basis of this higher concrete strength. Especially fibre-reinforced concrete would then be of great use in such a procedure, as has also been shown in tests and non-linear finite element analyses of spliced beams, e.g. Broo and Broo (1997). In addition, due to a more favourable relation between the tensile and compressive strength compared to that of plain concrete, the value of  $\omega_{crit}$  derived in equation (2.18) could be increased when using fibre-reinforced concrete. Further, depending on what fibre amount is used, the considerable increase in fracture energy in such concrete implies that a more rectangular stress distribution would be more accurate than the triangular one assumed in Figure 2.6b. Thus, by using fibre-reinforced concrete within the corner only, it is reasonable to believe that the mechanical reinforcement ratio that guarantees yielding of the reinforcement could be considerably increased, probably at least as high as  $\omega_{crit} = 0.060$ . Abdul-Wahab and Al-Roubai (1998), for instance, obtained an efficiency of 97% when the mechanical reinforcement ratio was 0.089 and the fibre volume used was 1%; see Appendix A. Thus, the use of higher concrete strength in the corner region can be of considerable advantage. Especially when using prefabricated members such a procedure seems to be a preferable method, while for *in situ* casting it may perhaps be somewhat more difficult to realise.

### **2.3.3 Estimation of corner efficiency in opening corners**

#### **2.3.3.1 General remarks**

From the comparison of different detailings in opening frame corners presented in Figure 2.13 it is evident that the scatter of the efficiencies obtained is quite large. Even so, some attempts have been made in the literature to propose an expression to estimate the efficiency of frame corners using detailing *Type 3* or *Type 4*. It is the author's opinion, though, that none have been very successful. Although such an expression is not proposed in this dissertation, the attempts previously reported are briefly summarised and discussed. For closing corners, though, it can be concluded that as long as flexural failure is obtained and side concrete spalling does not limit the corner capacity, the conventional evaluation method, introduced in Section 2.1.3, is sufficient to use when estimating the expected capacity.

### 2.3.3.2 Equilibrium model

As mentioned above, Nilsson derived an expression that is based on an equilibrium model, see equation (2.1), and a simplified version of it was presented in Section 2.2.1. Figure 2.25 compares the estimated efficiencies determined according to this method with those obtained in tests of detailing *Type 1*, *Type 2* and *Type 3*. The estimated efficiencies for detailings *Type 1* and *Type 3* were determined by calculating the tensile stress in the reinforcement by use of equation (2.8). For *Type 2*, though, the influence of the radial stirrups was accounted for by modifying equation (2.7) as

$$F_R = \max \left\{ \begin{array}{l} \frac{0.9f_{ct}bd_1}{\sqrt{1+\gamma^2}} + \frac{E_s}{E_c} f_{ct}A_{s,r} \\ f_{sy,r}A_{s,r} \cdot \cos \beta = \frac{2f_{sy,s}A_{s,r}}{1+\gamma^2} \end{array} \right\} \quad (2.18)$$

before setting it equal to the tensile force  $R$ . Here,  $E_s$  and  $E_c$  are the Young's modulus for steel and concrete, respectively;  $A_{s,s}$  is the cross-section area of the inclined stirrups and  $f_{sy,s}$  is their yield strength. The tensile stress in the main reinforcement was determined and then used to estimate the related moment capacity. The estimated efficiency was finally obtained by dividing this capacity by the estimated ultimate moment capacity in the critical section as defined in Section 2.1.3; the efficiency, though, was limited to 100%. From Figure 2.25 it can be seen that when the estimated efficiency is lower than 60% all but four cases are estimated on the safe side. However, of the tests for detailings *Type 1* and *Type 2* in which the estimated efficiency is higher than this, the method's prediction is generally on the unsafe side. When comparing the test results of the frame corners using reinforcement loops (i.e. *Type 3*) it is evident, though, that the equilibrium model clearly underestimates their efficiency. Hence, it seems safe to use the expression given in equation (2.10) to determine an upper limit on the mechanical reinforcement ratio, where yielding of the reinforcement is guaranteed when using the *Type 3* detailing.

According to the CEB-FIP Model Code, CEB (1993), the mean tensile strength,  $f_t$ , can be determined as

$$f_t = 0.30(f_c - 8)^{2/3} \quad (2.19)$$

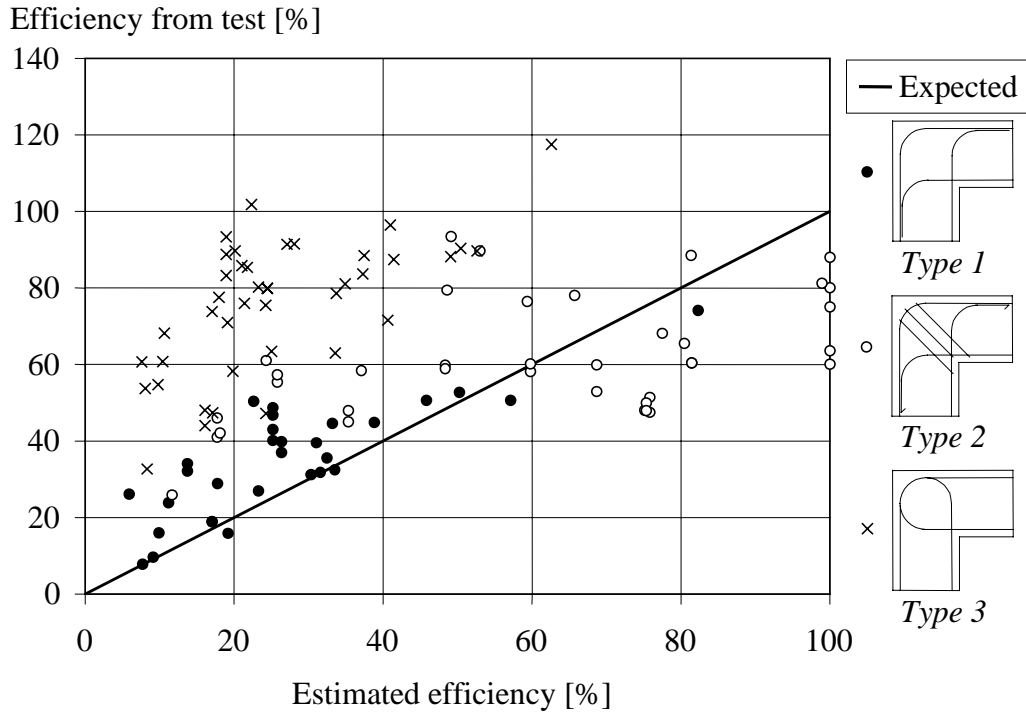


Figure 2.25 Comparison of efficiencies obtained in tests for detailings *Type 1*, *Type 2* and *Type 3* with that estimated by using a equilibrium model.

where  $f_c$  is the mean compressive cylinder strength. However, in the range of 15 to 50 MPa, a satisfactory approximation of this expression is

$$f_t \approx 0.075f_c \tag{2.20}$$

If using concrete with higher strength than this, up to strength of 80 MPa, the approximate relation

$$f_t \approx 0.067f_c \tag{2.21}$$

can be applied instead. Using these approximations together with equations (2.10) and (2.15) it is possible to derive a lower limit of the mechanical reinforcement ratio where the tensile reinforcement yields as

$$\omega_{crit} = \rho_{crit} \frac{f_{sy}}{f_c} \approx 0.033 \text{ when } 15 \leq f_c \leq 50 \text{ MPa} \tag{2.22a}$$

$$\approx 0.030 \text{ when } 50 < f_c \leq 80 \text{ MPa} \tag{2.22b}$$

### 2.3.3.3 Empirical expressions

Below, when comparing the efficiencies of tests using detail *Type 4*, the conventional evaluation method is used when determining the efficiencies. That is, the increase in estimated moment capacity due to the inclined bars is not taken into account, the reason being that this is the method used when the expressions presented below were originally derived.

Noor (1977) proposed two empirical expressions to estimate the moment capacity  $M_{uc}$  for frame corners reinforced with detailing *Type 3* or *Type 4*, respectively, i.e.

$$M_{uc}^{Type3} = (0.05 + 0.42\rho) \cdot bd \sqrt{f_{c,cube}} \quad (2.23)$$

and

$$M_{uc}^{Type4} = \left( 0.05 + 0.42\rho + 0.0035\rho_i \frac{f_{sy}}{\sqrt{f_{c,cube}}} \right) \cdot bd \sqrt{f_{c,cube}} \quad (2.24)$$

based on his own tests and tests reported by Swann (1969), Mayfield *et al.* (1972), and Nilsson (1973). Here  $\rho$  and  $\rho_i$  are the reinforcement ratios of the reinforcement loops and the inclined bars, respectively, and  $f_{c,cube}$  is the cube compressive strength of the concrete. Noor also proposed a lower limit

$$M_{uc} \geq 0.16 \cdot bd \sqrt{f_{c,cube}} \quad (2.25)$$

determined from test results of frame corners using the *Type 1* detailing.

Further, Abdul-Wahab and Al-Roubai (1998) recently proposed an empirical expression to estimate the moment capacity of opening frame corners reinforced with detailing *Type 3* or *Type 4*. Here it is also possible to take into account the corner angle  $\alpha$  and whether fibre-reinforced concrete (FRC) is used or not:

$$M_{uc} = \frac{K \cdot bd^2 \sqrt{f_{c,cube}}}{1 + \sin(\alpha/2)\cos(\alpha/2)} \quad (2.26)$$

where  $K = 0.471$  (detail *Type 3*)  
 $= 0.769$  (detail *Type 4*)  
 $= 0.610$  (detail *Type 3*, FRC)  
 $= 0.833$  (detail *Type 4*, FRC)

This expression has certain similarities to the equilibrium model discussed above, in that it depends on the corner dimensions  $b$  and  $d$  and also on the concrete strength ( $\sqrt{f_{c,cube}}$  corresponds here to the tensile strength  $f_t$ ). However, in the absence of a more thorough theoretical analysis the coefficient  $K$  was based on a total of 35 tests carried out by Abdul-Wahab and Al-Roubai, and Abdul-Wahab and Salman (1999), to match the positive effect that the reinforcement loops and possibly inclined bars have on the corner capacity.

A comparison of the corner efficiencies obtained when using these expressions to that obtained in tests is made in Figures 2.26 and 2.27. From these figures it is also evident that the predictions made using Noor's expression are far from satisfactory, the worst case predicting an efficiency of more than 100% (no limitation is given) but not even reaching 40% real efficiency. Consequently, it would be unsafe to use this expression in the design of an opening frame corner. However, Abdul-Wahab and Al-Roubai are rather successful in their attempt to predict a capacity on the safe side. The drawback is that the predictions made in several cases underestimate the capacity considerably. A major reason for this is that their expression does not take into account the amount of reinforcement in the corner or what strength it has, i.e. neglecting two parameters that have proven to have a substantial influence on the corner efficiency. Although a useful start, such an expression, to be fully satisfying, should also be able to take into account these two important parameters. Further, it is not clear what minimum ratio of inclined bars must be present in the corner to use the  $K$ -value for the *Type 4* detailing. The amount of inclined reinforcement used in the comparison of detailing *Type 4* made in Figure 2.27 is never lower than 45% of the main reinforcement. Therefore, it is the author's recommendation that if the inclined reinforcement amount is lower than this the coefficient  $K$  for detailing *Type 3* should be used.

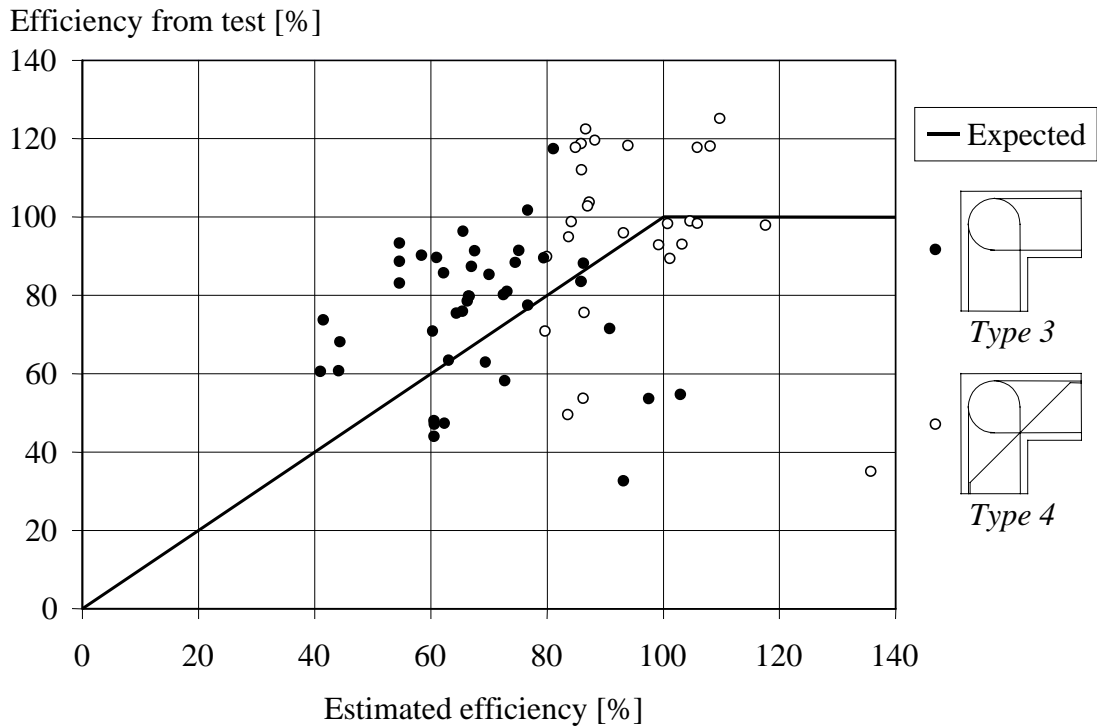


Figure 2.26 Comparison of efficiencies obtained in tests for detailings *Type 3* and *Type 4*, with the expressions in equations (2.19) and (2.20), respectively, given by Noor (1977).

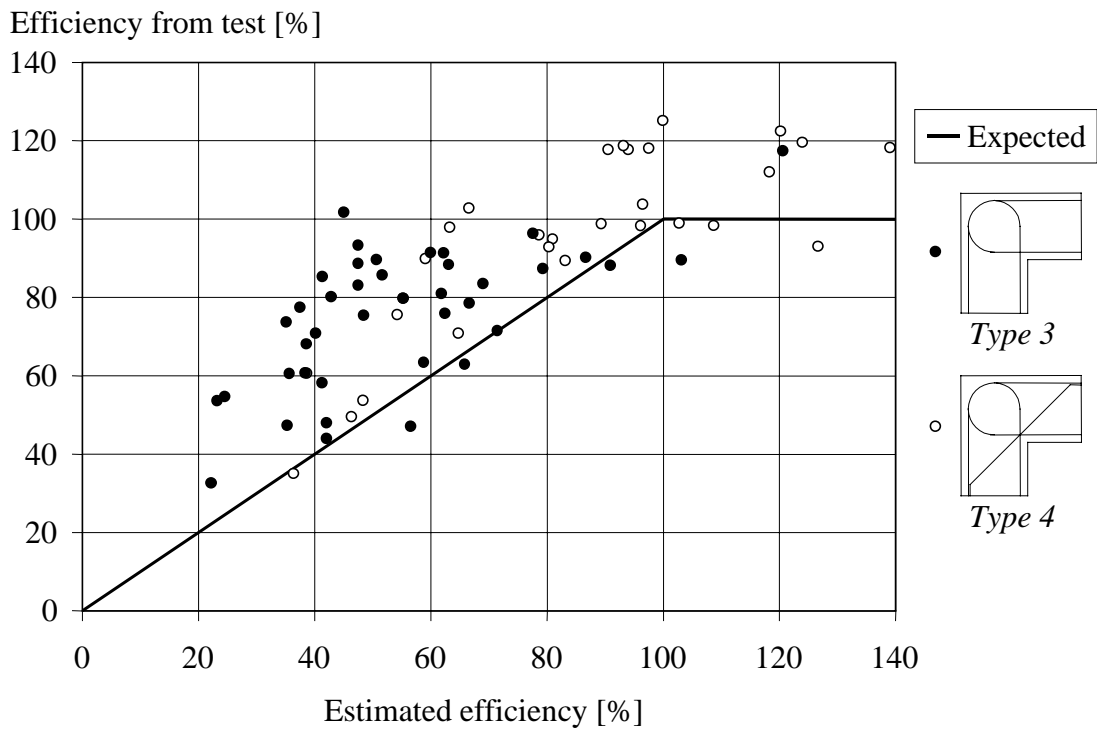


Figure 2.27 Efficiencies obtained in tests for detailings *Type 3* and *Type 4* compared with the prediction by equation (2.22) given by Abdul-Wahab and Al-Roubai (1998).

## **2.4 Discussion**

### **2.4.1 Opening corners**

#### **2.4.1.1 Choosing detailing**

The comparison made in Section 2.3.2.1 of the structural behaviour of opening corners, regarding whether to use inclined bars or not, suggests that if the moment distribution close to the corner is not constant the adding of inclined bars does not have the effect intended. Consequently, in a real structure the final failure will most likely take place within the corner region. This together with the discussion presented in Paper I, shows that the inclined bars can just as well be replaced by reinforcement loops that are simpler to position, i.e. the detailing proposed in Figure 1.1c. Still, it is important to point out that this solution also is unsuccessful in guaranteeing full efficiency. However, the aim of adding extra reinforcement loops is to provide a detailing that leads to a structural response similar to that obtained when using the generally accepted detailing using inclined bars proposed by Nilsson (1973). The presence of such extra reinforcement provides an additional strength to the corner so that its final capacity corresponds to what would have been obtained in the original detailing if fulfilling the requirement of full efficiency. It should be emphasised that even though the capacities obtained will be approximately the same, the total structural response will differ. In the latter case a ductile response similar to that of a reinforced beam would, due to the expected yielding of the reinforcement, have been the result. In the former, though, final failure will occur due to loss of anchorage when the compressed concrete outside the loops is pushed off. Due to this, reinforcement yielding is not reached, and accordingly the joint ductility is affected negatively. Nevertheless, tests by the author of opening corners, presented in Paper I, show that a ductile response is still possible. In two of these tests, the reinforcement loops even yielded at the inside of the corner but still full efficiency was not obtained. It may therefore be argued that the statements made in Section 2.2.1 that reinforcement yielding will result in full efficiency is not true. Yet, this can be explained by the occurrence of side concrete spalling in both tests. The bars at which the strain was registered were positioned far from the concrete edges and were therefore not affected by the loss of side concrete cover. Instead, the strain in these bars increased in order to balance the external load when the outer reinforcement loops unloaded. Consequently, it can be concluded that while neither of these detailings reaches an efficiency of 100%, they may still satisfy the ductility requirement set in Section 2.1.1. If the detailing is based on the recommendations given by Nilsson, in which the

amount of inclined bars shall be at least half that of the main reinforcement, equation (2.16) states that an amount of at least 35% extra reinforcement loops can be used instead, i.e.  $A_s^* = 1.35A_s$ . As a result of the author's work this solution is also what is now prescribed in the present Swedish Shelter Regulations, Swedish Rescue Services Agency (1998).

Before continuing the discussion it must be clarified that the use of inclined bars, in a structural sense, is not inferior to the detailing proposed herein, using reinforcement loops only. Inclined bars may even result in a better solution since there is then still a chance that the final failure will occur outside the corner region. Tests carried out by the author, though (see Paper I), indicated that *if* a failure does occur within the corner, then the presence of a larger amount of reinforcement loops might have a positive influence on the post-peak ductility. The major advantage with the detailing using just reinforcement loops, however, is that it may be considerably easier to carry out and also presents some other advantages as initially discussed in Section 1.2. Nevertheless, perhaps the greatest gain is that the designer may now have the freedom to choose the detailing that he or she thinks fits best. There may for instance be cases where it is regarded as easier to add inclined bars to the detailing rather than extra reinforcement loops, and then such a detailing should of course be used.

#### **2.4.1.2 Expected efficiency**

In Section 2.3.3.2 it was shown that an upper limit of the mechanical reinforcement ratio, at which the tensile reinforcement is guaranteed to yield within the corner, could be derived as  $\omega_{crit} = 0.033$ . Thus, it would be appropriate to use the *Type 3* detailing without adding any extra reinforcement loops when fulfilling this requirement. However, it seems reasonable that even though a frame corner with a mechanical reinforcement ratio of, say, 0.040 would need some extra reinforcement to reach the moment capacity wanted, it would probably not need all the extra 35% of reinforcement loops as is currently the case. At what ratio the full amount of extra reinforcement loops needs to be added is not clear, but an attempt is made here to give a reasonable estimation that can be used in practice. To do this, the expression proposed by Abdul-Wahab and Al-Roubai (1998) presented in Section 2.3.3.3 is used. If approximating the estimated moment capacity as

$$M_u = 0.9f_{sy}A_s \quad (2.27)$$



and set this equal to the estimated capacity in equation (2.26), it is possible to derive a maximum reinforcement ratio where the efficiency of the detailing reaches 100%. Using  $K = 0.471$  (i.e. reinforcement loops in plain concrete) and setting  $\alpha = 90^\circ$  the maximum reinforcement ratio can be written as

$$\rho = 0.349 \frac{\sqrt{f_{c,cube}}}{f_{sy}} \quad (2.28)$$

which is similar to the expression derived in equation (2.10). When evaluating the test results from different researchers the relation between the compressive cube strength and compressive cylinder strength was set to  $f_{c,cube} = 1.35f_c$ ; see Appendix A. Using the same relation here, the mechanical reinforcement ratio can be expressed as

$$\omega_s = \frac{0.405}{\sqrt{f_c}} \quad (2.29)$$

This expression is compared to that derived by the author in Figure 2.28, and from this it is clear that the latter seems to be quite conservative compared to the former. However, this is mainly due to how the expressions were derived. The critical reinforcement ratio proposed by the author is based on the equilibrium model for the *Type 1* detailing presented in Section 2.2.1, while the expression proposed by Abdul-Wahab and Al-Roubai is an empirical relation based directly on tests results of the *Type 3* detailing. Further, it should be pointed out that the former has an advantage since it predicts a mechanical reinforcement ratio where the reinforcement is guaranteed to yield before failure of the corner. This is not the case in the latter expression, which in some cases overestimates the capacity at high-predicted efficiencies. Therefore, the limit of  $\omega_s = 0.033$  is herein also preferred. Nevertheless, the expression in equation (2.29) may still be used to estimate at which mechanical reinforcement ratio all the extra amount of 35% reinforcement loops must be added. From Figure 2.28 it can be seen that the value of this expression decreases with increasing value of the compressive strength. Abdul-Wahab and Al-Roubai give no limit on the concrete strength for using their expression. But, the maximum cube strength used in the tests on which they based their expression was about 30 to 40 MPa; using the relation  $f_{c,cube} = 1.35f_{c,cyl}$  as above, this corresponds to a (cylinder) compressive strength of about 22 to 30 MPa. Further, as previously stated in Section 2.3.1, the maximum compressive strength used in all the tests that are compared in Figure 2.13 was approximately 52 MPa. This indicates that the expression proposed by Abdul-Wahab and Al-Roubai should be valid for concrete strengths up to at least 50 MPa. Hence, using  $f_c = 50$  MPa in equation (2.29) yields a mechanical reinforce-

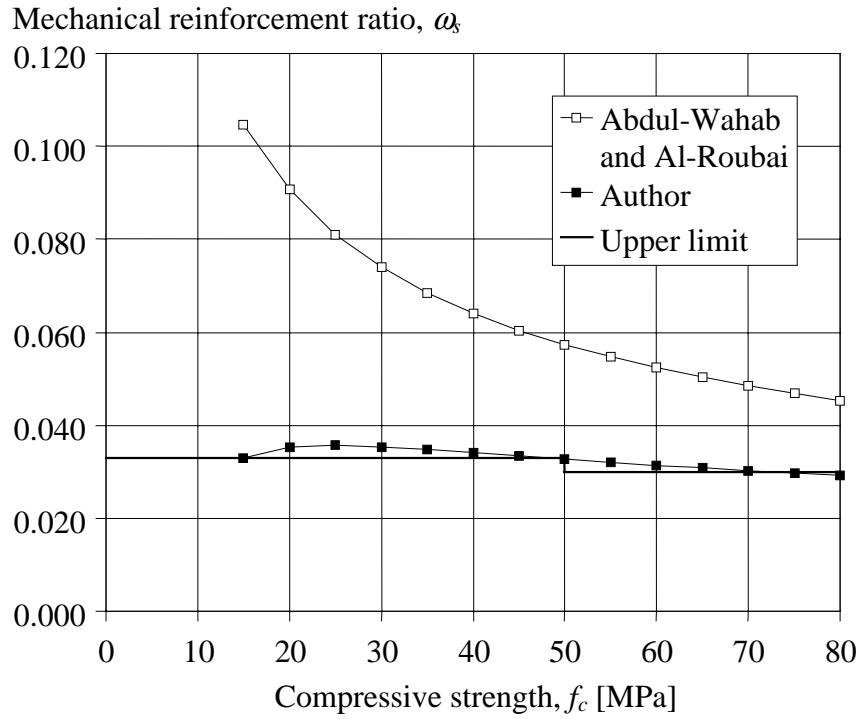


Figure 2.28 Comparison of upper limit of the mechanical reinforcement ratio when yielding of the tensile reinforcement can be guaranteed.

ment ratio  $\omega_s = 0.058$ . It is important to point out that this value refers to the mechanical reinforcement ratio *before* adding any extra reinforcement loops; once they are added, the resulting mechanical reinforcement ratio will instead be  $\omega_s^* = 1.35 \cdot \omega_s = 0.078$ . Hereby, an upper and a lower limit of  $\omega_s$  are derived in which the amount of extra reinforcement loops necessary is 0 and 35%, respectively. Recalling that the aim of adding such extra loops by 35%, thus getting a theoretical moment capacity of

$$M_{uc}^* = f_{sy} A_s^* \cdot z^* = 1.35 \cdot f_{sy} A_s \cdot z^* \quad (2.30)$$

was to make it possible to obtain a corner capacity at least as large as that obtained by the original detailing if full efficiency would have been reached there; i.e.

$$M_{uc} = f_{sy} A_s \cdot z \quad (2.31)$$

Hence, if approximating the internal lever arms as  $z^* = z$ , an estimated efficiency can be determined as

$$\eta = \frac{M_{uc}}{M_{uc}^*} \approx 0.74 \quad (2.32)$$

These results can be summarised as shown in Table 2.1. When  $\omega_s \geq 0.058$  the minimum efficiency expected is 74% while for  $\omega_s \leq 0.033$  it is 100%; between these values a linear interpolation can be used. However, as mentioned in Section 2.3.1, it is not recommended to use the *Type 3* detailing for  $\omega_s > 0.200$  and, since 35% extra reinforcement loops are added, this means that the maximum ratio allowed before adding such loops is  $\omega_s = 0.148$ .

Table 2.1 Expected efficiency when using different mechanical reinforcement ratios. Values are compared to test results in Figure 2.27.

Mechanical reinforcement ratio, $\omega_s$ <sup>1</sup>	Amount of extra reinforcement loops, $\gamma$ [%]	Resulting mechanical reinforcement ratio, $\omega_s^*$ <sup>2</sup>	Expected efficiency, $\eta$ [%]
$0.033 \leq \omega_s$	0	$0.033 \leq \omega_s^*$	100
$0.033 < \omega_s \leq 0.058$	$0 < \gamma \leq 35$	$0.033 < \omega_s^* \leq 0.078$	$100 > \eta \geq 74$
$0.058 < \omega_s \leq 0.148$	35	$0.078 < \omega_s^* \leq 0.200$	74

<sup>1</sup>Before adding extra reinforcement loops.

<sup>2</sup>After adding extra reinforcement loops.

Since the work presented herein was initiated to examine the use of reinforcement detailings in civil defence shelters, it is also of interest to compare the limits of the mechanical reinforcement ratio with that allowed in the Swedish Shelter Regulations, Swedish Rescue Services Agency (1998). Here, the minimum reinforcement ratio is set to  $\rho = 0.14\%$ . Further, the concrete used in Swedish shelters shall be of at least strength class K30, resulting in a mean compressive cylinder strength of about 27 MPa; the mean yield strength of the hot-rolled deformed bars of type K500 presently used in Sweden is about 550 MPa. Accordingly, the minimum reinforcement ratio in such shelters corresponds to a mechanical reinforcement ratio  $\omega_{shelter}^{\min} \approx 0.029$ , i.e. somewhat lower than  $\omega_s = 0.033$  proposed in Table 2.1 at which yielding of the reinforcement is guaranteed prior to corner failure. The maximum reinforcement ratio allowed in the Swedish Shelter Regulations, though, is 1.1%. Combined with the mean strength values used above, this results in a mechanical reinforcement ratio  $\omega_{shelter}^{\max} = 0.224$ , i.e. a value higher than the upper limit of 0.200. This indicates that if using such high reinforcement ratios, concrete of higher strength than K30 is required to obtain an adequate behaviour of the detailing.

### 2.4.1.3 Use of mechanical reinforcement ratio in the design

Previously it has been discussed what amount of extra reinforcement loops should be added at different mechanical reinforcement ratios. However, so far the value of  $\omega_s$  has always been based on the mean strength values for both concrete and reinforcement. It can be justly argued, though, that it is on the unsafe side to rely entirely on such mean values when determining limits to be used in the design. Further, the experimental results referred to herein were obtained in tests carried out during a relatively short time; i.e. the tests took not more than perhaps an hour or two to carry out. To the author's knowledge, no tests on opening or closing corners are reported in the literature in which sustained loading has been used. Nevertheless, it is commonly accepted that the strength of concrete usually is lower during such load conditions. In both the Swedish Concrete Code BBK 94, Boverket (1994), and in Eurocode 2, CEN (1991), this phenomenon is taken into account by multiplying the concrete compressive strength with a factor of 0.85. In the former, this factor is already built into the characteristic values, while in the latter it has to be included within the calculations to determine the sectional capacity in the ultimate limit state. From this it is clear that it is important to discuss how the mechanical reinforcement ratio should be determined in the design of a structure. A suggestion of how to do so in the design of concrete frame corners is therefore presented below.

A comparison is again made with the recommendations given by Nilsson (1973) who concluded that the *Type 4* detailing should be applicable in opening frame corners if the reinforcement ratio was lower than 1.2% and 0.8% when the two different Swedish reinforcement grades Ks40 and Ks60, respectively, were used. In the Swedish Concrete Code BBK 94, Boverket (1994), this was interpreted as

$$\rho \leq \frac{5}{f_{yk}} \quad (2.33)$$

where  $f_{yk}$  is the characteristic yield strength of the reinforcement. Since this value for Ks40 and Ks60 was approximately 400 and 600 MPa, respectively, it seems like a sound and rather accurate simplification. However, if this reinforcement ratio is to be translated to a corresponding mechanical reinforcement ratio, and thus enable a comparison to the limit of  $\omega_s \leq 0.200$  proposed herein, one has to decide what value shall be used for the concrete strength. The concrete strength used by Nilsson varied somewhat, but can generally be said to have had a mean compressive cube strength of about 25 to 35 MPa. Considering that his curing conditions were such that these strengths were perhaps about 5% lower than what

would have been obtained using the curing conditions described by the Swedish Standard, BST Byggstandardiseringen (1991), it can be said that this concrete approximately corresponds to that obtained in strength class K20 to K30 today.

Since the characteristic yield strength is used in the expression given in equation (2.33) it seems reasonable to use the characteristic strength for concrete too. For concrete of strength class K30 this is, according to BBK 94,  $f_{ck} = 21.5$  MPa and using this strength results in a mechanical reinforcement ratio, based entirely on characteristic values,  $\omega_{sk} = 0.232$ ; i.e. a value that is somewhat higher than that proposed herein. If instead using the recommendation given by Nilsson, this results in  $\omega_{sk} = 0.223$  which still is a little bit too high. It is worth noting, though, that the maximum mechanical reinforcement ratio used by Nilsson never exceeded 0.200 (see Appendix A), thus satisfying the maximum value of  $\omega_s$  proposed by the author.

Therefore, by using the same reasoning as when writing the Swedish concrete codes this, suggests that it should be sufficient to use the characteristic values of concrete and reinforcement to determine  $\omega_s$ . The advantages of using these values are that they are well known by designers and that, at least in the Swedish regulations, they also include the influence of long-term loading. If following for example Eurocode 2, in which the long-term influence is not included in the characteristic values, this effect has to be taken into account when determining  $\omega_s$ .

However, since the idea is that the reinforcement should yield to obtain a fully acceptable detailing, it is important not to underestimate the reinforcement yield strength. This indicates that it might be more correct (i.e. safer) to use the mean yield strength instead of the characteristic yield strength when determining what mechanical reinforcement ratio a section in a reinforced concrete structure corresponds to. It can also be argued that if yielding is to be obtained in the corner, prior to failure, it should be more correct to use an upper characteristic value on the reinforcement yield strength. However, no recommendations of such characteristic values are given in, for example BBK 94, and an approximate value on the mean tensile strength is therefore used. Based on experience of reinforcement tests (type K500) on various bar diameters carried out at the Division of Concrete Structures at Chalmers University of Technology, it is the author's opinion that the mean yield strength usually is at least 10% higher than that of the corresponding characteristic strength. Accordingly, the mechanical reinforcement ratio could in the design process approximately be determined as

$$\omega_s = \rho \frac{f_{sy}}{f_{ck}} \approx \rho \frac{1.1 \cdot f_{yk}}{f_{ck}} \quad (2.34)$$

Using this expression to recalculate the mechanical reinforcement ratios of the test results of detailing *Type 3*, the relations shown in Figure 2.29 can be determined. The results are also compared to the relation presented in Table 2.1, and this indicates that the limitations and efficiencies presented there should be appropriate to use.

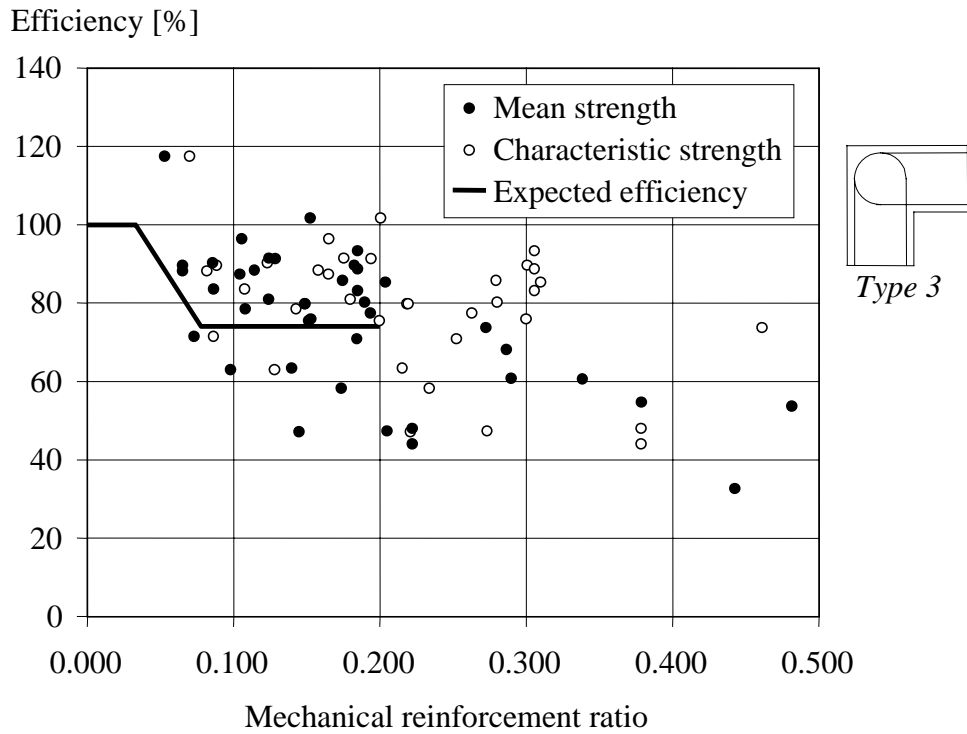


Figure 2.29 Comparison of test results when the mechanical reinforcement ratio is based on the mean and characteristic compressive strengths. The “expected efficiency” refers to the values given in Table 2.1.

## 2.4.2 Closing corners

As discussed in Section 2.2.2 the reinforcement detailing in closing frame corners causes far fewer problems than that in opening corners. The test results suggest that both detailings examined would be acceptable for mechanical reinforcement ratios as high as  $\omega_s = 0.200$ . For higher values, the test data are somewhat too scarce to provide a definite statement. It seems likely, though, that these detailings will be effective only up to a certain ratio; Stroband and Kolpa (1983), for instance, suggest that  $\omega_s \leq 0.240$  if crushing of the diagonal compressive strut is to be avoided. However, of the three failure types mentioned in Section 2.2.2, spalling of the side concrete cover seems to be more dangerous when using spliced reinforcement loops within the corner. Here, it is primarily not the mechanical reinforcement ratio that is important, but rather what combination of bending radius, bar diameter, side concrete cover, and concrete and reinforcement strength is used. A very limited comparison with the tests reported in Paper I suggests that the expressions given in the literature may be inadequate to use for spliced reinforcement loops in frame corners. Nevertheless, as discussed in Section 2.2.3, whether this kind of failure is dangerous or not depends very much on the number of bars used in the corner; a greater number of small bars is better than large but few bars. Generally, though, it can be stated that spalling of the side concrete cover is not really a problem in wall-slab joints, while in beam-column connections it may be of major importance. As is the case for opening moment, however, an increase in concrete strength within the corner may be the solution to this kind of problem. When determining the mechanical reinforcement ratio in the design of closing moments, the approach described in Section 2.4.1.3 can be used.

As discussed in Section 2.2.1 and shown in Figure 2.13, the *Type 1* detailing is very inefficient for opening corners. This might not be a problem in statically loaded structures where it is known that the corner will not be subjected to any opening moments. A civil defence shelter, though, must be able to withstand highly transient loads such as the blast pressure of a bomb exploding nearby. Therefore, the corner regions will also be subjected to both opening and closing moments. Even though the stresses due to opening moment in a corner may be substantially lower than what it was primarily designed for in closing moment, they may very well still exceed the capacity provided by the *Type 1* detailing. The *Type 3* detailing, though, is able to resist opening moments that are at least about 75% of the closing moment. Thus, by replacing the conventional detailing (i.e. *Type 1*) with the new proposal (*Type 3*), a considerable improvement of the structure's total behaviour is also obtained. Consequently, this is what has been done in the present Swedish Shelter Regulations.

## 2.5 Concluding remarks

The use of inclined bars in opening frame corners may not be as efficient as commonly thought. Instead the inclined bars may as well be replaced by an equivalent amount of extra reinforcement loops, thus resulting in a detailing that may be considerably easier to carry out at the construction site. Neither detailing, though, fulfils the requirement of full efficiency as it is defined herein (new evaluation method, see Section 2.1.3) unless the mechanical reinforcement ratio is sufficiently low. It is common to relate the corner efficiency to the reinforcement ratio. However, the results herein show that the reinforcement and concrete strengths also play a vital part for the corner behaviour and, therefore, the use of the mechanical reinforcement ratio  $\omega_s$  is a better approach. Further, comparisons of test results on opening corners indicate that the use of many small bars in favour of a few large ones has an advantageous effect on the corner behaviour. The ratio between the effective height and the bar diameter of the loops also seems to have a positive effect on the efficiency, since this decreases the risk of side concrete spalling. An upper limit of the mechanical reinforcement ratio,  $\omega_s = 0.033$ , was derived for which full efficiency is guaranteed, provided that reinforcement loops such as those proposed herein are used. Due to this, some possible solutions that may reach higher efficiency are also discussed and it is concluded that perhaps the best method, if using high reinforcement ratios and full efficiency still is to be achieved, is to increase the concrete strength within the corner. Fibre-reinforced concrete is then believed to be especially advantageous, not least due to its considerably larger fracture energy in tension. Moreover, it is concluded that if inclined bars are to be used it is important not to splice reinforcement loops and straight bars just outside the corner region.

Frame corners subjected to closing moment are less sensitive to which reinforcement detailing is used. Consequently, even though test results indicate that the use of reinforcement loops causes higher splitting stresses, this detailing has proven to be at least as efficient as the conventional one. An important reason is that the negative influence due to eventual spalling of the side concrete cover will be of minor, if any, importance in a civil defence shelter. Here, a corner region will be confined in the transverse direction due to the three-dimensional structure, and if this is not enough, the large numbers of bars in a wall-slab connection in such a structure ensure that the change in response will be negligible. In a beam-column joint, though, side concrete spalling may become a major problem, so this kind of failure cannot be neglected in such structures. Therefore, it is also a bit worrying that the expressions found in different codes do not seem to be fully reliable for predicting the initiation of such splitting cracks when reinforcement loops are used in frame corners. Nevertheless, it was concluded



that the use of the new detailing in closing corners is a considerable improvement in a civil defence shelter, since such corners may be subjected to both opening and closing moments during the transient loading they are designed to withstand. Consequently, the findings presented herein strongly suggest that the new reinforcement proposal of spliced reinforcement loops within the corner, introduced in Section 1.1 is suitable to replace the conventional detailings in both opening and closing frame corners in civil defence shelters. In opening corners, though, an extra amount of up to 35% extra reinforcement may be required. As a result of the work presented here, this detailing is now prescribed in the present Swedish Shelter Regulations, Swedish Rescue Services Agency (1998).



## **3 Non-linear Finite Element Analyses of Concrete Structures**

### **3.1 Why use finite element modelling?**

When studying the response of a concrete structure subjected to external load, the traditional way is to carry out experiments in which different parameters are varied. The observations made may then be used to propose mechanical or empirical models that can adequately describe the structure's behaviour. However, not only is this approach quite expensive but it cannot be counted on to give all the information needed. Another approach is to make use of the advanced computational techniques available today. By using the non-linear finite element method, in which the concrete material models are based on non-linear fracture mechanics to account for cracking, together with plasticity models for the reinforcement steel and the concrete in compression, the need for experiments can be greatly reduced. In such a finite element analysis, it is possible to evaluate the response of a structure more thoroughly than can be done in an experiment. However, the experiments cannot be replaced completely since they are still vital to check whether the finite element simulations correspond to reality. This means that even if both methods have their advantages when used alone, they can become an even more powerful tool when used together. Accordingly, in combination with the experiments, the use of non-linear finite element analyses will result in a better understanding and prediction of the mechanical behaviour in a structure during loading to failure.

This chapter tries to give a brief background for the use of non-linear finite element analyses when simulating the behaviour of concrete structures. Especially the problems associated with localisation, which occurs when a crack is initiated or the peak strength of concrete is reached, are dealt with. Further, results from finite element studies on concrete frame corners are presented and briefly discussed.

### **3.2 Fracture mechanics for concrete**

The fracture mechanics models commonly used for concrete originate from studies of the initiation and propagation of a crack in a uniaxial concrete tensile test. In a concrete structure, cracking occurs when the tensile strength of concrete is reached. Figure 3.1 sketches the failure development of a crack in a concrete specimen subjected to increasing tensile deformation; a typical mean stress-displacement relation for such a test specimen is shown in

Figure 3.2. When the specimen is loaded in tension, microcracks form at local weak points (Figure 3.1b) and under increasing load these microcracks become connected to each other and are localised to a fracture zone at the weakest section (Figure 3.1c). After the maximum load is reached, the tensile strength in the fracture zone decreases with increasing deformation, while the strain outside the zone decreases (Figure 3.1d). Eventually, a true crack that cannot transmit any tensile stresses is formed in the zone (Figure 3.1e). The concrete around the formed crack, which has never reached the tensile strength, will then unload completely and a redistribution of stresses and deformations in the structure takes place.

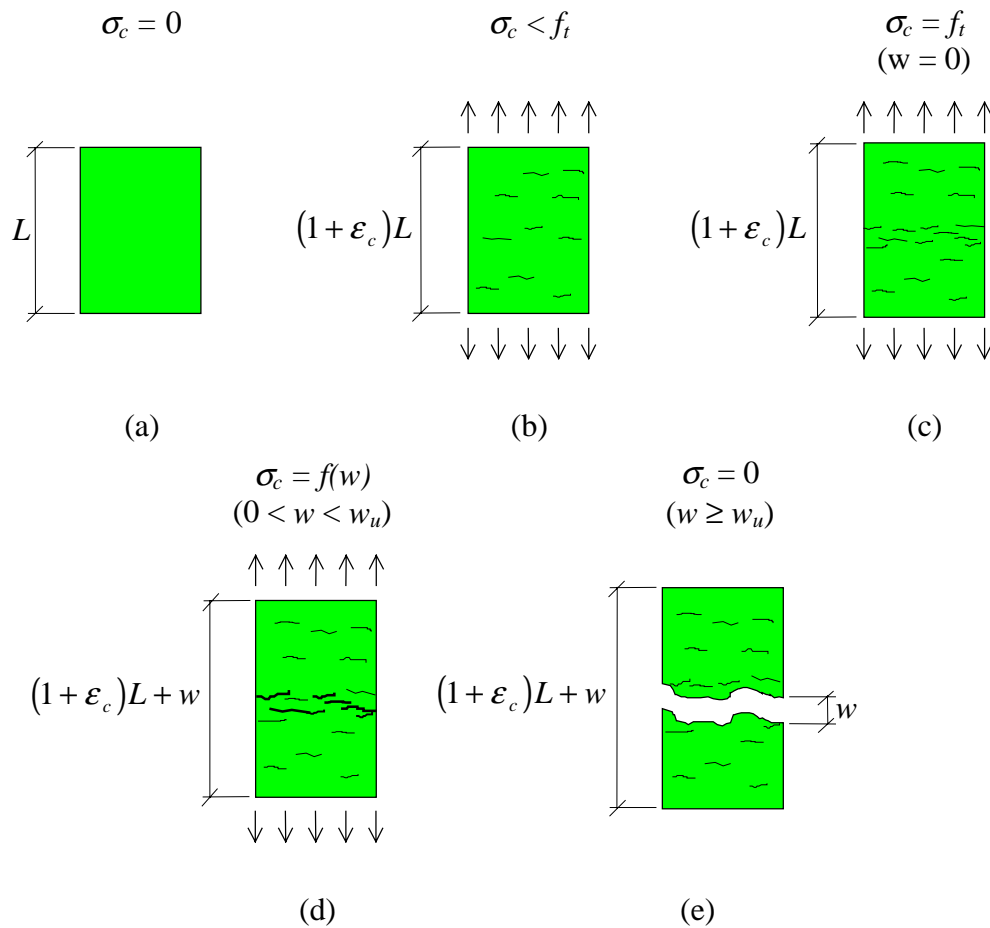


Figure 3.1 Stages in the formation of a crack in a concrete specimen subjected to increasing elongation.

Once a fracture zone has formed, the stress transferred through the zone depends upon the crack opening  $w$  and can be defined as  $\sigma_c = f(w)$ , where  $f(w)$  is a function that describes the softening behaviour of the concrete; see Figure 3.2. The area under the softening curve,  $f(w)$ , represents the energy release when concrete cracks and is, according to Hillerborg

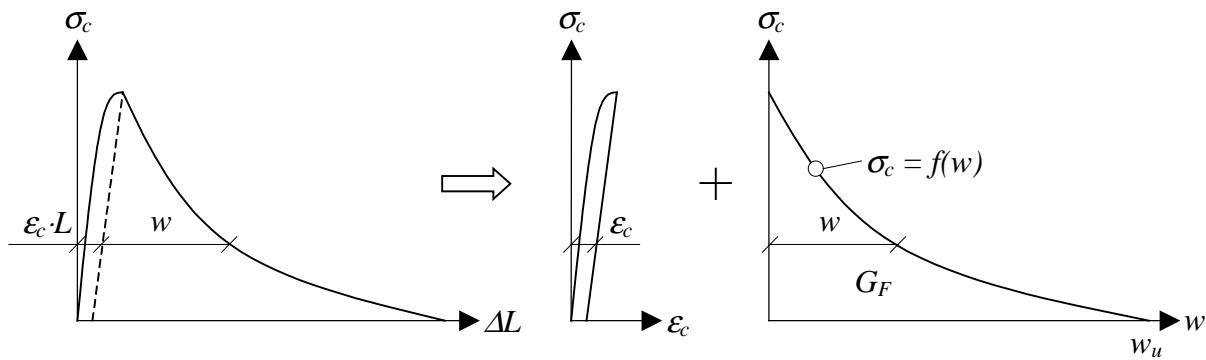


Figure 3.2 Mean stress-displacement relation for a uniaxial tensile test specimen. The displacement is separated into a stress-strain relation and a stress-crack opening relation. The area under the softening curve  $f(w)$  represents the fracture energy  $G_F$ .

*et al.* (1976), the mean energy per unit area of a formed crack. This energy, called the fracture energy and denoted  $G_F$ , is an essential concept when modelling cracking in concrete. Fracture mechanics for concrete and concrete structures in general is treated by, for instance, Elfgren (1989), and Hofstetter and Mang (1995).

### 3.3 Crack models

#### 3.3.1 General

In finite element modelling of cracks in concrete, there are three major concepts for treating cracks: the discrete crack approach, the smeared crack approach and the embedded crack approach. In this section, only the principal differences in these approaches are mentioned. More thorough descriptions of them can be found in, for example, Hofstetter and Mang (1995) or Jirasek (1999). A historical background of different crack models is not given herein but may be found in, for example, Kwak and Filippou (1990), or de Borst (1995).

Common to all models is that a crack is initiated when it fulfils a so-called crack initiation criterion. This is usually taken to be when the maximum principal stress reaches the tensile strength of the material, although there are variants considering, for example, the influence of the multiaxial stress state. Once initiated, the crack response is described by a stress-displacement or stress-strain relation based on the fracture energy in the material.

### **3.3.2 Discrete crack models**

In the discrete crack approach, the crack is modelled as a geometrical discontinuity and separate elements are used to simulate the cracks and the material between the cracks. It can be said that the method lumps the deformation due to cracking into discontinuous displacements. The fictitious crack model presented by Hillerborg *et al.* (1976), in which the concept of fracture energy was first introduced, is such a model and the crack response is here described by a stress-crack opening relation. However, since separate elements are used to model a crack in the discrete crack approach, the possible crack path must be assumed in advance and the finite element mesh arranged so that the crack path follows the element boundaries. This is a serious drawback of the approach; a great amount of work is required to establish the finite element mesh since the user has to decide where and how the cracks may arise. It also imposes a limitation on the spontaneous crack pattern.

### **3.3.3 Smearred crack models**

According to Rots (1988), the smeared crack approach is the counterpart of the discrete crack approach. Here, the localised non-linearity of the crack is “smeared” out over the finite element, i.e. all the material deformations, including the crack, are considered in the same element and hence, cracks may form in each integration point within the element. Accordingly, a cracked solid is modelled as a continuum allowing the cracked material to be described with a stress-strain relation. As this means that the crack pattern need not be taken into account in advance, the smeared crack approach is a more attractive procedure than the discrete crack approach. The smeared crack models reported in the literature can be subdivided into the following: fixed orthogonal cracks, fixed non-orthogonal cracks, rotating cracks and plasticity models.

In the first two kind of model, once a crack is initiated it is permanently locked in a direction perpendicular to the maximum principal stress at the time of initiation. Both methods allow the formation of additional cracks at the same point. However, as indicated by its name, in a fixed orthogonal crack model such cracks may only form perpendicular to already initiated cracks. In non-orthogonal models, though, this limitation does not exist. Instead, the number of cracks that may form at an integration point is determined by a threshold angle chosen by the user. A new crack may only arise if it forms at an angle to already existing cracks that exceeds the threshold angle. Further, once initiated a fixed crack is never removed. This

means that even though the crack at a later stage closes completely it will still affect the initiation of further cracks at the same integration point. Hence, as schematically shown in Figure 3.3, the principal stresses may also become substantially larger than the tensile strength without causing a new crack. To take into account this possible stress-locking, the concept of reduced shear stiffness over the crack is introduced by the use of a so-called shear retention factor  $\beta$ . This means that the shear modulus of the cracked concrete,  $G_{crack}$ , is given as

$$G_{crack} = \beta G_c \quad (3.1)$$

where  $G_c$  is the shear modulus of the uncracked concrete and  $0 \leq \beta \leq 1$ .

Non-orthogonal models, though, due to their lower restriction on secondary cracks, are less sensitive to such locking than orthogonal models.

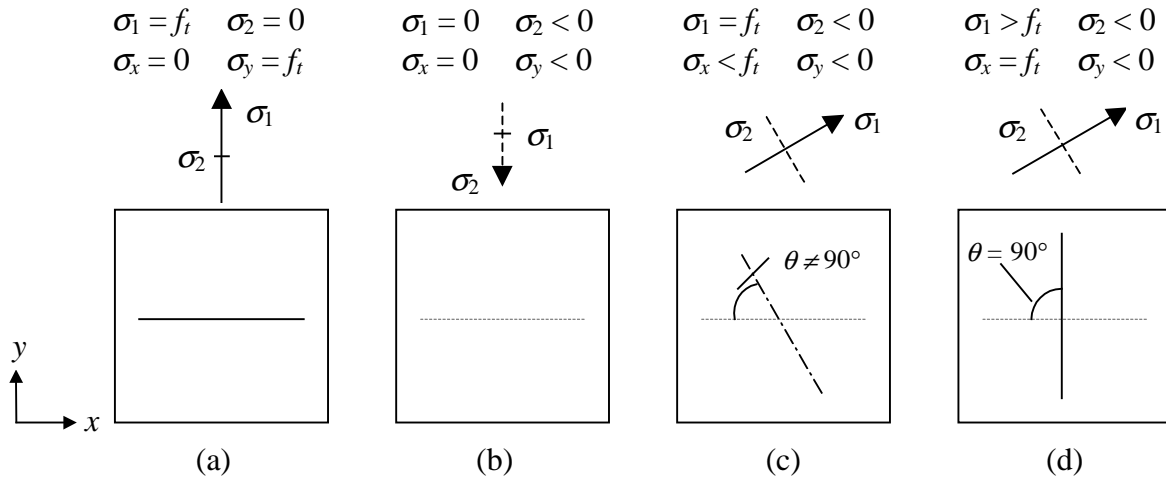


Figure 3.3 Schematic view of the initiation of a first and second cracks in a fixed non-orthogonal crack model: (a) initiation of horizontal crack; (b) crack closes; (c) principal stress reaches tensile strength, angle  $\theta \leq 90^\circ$ , though, and a new crack cannot form; (d) vertical crack forms when  $\sigma_x = f_t$ , note that  $\sigma_1 > f_t$ .

The rotating crack model was developed as an alternative to the non-orthogonal crack model described above. In this model the crack orientation follows the normal to the direction of the principal strain. However, to retain the consistency of using principal stress-strain curves to describe the cracked material response, the principal stress directions are forced to coincide with those of the principal strains; see Rots (1989). The effect can be interpreted as a single crack, whose orientation is continuously updated with respect to the present stress state. Hence, it may also be considered to act as a fixed non-orthogonal crack model in which the

threshold angle is set to  $0^\circ$ , Rots (1988). Up to three orthogonal cracks may appear at the same integration point, and thus there will be no shear stresses acting across the crack. Accordingly, there is no need to use a shear retention factor for cracked concrete. Hence, the rotating crack model has an advantage over the fixed crack approaches since the kind of stress-locking obtained there can be avoided; see Feenstra (1993). Crack models based on plasticity and utilising the Rankine yield criterion have the same advantage and also show approximately the same behaviour as that of rotating crack models, Feenstra (1993). These types of models have also proven to agree better with experimental results than does a fixed crack model; see Rots (1989) and Lundgren (1999).

The finite element analyses presented in Paper II were performed using fixed non-orthogonal cracks, and the dynamic analyses presented in Paper III used a fixed orthogonal crack model. Rotating cracks were not used because this approach was not implemented in the programme versions used; otherwise it would probably have been chosen due to its advantages regarding stress-locking.

### **3.3.4 Embedded crack models**

To simplify, it can be said that the embedded crack concept is something like a mixture of the discrete and the smeared crack approaches. According to Jirasek (1999) the embedded crack model combines the strong points of these two approaches. As in the smeared concept, no account has to be taken of where cracks may appear when meshing the structure. However, instead of spreading out the crack over the whole element volume, in the embedded crack model it is treated more like that in the discrete crack approach. The deformation due to the crack is here treated as a strain or displacement discontinuity in a localisation band within the element; e.g. Olofsson *et al.* (1995), Larsson *et al.* (1995) and Åkesson (1996). That is, in a case of a pure tensile situation all the deformation belonging to the crack is gathered within a zone across the element, as schematically shown for the three-node element in Figure 3.4a, and hence the response outside this zone will be elastic. If a smeared crack model had been used instead, the strain would have been smeared out over the element as shown in Figure 3.4b.



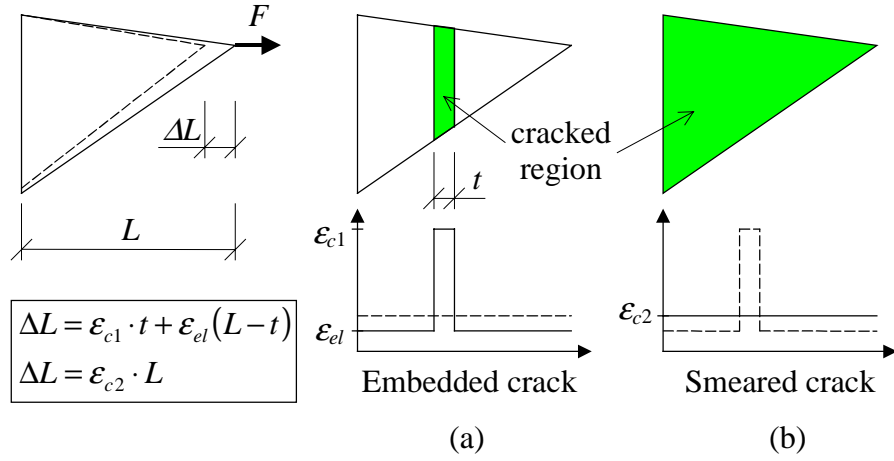


Figure 3.4 Schematic view of the strain distribution in a three-node element subjected to an elongation  $\Delta L$  when using (a) an embedded crack model, and (b) a smeared crack model.

## 3.4 Localisation

### 3.4.1 Tension

As mentioned above, a stress-crack opening relation is often used to simulate the softening curve of cracked concrete. There are many proposals of what this relation might look like, but since the bilinear relation given in Gylltoft (1983) has been used in all analyses in this work, it is also used in the coming discussion. The fracture energy  $G_F$  and tensile strength  $f_t$  are here used to calculate an ultimate crack opening  $w_u$  where the post-peak stress reaches zero; see Paper II or III. However, since the input data to the crack models used are based on stress-strain, the stress-crack opening relation has to be smeared over a certain distance, the crack extension  $l$ . Thereby, the ultimate crack strain  $\varepsilon_u$  can be determined as

$$\varepsilon_u = \frac{w_u}{l} = \frac{4G_F}{f_t l} \quad (3.2)$$

From this expression it is clear that the value of the crack extension  $l$  is just as important as the fracture energy  $G_F$  when determining the ultimate crack strain  $\varepsilon_u$ . Evidently, the numerical response will be accurate only if the width of the softening region obtained in an analysis is equal to the assumed crack extension  $l$ . It is therefore a very important issue to accurately determine this length prior to carrying out the analysis.

The crack pattern obtained in an analysis does differ from case to case depending on, for example, geometry, boundary conditions and load conditions. However, in the case of unreinforced concrete a crack usually localises within a row of elements as schematically shown in Figure 3.5a. In such a case, a correct crack extension would be to use the length of the element in which the crack localises. If using a smeared crack approach,  $l$  is usually set to  $l_{element}$ , the length of the element perpendicular to the crack; see Paper II. However, since the direction of the crack might be difficult to know in advance, or if cracks form in more than one direction in the element, a mean value is normally used. A common approximation in a two-dimensional model is to determine  $l_{element}$  as

$$l_{element} = \sqrt{A_{element}} \quad (3.3)$$

where  $A_{element}$  is the area of the element in question. Accordingly, in a mesh with different element sizes the length  $l$  also differs between elements of different size. If instead using the embedded crack model, it is considerably easier to determine this length, since here the width of the localisation band is what will represent the length  $l_{element}$ . In a reinforced concrete structure, though, it may be more complicated to determine the expected crack extension.

The above reasoning holds true also in a reinforced concrete structure in which the interaction between the reinforcement and the surrounding concrete is modelled accurately. In such a case the cracks will, as schematically shown in Figure 3.5b, appear in a way similar to that obtained in tests. However, if perfect bond is assumed in the modelling, i.e. if the nodes used to define the reinforcement and concrete elements are locked to each other so that the strains in both materials remain the same, the element length can no longer be used to determine the stress-strain relation. Instead of crack localisation, the cracks are to spread out over an even distance as shown in Figure 3.5c (this presumes, though, that the elements used are smaller than the mean crack spacing, as is the case in all the analyses carried out in this thesis). This smeared zone of cracks will then represent the discrete cracks observed in an experiment. Accordingly, a more satisfactory approximation of the crack extension should be to use the mean crack spacing  $s_m$ ; see de Borst (1995), Plos (1995) and Johansson (1996).

However, when the cracks propagate further into the structure, away from the reinforcement, they seem to localise in one or two elements. This suggests that the approximation of the crack extension as the mean crack spacing is incorrect in these unreinforced regions. Instead it seems more correct to approximate the crack extension as the element length. To further exemplify this, Figure 3.6a shows the crack pattern obtained in a closing corner when assuming perfect bond between reinforcement and concrete (static analysis of shelter,

presented in Paper III) and hence, the crack extension was approximated as the mean crack spacing. Still, as can be seen from the obtained crack pattern, this assumption is valid only close to the reinforcement in tension. For the concrete at a certain distance from the reinforcement, it would probably, as illustrated in Figure 3.6b, have been more correct to approximate the crack extension as the element length.

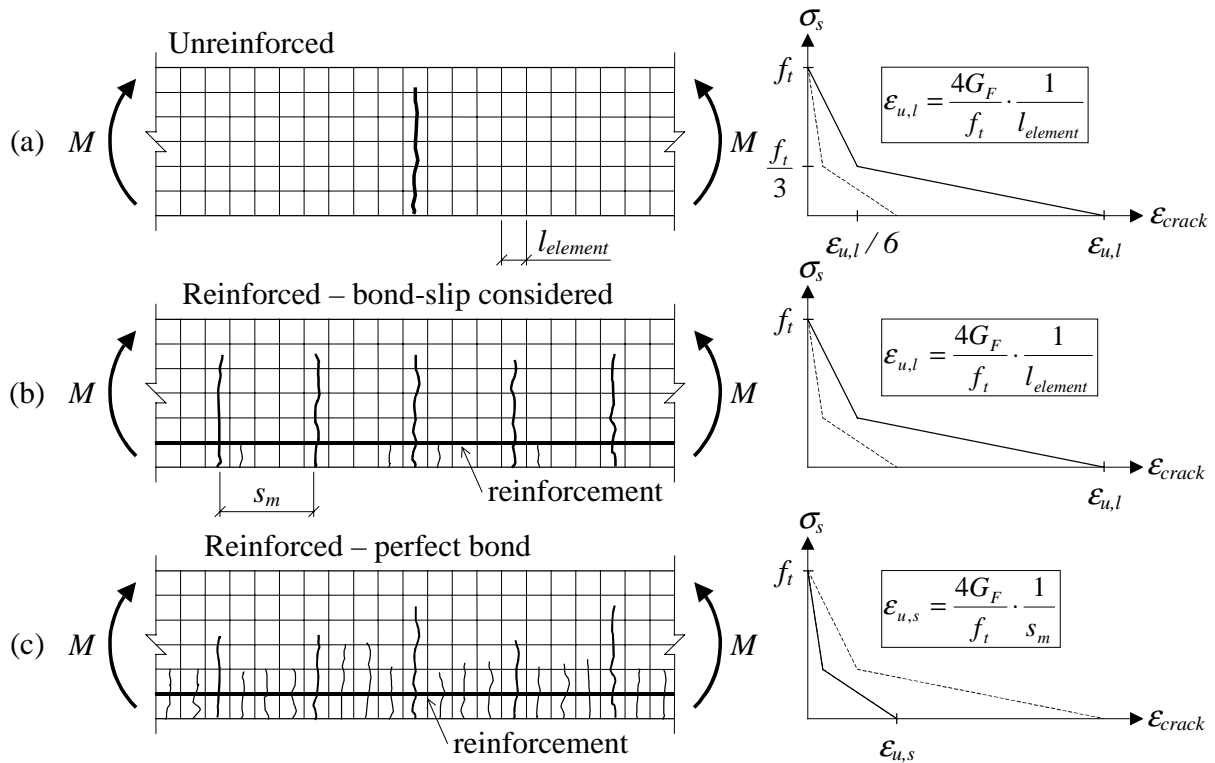


Figure 3.5 Schematic view of crack patterns obtained when modelling unreinforced and reinforced concrete. Filled line shows the stress-strain relation used; dashed lines are shown for comparison only.

From the discussion above it might seem that there may only be problems with localisation when assuming perfect bond. However, this is not true. Depending on, for instance, the size and orientation of the elements used and what load case is studied, one cannot be sure that the cracks will localise within one element even though accurately modelling the bond-slip relation; see for example Johansson (1997) and Lundgren (2000). Neither will the difficulty automatically be resolved by using the embedded crack model (Magnusson 2000), since it will encounter the same type of problem as the smeared crack approach, perhaps making it necessary to adjust the stress-strain relation used here too.

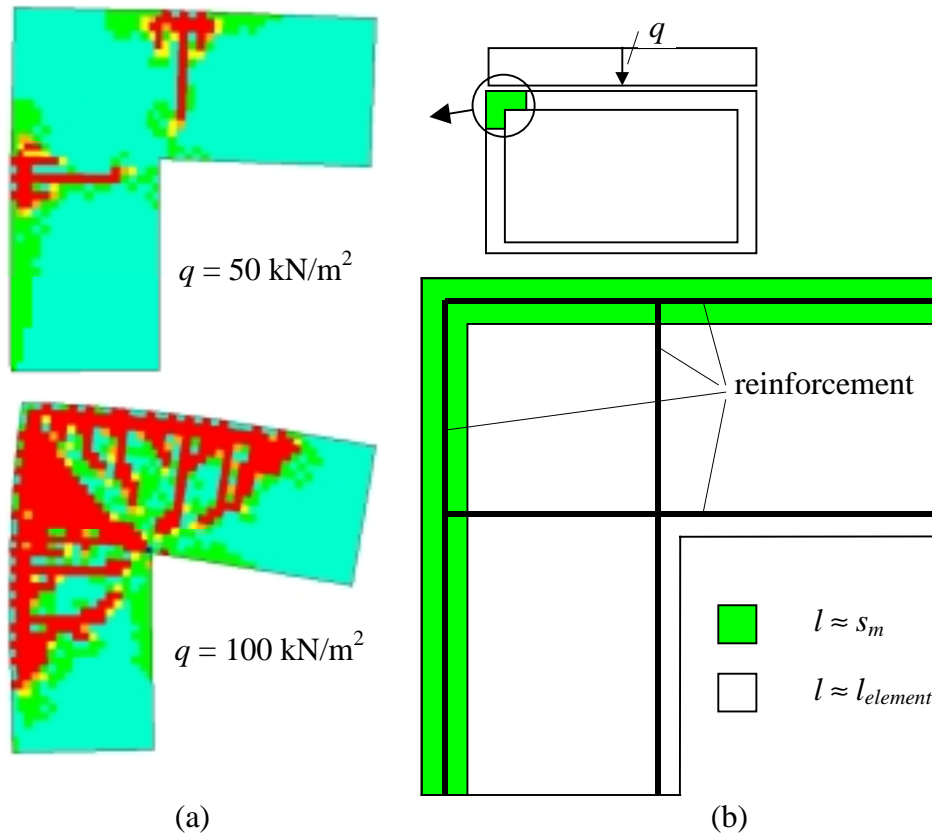


Figure 3.6 (a) Crack pattern in closing corner when assuming perfect bond; (b) approximation of crack extension  $l$  that should be rather accurate.

To summarise, if the crack extension is assumed as the mean crack spacing and this length is larger than the length of the elements used, the results obtained will probably be somewhat too brittle. On the other hand, by approximating the crack extension as the element length, the response will most likely be somewhat too ductile, even though the interaction between concrete and reinforcement is accurately dealt with. Hence, it may be important to carry out a sensitivity study to more thoroughly examine what influence the stress-strain relation used has on the response of the structure studied. A quite approximate way to do this is to vary the crack extension  $l$  used by, say, a factor of two: halved when using perfect bond and doubled when modelling the bond-slip. If this change has little effect on the result, then the analysis is more likely to be trusted. However, if such a change has large impact on the structural response one should be careful when interpreting the results. A correct approach would then be to modify the crack extension originally used in those parts where the assumptions proved to be invalid. A new analysis than has to be carried out and the validity of the assumptions checked. Evidently, this may lead to a cumbersome iteration process that may be quite time-consuming. But, if the post-peak ductility in tension proves to be vital, it may be the only way to obtain correct results.

### 3.4.2 Compression

That cracking can cause localisation problems may be easy to understand, but that this is also the case with concrete in compression might perhaps not be as obvious. Nevertheless, it has been stated by several researchers (e.g. van Mier 1984; Hillerborg 1988; van Mier *et al.* 1997; Lee and Willam 1997) that the post-peak response for compressed concrete is a localised phenomenon. Van Mier showed that the post-peak ductility, among other things, depends on the height of the concrete specimen used. Figure 3.7a shows the normalised stress-strain relation for uniaxial compressive tests on concrete prisms of height 50, 100 and 200 mm. According to this, a specimen with smaller height results in greater ductility. However, if instead comparing the displacement in the same specimens, the relations shown in Figure 3.7b are obtained. Consequently, it can be concluded that the corresponding stress-strain relations do not represent the concrete material behaviour but just a structural effect. The similarity to concrete in tension and the concept of fracture energy comes to mind. Hence, it seems reasonable to solve this in a way similar to that for concrete in tension, that is, introduce fracture energy for concrete in compression. This was done by, for example, Markeset (1993) and Feenstra (1993). However, the use of fracture energy is not enough, since as in the case of cracking, it is a displacement and not a strain that must be simulated. Therefore, there is also a need of a softening zone in which the localisation in compression may occur (compare the use of the crack extension  $l$  for cracking).

The stress-strain relations for concrete in compression given in the literature, e.g. CEB-FIP Model Code, CEB (1993), normally use the mean strain in the specimen and are therefore not suitable to be used as input data for finite element analyses in which the softening of concrete is to be simulated. Such relations, i.e. the measured displacement divided by the height of the specimen (300 mm in CEB-FIP Model Code), do not take into account that a localisation occurs in the material. Nevertheless, up to the maximum strength this is an appropriate approximation since the strain in the concrete thus far is quite homogeneous distributed. However, when reaching the post-peak part this is no longer the case and the material behaviour will be incorrect to use. If, for example, applying such a stress-strain relation in a finite element analysis where the softening zone in the analysis becomes 50 mm, this means that the post-peak relation given will be  $300 / 50 = 6$  times too steep. Not only does this result in a more brittle behaviour, but it may also lead to such numerical difficulties that a solution cannot be found. This is what happened in the finite element analyses presented in Paper II, and is also the reason why the post-peak stress-strain relation for concrete in compression there was modified in some of the analyses.

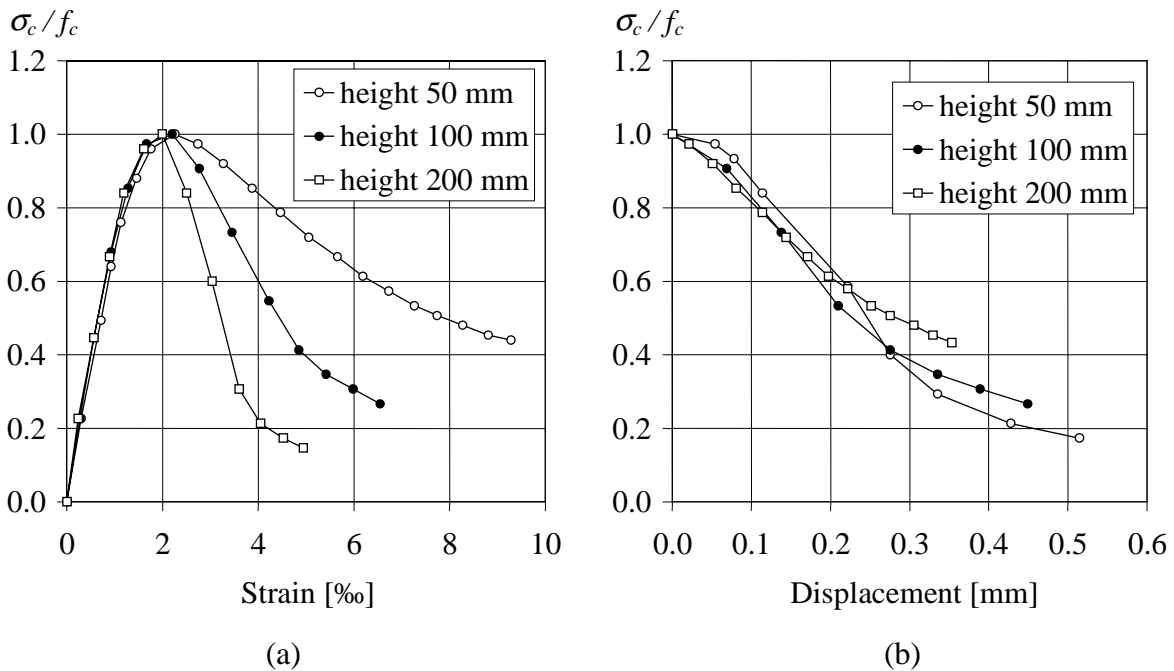


Figure 3.7 Post-peak behaviour of concrete prisms subjected to uniaxial compression: (a) normalised stress-strain relation; (b) normalised stress-displacement relation. Based on van Mier (1984).

If it is known over what length the concrete softening will take place in an analysis, it is easy to make the necessary modifications in the post-peak part of the stress-strain relation. Unfortunately, though, this length is generally unknown. For concrete in tension this length may, if accurate bond-slip relations are used as discussed in Section 3.4.1, be comparably easy to approximate to the element length. This is possible since the localisation due to cracking then generally occurs within one row of elements. However, for concrete in compression, this is usually not the case. The softening zone will here instead be smeared out over a number of elements, making it much more difficult to determine. Therefore, it is necessary to use a length larger than the element length to accurately consider the post-peak behaviour in compression. If this turns out to be important for the response that is to be studied, an iterative procedure similar to that proposed for concrete in tension may be carried out.

### 3.4.3 Possible solution

From the above it is evident that the localisation problems described are important issues to be resolved if more reliable finite element tools are to be obtained. A quite cumbersome and time-consuming iterative procedure was proposed above as an approximate way to handle this

and even though not a particularly good method, it still presents a possibility to solve the problems. Further, the size of the load steps used in an analysis (see Section 3.5) will also affect the final crack pattern; if large increments are used, the risk of a more diffuse crack pattern increases. Therefore, a somewhat more distinct crack pattern might be obtained by reducing the size of the load increments. However, it should also be remembered that too small load steps will not be practically possible due to the large execution time needed then.

According to Jirasec (1999), these localisation problems can be taken care of automatically in the material model by using so-called localisation limiters. Using this approach it is possible to supplement the stress-strain relation by an additional parameter that specifies the actual width of the softening zone, and to use a localisation limiter so that the numerically simulated softening zone gets the correct width. However, such models are not yet implemented in the finite element programmes used here and are therefore not further treated herein.

### **3.5 Numerical approach**

In a finite element analysis, where the non-linear behaviour of the material, the geometry, or both is taken into consideration, a system of simultaneous non-linear equations results. The relation between load and displacement then becomes non-linear, and the displacement at a given stage usually depends on previous displacements. To solve this system, the load is subdivided into increments; see Figure 3.8. At each load increment a linear approximation of the stiffness, representing a kind of linearised form of the relation between the load and the displacement, is established and the corresponding equilibrium equations are solved. Since the stiffness varies with the displacement, the internal forces of the structure are not in equilibrium with the external forces; this produces an error in the solution. Therefore, to minimise this error, an iterative solution procedure is used within each load increment and the solution is refined until a specified convergence criterion is satisfied.

Note, though, that when using an explicit integration method, such as that described in Section 6.3.2, equilibrium is satisfied without conducting any iterations. This is possible by fulfilling dynamic equilibrium instead of a static one in which the displacements at the next increment is based on the deformations and stiffness in the previous load steps only.

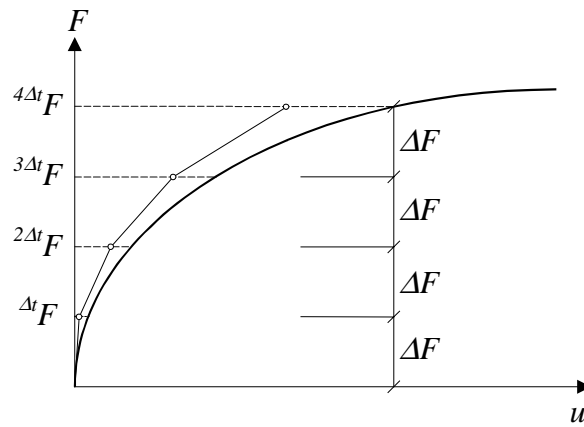


Figure 3.8 Increasing error of the solution when using the incremental load method without correction for a system with one degree of freedom.

There are several different iteration methods available that can be used in the solution process. The general procedure, though, is the same for all iteration methods; the difference is in how the stiffness matrix is determined. The iterative methods can be divided roughly into three categories: the tangent stiffness method, the initial stiffness method and the secant stiffness method, see Figure 3.9. In the tangent stiffness method, the stiffness matrix is determined at each iteration, resulting in a method that requires few iterations, but where every iteration is relatively time-consuming. In the initial stiffness method, the stiffness is determined at the beginning of each load step and it is then used throughout the whole iteration process within an increment. This method requires more iterations to reach convergence than the tangent stiffness method but, since the same stiffness matrix is used in each iteration within the increment, every iteration is faster. The secant stiffness method uses the information from previous solutions to update the inverse stiffness matrix in each iteration, which results in a convergence rate somewhere between that of the tangent and the initial stiffness methods. The iteration methods used in the analyses presented here were the Modified Newton-Raphson method (initial stiffness method) and the BFGS method (secant stiffness method). Of these, the latter were found to encounter fewer numerical problems when used. Further information on these iteration methods can be found in for instance Bathe (1996).



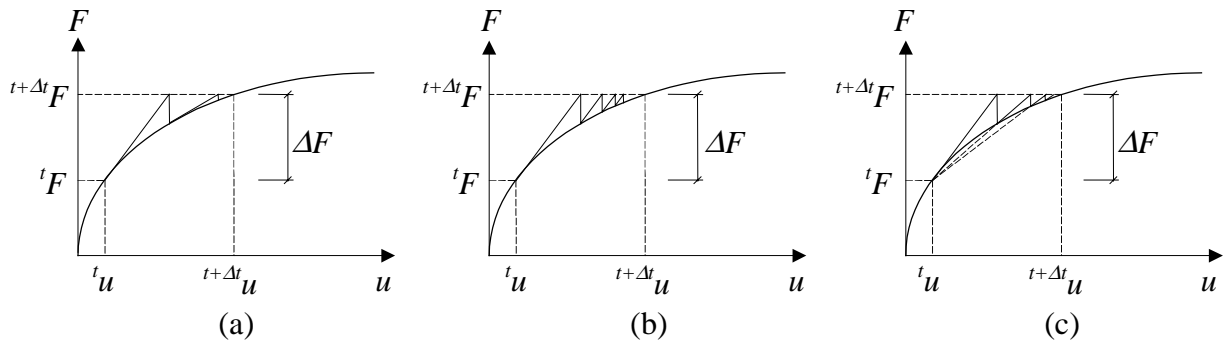


Figure 3.9 Schematic view of different iteration methods for a system with one degree of freedom: (a) tangent stiffness method, (b) initial stiffness method, (c) secant stiffness method.

### 3.6 Finite element analyses of frame corners

As stated in Section 3.1 the use of non-linear finite element analyses may considerably improve the understanding of the structural behaviour in reinforced concrete. Therefore, this tool has also been extensively used for the work presented herein, and naturally also in the study of frame corners. Paper II describes such analyses of closing frame corners in which the uses of the conventional and new reinforcement detailings as shown in Figure 1.1 (i.e. detailing *Type 1* and *Type 3*, respectively) were compared. These analyses were based on the second test series described in Paper I. Here, a low and high amount of reinforcement were used. However, due to the occurrence of side concrete spalling in the latter case, only the analyses of the former were included there. When conducting these analyses, numerical problems due to concrete crushing were encountered. This was due to the localisation problem described in Section 3.4.2 and was dealt with accordingly. Despite such problems, the analyses proved very valuable since they provided an improved insight into the response of the corner and resulted in increased knowledge and better understanding. Thus, it was also possible to predict rather accurately the difference in structural behaviour of a frame corner when using the different detailings studied. Accordingly, based on a combination of the observations made in the tests and the finite element analyses it was concluded that the new alternative (i.e. *Type 3*) is suitable to use instead of the conventional reinforcement detailing (*Type 1*).

Further, the analyses made it possible to examine what could happen if the reinforcement loops in the new detailing were positioned incorrectly by mistake. The case studied did seem to have a negligible influence on the overall behaviour and even though one should be aware

that this might not fully reflect reality, it still gave a basic idea of what might happen. This study also brought out one of the substantial advantages of using the finite element tool, i.e. making it possible to at least arbitrarily examine what can happen in a complicated case without having to carry out expensive and time-consuming tests. Hence, apart from providing important knowledge as such, it may for instance be used prior to experimental testing to determine what might be interesting to examine further in a test series.

Apart from the work by the author, two theses making use of the finite element tool in similar studies have recently been presented at the Division of Concrete Structures at Chalmers University of Technology, Plos (1995) and Lundgren (1999). Such analyses were also performed in two Master of Science projects in which the author acted as supervisor; e.g. Olsson (1996) and Johansson and Karlsson (1997). Due to the close resemblance to the work presented in this thesis, these works are briefly summarised below.

Plos, Olsson, and Johansson and Karlsson carried out two-dimensional plane stress analyses similar to those presented in Paper II, using the same material models and element types used there. The analyses by Lundgren, though, were more sophisticated; she was able to use a rotating crack model in combination with a much-improved bond model, developed by herself, in three-dimensional analyses. The work of Plos and Lundgren was limited to the study of closing corners using a detailing similar to the *Type 1* detailing shown in Figure 2.5. The analyses agreed well with the test results and they played an important part in the improved knowledge gained for the detailings studied. One conclusion of the work was that it should be appropriate to splice reinforcement bars within the corner; this has resulted in a change in the current bridge code used by the Swedish Road Administration.

As mentioned in the previous section, a test series comprising four frame corners reinforced with the *Type 3* detailing subjected to closing moment was carried out: two with a low reinforcement ratio and two with a high ratio. Analyses of the former were carried out by the author and are presented in Paper II and Johansson (1996); the latter, though, were not included in that study due to spalling of the side concrete cover. However, to further examine the corner behaviour for such high reinforcement ratios when side concrete spalling is prevented, non-linear finite element analyses were carried out and reported by Olsson (1996). Since plane stress was assumed, the spalling of the side concrete cover was not simulated and, consequently, the load capacity also became larger than obtained in the tests. Nevertheless, the initial stiffness was approximately the same as in the tests and the load capacity corresponded well with what would theoretically have been obtained if no side concrete spalling had

occurred. As in the analyses presented in Paper II, crushing of the concrete at the inside of the corner caused numerical problems at a stage considerably earlier than expected. However, this was not regarded as due to premature crushing but to the post-peak relation used for concrete in compression being too steep. Therefore, this part of the stress-strain curve was elongated in a way similar to that described in Paper II. The finite element analyses showed that an increased reinforcement amount caused a considerably larger part of the cracking to take place within the corner. Nevertheless, the critical sections were still obtained as schematically shown in Figure 2.4b and hence, a satisfying response with yielding of the reinforcement was still possible. Further, it was found that the construction joint obtained due to separate casting stages had negligible effect on the structural response, a crack forming in this section in either case.

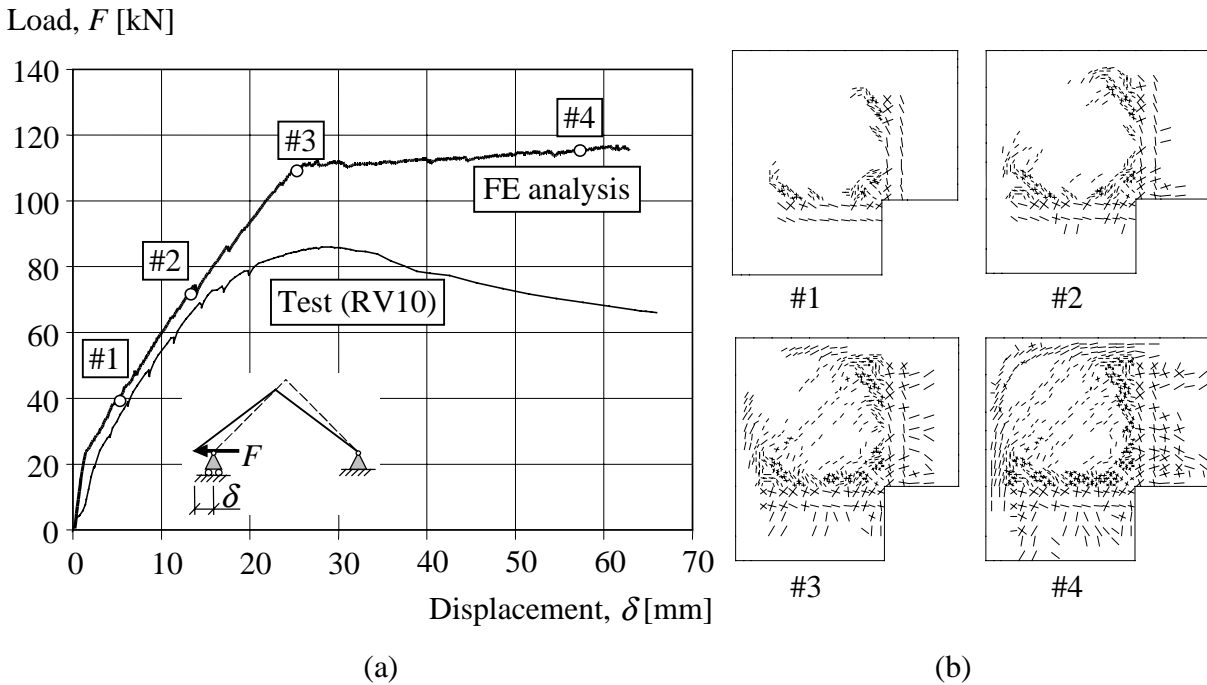


Figure 3.10 FE analyses of opening frame corner (specimen RV10, see Paper I): (a) comparison of load-displacement relations; (b) crack pattern at different load stages. Based on Johansson and Karlsson (1997).

Johansson and Karlsson (1997) carried out finite element analyses of the opening frame corners presented in Paper I. Unfortunately, though, they were not able to fully simulate the response observed in the tests carried out. Even though cracks formed around the reinforcement loops, this did not cause failure. Instead, the reinforcement yielded at the inside of the corner and a load plateau, different from that observed in the tests was obtained; see Figure 3.10. A possible reason for this is that shear-locking occurred, despite using a constant

shear retention value of 0.05, and prevented the failure from developing as expected; if the rotating crack concept had been used instead, a more realistic response might have been the result. Another probable reason for the different behaviour is that the two-dimensional plane stress model used to model the concrete was unable to take into account the loss of capacity due to the probable spalling initiation of the side concrete cover. Hence, all reinforcement bars were fully active in the analyses, while this most probably was not the case in the tests; see Paper I. Nevertheless, the analyses supported the conclusion drawn in Section 2.3.2.1 that the inclined bars used in the *Type 4* detailing may be replaced by an extra amount of reinforcement loops, thus transforming it into a *Type 3* detailing.

When studying the literature regarding the research on concrete frame corners, it is evident that most work carried out so far has been done by experimental studies. This is not that surprising since most research within the field was carried out from the late 1960s until the early 1980s and the availability of robust and reliable concrete material models are relatively new. Nevertheless, non-linear finite element analyses have also been used to some degree as shown in the previous two sections. Other researchers who have used non-linear finite element analyses to study the behaviour in frame corners are Krauthammer and co-workers, e.g. Marx (1993), Otani and Krauthammer (1997), and Ku and Krauthammer (1999); a summary of the results gained is given in Krauthammer (1998). Both two-dimensional and three-dimensional analyses of a concrete structure subjected to an internal explosion (i.e. opening moment) were made. As further discussed in Section 4.1, the pressure in such a load case is highly dynamic and thus very different from a static one. The dimensions of the structure studied were very large; see Figure 3.11. Especially notable is the large amount of inclined reinforcement, its amount being about five times that of tensile reinforcement at the inside of the smaller adjoining member, which was determined from the connection's shear capacity, see Marx (1993). Different reinforcement detailings were investigated; among other things, the influence of stirrups in the adjoining member and within the corner was examined. Further, the amount of inclined bars and their distance to the outside of the corner were varied.

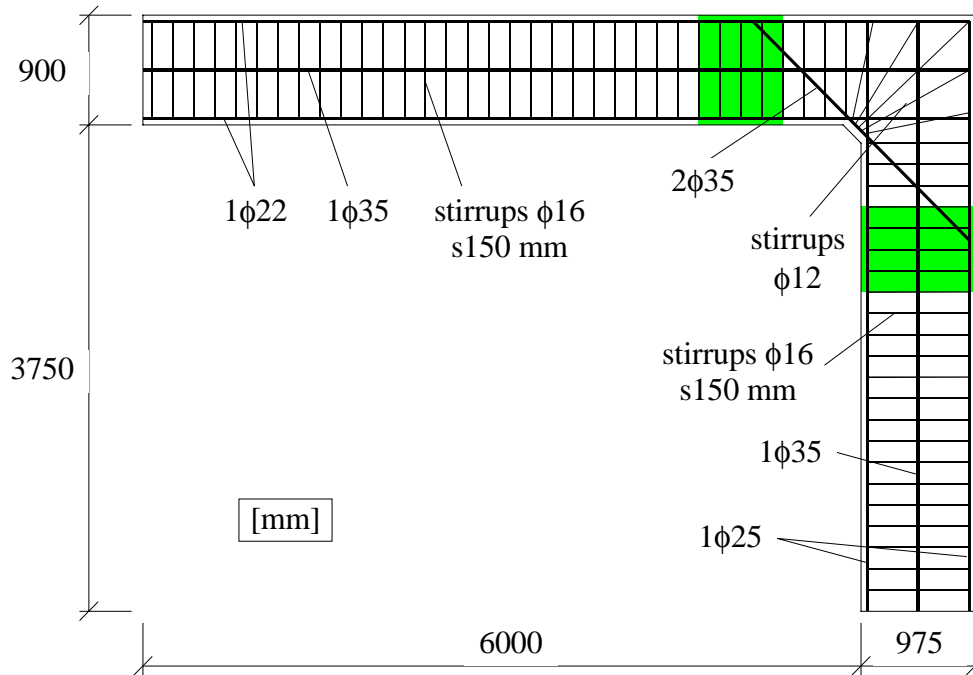


Figure 3.11 Approximate dimensions of frame corner studied by Krauthammer and co-workers. The reinforcement amounts given are valid for a strip of width 100 mm. The plastic zones obtained are marked with grey. Based on Krauthammer (1998).

In none of the analyses did the corner fail due to loss of the outside part of the corner, i.e. the type of failure commonly observed in static tests; see Section 2.2.1. Whether this was due to the impulse loading, the concrete model being unable to capture this type of failure, or to something else is not clear. Nevertheless, failure was instead obtained due to rupture of the reinforcement at the inside of the corner or, more commonly, failure within a plastic hinge formed in the region where the inclined bars reached the compressive zone; see Figure 3.11. A possible explanation for this response is that the amount of inclined bars in the corner was so much larger than that of the tensile reinforcement that the capacity of the plastic hinges was reached before the inside of the corner. Nevertheless, Krauthammer (1998) states that the results “confirmed that a connection detail based on static design should not be expected to survive the severe loading associated with explosive loads.” However, based on the reinforcement detailing used and the fact that concrete failure was not obtained within the corner, it seems to be a sound interpretation that the detailing itself was not insufficient. Instead, the results suggest that the design method used underestimated the amount of tensile reinforcement needed in both the corner and the adjoining members, and that this is the reason why failure was obtained in most of the cases examined.

### **3.7 Concluding remarks**

It has been shown that non-linear finite element analyses can be a very powerful tool in the study of reinforced concrete structures, for instance in the study of opening or closing frame corners. However, it is important to be aware that such analyses cannot completely replace the need of experimental testing; tests will always be needed since they describe the reality while the former just attempts to simulate it. Hence, certain phenomena may be observed in a test that the material models or element types used in the analyses are unable to reproduce correctly. On the other hand, though, finite element analyses may supply the means for further understanding and an extensive increase in knowledge of the often complicated response in reinforced concrete structures. Hence, this tool may make it possible to explain phenomena in a way that would simply not be possible by using only conventional testing and evaluation methods. Further, it must be pointed out that even though the analyses may be unable to describe the response quite correctly, they can still often be successfully employed to give the user a basic idea of what behaviour may be expected in a given situation. Non-linear finite element analyses may therefore also be a very useful tool when determining what experiments should be carried out. Consequently, it can be concluded that the two methods are used to their fullest advantage only when combined.

Several different crack models are available today in commercial finite element programmes, making it possible to obtain rather reliable results in analyses of reinforced concrete structures. However, the use of such an advanced tool also puts a high demand on the user. Without awareness of what the given input means and the ability to critically examine the results, it may lead to critical misjudgements in the interpretation of the response obtained. The post-peak behaviours for concrete in tension and compression, for instance, are both highly localised phenomena, making it difficult to determine a correct stress-strain relation to use in an analysis. To be able to simulate such a response accurately, the concept of fracture energy and the length of the softening region have to be considered. Hence, if one is not aware of this or how to handle it the results obtained may be quite incorrect. Even for an experienced user such localisation may still cause substantial problems in the modelling of a structure. This, then, is a field of great importance that is still to be elucidated.

# 4 Structural Behaviour at Dynamic Loading

## 4.1 General remarks

When designing a civil defence shelter according to the present Swedish Shelter Regulations, Swedish Rescue Services Agency (1998), dynamic load cases are not used. Instead, equivalent static load cases are employed to make calculations easier for the designer. As a weapon load, the long-term pressure (both positive and negative) due to a nuclear detonation at long range is assumed, and for the impact of falling debris from a collapsing building an equivalent static load is employed; see Figure 4.1a. However, the real loads that a shelter must be able to withstand are quite different and more similar to those shown in Figure 4.1b. The pressure, due to a nearby explosion, acting on the front shelter wall will present a very large peak pressure that decreases to zero within a couple of milliseconds. The impact, though, will be composed of a falling mass hitting the shelter with a certain velocity.

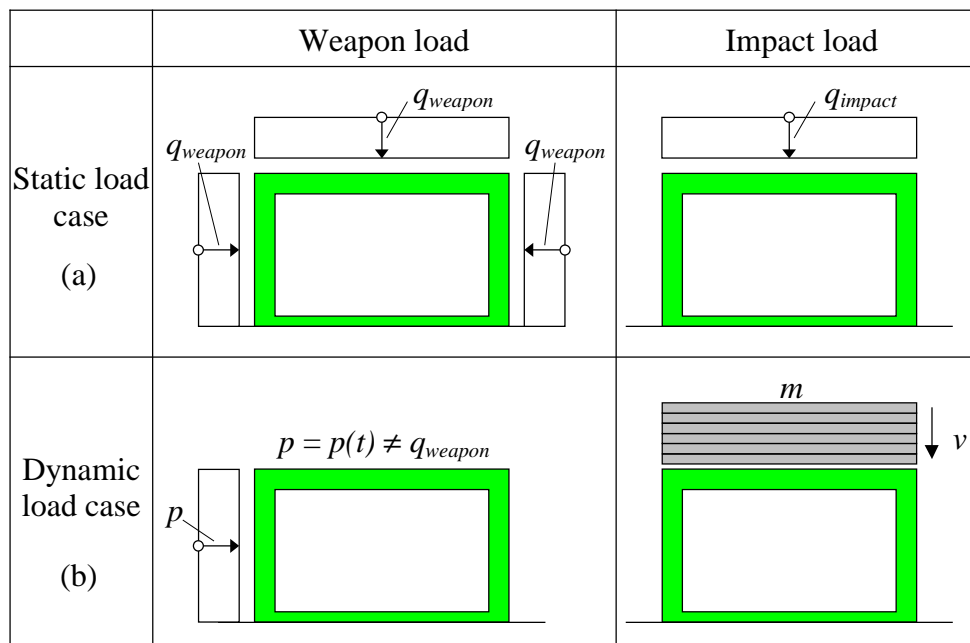


Figure 4.1 Comparison between (a) equivalent static loads and (b) probable dynamic loads that may act on a civil defence shelter.

To further study the effect of such highly dynamic load cases, non-linear finite element analyses were carried out; see Paper III. In accordance with the criterion in the Swedish Shelter Regulations, the time-dependent pressure due to an explosion of 125 kg TNT at a distance of five metres was used as the blast load. The impact of falling debris was based on

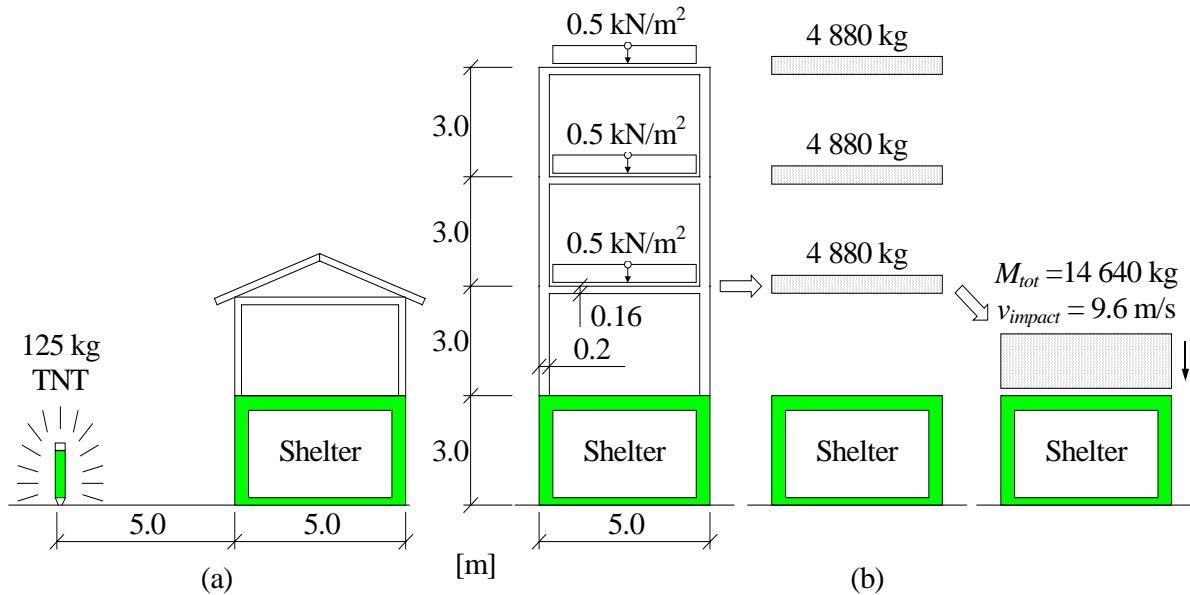


Figure 4.2 Dynamic load cases studied in Paper III using non-linear finite element analyses: a) pressure from blast load, and b) impact load due to falling masses.

the collapse of a three-story concrete building standing on top of the shelter, see Figure 4.2. However, to better understand the response obtained and the reasons for the choices made, a brief background about such extreme load cases is presented in the following sections.

## 4.2 Response at transient loading

A structure subjected to dynamic load may behave very differently compared to when it is loaded statically. This is especially true if the load applied is very intense, with a high peak value and acting during a very short time. Such so-called impulse loads, or highly transient loads, are obtained when for example a structure is subjected to the pressure from a nearby explosion or the impact from colliding objects, i.e. the kind of dynamic loads that may act on a civil defence shelter.

When a load is applied on a structure, stress waves caused by the load travel back and forth in the structure, “informing” all its parts of what is going on. The time it takes for this information to be distributed depends on the wave speed (i.e. the speed of sound in the material) and on the structure’s shape. The former may be determined as

$$c = \sqrt{\frac{E}{\rho}} \quad (4.1)$$



where  $E$  is Young's modulus and  $\rho$  is the density of the material, and will in normal-strength concrete be approximately 3,500 m/s. Accordingly, the time needed for this distribution is usually very short and normally does not cause any problems. However, as stated above, the pressure caused by a nearby explosion may not last more than a couple of milliseconds and will present an extremely high peak pressure. Consequently, the pressure will affect the structure but there will not be time enough for the information to spread through the structure, and hence a very different response may initially be obtained.

A good example of this is a simply supported beam (plain concrete) subjected to the impact of a drop weight hitting the beam with a certain speed; see Figure 4.3. The crack directly below the load would eventually form also with statically loading. However, the inclined shear cracks and the cracks at the top of the beam would not appear in such a case. The reason for their appearance is that, at the time of cracking, the supports are still unaware of the drop weight hitting the beam. Hence, this failure mode would be obtained regardless of whether the beam had been fixed, or as now, simply supported. Instead, the current boundary conditions can perhaps best be regarded as time-dependent fixed supports, where the locations of these supports move toward the ends of the beam with a speed equal to the wave speed in the beam. This would also explain the forming of bending cracks at the top of the beam. Another good example of how the initial behaviour may be affected due to such time-dependent boundary conditions is the initial behaviour of a shelter wall subjected to the impulse load from a nearby explosion, as shown in Paper III.

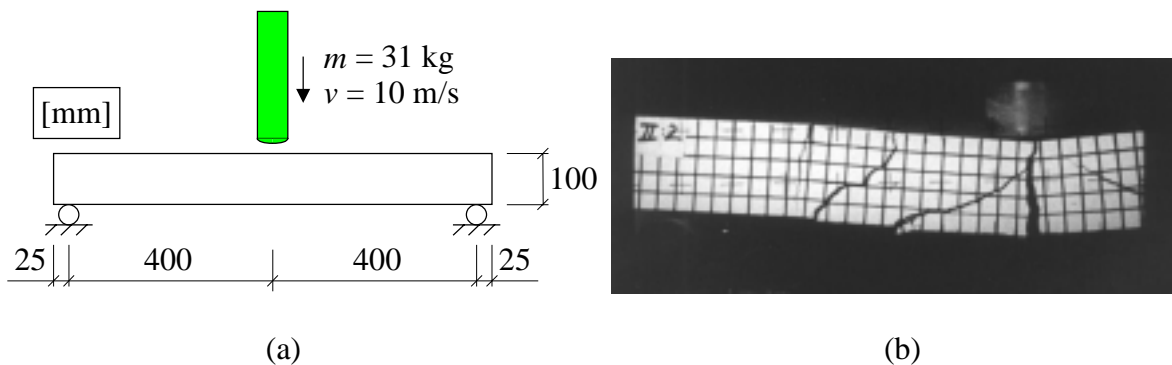


Figure 4.3 (a) Load set-up of simply supported beam with width 100 mm; (b) crack pattern obtained when subjected to the impact of falling drop weight. Based on Ågårdh and Laine (1997).

Based on the above, it is clear that the possibility of global force redistribution within a structure subjected to such loads may be very different from that in a statically loaded structure. Such a redistribution needs a certain amount of time to take place, a time that

evidently need not be available in a structure subjected to an impulse load. Accordingly, the ability of such a redistribution to take place may therefore also be reduced. Unfortunately, the possibility of such force redistribution is very important in structures subjected to impulse loads. This makes it even more important that the materials (especially the reinforcement) and the detailings used in such concrete structures can guarantee ductile behaviour. With this as a background, it is therefore disturbing that the reinforcement ductility used in Sweden has decreased quite considerably during the last ten to fifteen years. Even though it was recently decided that a more ductile reinforcement should now be made available in Sweden (Fundia 1999), the difference from the material properties of the steel used during the 1970s and 1980s are still great, see Johansson (1997). This statement is valid for both the strain at ultimate stress and the ratio between ultimate strength and yield strength.

Due to the small time periods during which an impulsive load may act, the gathering of test data becomes more difficult when conducting such experiments. As an example, in static tests it is usually possible to visually register and mark the forming of cracks during loading, information that tends to be vital when interpreting the test results. However, this is not possible in a transiently loaded structure; for such registration a high-speed camera is required. Further, the arrangements necessary when conducting, for example, explosion tests or drop tests may be far more difficult to carry out, compared to static tests. Therefore, the use of finite element analyses may become an even more powerful tool in such studies, since this tool makes it possible to continuously follow the response in the structure regardless of time. Moreover, the structural behaviour, considering for example the global inertia effects or the time-dependent boundary conditions, is taken into account automatically. A problem arises, though, due to the change in material behaviour of both concrete and steel when subjected to high strain rates. That is, when the load velocity of the material increases, its properties such as strength and stiffness also change. This is a very complicated field that has yet to be clarified; nevertheless, what influence a high strain rate has on, especially, concrete is further presented and discussed in Chapter 5. The numerical approach for such short-duration responses also differs from that suitable in static or quasi-static loading, and is therefore dealt with in Chapter 6.

Often it may not be practical or even necessary to use advanced finite element analyses to determine the global response of a structure subjected to a dynamic load. Instead, when solving such problems the mass, stiffness and external load of the structure may be transformed so that a single-degree-of-freedom system (SDOF system) can be used; see for instance Balazs (1997). This is made possible by converting these properties so that the work

carried out by the external and internal forces in the SDOF system is the same as the work carried out in the real structure. Further, an equivalent mass is used so that the kinetic energy generated in the SDOF system is the same as that in the real structure. Depending on what is sought, such an approximation may in many cases also be adequate. However, since the conversions made usually are based on static behaviour, this method is not able to take directly into account the time-dependent boundary conditions that may be very important when studying the initial behaviour of a structure. Therefore, an SDOF system may be highly unsuitable when studying the initial behaviour of a structure subjected to an impulse load, such as the beam shown in Figure 4.3. Hence, even though an SDOF model in many cases may be a useful tool it should be pointed out that it may be unsuitable due to its considerable coarseness; i.e. if for instance the crack pattern is of interest, a more detailed finite element analysis should of course also be used.

## **4.3 Blast load**

### **4.3.1 Explosive shock in air**

According to the English edition of the Swedish Shelter Regulations, Swedish Rescue Services Agency (1994), a civil defence shelter shall be able to withstand “the effect of a pressure wave corresponding to that produced by a 250 kilograms GP-bomb with 50 weight percent TNT which bursts freely outside at a distance of 5.0 metres from the outside of the shelter during free pressure release”. Further, the shelter shall endure the impact of splinter from such a bomb. Apart from these “close range” requirements, the shelter shall also resist the long-term pressure (overpressure of 50 kPa and underpressure of 8 kPa) from a nuclear bomb that detonates at a long distance. This section gives a very brief description of the blast waves generated by an explosion in free air, and is included to give the reader a background for the blast load used in the finite element analyses presented in Paper III. As stated in Section 1.4, though, the influence of splinter was not considered in these analyses. More information about the origin and development of blast loads may be found in, for example, Baker (1973) or Kinney and Graham (1985). The expressions given below are valid only for explosions of conventional weapons (i.e. not nuclear weapons).

An explosion is, according to Kinney and Graham, a phenomenon resulting from a sudden release of energy and whose magnitude is established by the amount of energy released. There are many different sources of such energy releases, but a generally accepted standard of

measurement for them is the energy released in the explosion of TNT. Thus, different explosives are generally considered in TNT-equivalencies and, since energy is proportional to mass, it is also common to specify the explosives in terms of mass instead of energy.

The energy release of an explosion will push back the surrounding atmosphere and a blast wave, travelling faster than the speed of sound, will form. A typical pressure-time relation of an ideal blast wave is shown in Figure 4.4. The explosion detonates at time  $t = 0$  and after a certain time  $t_a$ , the wave front reaches the target. The pressure in the wave front will rise from the ambient pressure,  $p_0$  (in our case the air pressure  $\approx 100$  kPa), to  $p_0 + P_s^+$  during a very short time (a couple of microseconds). The pressure then decays to the ambient pressure again at time  $t_a + T^+$  ending the positive phase. A negative phase will then form with amplitude of  $p_0 - P_s^-$  when the rush of air toward the explosion centre forms a partial vacuum. Eventually the pressure will be back to  $p_0$  at total time  $t_a + T^+ + T^-$ . The portion of the time history above the ambient pressure  $p_0$  is called the positive phase and the portion below  $p_0$  is called the negative phase. The positive and negative impulse intensities can be defined as shown in equations (4.2) and (4.3) respectively.

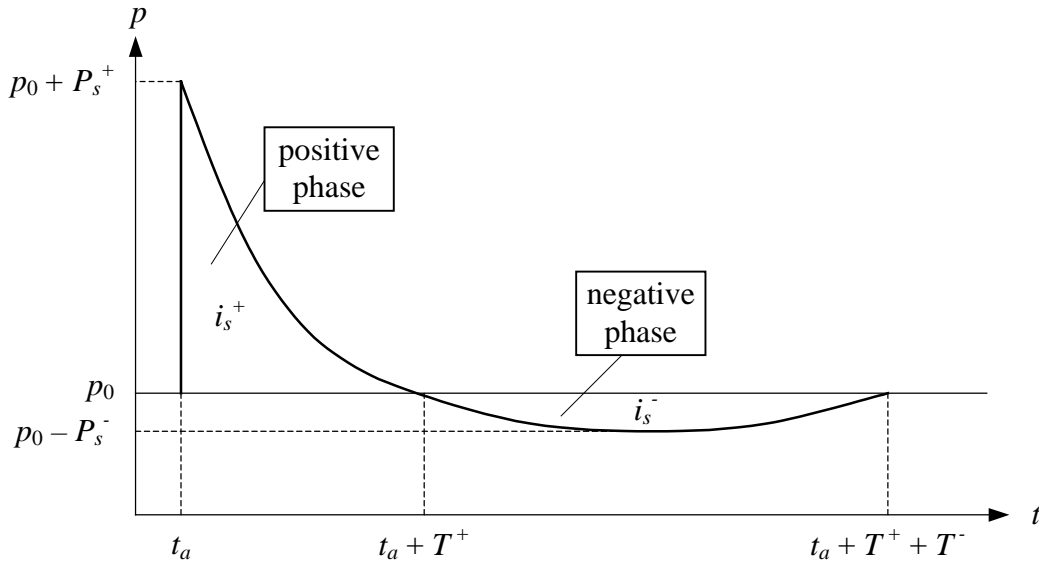


Figure 4.4 Schematic view of an ideal blast wave.

$$i^+ = \int_{t_a}^{t_a+T^+} (p(t) - p_0) dt \quad (4.2)$$

$$i^- = \int_{t_a+T^+}^{t_a+T^++T^-} (p_0 - p(t)) dt \quad (4.3)$$

The positive impulse  $i^+$  together with the peak pressure  $P_s^+$  and the duration  $T^+$  are important parameters that are used to describe the shape of the blast load. Different researchers have proposed several “blast wave shapes” with varying complexities. Baker (1973) describes six of these, where the simplest one is a linear function involving only two parameters and the most complex is an exponential function including five parameters. Because of its simplicity and allowance of accurate matching to observed parameters, Baker propose the use of

$$p(t) = p_0 + P_s^+ \left| 1 - \frac{t}{T^+} \right| e^{-\alpha t/T^+} \quad (4.4)$$

where  $t$  is time after shock arrival (i.e., measured after the arrival time,  $t_a$ ) and  $\alpha$  is a wave form parameter that describes the rate of decay of the overpressure. This expression is also proposed by Kinney and Graham (1985) and used in both ConWep (1992) and FortH 2 (1987). Consequently, it has also been used in this work to determine the pressure-time relation for an explosion. Combining equations (4.2) and (4.4) gives

$$i^+ = P_s^+ T^+ \left[ \frac{1}{\alpha} - \frac{1}{\alpha^2} (1 - e^{-\alpha}) \right] \quad (4.5)$$

from which  $\alpha$  can be obtained. The corresponding relations for the negative phase have, according to Baker been almost totally ignored by researchers. A probable reason is that most investigators have considered the negative phase as relatively unimportant compared to the positive phase, or that they have encountered difficulties in accurately measuring its characteristics. According to Baker, the only expression proposed for the negative phase is that proposed by Brode (1955), in equation (4.6). Here, time is measured from the start of the negative phase  $t_a + T^+$ . The negative phase, though, was neglected in the analyses presented in Paper III.

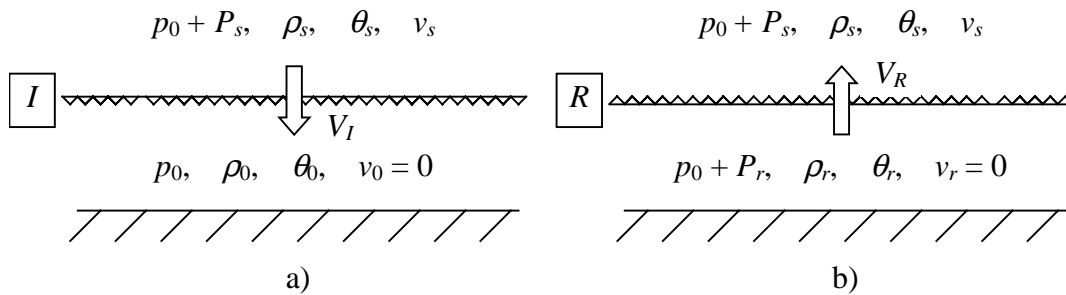
$$p(t) = p_0 - P_s^- \left| \frac{t}{T^-} \right| e^{-4t/T^-} \quad (4.6)$$

### 4.3.2 Reflection of shock waves

The information given above is valid for a blast wave that is free to develop in free air without any kind of disturbances. However, when a blast wave encounters a denser object, its characteristics will change dramatically. Thus, in order to better understand the pressure-time shape of a blast load acting on a structure, it is helpful to be at least vaguely aware of what

happens when a shock wave is reflected from a denser surface or diffracted around an object. The former topic is treated here and the latter in Section 4.3.3.

The simplest case of reflection is normal reflection, where the shock wave hits a dense surface at a right angle. In Figure 4.5a the incident shock wave  $I$  is approaching the wall with a velocity  $V_I$ . The conditions in front of the wave are the ones for still air (indicated by the subscript 0) while the conditions immediately behind are those for a free-air shock with a given pressure ( $p_0 + P_s$ ), density ( $\rho_s$ ), temperature ( $\theta_s$ ) and particle velocity ( $u_s$ ). Immediately after reflection at the wall (Figure 1b) the reflecting wave moves away from the wall into the region associated with the incident wave at a velocity  $V_R$ . At the wall surface the pressure ( $p_0 + P_r$ ), density ( $\rho_r$ ) and temperature ( $\theta_r$ ) are all increased to a value above that of the incident wave, while the particle velocity is reduced to zero. The overpressure,  $P_r$ , is called the reflected pressure and can be several times as high as the pressure,  $P_s$ , of the incident wave. For weak shocks ( $P_s \ll p_0$ ) where acoustic approximations are valid, the reflected overpressure will be twice as high as that of the incident wave. For stronger shocks this ratio can be increased considerably and can, according to Baker (1973), in extreme cases perhaps be as high as 20 or more.



angle  $\alpha_{l,crit}$ , such that the reflection described above is not possible for  $\alpha_l > \alpha_{l,crit}$ . What value this critical angle has depends on the velocity of the incident shock; see Kinney and Graham (1985). For a wave velocity of Mach 1.5 (where Mach 1.0 is the speed of sound) and above,  $\alpha_{l,crit} \approx 40^\circ$ . This is the so-called Mach reflection, a complex but important phenomenon that is further described below.

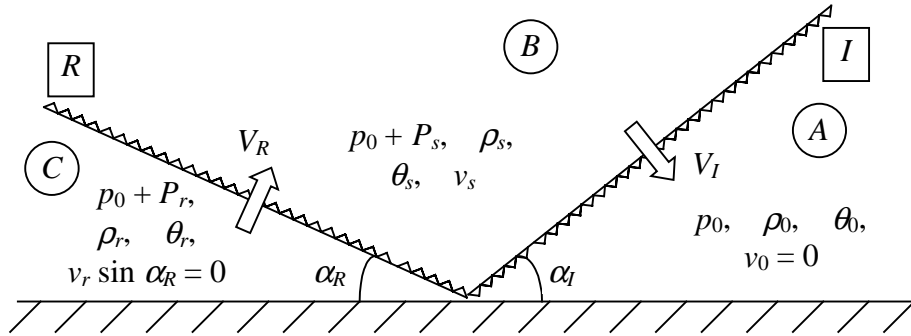


Figure 4.6 Ordinary oblique reflection of a plane shock from a rigid wall. Based on Baker (1973).

When the incident wave hits a surface at the critical angle  $\alpha_{l,crit}$  or more steeply a Mach reflection occurs. Now, in contrast to the ordinary oblique reflection, the wave will not bounce away directly. Instead it spurts away along the surface before being reflected. This has the effect that a new shock wave, a Mach stem, takes form almost perpendicular to the surface. As the shock system moves along the surface, the height of the Mach stem increases. This means that the intersection point between the Mach stem and the incident and reflected shock, the so-called triple point, will get further away from the surface as the shock system moves.

In Figure 4.7 the reflection process of a strong shock waves, separated into three stages, is shown. In the first stage the incident wave  $I_1$  has just touched the reflecting surface. The reflected pressure will then be more than twice as high as anywhere else on the incident wave. As the incident wave expands, so does the reflected wave. The reflected wave, however, will not be spherical since the angle of reflection  $\alpha_R$  is less than the angle of the incident wave  $\alpha_l$  (a reflected acoustic wave, however, would be spherical due to equal angles  $\alpha_l$  and  $\alpha_R$ ). At a certain distance from the charge C, the incident angle  $\alpha_l$  is equal to the critical angle  $\alpha_{l,crit}$  which means that a Mach stem is formed (stage two in Figure 4.7). As the shock system expands further, the Mach stem grows rapidly and “swallows” the inclined and reflected waves above it, as shown by the line  $\rho$ , which describes the line of the triple point. In stage three, the Mach stem dominates the shock close to the surface and an almost vertical shock

front has formed. Further, the pressure in the Mach stem and in the neighbourhood of the triple point will be considerably larger than those in  $I_3$ . This means that depending on the distance to a given target and the height of the target, the whole target may or may not be hit by a uniformly distributed pressure at the same time.

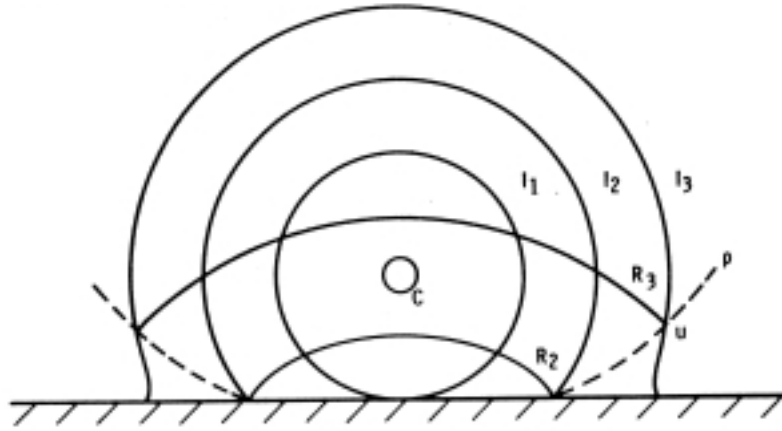


Figure 4.7 Reflection of strong shock waves. From Baker (1973).

### 4.3.3 Diffraction of shock waves

All information given here about the diffraction of shock waves is based on Baker (1973). When a shock wave encounters a solid object, such as a building, a complicated interaction termed diffraction occurs. The process of a plane shock wave hitting a two-dimensional structure is sketched in Figure 4.8. When the incident wave,  $I$ , strikes the wall a reflected wave,  $R$ , moves in the opposite direction and the pressure at the wall surface increases instantaneously from  $p_0 + P_s$  to  $p_0 + P_r$ . Above the wall, however, the incident wave continues its movement relatively undisturbed and the pressure remains at  $p_0 + P_s$ . Due to the difference in pressures at the upper left corner of the wall, the reflected pressure will decrease as a rarefaction wave moves down the wall. A vortex of spinning air with low overpressures at its centre will then form at the corner, thus further decreasing the pressure in this region. In the stage shown in Figure 4.8b the pressure at the lower part of the front wall is still  $p_0 + P_r$  while the upper part has a pressure similar to that in the incident wave. As the shock wave reaches the back wall of the structure, the shock wave diffracts around the corner (Figure 4.8c) and a second vortex is formed. The pressure on the back wall behind this diffracted shock front is somewhat less than  $p_0 + P_s$  while the pressure in front of it is equal to the ambient pressure  $p_0$ ; at the roof the pressure is still close to  $p_0 + P_s$ . At the front wall, the rarefaction wave has negated the reflected wave and the pressure is now  $p_0 + q$ , where  $q$  is the dynamic pressure.



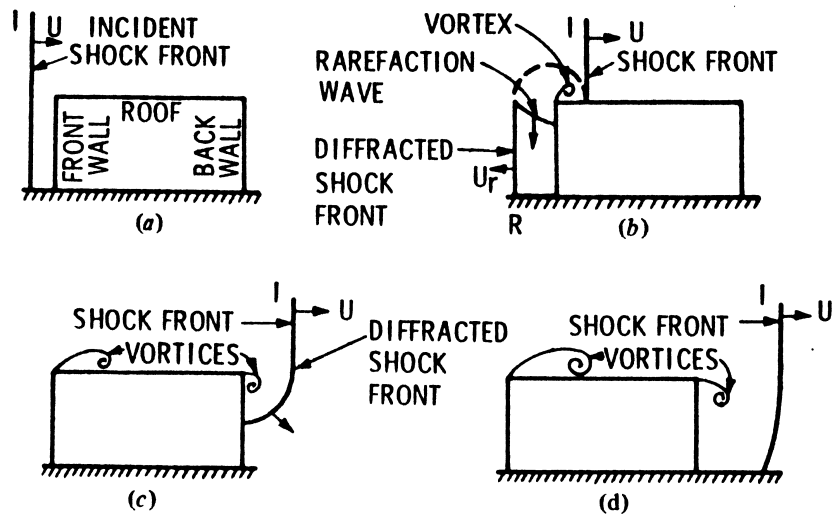


Figure 4.8 Diffraction of shock front over a two-dimensional structure. From Baker (1973).

The behaviour described above will depend on the geometrical dimensions of the solid object. If the width of the object is large, the rarefaction wave may have negated the reflected wave before the shock front reaches the back wall, *etc.* Diffraction is, of course, also valid for a three-dimensional structure. In this case the shock wave can also diffract at the sides of the structure.

#### 4.3.4 Pressure-time relation used in finite element analyses

From Sections 4.3.2 and 4.3.3 it is clear that it is very complicated to determine a correct pressure-time relation for various parts of a real structure; apart from the difficulty of taking into account different reflections, the load also depends on the structure's geometry. Therefore, certain simplifications have been necessary in the study. As quoted in Section 4.3.1 the Swedish Shelter Regulations clearly state that the weapon load chosen corresponds to that of an explosion in free air where the pressure release is free. Thus, the interpretation made was that reflection from the ground could be neglected. This may also hold true for the diffraction. Nevertheless, the following reasoning was used to justify the disregard of the diffraction effect. The analyses carried out only model a single strip of the shelter. This approximation should be appropriate if the out-of-plane length of the shelter is large enough and the bearing capacity in the transverse direction can be neglected. In this way the problem with diffraction at the end walls can be avoided. This would also be the case with the diffraction at the front wall if the wall is high enough, i.e., a building is on top of the shelter. Therefore, the shelter subjected to a blast load was assumed to have some kind of

light structure (i.e., wooden building) on top which would delay the diffraction in such a way that it can be neglected. With these approximations the pressure-time relation can be calculated according to the equations given in Section 4.3.1.

For a charge of 125 kg TNT (250 kg bomb with 50 weight percent TNT) exploding at a distance of 5 metres, ConWep (1992) gives blast parameters as shown in Table 2.1. Hereby, the factor  $\alpha$  in equation (4.5) can be determined for the reflected wave ( $\alpha = 15.00$ ) and the pressure-time relation for the positive phase be expressed according to equation (4.4). The result is shown in Paper III, and from this it can be seen that the pressure decreases very rapidly from a value of about 5 MPa at the time of arrival to a pressure of 22 kPa after just 3 ms. The approximated pressure-time relation used in the finite element analyses leads to a somewhat increased impulse intensity of about 6%. However, this approximation is believed to be negligible compared to other uncertainties in the blast analyses.

## 4.4 Impact load

A shelter may be exposed to falling masses as a result of weapon impact on a nearby building. Therefore, it must be designed to withstand such a load. However, as is the case with the weapon load, an impact load is a complicated dynamic load case, and consequently, it is not realistic for a designer to use such a load in the design of a civil defence shelter. Therefore, when revising the regulations in the 1970s there was a demand for an expression of an equivalent static load that could be used in the design process. An early approach for such a static load was presented by Hallgren and Granström (1975) and further simplified by Hallgren and Granström (1977). After this, some minor changes have been made and the equivalent static load given in the present Swedish Shelter Regulations, Swedish Rescue Service Agencies (1998), is now expressed as

$$q_{\text{impact}} = 1.4 \cdot m \cdot \sqrt{h_t} \quad (4.7)$$

where  $m$  is the dead weight per square meter of the building above the shelter (units given in  $\text{kN/m}^2$ ) and  $h_t$  is the distance from the centre point of this building to the top of the shelter. The expression given in equation (4.7) is based on an SDOF system where the following assumptions are made:

- the behaviour of the structure is fully plastic;
- plastic impact between falling mass and shelter roof;
- the falling mass hit the shelter roof with a constant amount per time unit.

Other important assumptions made are, for example, that all the impact energy dissipates due to bending and that the active time, i.e. the time it takes for all the mass to hit the shelter, is set to 0.5 s. Hallgren and Granström (1977) stated that the latter assumption probably is somewhat optimistic but that this to a large degree should be compensated by the former, that no energy is consumed due to crushing or shear at the supports. Apart from the work by Hallgren and Granström, the derivation of this expression may also be found in Johansson (1999b). Impact loading due to falling masses has experimentally and theoretically been examined by, for example, Sundquist (1977, 1978, 1979) and Andersson (1985, 1987a, b).

The collapse sequence of the building, assumed in the derivation of equation (4.7), starts at the top and proceeds downward, thus dragging the underlying floors along in its fall; see Figure 4.9. The top floor slab is assumed to start falling with an initial velocity of zero and accelerate until it hits the underlying floor. Its movement is then decreased due to plastic impact and breaking of the slab hit. The two slabs then continue to fall down with a velocity corresponding to the reduced kinetic energy. This process is repeated until the roof of the shelter is reached. Assuming plastic impact between the impacting floors, the kinetic energy of the falling mass just prior to its impact with the shelter roof may be expressed as

$$E_{impact} = M_{tot} gH \cdot \frac{1}{n^3} \sum_{i=1}^n i^2 - E_B \frac{n^2 + n + 2}{2n} \quad (4.8)$$

where  $M_{tot}$  is the total falling mass of the building above the shelter,  $g$  is gravity,  $H$  is the total height of the building above the shelter roof,  $n$  is the number of floors and  $E_B$  is the energy needed to break one floor slab in the collapsing building. A derivation of this expression can be found in, for instance, Hallgren and Granström (1977) or Andersson (1985). Due to uncertainty about the capacity of each floor slab, though, the energy term  $E_B$  was set to zero when determining the impact velocity  $v_{impact}$  in the finite element analyses, and it could then be determined as (given  $n = 3$  and  $H = 9$  m)

$$v_{impact} = \sqrt{\frac{2 \cdot E_{impact}}{M_{tot}}} = \sqrt{2gH \cdot \frac{1}{n^3} \sum_{i=1}^n i^2} = 9.6 \text{ m/s} \quad (4.9)$$

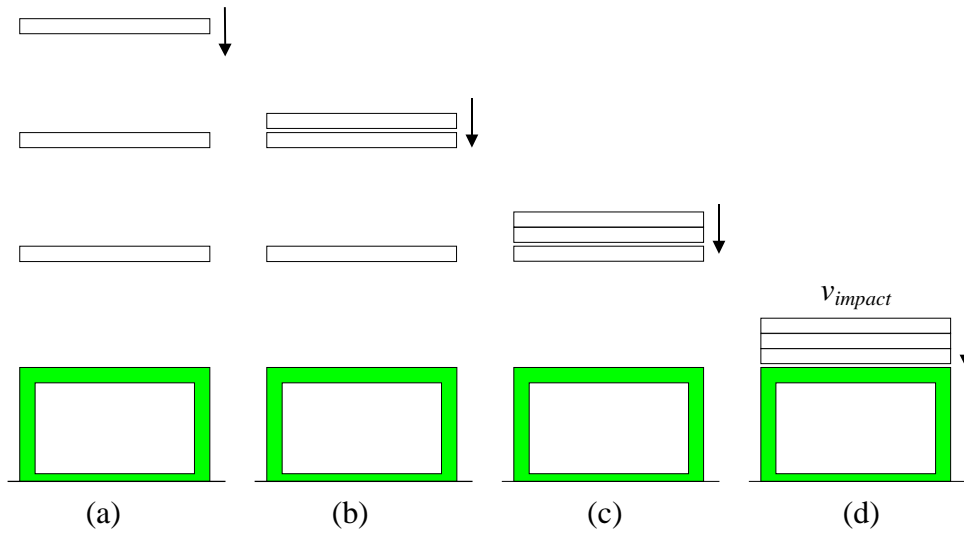
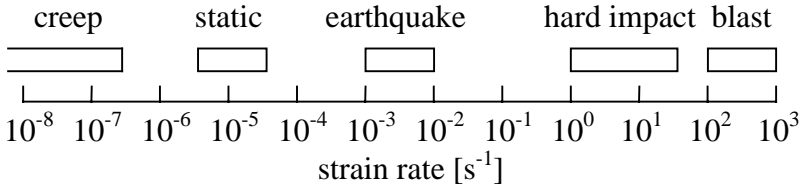


Figure 4.9 Schematic description of collapse sequence assumed: (a) the third floor starts to fall with zero initial velocity; (b) third floor is about to hit second floor; (c) after plastic impact between third and second floor they continue downward to first floor; (d) all three floors falling with the same velocity just before hitting the shelter roof.



## 5.2 Testing at high strain rates

It is commonly accepted that the mechanical properties of concrete are affected by the rate of loading. Several researchers have examined the magnitude of the dynamic increase factor (DIF), i.e. the ratio between the dynamic strength and static strength, for different strain rates and it has been found that an increased strain rate also results in an increased material strength; see Figures 5.2 and 5.3. The large scatter in these figures, though, clearly indicates the considerable difficulties present when the influence of the strain rate is to be determined. According to Bischoff and Perry (1991) the kind of dynamic testing necessary is much more complicated to carry out and evaluate than similar static tests. Therefore, it is also more important to consider what influence different parameters may have on the test results. Hence, the large scatter shown in Figures 5.2 and 5.3 can at least partially be explained by a mixed usage of important parameters such as: concrete strength, specimen dimension, moisture content and test method. Further, the evaluations of the test results have not been made similarly. Therefore, Bischoff and Perry conclude that the results summarised in Figure 5.2 are not necessarily comparable with each other, and that such results therefore have to be interpreted with great care since they depend on both the test method and the evaluation method.

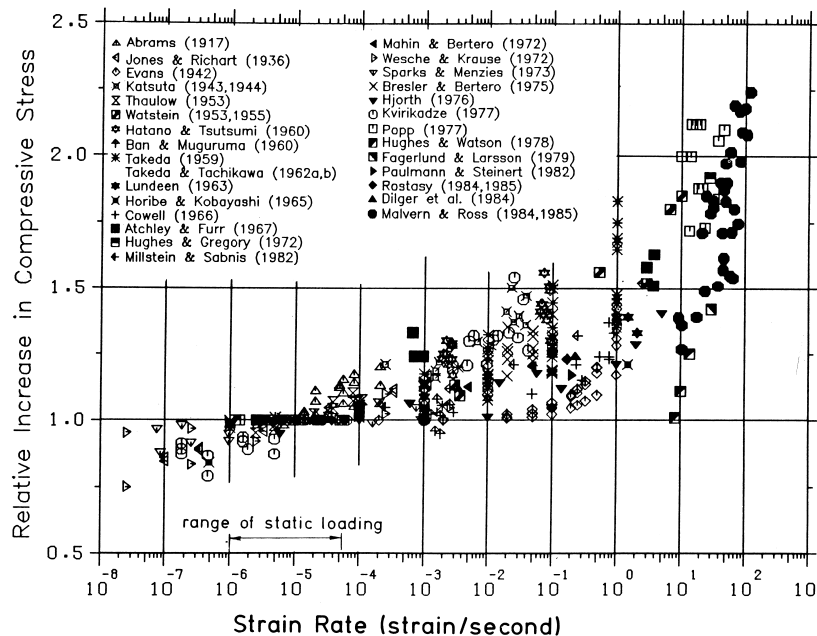


Figure 5.2 Strain rate effect on the compressive strength of concrete. From Bischoff and Perry (1991).

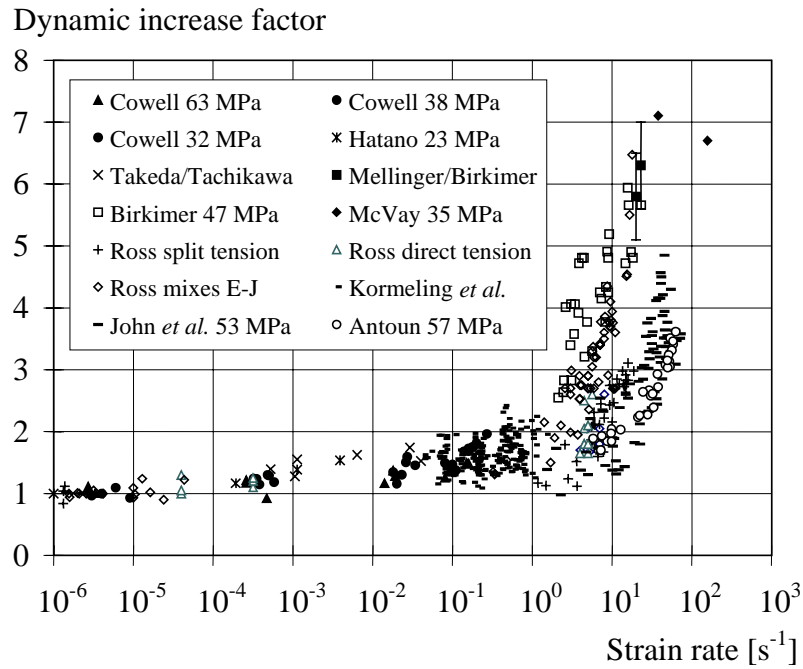


Figure 5.3 Strain rate effect on the concrete tensile strength. Based on Malvar and Ross (1998).

As an example of the difficulties encountered when evaluating dynamic test results, Figure 5.4 shows the load-time relations of concrete prisms subjected to shear where the load was measured at both the top and bottom of the specimens; see Chung (1978). From this it is clear that there is a difference in load registered at the upper and lower load cells. This is due to the inclusion of inertia forces in the load system, and because it takes a certain time for the compressive wave to travel through the specimen. Hence, a certain amount of load (depending on what strain rate is used) will be applied at the top of the specimen before the information from the middle part of the prism reaches the upper part, “informing” it of the specimen’s failure. Consequently, the load registered in the top load cell is not representative for the capacity of the prism; instead it is the load cell at the bottom that represents the true material capacity. From this Bischoff and Perry conclude that the influence of the inertia forces can be minimised by positioning the load cell at the specimen side opposite to that of loading.

Further, when evaluating a dynamic test it is important to be aware that a travelling wave is transmitted and reflected each time it reaches a new material and/or different cross-section. Depending on the test set-up, this may result in the original compressive wave soon being divided into a complicated series of stress waves that bounce back and forth in the specimen, making it difficult to evaluate the test results obtained. Figure 5.5 shows a schematic view from Hughes and Gregory (1972) of how a compressive wave is diverted into a complicated series of tensile and compressive waves. Hence, it is important to account for the wave

propagation in a structure in the evaluation of dynamic test results; if not, such diversions may considerably affect the final conclusions. However, according to Hughes and Gregory the problem can be solved by using a load column that is long enough, so that the reflected wave does not reach the specimen again until failure is already achieved. This is also a technique that is used in the so-called Split-Hopkinson bar as described by, for instance, Reinhardt *et al.* (1985).

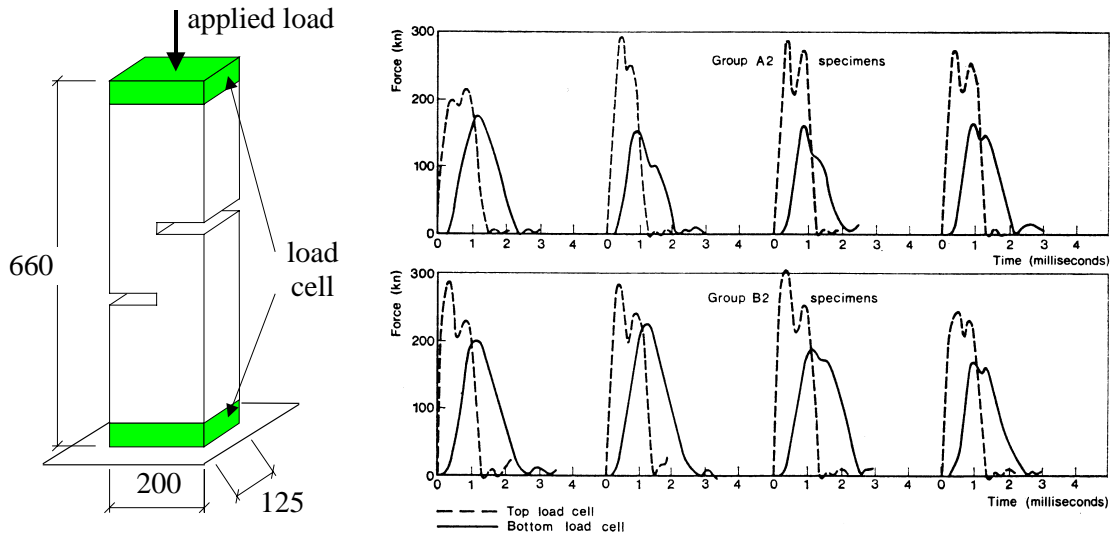


Figure 5.4 Typical load-time relations for shear-loaded concrete prism at a strain rate of  $\dot{\epsilon} \approx 0.3 \text{ s}^{-1}$ . From Chung (1978).

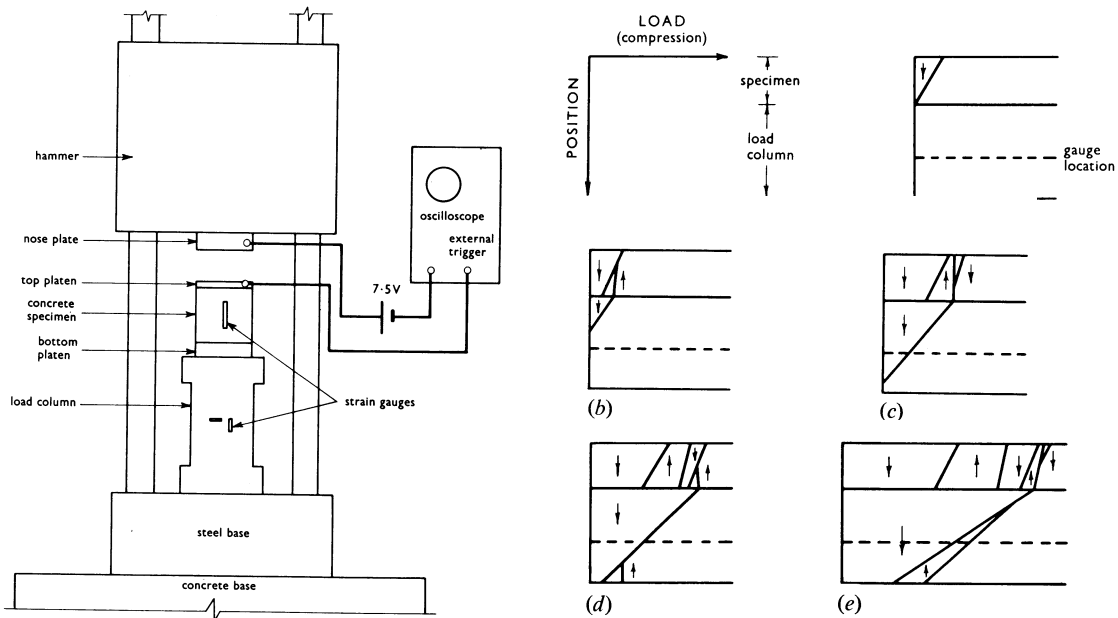


Figure 5.5 Schematic view of the diversion of a compressive wave into a complicated series of tensile and compressive waves bouncing back and forth.



### 5.3 Strain rate influence of concrete strength

Various researchers have proposed expressions that try to describe how the concrete strength depends on the strain rate. Such proposals for concrete in compression have, for instance, been made by Seabold (1970), Dilger *et al.* (1984), Soroushian *et al.* (1986) and the CEB-FIP Model Code, CEB (1993); proposals for concrete in tension can, for example, be found in CEB (1993), Ross *et al.* (1996), and Malvar and Ross (1998). These expressions, though, differ considerably as to appearance, and in some cases also as to what properties they depend on. The expressions reported in Seabold, Dilger and Soroushian *et al.* just give a DIF as a function of the strain rate; the latter, though, differs between wet and dry concrete (i.e. concrete that has been prevented from drying out and whose micropores thereby contain free water). Ross *et al.* proposed a more complicated expression that takes into account parameters such as the fracture toughness and compressive strength of the concrete. However, perhaps the most accepted relations are those presented in the CEB-FIP Model Code where the DIF of concrete in both tension and compression is related to its static compressive strength. The expression proposed by Malvar and Ross for concrete in tension is also an improvement of that in the Model Code. The different proposals mentioned above are compared in Figures 5.6 and 5.7. From these it is also clear that there is uncertainty about what effect the strain rate has. Further comparisons are thus hereafter made with the expressions given in CEB (1993) and Malvar and Ross (1998).

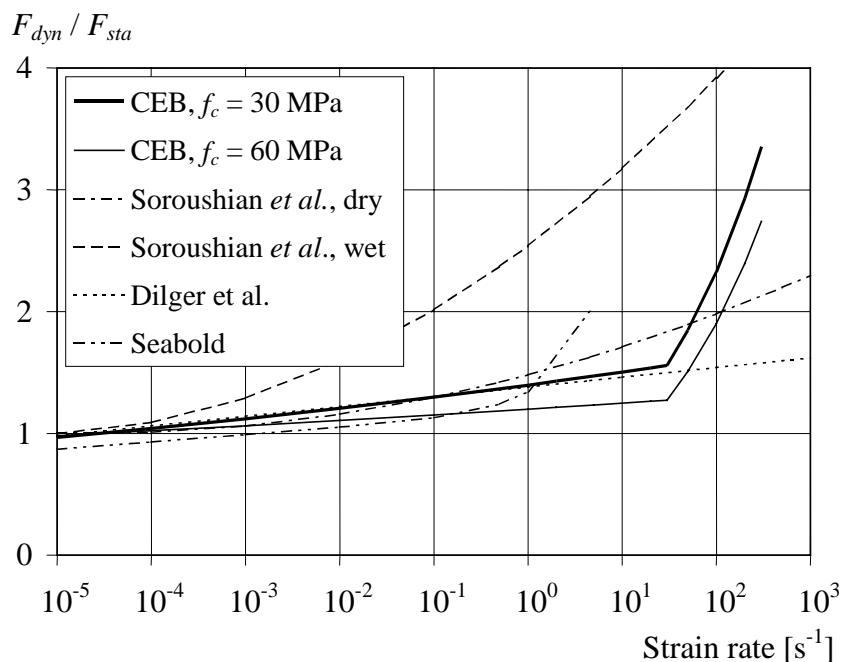


Figure 5.6 Comparison of DIF-strain rate relations for concrete in compression, given in the literature.

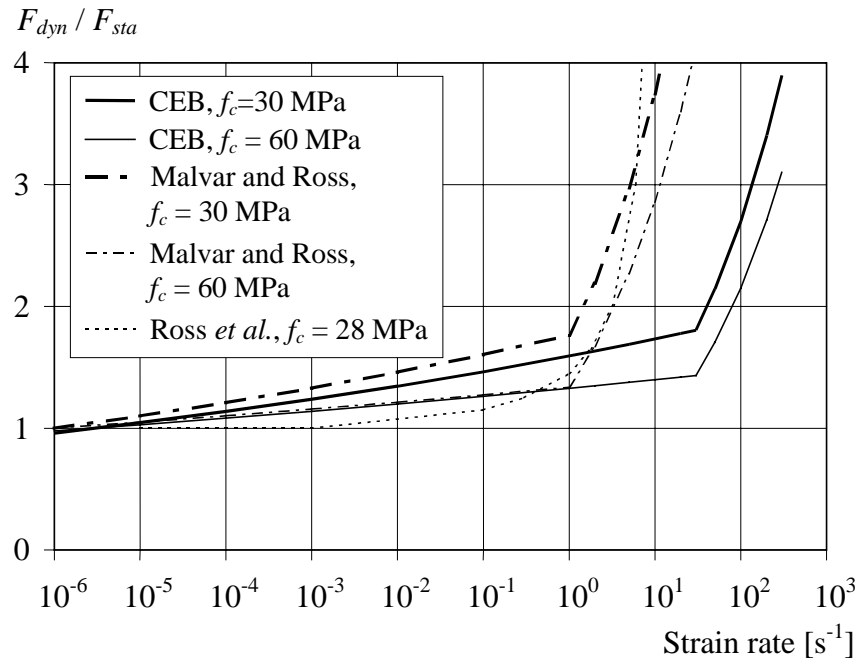


Figure 5.7 Comparison of DIF-strain rate relations for concrete in tension, given in the literature.

## 5.4 Possible explanations for the increase in concrete strength

### 5.4.1 Characterisation of strain rate effects

The strain rate effect in concrete can, somewhat simplified, be divided into two different kinds: viscous and structural effects. The former, which leads to relatively moderate strength enhancements at increased strain rate, can be said to occur at strain rates up to the so-called transition zone; see Figure 5.8. A commonly accepted theory is that this increase is largely due to the presence of free water in the concrete micropores, see further in Section 5.4.2. Since this is also an explanation that the author supports, it is treated in somewhat more detail herein. At strain rates above that of the transition zone the strength increase is more dramatic because structural effects, i.e. inertia and confinement, dominate the dynamic strength contribution. This is further discussed in Section 5.4.3.

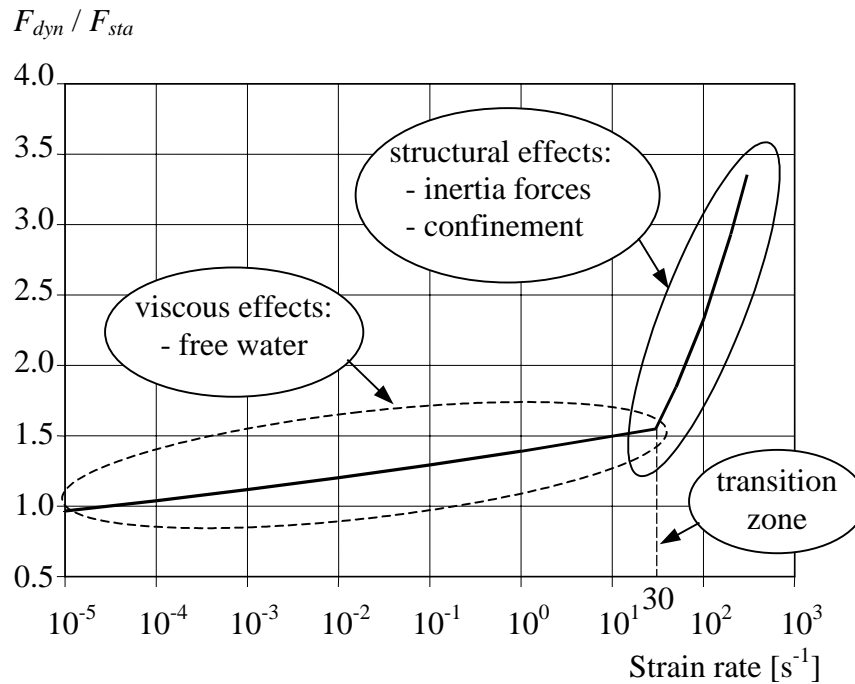


Figure 5.8 Schematic view of the strain rates at which the viscous and structural effects, respectively, are dominant.

### 5.4.2 Viscous effects

It is commonly accepted that the non-linearity of the concrete decreases with increasing strain rate. According to Zielinski *et al.* (1981) this is due to the difference in crack propagation obtained at higher load rates compared to that of static loading. When the load is applied slowly, it is possible for the cracks to propagate in a way that demands lower energy consumption. Hence, it is possible for the cracks to pass around strong aggregates and form in the weaker zones. However, at high strain rates, when a large amount of energy is introduced in the specimen during a very short period of time, this is no longer possible to the same extent. Instead, the cracks are forced to take a shorter route and propagate through stronger zones which, if loaded at lower strain rates, it would otherwise have avoided. Consequently, the crack propagation will also differ from that in a static case as schematically shown in Figure 5.9. If the load velocity is high enough, the cracks may even propagate through the aggregates instead of through weaker cement paste; see Rossi (1991a). Thereby, the material homogeneity increases, which results in a stiffer behaviour and higher strength of the concrete. This failure mode is similar to that obtained in static testing of high-strength concrete, e.g. by Claeson (1998). Therefore, it is tempting to compare the behaviour of normal-strength concrete subjected to high strain rates with that of statically loaded high-

strength concrete. In both cases the cracks may propagate through the aggregates and the material's non-linearity is quite restricted before maximum strength. This thought is also supported by Zielinski (1982) and Taerwe (1993) who state that “a fast-moving crack may grow more easily through stronger zones of material” and “the smoothness of the fracture surface is mainly related to the speed of crack propagation”, respectively. Further, Zielinski has shown that multiple fracture zones are possible at high strain rates, resulting in higher energy consumption during the fracture process. This can then, as schematically shown in Figure 5.10, also lead to larger strains and increased strength compared to that of static tests.

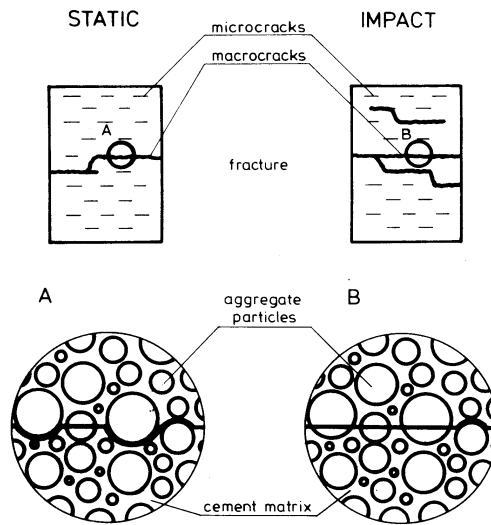


Figure 5.9 Schematic difference in crack propagation of specimen loaded in tension during static or impact conditions. From Zielinski (1982).

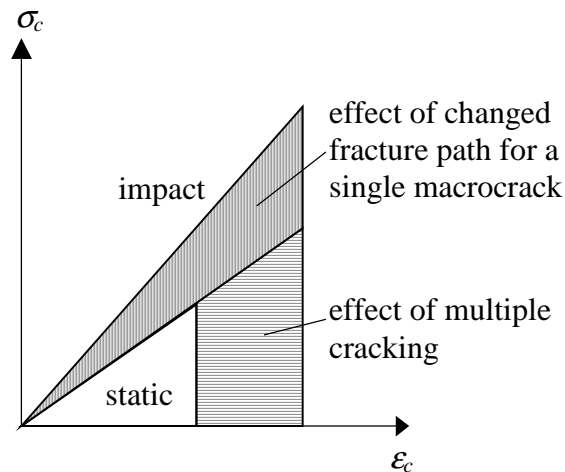


Figure 5.10 Schematic view of the fracture mechanism's influence on the stress-strain relation for concrete in tension. Based on Zielinski (1982).

The relations presented by Soroushian *et al.* in Figure 5.6 indicate that wet concrete, i.e. concrete that has been prevented from drying out and whose micropores thereby contain free water, is more sensitive to high strain rates than dry concrete. This observation agrees well with those by other researchers, e.g. Kaplan (1980), Reinhardt *et al.* (1990) and Rossi *et al.* (1994). They suggest that the fundamental cause of changed crack propagation, and thus higher strength and stiffness, observed in concrete at high strain rates is the presence of free water in the micropores of the concrete.

Reinhardt *et al.* (1990) present the results from a pilot test series in which the effects of high strain rate are examined for concrete in tension. Twenty cylindrical specimens ( $\phi 74 \times 100$  mm) were cast using a so-called micro concrete with a maximum aggregate size of 2 mm. Seven days after casting the specimens were demoulded. Half of them were then prevented from drying and the other ten were dried in an oven at 105°C for five days. Hereby, the relative humidity of the wet and dry specimens was more or less 100% and 0%, respectively, at the day of testing. The specimens were tested in a Split-Hopkinson bar at strain rates between 0.50 and 1.25 s<sup>-1</sup> and it was found that the capacity of the wet specimens was very sensitive to the strain rate while the dry ones remained unaffected. In a continuous study of the above, Rossi *et al.* (1994) examined the behaviour of more “normal” concrete using a maximum aggregate size of 10 mm. The dimensions of the specimens were the same but the dry specimens were now oven-dried for three weeks. Further, the influence of different water-cement ratios (w/c ratios) was examined in the wet specimens. The results of this study are summarised in Figures 5.11 and 5.12, from which it is also clear that wet concrete is far more sensitive to high strain rates than dry concrete. However, as distinct from the observations made by Reinhardt *et al.* with the micro concrete, the dry concrete here showed a certain sensitivity to the strain rate. Rossi *et al.* give three possible explanations for this: it might be due to a physical phenomenon other than the presence of free water; inertia forces can possibly affect the results obtained from the Hopkinson bar; and finally, the dry specimens probably cannot be regarded as totally dried out since this would demand a very large amount of energy. The last hypothesis was also confirmed in tests on specimens that had been dried for one week only. From Figure 5.11 it can also be seen that the influence of the strain rate increases with increased value of the w/c ratio. However, a closer look reveals that the absolute increase in strength (i.e.  $f_{t,dyn} - f_{t,sta}$ ) was more or less independent of the w/c ratio of the concrete; see Figure 5.12. These results are also useful when comparing the strain rate sensitivity of concrete of different static strength as discussed in Section 5.5.

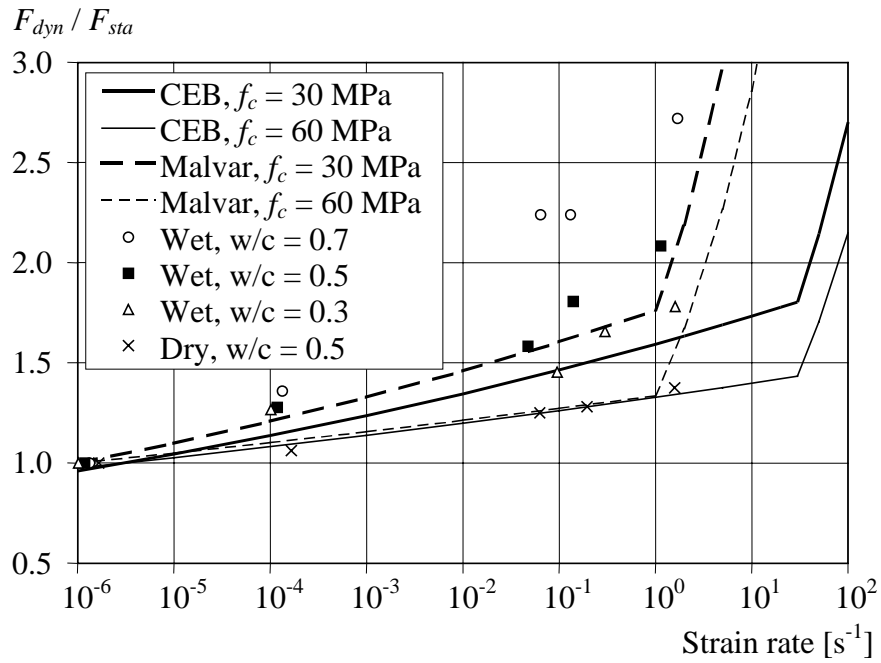


Figure 5.11 Influence of strain rate on the tensile strength for wet and dry concrete when the w/c ratio is varied. Each point represents an average of between six and eleven tests. Based on test data presented in Rossi *et al.* (1994).

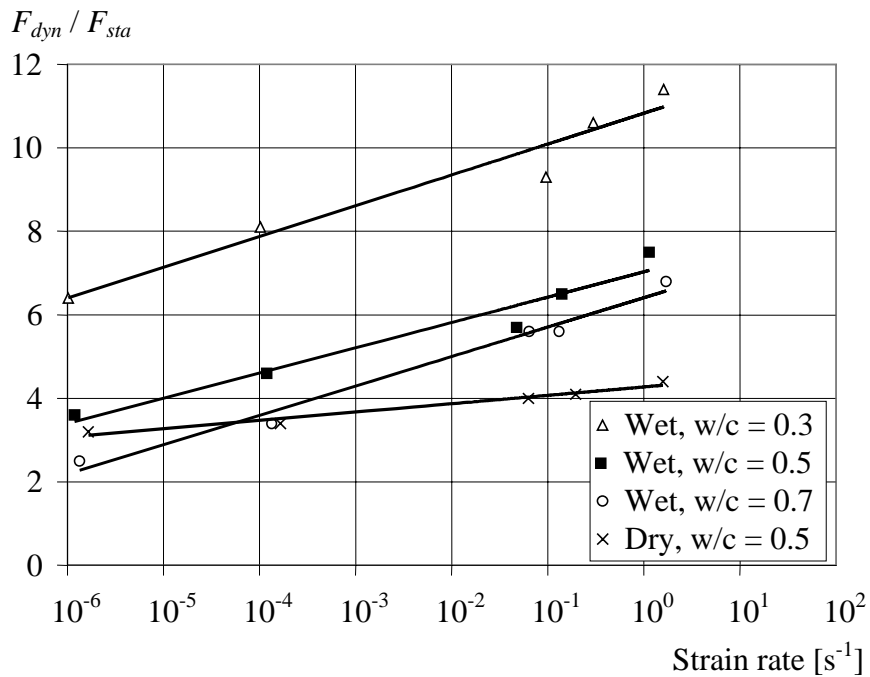


Figure 5.12 Difference in concrete tensile strength at various strain rates and w/c ratios. The continuous lines are logarithmic regressions. Based on test data presented in Rossi *et al.* (1994).

Kaplan (1980) explains that a probable reason for the influence of the moisture content at high strain rate is the presence of free water in the concrete micropores. When a concrete specimen is loaded in compression the pores tend to close, thus forcing any water present to move within the specimen. This movement gives rise to an inner pressure which depends on the pore size, the amount of free water in the pore and the closing speed of the pore. Such an internal pressure may help the solid phase of the concrete to resist the external force, thus delaying the crack initiation so that a higher compressive strength is obtained. A similar hypothesis is proposed in Rossi (1991a) to describe the physical cause of increased tensile strength. Rossi explains that a possible physical explanation can be found by the use of the so-called Stéfán effect. Simplified, it can be said that the presence of a thin viscous film (e.g. water) trapped between two plane and parallel plates that move apart gives rise to a resisting force. In a concrete structure the walls of the micropores can be approximated as such plates and, when a tensile force tries to open the pore, a counteracting force  $F_s$  arises that hinders the separation. Accordingly, the influence of free water within the concrete micropores strengthens the cement paste, making it so strong that cracks may propagate through the aggregates rather than in the normally weaker zones of the cement matrix; see Rossi (1991b). Consequently, a larger external force is needed which results in a higher strength. Thus, even though not explaining the strain rate phenomenon in exactly the same way, the statements of Zielinski and Rossi and co-workers can in a sense still be regarded as rather similar. They all agree that the geometry of the fracture plane changes with increasing strain rate, i.e. leading to aggregate fracture instead of fracture in the weaker cement paste.

The resisting force  $F_s$  due to the Stéfán effect can, according to Rossi, be expressed as

$$F_s = \frac{3\eta V^2}{2\pi h^5} \dot{h} \quad (5.1)$$

where  $\eta$  is the liquid viscosity,  $V$  is its volume,  $h$  is the initial distance between the two plates that separate and  $\dot{h}$  is the velocity of separation. However, Rossi emphasises that this expression not should be used to determine the value of  $F_s$  but just be regarded as an explanatory model to simplify the understanding of what happens in the concrete. If used thus, it can also be seen from the expression that the size of the pore has a considerably larger effect than the amount of free water, and that the restraining force is proportional to the velocity of separation.

It is highly interesting to note that Han (1996) makes use of the same explanations in his thesis about long-term effects in high-strength concrete. This indicates that it is the same phenomenon that causes the change in concrete strength for both long-time loading and loading at very high strain rates. Both phenomena described above will have a positive effect on the concrete strength in compression. In tension, though, only the Stéfán effect influences the change in strength, which according to Han means that the strain rate effect in absolute terms will also have a larger effect for concrete in compression than in tension. This is opposite to a common opinion in the literature, e.g. CEB (1993) and Ross *et al.* (1995), that the strain rate sensitivity is higher for concrete in tension than it is for concrete in compression. However, this is probably due to different definitions of “sensitivity”. The absolute increase at high strain rates is undoubtedly higher in compression, but due to the comparably low static tensile strength its *relative* strength increase (i.e. DIF) is higher in tension than in compression; see also Figure 5.12.

### 5.4.3 Structural effects

The summarised test results presented in Figures 5.2 and 5.3 indicate that there is a sudden increase in concrete strength with increasing strain rate at a certain critical strain rate. Of the expressions discussed in Section 5.3 and shown in Figures 5.6 and 5.7 only those of CEB (1993), Ross *et al.* (1996) and Malvar and Ross (1998) try to take this so-called transition zone into account. According to CEB this occurs at a strain rate of  $30 \text{ s}^{-1}$  for concrete in both tension or compression. Ross *et al.*, though, differ between these two stress cases and state that the transition zone for dry concrete in tension occurs somewhere in the interval of 1 to  $10 \text{ s}^{-1}$  while the corresponding strain rates for concrete in compression are 60 to  $80 \text{ s}^{-1}$ . This use of different transition zones for concrete in tension and compression corresponds better to the observations made in tests; compare Figures 5.2 and 5.3. This also suggests that the location of the transition zone given in CEB is not valid; a change by a factor of ten, so it appears at a strain rate of about  $3 \text{ s}^{-1}$ , seems more reasonable. This is why Malvar and Ross (1998) proposed a modification to the CEB expression for concrete in tension, in which the transition zone was set to occur at a strain rate of  $1 \text{ s}^{-1}$ . However, none of these references tries to give any physical explanation for why this sudden increase occurs at all.

Rossi and Toutlemonde (1996), though, state that the increase in tensile strength up to a strain rate of about  $1 \text{ s}^{-1}$  is due to the viscous effects described by the Stéfán model. After this, the inertia forces are no longer negligible and at a strain rate higher than  $10 \text{ s}^{-1}$  their contribution



is dominating. This statement is also supported by findings of Weerheijm (1992), who developed a model based on linear elastic fracture mechanics to study the strain rate effect on concrete tensile strength. Using this he was able to show that the steep increase in strength obtained at high strain rates is caused by changed stress and energy distribution due to inertia effects around the concrete crack tips. Hence, this phenomenon is not a material effect but a structural response and its effect should therefore not be included in the constitutive model in, for example, a finite element code. This may be true if the modelling treats aggregates and cement paste as separate elements. However, if the concrete for instance is approximated as a homogeneous material, something that is commonly assumed when modelling concrete structures, this is not the case. Therefore, as argued by Malvar and Ross (1999), if the numerical model used is unable to take this inertia phenomenon into account automatically, then the steep increase still has to be considered in the material model used.

Whether this explanation about the effect of the inertia forces at the crack tips can be used for concrete in compression too is not entirely clear, even though it seems quite reasonable since the compressive failure also is governed by cracking. Bischoff and Perry (1991), however, reason that the sudden increase for concrete in compression is due to inertia confinement effects. When the concrete is loaded sufficiently fast, it will not have time to react and a stress state similar to that of plain strain is obtained, thus resulting in a substantial increase in strength because of the multiaxial stress state. The presence and influence of such inertia confinement were also shown in finite element analyses of concrete specimens loaded in compression at strain rates ranging from 300 to 700 s<sup>-1</sup>, by Georgin *et al.* (1998). The effect of confinement due to high strain rates has also been shown in Johansson (1999a).

## **5.5 Effect of concrete strength on strain rate sensitivity**

From the above it is evident that the presence of free water, in combination with the size of the concrete micropores, greatly affects the strain rate sensitivity of the concrete. Generally, it can be said that high-strength concrete has a finer pore system but also contains a lower amount of free water. However, according to Han (1996), the relation between amount of free water and size of the pore structure of such concrete is higher than it is in concrete with lower strength; thus, the higher the strength of the concrete, the higher the strain rate sensitivity should be. Figure 5.13 compares the influence of strain rate (sustained and static loading) for concrete in compression with static strengths of about 28 kN and 95 kN, respectively. These results indicate that high-strength concrete obtains a relatively large contribution from the

internal pore pressure due to free water even for strain rates corresponding to that of static loading; the capacity of the normal-strength concrete, though, is more or less unaffected. The reason is that the micropores in the stronger concrete are so small that the movement of free water even for very low strain rates results in a substantial contribution to the total strength. For the normal-strength concrete, though, the amount of free water in relation to the size of the micropores is so low that its contribution is still negligible. Based on this, it can be concluded that a part of the static strength for concrete of higher strength is made up of contributions from the viscous effects in the material's micropores. Hence, a part of this potential “reserve” in strength has already been used before the strain rate even has passed that corresponding to static loading.

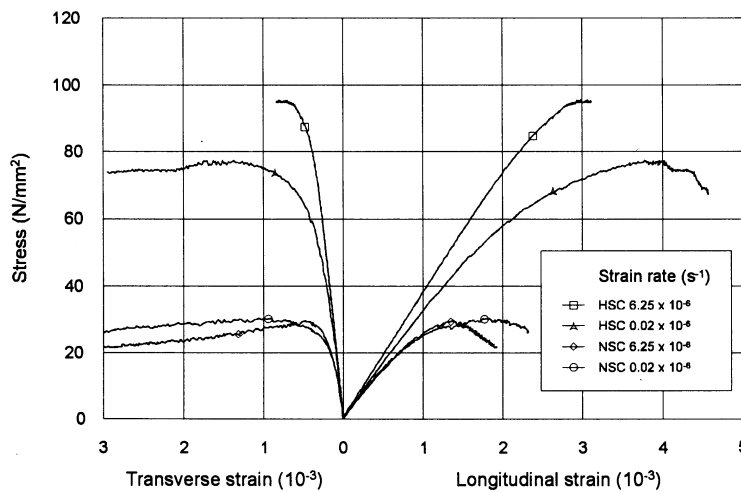


Figure 5.13 Comparison of stress-strain relations obtained for concrete of different strengths when the strain rate is varied. The strain rates given refer to the transverse strain rate where the higher value corresponds to static loading. From Han (1996).

Nevertheless, at sufficiently high strain rates the presence of free water also affects the strength of normal-strength concrete. This contribution, according to the results obtained by Rossi *et al.* (1994) as shown in Figure 5.11, is approximately the same independently of the static strength of the concrete. Compared with the static strength, though, the strain rate sensitivity will increase with decreasing static strength. This idea corresponds well with the expressions presented in CEB (1993) where the static strength of the concrete is taken into account. As shown in Figures 5.6 and 5.7 the increase in strength due to strain rate is higher for low-strength concrete. However, in absolute terms, the increase is more or less the same in both tension and compression, respectively; see Figure 5.14.

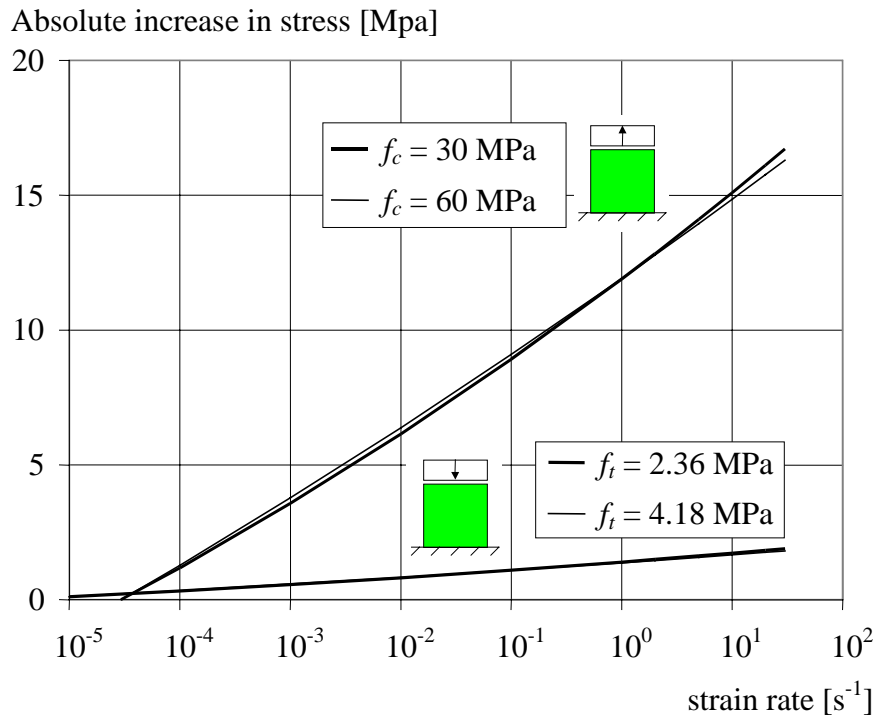


Figure 5.14 Contribution of strength due to strain rate effects lower than  $30 \text{ s}^{-1}$  for different concrete strengths. According to CEB (1993).

The conclusions drawn above, regarding what influence the static strength has on the strain rate sensitivity, are not supported by everyone. Bischoff and Perry (1992) state, in their summary of the strain rate influence of compressive strength, that many researchers concluded that concrete of high static strength is less sensitive to high strain rates. However, they also point out that they do not agree that their summary indicates that this would be the case. Based on the results presented in Figure 5.12 it still seems reasonable to take into account the static strength of the concrete, as is done in CEB (1993) and Malvar and Ross (1998), when determining what influence high strain rates have.

As discussed in Section 5.4.3 the transition zone, i.e. the steep increase in strength, for concrete in tension appears at a strain rate that is approximately ten times lower than that for compressed concrete. It was concluded that the reason for this phenomenon was the influence of inertia forces within the material. The inertia effects will be negligible until such high strain rates are reached that the inertia forces within the concrete at least attain a value reasonably close to that of the static strength. Evidently, the lower the value these forces have to attain the lower is the required strain rate, and accordingly inertia effects should influence low-strength concrete earlier than high-strength concrete. Based on this reasoning, it is the author's belief that the static strength also affects the strain rate at which the transition zone appears. Apart

from the apparent difference in positioning of the transition zone for concrete in tension and compression, this thought is also supported by calculations made by Weerheijm as shown in Figure 5.15 and by the author using a SDOF model; see Johansson (1999a). Weerheijm examined the strain rate sensitivity for concrete of different strengths (tensile strength equal to 2.98 and 1.63 MPa for Mixes A and B, respectively) and whether the fracture energy was rate-dependent or not. Here the dynamic increase factor is shown as a function of the stress rate. However, the Young's modulus used was in the range of about 31 to 34 GPa; thus, a stress rate of 1 GPa/s corresponds to a strain rate of about  $30 \text{ s}^{-1}$ .

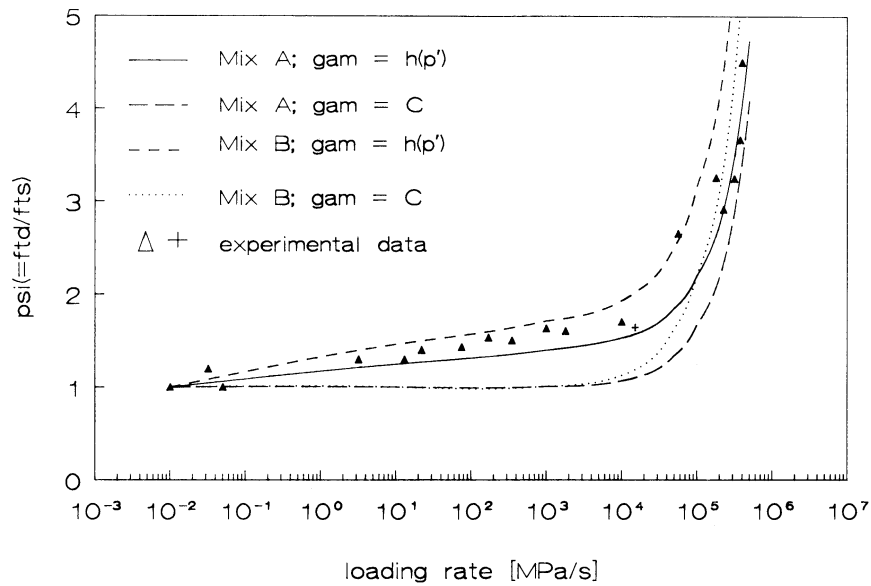


Figure 5.15 Predicted rate effect for different concrete qualities subjected to tension, with and without use of rate-dependent fracture energy ( $\text{gam} = h(p')$  and  $\text{gam} = C$ , respectively). Based on Weerheijm (1992).

## 5.6 Effect of strain rate on other material parameters

As with the strength, the strain rate also affects the concrete Young's modulus even though its influence on the latter is not as large as that of the strength. Rossi and Toutlemonde explain that this is because the viscous effects described above do not affect the concrete aggregates and, since these have the greatest importance for the value of the Young's modulus, a lower sensitivity is obtained. Nevertheless, Reinhardt (1982) and Rossi *et al.* (1992) state that the rate sensitivity of Young's modulus increases with increased value of the w/c ratio. A high value of w/c can be interpreted as concrete of low strength, which suggests that the static strength perhaps would affect the strain rate sensitivity of Young's modulus. However, no

such consideration is taken in either CEB (1993) or Soroushian *et al.* (1986). The strain rate effect according to these references is compared in Figure 5.16a; the former differs between the sensitivities in compression and tension. To the author's knowledge, there are no reports in the literature stating that either of them exhibits a transition zone where the influence of the strain rate suddenly increases.

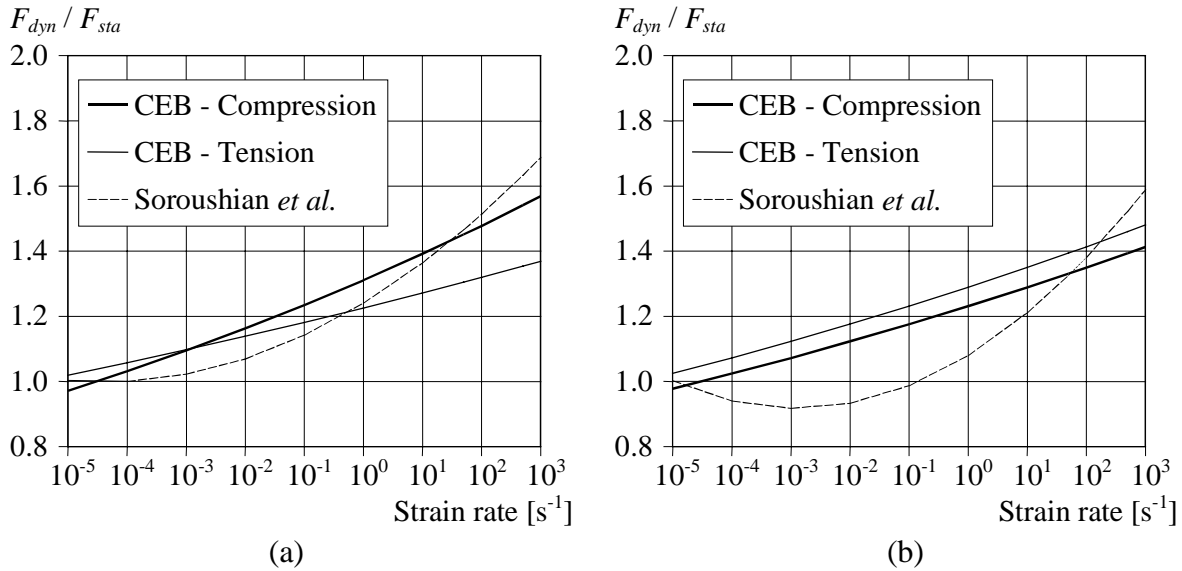


Figure 5.16 Influence of strain rate on: (a) Young's modulus, (b) strain at maximum stress. Based on CEB (1988, 1993) and Soroushian *et al.* (1986). The former differs between the rate sensitivities of concrete in compression and tension.

The strain rate effect on the strain at maximum stress is according to Bischoff and Perry (1991), unclear. In their summary of results reported in the literature they found contradictory test results, stating that the strain at maximum stress may both increase and decrease with increasing strain rate. Nevertheless, Bischoff and Perry think that the results indicate that the strain does increase with increasing strain rate. The expressions given by CEB Bulletin d'Information No 187, CEB (1988), and Soroushian *et al.* are presented in Figure 5.16b; none of the expressions take the static strength into account.

How the fracture energy changes with increasing strain rate has not been examined to a large degree, even though Ulfkjaer *et al.* (1996) state that it does increase at higher strain rates. This is also supported by CEB (1988) which gives an expression based on the velocity of the crack opening. Weerheijm (1992), though, states that this is not the case. Instead, the increase in deformation capacity and fracture energy observed in tests is due to multiple fracture and

failure zones. Hence, according to this, the strain rate effect on fracture energy should be a structural effect and not part of the material behaviour itself.

The research carried out on what influence high strain rates have on the bond strength is very limited. However, Vos and Reinhardt (1980) and Yan and Mindess (1998) have shown that the bond strength increases with increasing strain rates. Based on these, Malvar (1997) states that the increase in bond strength at high strain rates can be approximated to be affected in the same way as concrete.

## **5.7 Influence of strain rate on reinforcement**

As is the case for concrete, the reinforcement steel is also affected by high strain rates. It is agreed that both the yield and the ultimate stresses increase at high strain rates and that the Young's modulus remains unchanged. However, about the ultimate strain, i.e. the strain at ultimate stress, there seems to be a disagreement. Malvar (1998), who presents a thorough review of tests at high strain rates of reinforcement bars used in the U.S., states that the ultimate strain is unaffected by the strain rate. According to Limberger *et al.* (1982) and CEB Bulletin d'Information No 187, CEB (1988), though, the ultimate strain increases with increased strain rate. Further, how much the yield and ultimate stresses increase with increasing strain rate differs quite considerably. Figure 5.17 shows a comparison of the increase given by Malvar and CEB for a hot rolled deformed bar with a static yield strength of 500 MPa and an ultimate strength of 550 MPa. The expressions given by the former are valid for strain rates between  $10^{-4}$  and  $10 \text{ s}^{-1}$  while no limit is given for the expressions in the latter. From this, it is quite clear that there is a very significant difference. It is of special interest to note that the increase in ultimate strength according to Malvar is considerably lower than that of the yield strength. The corresponding increase factors from CEB, though, show a slightly larger increase for the latter compared to the former, thus suggesting that the reinforcement would become more ductile at high strain rates; the findings of Malvar suggest the opposite.

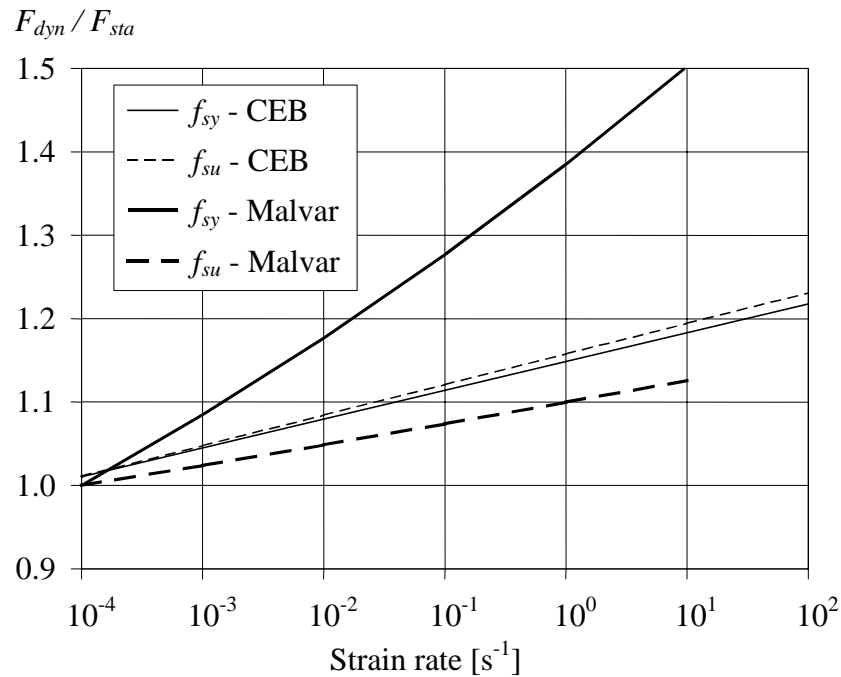


Figure 5.17 Influence of strain rate on yield and ultimate stresses of reinforcement steel with static yield strength  $f_{sy} = 500$  MPa and ultimate strength  $f_{su} = 550$  MPa.. Based on CEB (1988) and Malvar (1997).

## 5.8 Strain rate mesh dependency in finite element analyses

As shown in the previous sections of this chapter, the concrete material properties change significantly when subjected to high loading rates. Hence, it is also evident that to obtain an accurate structural behaviour when modelling concrete structures subjected to such loads it may also be necessary to take these effects into account. This is possible by including the strain rate effect in the constitutive concrete material models. Such constitutive modelling has been performed by several researchers, e.g. Nilsson (1979), Suaris and Shah (1985), Chandra and Krauthammer (1996), Schmidt-Hurtienne *et al.* (1998), Georgin *et al.* (1998), Serecombe *et al.* (1998), and Eibl and Schmidt-Hurtienne (1999). This field, though, was not included in the scope of the work presented in this thesis and is therefore not further treated here. Nevertheless, some observations and experiences, regarding the consideration of strain rate effects in the finite element programme ABAQUS/Explicit, HKS (1998), are presented and briefly discussed.

A dynamically loaded concrete structure will encounter the same type of problems as a statically loaded one. However, it will be shown below that when the strain rate effect is taken into account in the constitutive models, the results obtained may also become mesh-dependent. This is, for instance, the case in the strain-rate-dependent model supplied in the finite element programme ABAQUS/Explicit, used for the dynamic analyses presented here. In Section 3.4 it was discussed how the difficulties with localisation obtained for concrete in tension and compression may be treated. It was concluded that the mesh dependency might be largely dealt with by the use of fracture mechanics and by accurately taking into account within what length the softening takes place. When modelling the cracking of unreinforced concrete or reinforced concrete, where the interaction between the reinforcement and concrete is accurately taken into account, the so-called crack extension is directly related to the length of the independent element. Hence, since the crack strain represents a crack opening, the stress-strain relation for a smaller element will also be more ductile than in a larger element. Therefore, if the crack opening velocity is to be the same, independently of the element mesh used, the strain rate in a smaller element will also be higher than in a larger one. This is further exemplified below.

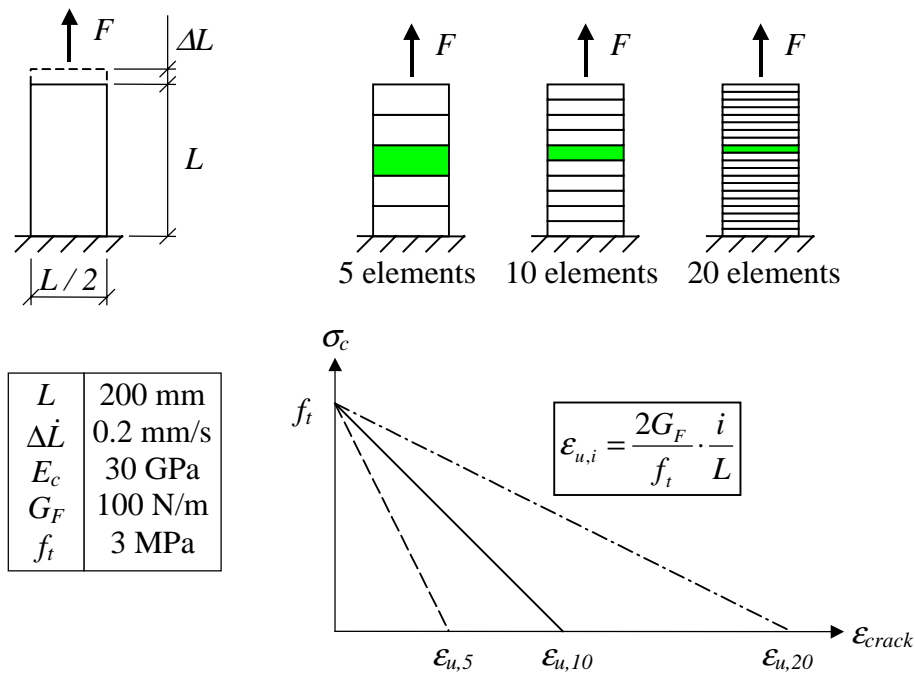


Figure 5.18 Concrete prism subjected to elongation. The marked elements were modelled as shown in the stress-crack strain relation; the rest of the elements were linear elastic.



Figure 5.18 shows a concrete prism, of length 0.2 m and cross-section 100 x 100 mm, subjected to an elongation in displacement-controlled loading at speed  $\dot{\Delta L}$ . The prism was modelled by using three different element meshes made up of 5, 10 or 20 beam elements. One element in each mesh, positioned approximately in the prism midsection, was modelled as non-linear with a tensile strength and a linear stress-crack strain relation using von Mises plasticity; the rest of the elements were modelled as linear elastic. As mentioned above, the stress-strain relations used are related to the size of the cracking element, hence assuring that the resulting force-elongation relation will be the same independently of what element mesh was used.

Figure 5.19a shows the strain rate obtained in the cracking element. Initially, it is the same for all three meshes. However, when the tensile strength is reached at an elongation of  $\Delta L = 0.02$  mm and cracking is initiated, a localisation is obtained in the cracked element; the rest of the elements in the prism unload. The strain rate will then also be considerably affected, obtaining a value inversely proportional to the length of the element. This has no effect, though, if the material model used is strain-rate-independent; the load-elongation relation will then be the same independently of what mesh is used. However, if the strain rate effect is included in the concrete constitutive model it may cause a considerable change in the general behaviour.

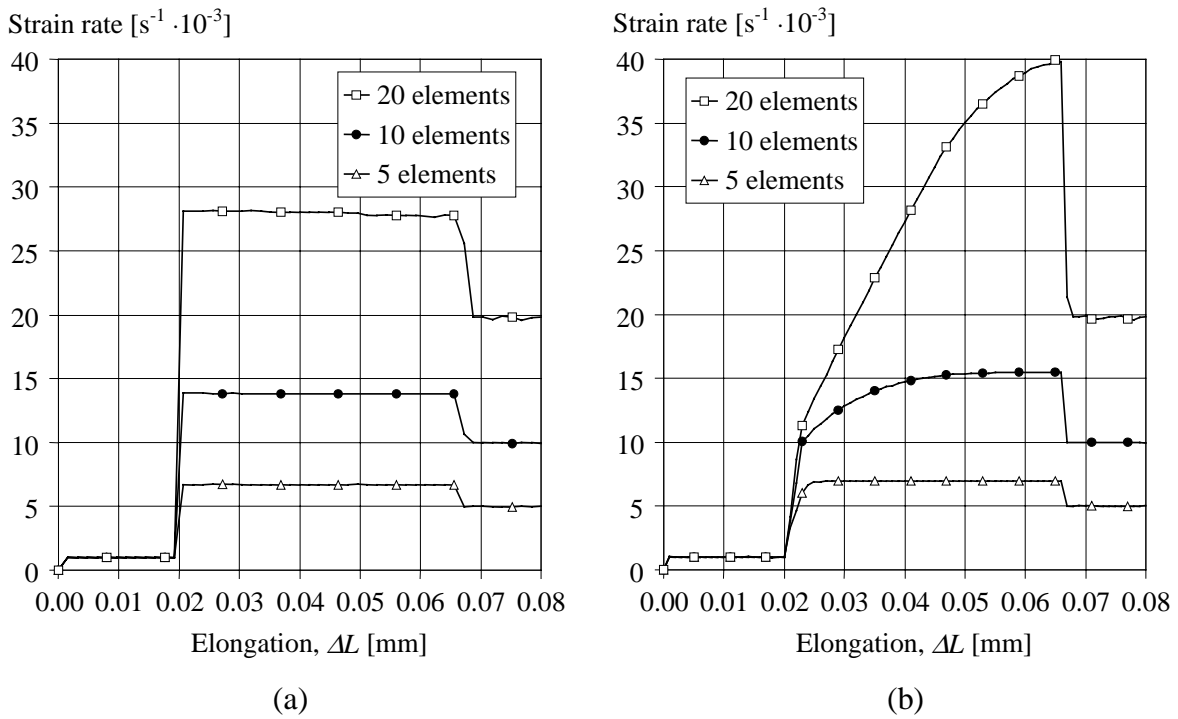


Figure 5.19 Strain rate in cracking element when the material model is: (a) non-rate-dependent; (b) rate-dependent.

The stress-crack strain relation was modelled with von Mises plasticity since it was then possible to include the strain rate effect by using a viscoplastic model. The rate-dependency used is shown in Figure 5.20a. This DIF-strain rate relation is related to that obtained for concrete in tension for  $f_c = 30$  MPa when the expression proposed by Malvar and Ross (1998) is used. However, to simplify the comparison made here, the elongation velocity  $\Delta\dot{L}$  of the concrete prism was chosen so that the inertia effects became negligible. This, though, leads to strain rates that are small compared to that necessary to reach the transition zone for concrete in tension. Therefore, the DIF-strain rate relation proposed by Malvar and Ross was modified to correspond better with the conditions used here. The strain rate was reduced by a factor of 100; i.e. the location of the transition zone originally proposed to take place at  $\dot{\epsilon} = 1 \text{ s}^{-1}$  was changed to appear at  $\dot{\epsilon} = 0.01 \text{ s}^{-1}$ . Further, the DIF was normalised with respect to the original DIF at  $\dot{\epsilon} = 0.1 \text{ s}^{-1}$ , thus reducing it to one at this strain rate.

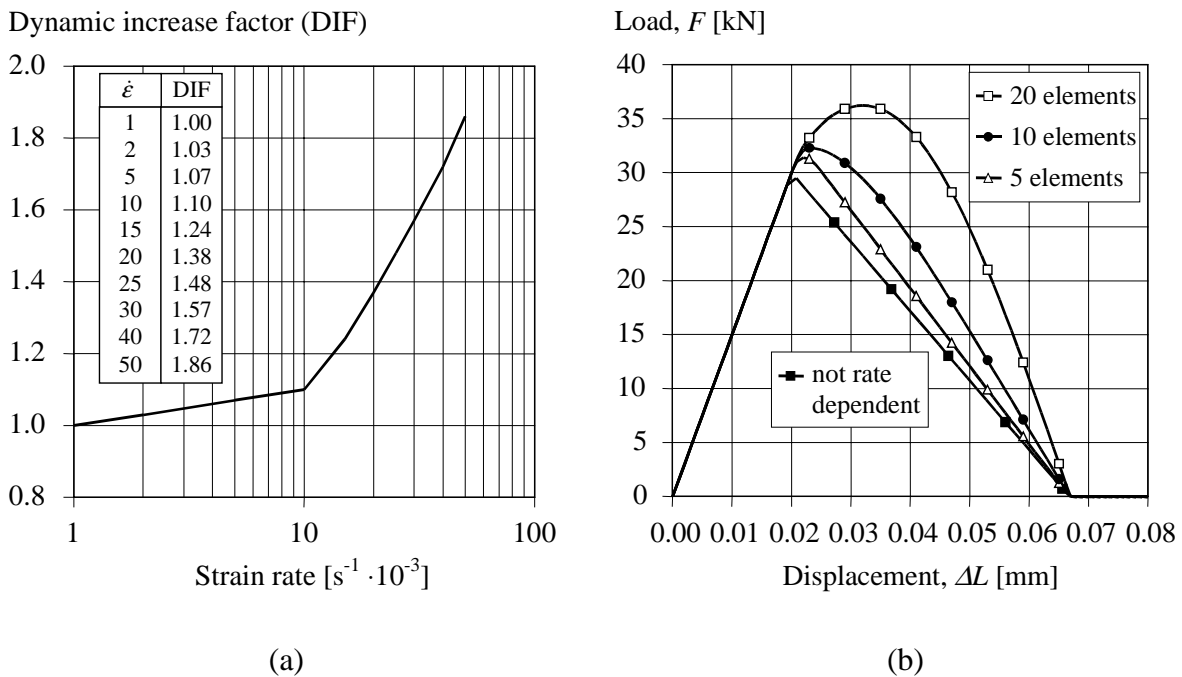


Figure 5.20 (a) DIF-strain rate relation used in the rate-dependent analyses, and (b) load-elongation relations obtained when modelling the concrete prism with different numbers of elements. The relation obtained for the rate-independent analyses is shown for comparison.

The inclusion of rate-dependency affected the strain rate as shown in Figure 5.19b. When comparing the resulting load-elongation relations in Figure 5.20b it is also evident that the different strain rates obtained had a substantial effect. The difference in maximum load when using 5 or 10 elements is comparably small. Even though the strain rate increases by a factor

of two; its effect on the material properties is still about the same. However, the increase in load capacity is more apparent for the prism modelled by 20 elements. Here, the strain rate at maximum load has passed the transition zone and the DIF is therefore considerably increased. From this it can be concluded that, depending on which side of the transition zone the resulting strain rates are obtained at, a change in element size may have a very significant effect on the final result. Using different DIF-strain rate relations for different mesh sizes could perhaps partly solve this problem, but it is still to be determined what element length corresponds to the original DIF-strain rate relation proposed by for instance, Malvar and Ross. Until then, it is the author's opinion that the use of rate-dependent material models, such as those in ABAQUS/Explicit, should be exercised with great care. This is also the reason why the reinforcement in the shelter analyses presented in Paper III was not modelled as a rate-dependent material.



## 6 Numerical solution methods for dynamic problems

### 6.1 General

The equilibrium equation for a dynamic problem can be written as

$$M\ddot{U} + C\dot{U} + KU = P \quad (6.1)$$

where  $M$ ,  $C$  and  $K$  represent the mass, damping and stiffness matrices;  $\ddot{U}$ ,  $\dot{U}$  and  $U$  are the acceleration, velocity and displacement vectors, respectively. When using numerical methods to solve this equation, two different classes of methods are, according to Bathe (1996), generally used: the mode superposition and direct integration methods. The choice of which method is best to use is determined by the numerical effectiveness. The dynamic analyses presented in this thesis, though, have only made use of the latter, so the former is mentioned very briefly. For a more thorough description of mode superposition, see for instance Bathe (1996).

### 6.2 Mode superposition

In the mode superposition method, the dynamic equilibrium equation (6.1) is first transformed into a form in which is less costly to solve. The transformation matrix used may be established by neglecting the damping and using the displacement solutions of the free-vibration equilibrium equations

$$M\ddot{U} + KU = 0 \quad (6.2)$$

To solve this, the displacement can be assumed to be have the form

$$U = \phi \sin \omega(t - t_0) \quad (6.3)$$

where  $\phi$  is a vector of order  $n$  describing the shapes of the  $n$  first modes,  $\omega$  is the angular frequency,  $t$  is time and  $t_0$  is a time constant. Combining equations (6.2) and (6.3) an eigenproblem of the form

$$K\phi = \omega^2 M\phi \quad (6.4)$$

is obtained. The eigenvalues and their corresponding eigenvectors are found, and the latter form the transformation matrix. As shown in for example Bathe, the use of this transformation

matrix yields a decoupled system of equations, which means that the response of the modes in the analysed structure can be determined individually. These modes can then be superposed and the response of the whole structure determined. Thus, the advantage with a mode superposition analysis is that not all modes have to be considered; instead only those believed to affect the response of the structure studied need to be taken into account. This is the primary reason why this procedure can be much more effective than direct integration methods. However, it also means that the effectiveness depends on how many modes have to be taken into account, something that usually depends on a combination of the geometry of the structure, the distribution in time and space of the load, and the load frequency content. A harmonically loaded structure needs a small number of modes, while for example a highly transient load, such as a blast load, needs substantially more modes to obtain an accurate solution. Further, the method might not be very effective for solving non-linear problems. The mode superposition procedure is well suited to solve strictly linear problems where a higher cost-efficiency often can be achieved, compared to a direct integration method. However, for non-linear problems the mode forms will vary with time, which means that they will have to be recalculated in each step, thus making the method far less attractive for such problems. According to Bathe, mode superposition only efficient for non-linear dynamic problems only if a relatively small number of modes is necessary; if this criterion cannot be met, then direct integration should be used instead.

## **6.3 Direct integration methods**

### **6.3.1 General**

When solving a problem by using a direct integration method, the expression in equation (6.1) is solved numerically through an incremental process. The term “direct” means that no transformation to another form of this expression takes place prior to the numerical integration. The direct integration methods are, according to Bergan *et al.* (1986), commonly classified into two groups: explicit and implicit methods. The essential difference between these two classes can be said to be *when* in time the equilibrium of equation (6.1) is solved. For the explicit methods, the displacement vector  ${}^{t+\Delta t}U$  is solved by using the equilibrium at time  $t$ ; for the implicit methods it is instead solved at time  $t+\Delta t$ ; compare equations (6.5) and (6.6) respectively.

$$M {}^t\ddot{U} + C {}^t\dot{U} + K {}^tU = {}^tP \quad (6.5)$$

$$M {}^{t+\Delta t}\ddot{U} + C {}^{t+\Delta t}\dot{U} + K {}^{t+\Delta t}U = {}^{t+\Delta t}P \quad (6.6)$$

The index used refers to what time the parameter used belongs to; e.g.  ${}^t\ddot{U}$  indicates the acceleration at time  $t$  and  ${}^{t+\Delta t}\dot{U}$  refers to the velocity at time  $t+\Delta t$ . Here,  $M$ ,  $C$  and  $K$  are assumed to be constant in time.

Several integration methods have been developed, of which many can be said to be special cases of the more generalised Newmark method which is briefly treated here; for more information the reader is referred to, for instance, Hughes (1987) or Bathe (1996). In the Newmark method, the velocity and displacement vectors are expressed as

$${}^{t+\Delta t}\dot{U} = {}^t\dot{U} + \Delta t \left[ (1 - \delta) {}^t\ddot{U} + \delta {}^{t+\Delta t}\ddot{U} \right] \quad (6.7)$$

$${}^{t+\Delta t}U = {}^tU + \Delta t {}^t\dot{U} + \Delta t^2 \left[ \left( \frac{1}{2} - \alpha \right) {}^t\ddot{U} + \alpha {}^{t+\Delta t}\ddot{U} \right] \quad (6.8)$$

where  $\delta$  and  $\alpha$  are parameters that are used to obtain accuracy and stability, respectively. According to Bergan *et al.* (1986) the former is used to control the numerical damping in the solution algorithm, and the latter is used to control what solution method is used. To better illustrate the difference between explicit and implicit integration methods, the explicit central difference method and the implicit trapezoidal rule (also referred to as the constant-average acceleration method) are presented below. To better visualise the difference between the methods, initially only linear problems are treated here; the influence of non-linear behaviour is discussed in Section 6.3.4.

### 6.3.2 Explicit integration method

By setting the numerical damping to zero, i.e.  $\delta = 0.5$ , and using  $\alpha = 0$  in the Newmark method, the central difference method is obtained, which is a commonly used explicit method. Using the values given above for  $\delta$  and  $\alpha$  in equations (6.7) and (6.8), and assuming a constant time step  $\Delta t$ , the acceleration and velocity at time  $t$  can be expressed as

$${}^t\ddot{U} = \frac{1}{\Delta t^2} \left( {}^{t+\Delta t}U - 2 {}^tU + {}^{t-\Delta t}U \right) \quad (6.9)$$

$${}^t\dot{U} = \frac{1}{2\Delta t} \left( {}^{t+\Delta t}U - {}^{t-\Delta t}U \right) \quad (6.10)$$

The solution for the displacement  $U$  at time  $t+\Delta t$  is then obtained by combining these two expressions with that in equation (6.5) and an expression for  ${}^{t+\Delta t}U$  can be derived as

$${}^{t+\Delta t}U = \left( \frac{M}{\Delta t^2} + \frac{C}{2\Delta t} \right)^{-1} \left( {}^tP - \left[ K - \frac{2M}{\Delta t^2} \right] {}^tU - \left[ \frac{M}{\Delta t^2} - \frac{C}{2\Delta t} \right] {}^{t-\Delta t}U \right) \quad (6.11)$$

Since all terms on the right-hand side are known from time  $t-\Delta t$  or time  $t$ , the displacement  ${}^{t+\Delta t}U$  can be explicitly determined.

It can be shown that the central difference method is conditionally stable, i.e. that the time step  $\Delta t$  used in equation (6.11) has to be less than or equal to a critical time step  $\Delta t_{cr}$  if an acceptable solution is to be obtained; see also Section 6.3.5. This critical time step is normally very small, which usually means that it takes a lot of increments for the analysis to cover the time period that is to be examined. Consequently, an important criterion for the method to be of practical use is that the response in each increment can be solved very effectively. However, this is possible by neglecting the effect of damping or making sure to use a diagonal damping matrix, and by using a lumped (i.e. diagonal) mass matrix. Thereby, the inverted part in equation (6.11) can easily be determined and  ${}^{t+\Delta t}U$  solved by the use of ordinary matrix multiplication. Hence, a fast and effective solution method is obtained since the calculations necessary in each increment become very “cheap”.

As shown in equation (6.11) the calculation of  ${}^{t+\Delta t}U$  makes use of both  ${}^tU$  and  ${}^{t-\Delta t}U$ . However, this means that when solving the displacement at time  $\Delta t$  information about the displacement at time  $-\Delta t$  is needed. Hence, to calculate the displacement at time  $\Delta t$  it is necessary to use a special starting procedure that according to Bathe is expressed as

$${}^{-\Delta t}U = {}^0U - \Delta t {}^0\dot{U} + \frac{\Delta t^2}{2} {}^0\ddot{U} \quad (6.12)$$



### 6.3.3 Implicit integration method

If  $\delta$  and  $\alpha$  are set to 0.5 and 0.25, respectively, in the Newmark method the so-called trapezoidal rule is obtained. Thus, the velocity and displacement vectors can be written as

$${}^{t+\Delta t}\dot{U} = {}^t\dot{U} + \frac{\Delta t}{2} ({}^t\ddot{U} + {}^{t+\Delta t}\ddot{U}) \quad (6.13)$$

$${}^{t+\Delta t}U = {}^tU + \Delta t {}^t\dot{U} + \frac{\Delta t^2}{4} ({}^t\ddot{U} + {}^{t+\Delta t}\ddot{U}) \quad (6.14)$$

and by using these expressions in equation (6.6) the displacement at time  $t+\Delta t$  can be derived as

$${}^{t+\Delta t}U = \left( \frac{4M}{\Delta t^2} + \frac{2C}{\Delta t} + K \right)^{-1} \left( {}^{t+\Delta t}P + M {}^t\ddot{U} + \left[ \frac{4M}{\Delta t} + C \right] {}^t\dot{U} + \left[ \frac{4M}{\Delta t^2} + \frac{2C}{\Delta t} \right] {}^tU \right) \quad (6.15)$$

Contrary to the central difference method, the trapezoidal rule is unconditionally stable; that is, the stability of the solution remains independent of what value of the time step  $\Delta t$  is used. Neither does it need a special starting procedure since the displacement at time  $t+\Delta t$  only depends on parameters at time  $t$  and  $t+\Delta t$ . This is the unconditionally stable method originally proposed by Newmark and is, according to Bathe, also the one which has the most desirable accuracy characteristic. A closer look at the expression in equation (6.15) reveals that the stiffness matrix  $K$  is included in the term that has to be inverted (i.e. the *effective* stiffness matrix) to obtain the displacement  ${}^{t+\Delta t}U$ . Due to this requirement each increment will be far more “expensive” in this method than the central difference method, where this procedure is not necessary; compare equation (6.11). Finally, it is worth noting that if the effect of inertia and damping is neglected in the expression given in equation (6.15) it is reduced to a static analysis, i.e. if  $C$  and  $M$  is set to zero the static solution is obtained for a time-dependent load. Doing the same with the central difference method, though, is not possible.

### 6.3.4 Solution of non-linear problems

The expressions to determine the displacement at time  $t+\Delta t$  by an explicit and an implicit method were derived in equations (6.11) and (6.15), respectively. It has been discussed above that the treatment of the stiffness matrix differs in the two methods. However, in the foregoing, only linear problems were treated; thus the stiffness matrix  $K$  was also constant. If

the problem is non-linear, there are more differences in how a solution is obtained in the different analyses. If assuming non-linear material behaviour, the stiffness matrix  $K$  will no longer be constant; instead at time  $t$  it depends on the displacement  ${}^tU$ . Accordingly equations (6.11) and (6.15) can be rewritten as

$${}^{t+\Delta t}U = \left( \frac{M}{\Delta t^2} + \frac{C}{2\Delta t} \right)^{-1} \left( {}^tP - \left[ {}^tK - \frac{2M}{\Delta t^2} \right] {}^tU - \left[ \frac{M}{\Delta t^2} - \frac{C}{2\Delta t} \right] {}^{t-\Delta t}U \right) \quad (6.16)$$

and

$${}^{t+\Delta t}U = \left( \frac{4M}{\Delta t^2} + \frac{2C}{\Delta t} + {}^{t+\Delta t}K \right)^{-1} \left( {}^{t+\Delta t}P + M {}^t\ddot{U} + \left[ \frac{4M}{\Delta t} + C \right] {}^t\dot{U} + \left[ \frac{4M}{\Delta t^2} + \frac{2C}{\Delta t} \right] {}^tU \right) \quad (6.17)$$

respectively. Above, it has been assumed that only the stiffness matrix depends on time, and that the mass and damping remain constant. For the solution of  ${}^{t+\Delta t}U$  using the explicit central difference method in equation (6.16) there will not be any essential changes, the distinction being that the stiffness is now time-dependent. Consequently, since  ${}^{t+\Delta t}U$  depends only on values already known, the same procedure as in the linear case can be used. However, this is not the case for the implicit trapezoidal rule. Here  ${}^{t+\Delta t}U$  depends on  ${}^{t+\Delta t}K$ , which in turn depends on  ${}^{t+\Delta t}U$ . Hence, the use of an iteration process is necessary to reach a solution, thus making the method even more “expensive”. To summarise, when using an explicit method it does not matter whether the problem is linear or non-linear; the time needed to solve the problem will be the same anyway. But, for an implicit method it will have a large effect, since a non-linear problem has to be solved with the help of an iteration process.

### 6.3.5 Stability

It was mentioned above that the central difference method is conditionally stable, and that its major disadvantage was that it has to make use of an often very small time step  $\Delta t$ . Contrary to this, the implicit trapezoidal rule is unconditionally stable, meaning that there is no such limitation on what time step can be used. That a solution is stable means that any errors in the solution, due for example to round-off in the computer, do not grow in the continuous calculation. However, as already noted, the stability of a solution can be guaranteed by using a sufficiently small time step  $\Delta t$  so that the response in the highest-frequency component is

accurately predicted. Considering the stability of integration methods, one distinguishes between conditionally stable and unconditionally stable procedures. In the Newmark method, the latter is the case if the following conditions are fulfilled:

$$\delta \geq 0.5 \quad (6.18)$$

$$\alpha \geq 0.25(\delta + 0.5)^2 \quad (6.19)$$

However, if the values of  $\delta$  and/or  $\alpha$  do not meet these conditions, the integration method becomes conditionally stable. The critical time step  $\Delta t_{cr}$  needed in such a case can, for an undamped, system be determined as

$$\Delta t_{cr} = \frac{1}{\omega_{max}} \frac{1}{\sqrt{0.25(\delta + 0.5)^2 - \alpha}} \quad (6.20)$$

where  $\omega_{max}$  is the maximum angular frequency for any component in the system. Comparing the values of  $\delta = 0.5$  and  $\alpha = 0$ , i.e. the values used to obtain the central difference method, with the conditions given above, it is evident that this method is conditionally stable and that its critical time step necessary to obtain stability is

$$\Delta t_{cr} = \frac{2}{\omega_{max}} \quad (6.21)$$

According to Bathe the critical time step is independent of damping; in ABAQUS/Explicit, though, a somewhat different variant of the central difference method described here is used, which also causes the critical time step to depend on the damping, see Section 6.3.8. A physical interpretation of this time limit, which perhaps is easier to understand, is that the critical time step  $\Delta t_{cr}$  in equation (6.21) corresponds to the minimum time it takes for a stress wave to travel through any finite element included in the analysis. Thus, the use of this time step guarantees that no wave passes an element without it being able to respond. If the time step used is larger than the critical time step, the lack of response causes loss of information and results in an unstable solution.

By making a similar comparison to the trapezoidal rule ( $\delta = 0.5$  and  $\alpha = 0.25$ ) it is found that this method fulfils the conditions given in equations (6.16) and (6.17) and therefore is unconditionally stable. Thus, regarding only the stability of the solution, the time step used could be of any value. However, even though this usually means that the time step used in an implicit method can be considerably larger than what is the case in an explicit method, its size is still of utmost importance to obtain an accurate solution.

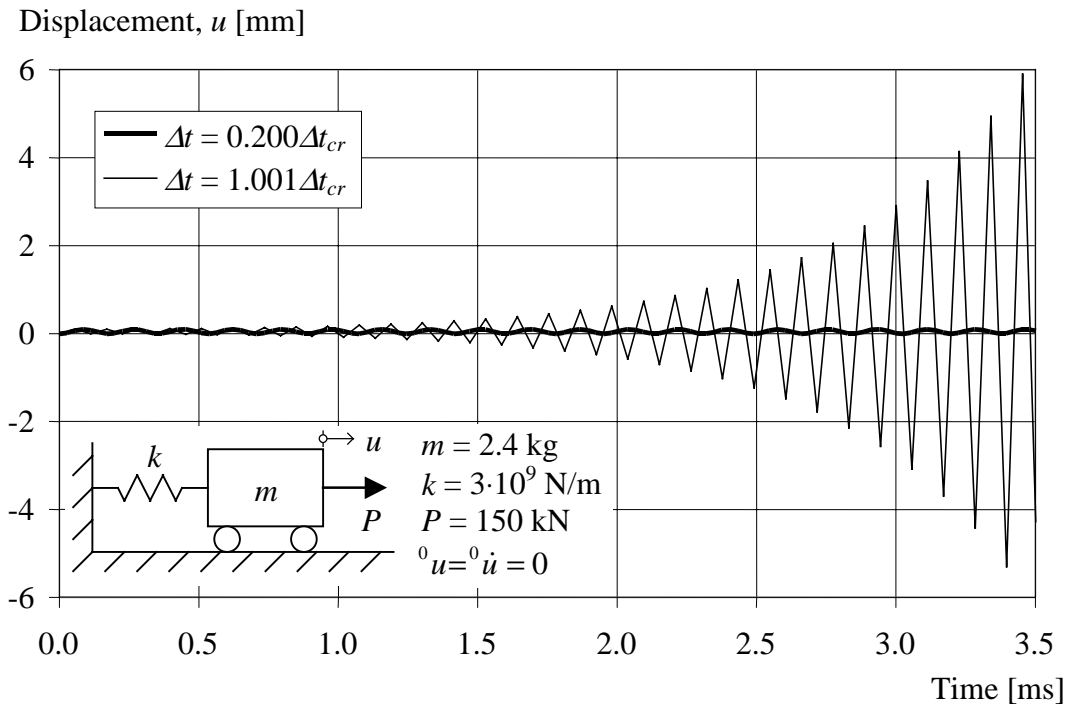


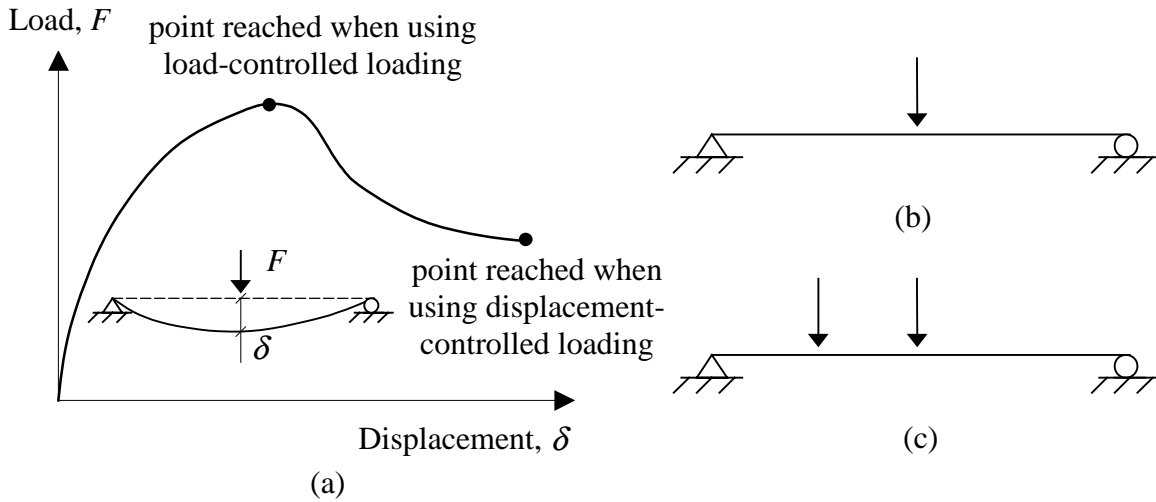
Figure 6.1 Comparison of stable and unstable solutions of SDOF system when the central difference method is used. The stable solution ( $\Delta t = 0.200\Delta t_{cr}$ ) corresponds to the exact one.

Figure 6.1 illustrates what effect a too large time step has on a linear, undamped single-degree-of-freedom system (SDOF system) when this is solved by using the central difference method. From the figure it is evident that the error in the solution increases very quickly to such proportions that it soon becomes useless.

### 6.3.6 Way of loading

The usual way to apply the load of a structure is to use load-controlled or displacement-controlled loading. The problem with the former is that it is not possible to follow the post-peak behaviour of a structure, i.e. the response after maximum load, something that is of utmost importance when studying the ductility of a structure; see Figure 6.2a. Depending on the load condition, it may be possible to solve this by loading the structure through direct displacement-control instead, thus also enabling the post-peak response to be described in the solution. However, for many cases this solution is not possible since there are no node or nodes suitable to represent the load or load combination that is to be used. A simple example of such a case is a simply supported beam loaded by two point loads as shown in Figure 6.2c. In a static or implicit analysis, in which iterations are used, it would be possible to use a so-

called arch length method to follow the response until final failure; but in an explicit method this is, to the author's knowledge, not possible since no iterations are carried out. It would perhaps be possible to follow the post-peak response using load-controlled loading also but then an iterative procedure including the external load and the displacement in the controlled node would be necessary. Therefore, regarding the possibility to model different load cases, an explicit method is at a disadvantage of an implicit one.



Figur 6.2 (a) Schematic view showing the difference in response that it is possible to follow when using load-controlled or displacement-controlled loading. Example of load case where it is (b) possible, and (c) not possible, to use direct displacement controlled loading.

Apart from displacement-controlled loading, it is also possible in dynamic analyses to apply the load as velocity-controlled as well. The advantage of this method is that the load then is applied more “smoothly” than is the case using displacement-controlled loading. Thus, it is possible to avoid acceleration terms approaching infinity as schematically shown in Figure 6.3.

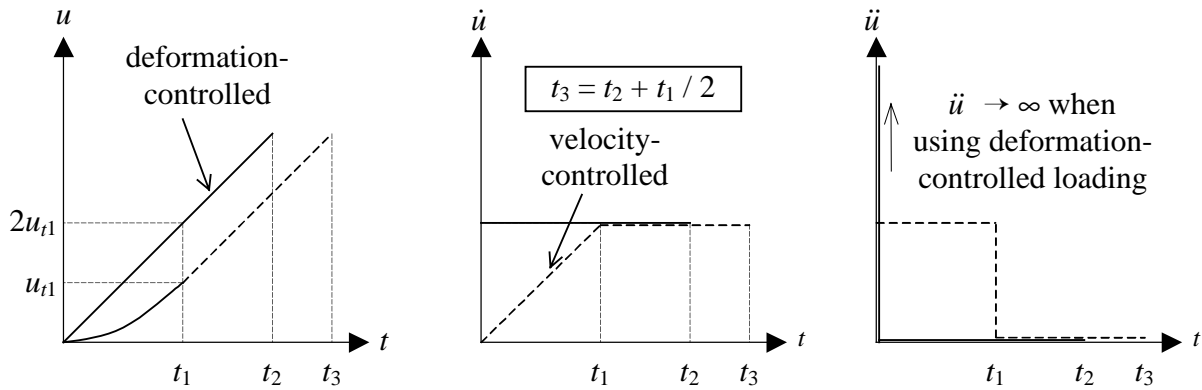


Figure 6.3 Schematic view of the difference in deformation, velocity and acceleration terms when using deformation-controlled or velocity-controlled loading.

### 6.3.7 Choosing integration method

Which integration method should be used for a specific problem depends to a large degree on the “calculation cost” of solving the problem. Due to the usually small time step allowed in an explicit analysis, this method is normally used only when the load can be applied during a relatively short time, e.g. blast load analyses on buildings or crash analyses of cars. Even though it is possible to use an implicit method for these kinds of problems too, the solution time needed is usually much higher than that needed by the explicit method. In other dynamic cases, however, in which the loading lasts during a longer time of perhaps a couple of seconds, the conditions are reversed. Here, implicit methods are more suitable since a larger time step can be used, while the explicit method still has to fulfil the requirement on its critical time step, resulting in very long execution times. The characteristic ability of the explicit method to always obtain equilibrium without using iterations, though, transforms it to a robust method that makes it attractive to use also for static problems. This, in combination with the fact that it is an effective tool in contact problems, has enabled it to be used frequently in metal sheeting analyses in, for example, the car industry; see e.g. Mattiasson *et al.* (1991). Further, it has successfully been used in analyses of statically loaded concrete structures, e.g. by Johansson (1998) and Martinez and Sanchez (2000).

### 6.3.8 Central difference method in ABAQUS/Explicit

The central difference method used in ABAQUS/Explicit, HKS (1997), is somewhat different from the one described in Section 6.3.2 and is therefore treated briefly here. The expression in equation (6.9) for the acceleration remains the same but the velocity in equation (6.10) is changed to

$${}^{t-\Delta t/2}\dot{U} = \frac{1}{\Delta t} \left( {}^tU - {}^{t-\Delta t}U \right) \quad (6.22)$$

i.e. the velocity is specified at time  $t-\Delta t/2$  instead of time  $t$ . By combining equations (6.5), (6.9) and (6.22) it is possible to derive an expression for the displacement at time  $t+\Delta t$  corresponding to that shown in equation (6.11) and the displacement  ${}^{t+\Delta t}U$  can then be derived as

$${}^{t+\Delta t}U = \Delta t^2 M^{-1} \left( {}^tP - \left[ K - \frac{2M}{\Delta t^2} - \frac{C}{\Delta t} \right] {}^tU - \left[ \frac{M}{\Delta t^2} - \frac{C}{\Delta t} \right] {}^{t-\Delta t}U \right) \quad (6.23)$$

As is the case in equation (6.11) all parameters on the right-hand side are known and the displacement  ${}^{t+\Delta t}U$  can therefore be determined explicitly. Further, from this it can be seen that the damping matrix  $C$  is no longer part of the term that has to be inverted. Accordingly, any type of damping can now be taken into account without affecting the efficiency of the calculation. The mass matrix, though, still has to be lumped to ensure that a quick solution of  $M^{-1}$  is possible. This kind of central difference method gives the same accuracy as that previously described. However, contrary to the original method discussed in Section 6.3.2 the damping coefficient now influences the stability of the solution:

$$\Delta t_{cr} = \frac{2}{\omega_{\max}} \left( \sqrt{1 + \xi^2} - \xi \right) \quad (6.24)$$

and hence the critical time step  $\Delta t_{cr}$  becomes a function of the damping coefficient  $\xi$ .





## 7 Conclusions

### 7.1 General

The main aim of this research project was to evaluate a new design proposal of the reinforcement detailing in concrete frame corners of Swedish civil defence shelters, and to examine whether this detailing, consisting of reinforcement loops spliced within the corner, is appropriate to replace the detailings previously used in closing and opening frame corners. This part of the study was carried out by a combination of a literature survey, experimental testing and non-linear finite element analyses. Further, since a civil defence shelter must be able to withstand highly dynamic load cases, where the structural response might be quite different, another aim was to increase the knowledge of what structural response is obtained when subjected to such loads and to examine whether the conclusions drawn from static tests and analyses could also be used in such a case. This was dealt with by studying a civil defence shelter, subjected to a blast load from an explosion or falling masses from a collapsing building, using dynamic non-linear finite element analyses.

The reinforcement detailings used in opening frame corners are very critical for what response will be obtained. A common approach is to use reinforcement loops combined with inclined bars positioned at the inside of the corner. However, it is shown herein that the use of such inclined bars may not be as efficient as commonly thought. Instead they may as well be replaced by an equivalent amount of extra reinforcement loops, thus resulting in a detailing that may be considerably easier to carry out. Neither detailing, though, is guaranteed to fulfil the requirement of full efficiency, as it is defined here, unless the mechanical reinforcement is lower than an upper limit, here derived to be  $\omega_s = 0.033$  for concrete of compressive strength less than 50 MPa. This might be difficult to fulfil if using high reinforcement ratios, and a discussion of possible solutions is therefore presented. It was found that the best method probably is to increase the concrete strength within the corner, especially by the use of fibre-reinforced concrete. Although full efficiency of such a corner detailing may not be achieved, a ductile behaviour may very well still be obtained. Further, it was concluded that if inclined bars are to be used it is important not to splice the reinforcement loops and straight bars just outside the corner region.

Contrary to opening corners, frame corners subjected to closing moment are less sensitive to what reinforcement detailing is used. Accordingly, even though test results indicate that the use of reinforcement loops causes increased risk of concrete side spalling, the new proposal

has proven to be at least as efficient as the conventional one. The negative influence due to such spalling of the side concrete cover will, in a wall-slab connection, be of minor importance due to the large number of bars present. In a beam-column joint, though, this is not necessarily the case and special attention must be given to the spalling phenomenon in such structures since it may have great influence on the final capacity.

In the dynamic analyses of a shelter it was found that the global response of a structure subjected to a blast load, in the initial stage, may be very different from that of a static load. A major reason is that the boundary conditions of a structure subjected to high-rate loading may be regarded as time-dependent. Nevertheless, the results obtained indicate that no critical cracks will form within the corner region, and it therefore seems reasonable to believe that the response within such a corner will be similar to that obtained in a statically loaded structure. Accordingly, even though the structural behaviour may be completely different in static and transient loaded structures the local behaviour may still be rather similar. Consequently, it can be concluded that it is suitable to replace the conventional detailings in both opening and closing frame corners in civil defence shelters with the new reinforcement proposal of spliced reinforcement loops within the corner. In opening corners, though, an additional reinforcement amount up to 35% may be required. As a result of the work presented herein, this detailing is now prescribed in the present Swedish Shelter Regulations, Swedish Rescue Services Agency (1998).

The non-linear finite element analyses carried out within the scope of this work have shown that the finite element method can be a very powerful tool in the study of reinforced concrete structures. Such analyses may supply the means for further understanding and increased knowledge of the often complicated response in reinforced concrete structures, making it possible to explain phenomena in a way that would not be possible by using only conventional testing and evaluation methods. Nevertheless, it is important to remember that experimental testing cannot be neglected since they always describe the reality, while the former is just an attempt to simulate it. Hence, while both methods have certain advantages when used alone, they will only be at their fullest advantage when combined. However, the use of such an advanced tool also puts a high demand on the user. The post-peak behaviours for concrete in tension and compression, for instance, are both highly localised phenomena, making it difficult to determine a correct stress-strain relation to use in an analysis. To be able to accurately simulate such a response the concept of fracture energy and the length of the softening region have to be considered. For concrete in tension this is a fully accepted approach, whereas for concrete in compression it is still not commonly used. Thus, the stress-

strain relations for the latter, which can be found in the literature, cannot be used directly in a finite element analysis since they are related to the height of the specimens used when evaluating it, and not the zone in which softening will take place in an analysis.

Concrete structures subjected to high loading rates will also exhibit high strain rates that influence the material properties of both concrete and reinforcement. Hence, it may be important to include those effects when modelling concrete structures subjected to transient loading. However, it was found that the strain rate obtained might depend on what element sizes are used (this is, for instance, the case in the programme ABAQUS/Explicit used herein) and the material properties then also become mesh-dependent. Therefore, it was concluded that rate dependent material models have to be used with great care if the results are to be trusted.

## **7.2 Suggestions for future research**

The static analyses carried out herein showed some shortcomings regarding their possibility to predict the occurrence of side concrete spalling and the loss of the compressed concrete at the outside of opening frame corners. The former deficiency was due to the use of two-dimensional plane stress elements, while the latter was because of the concrete material models used. In both cases, the anchorage of the reinforcement loops is vital for the response obtained. Therefore, it is important that the stress state surrounding the reinforcement bars is accurately accounted for when modelling the interaction between reinforcement and concrete, so that the loss of concrete cover is also reflected in the loops' bond behaviour. This is possible by using, for instance, the bond model proposed by Lundgren (1999). Accordingly, three-dimensional finite element analyses, including more sophisticated crack models than those used herein, so that the loss of the concrete part at the outside of the corner is accurately described, and incorporating Lundgren's bond model, would be highly informative in the future study of concrete frame corners. Such analyses could then be used to increase the understanding of response observed in tests. In such a study it would also be comparatively easy to include the effect of haunches and/or different sizes of the corner.

The advantage of spliced reinforcement loops in joint connections has been shown for the case of opening and closing frame corners with an angle of  $90^\circ$ . Moreover, such a solution can undoubtedly be used successfully also for other types of connections, e.g. T-joints or splicing between two beam sections as shown in Figure 7.1. The latter was briefly treated within the scope of this work, in Appendix B and Grassl (1999), but further work is needed to fully understand the structural response obtained.

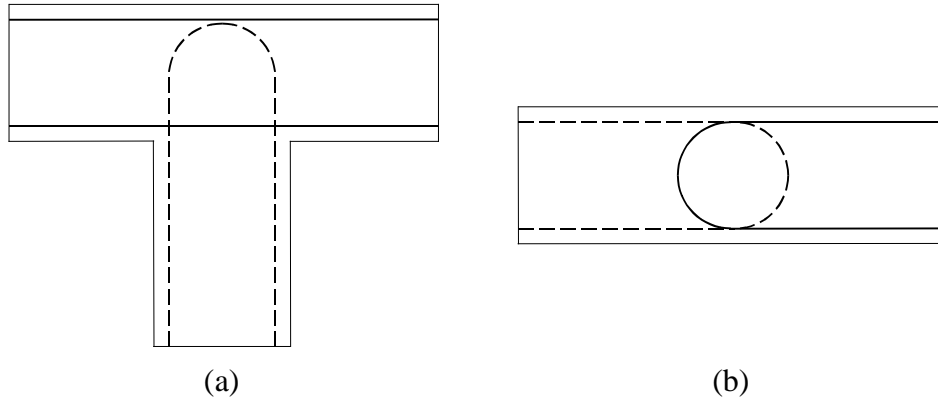


Figure 7.1 Possible joint connections where the splicing of reinforcement loops could be of use: (a) T-joint and (b) beam connection.

The dynamic analyses carried out herein could only take into account the influence of high strain rates on the material properties used in a very approximate way. It would be valuable to further examine what effects might emerge if the influence is considered more accurately. In addition, apart from the pressure of a nearby explosion there will also be the effects of splinter hitting the structure before, after or simultaneously with the blast load. Due to its complexity, this process was not incorporated in the present study. Nevertheless, it may be very important for the structural response and further investigation is therefore necessary.

## References

- Abdul-Wahab H.M.S. and Ali W.A. (1989): Strength and Behaviour of Reinforced Concrete Obtuse Corners under Opening Bending Moments. *ACI Structural Journal*, Vol. 86, No. 6, pp. 679-685.
- Abdul-Wahab H.M.S. and Al-Roubai A.A.M. (1998): Strength and behaviour of steel fibre reinforced concrete corners under opening bending moment, *Magazine of Concrete Research*, Vol. 50, No. 4, pp. 305-318.
- Abdul-Wahab H.M.S. and Salman S.A.R. (1999): Effect of Corner Angle on Efficiency of Reinforced Concrete Joints under Opening Bending Moment, *ACI Structural Journal* Vol. 96, No. 1, pp. 115-121.
- Anderson L. (1985): Inverkan på skyddsrum av byggnadsras (Influence of collapse load on Civil defence Shelters – Static and Dynamic Loaded Concrete Strips. In Swedish). Department of Building Statics and Structural Engineering, Royale Institute of Technology, Message No. 141, Stockholm, Sweden.
- Anderson L. (1987a): Statisk and dynamisk belastning av betongplattstrimlor (Static and Dynamic Loading of Concrete Strips. In Swedish). Department of Building Statics and Structural Engineering, Royale Institute of Technology, Message No. 145, Stockholm, Sweden.
- Anderson L. (1987b): Energiåtgång vid dynamisk engångslast på betongplattor, Del 1 (Energy dissipation at impact loading of concrete slabs, Part 1. In Swedish). Department of Building Statics and Structural Engineering, Royale Institute of Technology, Message No. 148, Stockholm, Sweden.
- Baker W.E. (1973): *Explosions in air*. University of Texas press, Austin, USA.
- Balasz P. (1997): Beräkningsmetoder vid stötvågsbelastade konstruktioner (Methods for Calculations of Blast Loaded Structural Behaviour. In Swedish). Department of Weapons and Protection, National Defence Research Establishment, FOA-R97-00473-311, Stockholm, Sweden.

- Balint P.S. and Taylor H.P.J. (1972): Reinforcement Detailing of Frame Corner Joints with Particular Reference to Opening Corners, Technical Report 42.462, Cement and Concrete Association, London, England.
- Bathe K-J. (1996): Finite Element Procedures. Prentice-Hall, Englewood Cliffs, New Jersey.
- Betonghandboken (1990): Betonghandboken – Konstruktion, utgåva 2 (Concrete Handbook Design, Second Edition. In Swedish). Edited by Cederwall K., Lorentsen M. and Östlund L., AB Svensk Byggtjänst, Stockholm, Sweden.
- Betonghandboken (1994): Betonghandboken – Material, utgåva 2 (Concrete Handbook Material, Second Edition. In Swedish). Edited by Ljungkrantz C., Möller G. and Petersons N., AB Svensk Byggtjänst, Stockholm, Sweden.
- Boverket (1994): Boverkets handbok för Betongkonstruktioner BBK 94, Band 1, Konstruktion (Boverket's Handbook for Concrete Structures, BBK 94, Vol. 1, Design. In Swedish). Boverket, Byggavdelningen, Karlskrona, Sweden.
- Bergan P.G., Larsen P.K. and Mollestad E. (1986): Svingning av konstruksjoner, Andra utgåvan (Vibration of Structures. In Norwegian). Tapir, Trondheim, Norway.
- Bischoff P.H. and Perry S.H. (1991): Compressive behaviour of concrete at high strain rates. Materials and Structures, 1991, 24, pp. 425-450.
- Brode H.L. (1955): Numerical Solutions of Spherical Blast Waves. Jour. Appl. Phys., Vol. 26, No. 6, pp 766-775.
- Broo H. and Broo M. (1997): Fog av högpresterande fiberbetong i prefabricerad brobanepatta (Joint of High-Strength Concrete in Prefabricated Bridge Slab. In Swedish). Division of Concrete Structures, Chalmers Univeristy of Technology, Master Thesis 97:2, Göteborg, Sweden.
- BST Byggstandardiseringen (1991): Betongprovning med Svensk Standard, BST handbok 12, utgåva 6 (Concrete Testing according to Swedish Standard, BST Handbook 12, sixth edition. In Swedish), SIS – standardiseringskommisionen i Sverige and Svensk Byggtjänst, Stockholm, Sweden.

- CEB (1988): Concrete Structures under Impact and Impulsive Loading. CEB Bulletin d'Information No 187, Lausanne, Switzerland.
- CEB (1993): CEB-FIP Model Code 1990, Design Code. Thomas Telford, Lausanne, Switzerland.
- CEN (1991): Eurocode 2: Design of concrete structures - Part 1: General rules and rules for buildings. European Committee for Standardization.
- Chandra D. and Krauthammer T. (1996): Rate-Sensitive Micromechanical Damagae Model for Brittle Solid. Journal of Engineering Mechanics, Vol. 122, No. 5, pp. 412-422.
- Chung H.W. (1978): Shear strength of concrete joints under dynamic loads. Concrete, mar 1978, pp. 27-29.
- Claeson C. (1998): Structural Behaviour of Reinforced High-Strength Concrete Columns. Division of Concrete Structures, Chalmers Univeristy of Technology, Ph.D. Thesis, Publication 98:1, Göteborg, Sweden.
- ConWep (1992): ConWep – Collection of conventional weapons effects calculations based on TM 5-855-1, Fundamentals of Protective Design for Conventional Weapons, U.S. Army Engineer Waterways Experiment Station, Vicksburg, USA.
- de Borst R. (1999): Analyses of Reinforced Concrete In a Historical Perspective. Nordic Symposium on Modern Design of Concrete Structures, Aalborg University, Denmark, pp. 261-299.
- Dilger W.H., Kand R. and Kowalczyk R. (1984): Ductility of Plain and Confined Concrete Under Different Strain Rates. ACI Journal, Jan-Feb, pp. 73-81.
- Dragosavic M., van den Beukel A. and Gijsbers F.B.J. (1975): Loop connections between precast concrete components loaded in bending. HERON, Vol. 20, No. 3, Delft, The Netherlands.

- Ekengren B. (1996): Ramhörn i skyddsrum - licentiatinledning (Frame Corners in Civil Defence Shelters – Introduction to Discussion at Licentiate Seminar. In Swedish). Swedish Rescue Services Agency, Karlstad, Sweden.
- Ekengren B. (1998): Förändrade regler för skyddsrum (Changed Regulations for Civil Defence Shelters. In Swedish). Bygg & Teknik, 6/98, Stockholm, Sweden, pp. 29-32.
- Eibl J. and Schmidt-Hurtienne B. (1999): Strain-Rate-Sensitive Constitutive Law for Concrete. *Journal of Engineering Mechanics*, Vol. 125, No. 12, pp. 1411-1420.
- Elfgren L., editor (1989): *Fracture Mechanics of Concrete Structures, From Theory to Applications*. Report of the technical committee 90-FMA Fracture Mechanics to Concrete - Application, RILEM. Chapman and Hall, London.
- Elinder U. and Hallhagen B. (1967): Spjälkningsrisk vid böckad buntad armering (Risk of spalling when using bent bundled reinforcement bars. In Swedish). The Royal Institute of Technology, Stockholm, Sweden.
- Feenstra P.H. (1993): *Computational aspects of biaxial stress in plain and reinforced concrete*. Delft University, Delft University Press, Delft, The Netherlands.
- FortH 2 (1987): *Fortifikationshandbok del 2, Kapitel 4-6 (Fortification's Handbook part 2, Chapter 4-6*. In Swedish). Försvarets Läromedelscentral, Stockholm, Sweden.
- Franz G. and Timm G. (1973): *Versuche zur Haken- und Schlaufenverbindung bei biegebeanspruchten Platten (Test of Hook and Loop Connections for Slabs Subjected to Bending*. In German.) *Deutscher Ausschuss für Stahlbeton*, Heft 226, pp. 23-54.
- Fundia (1999): *Letter of information regarding reinforcement type B500BT (In Swedish)*. August, Halmstad, Sweden.
- Georgin J.F., Reynouard J.M. and Nerabet O. (1998): *Modelling of concrete at high strain rate*. *Computational Modelling of Concrete Structure*, Edited by de Borst, Bicanic, Mang and Meschke, Balkema, Rotterdam, The Netherlands, pp. 593-601.



- Grassl P. (1999): Splicing of Reinforcement Loops in Beams: Experiments and Non-linear Finite Element Analyses. Division of Concrete Structures, Chalmers University of Technology, Master Thesis 99:4, Göteborg, Sweden.
- Gylltoft K. (1983): Fracture Mechanics Models for Fatigue in Concrete Structures. Division of Structural Engineering, Luleå University of Technology, Doctoral Thesis 1983:25D, Luleå, Sweden.
- Hallgren P. and Granström S. (1977): Ras mot Skyddsrumstak - beräkningsmodell (Impact load on shelter roof. In Swedish). Tyréns, Stockholm, Sweden.
- Hallgren P. and Granström S. (1975): Takplattans motståndsförmåga mot ras - fallförsök i Svanö fabrik (The resistance of the roof slab against impact loads – impact tests in Svanö Factory. In Swedish). Tyréns, Stockholm, Sweden.
- Han N. (1996): Time Dependent Behaviour of High Strength Concrete. Delft University of Technology, Delft University Press, Delft, The Netherlands.
- HKS (1998): ABAQUS/Explicit User's Manual, Version 5.7. Hibbit, Karlsson and Sorensen Inc. Pawtucket, USA.
- Hillerborg A., Modéer M. and Petersson P-E. (1976): Analysis of Crack Formation and Crack Growth in Concrete by means of Fracture Mechanics and Finite Elements. Cement and Concrete Research, Vol. 6, No. 6, pp. 773-782.
- Hillerborg A. (1988): Rotational Capacity of Reinforced Concrete Beams. Nordic Concrete Research, No. 7, Oslo, Norway, pp. 121-134.
- Hofstetter G. and Mang H.A. (1995): Computational Mechanics of Reinforced Concrete Structures. Vieweg & Sohn Verlagsgesellschaft, Braunschweig, Germany.
- Hughes B.P., and Gregory R. (1972): Concrete subjected to high rates of loading in compression. Magazine of Concrete Research, Vol. 24, No. 78, pp. 25-36.
- Hughes T.J.R. (1987): The Finite Element Method, Linear Static and Dynamic Finite Element Analyses. Prentice-Hall, Englewood Cliffs, New Jersey, USA.

- Jackson N. (1995): Design of reinforced concrete opening corners, *The Structural Engineer*, Vol. 73, No. 13, pp. 209-213.
- Jirasek M. (1999): Numerical Modelling of Deformation and Failure of Materials. Short course held at Rheinisch-Westfälische Technische Hochschule, Aachen, Germany.
- Johansson J.P.M. and Karlsson S. (1997): Nytt armeringsutförande i betongramhörns utsatta för positivt moment (New Reinforcement Detailing in Concrete Frame Corners Subjected to Positive Moment – in Swedish). Division of Concrete Structures, Chalmers University of Technology, Master Thesis 97:5, Göteborg, Sweden.
- Johansson M. (1996): New Reinforcement Detailing in Concrete Frame Corners of Civil Defence Shelters: Non-linear Finite Element Analyses and Experiments. Division of Concrete Structures, Chalmers University of Technology, Licentiate Thesis, Publication 96:1, Göteborg, Sweden.
- Johansson M. (1997): Armeringsseghetens inverkan på deformationsförmågan hos betongkonstruktioner (Influence of Reinforcement Ductility on the Deformation Capacity of Concrete Structures. In Swedish). Division of Concrete Structures, Chalmers University of Technology, Report 97:1, Göteborg, Sweden.
- Johansson M. (1998): Betongens töjningshastighetsberoende and explicit lösningsmetodik (Strain Rate Effects in Concrete and Explicit solution Methods. In Swedish). Division of Concrete Structures, Chalmers University of Technology, Report 98:2, Göteborg, Sweden.
- Johansson M. (1999a): Strain Rate Dependency in Concrete Explained by a SDOF model. Presented in *Material Test Procedures in Support of Dynamic Material Modelling*, Edited by Ågårdh L., FOA Defence Research Establishment, FOA-R-99-01227-311, Stockholm, Sweden.
- Johansson M. (1999b): Non-linear Finite Element Analyses of Civil Defence Shelter Subjected to Explosion Load or Impact Load. Division of Concrete Structures, Chalmers University of Technology, Report 99:8, Göteborg, Sweden.

- Kaplan S.A. (1980): Factors affecting the relationship between rate of loading and measured compressive strength of concrete. Magazine of Concrete Research, Vol. 32, No. 111, pp. 79-88.
- Karlsson M. (1999): Armeringsutformning i ramhörn and knutar (Reinforcement Detailing in Frame Corners and Joints. In Swedish). Teknikområde Anläggning, NCC Teknik, Göteborg, Sweden.
- Kinney G. F. and Graham K. J. (1985): Explosive shocks in air, Second Edition. Springer-Verlag, New York, USA.
- Kordina K. and Fuchs G. (1970): Untersuchungen zur Anwendung von hakenförmigen Übergreifungsstößen in Rahmenecken (Examination of the use of Reinforcement Loops in Frame Corners. In German). Institut für Baustoffkunde und Stahlbetonbau, Der Technischen Universität Braunschweig, Braunschweig, Germany.
- Kordina K. and Fuchs G. (1973): Untersuchungen an Übergreifungs-Vollstößen mit hakenförmig-gebogenen Rippenstählen (Studies of Splicing of Hook-formed Bars. In German). Deutscher Ausschuss für Stahlbeton, Heft 226, pp. 55-81.
- Kordina K. (1984): Bewehrungsführung in Ecken und Rahmenknoten (Reinforcement Design of Corners and Joints in Reinforced Concrete Frame Structures. In German). Deutscher Ausschuss für Stahlbeton, Heft 354, pp 5-93.
- Krauthammer T. (1998): Structural Concrete and Steel Connections for Blast Resistant Design. Transient loading and response of structures, Edited by Langseth M. and Krauthammer T., Trondheim, Norway, pp. 161-195.
- Ku C-K. and Krauthammer T. (1999): Numerical Assessment of Reinforced Concrete Knee-Joints under Explosively Applied Loads. ACI Structural Journal, Vol. 96, No. 2, pp. 239-247.
- Kwak H-G. and Filippou F.C. (1990): Finite Element Analysis of Reinforced Concrete Structures under Monotonic Loads. Department of Civil Engineering, University of California Berkeley, Report No. UCB/SEMM-90/14, California, USA.

- Larsson L., Runesson K. and Åkesson M. (1995): Embedded Cohesive Crack Models Based on Regularized Discontinuous Displacements. *Fracture Mechanics of Concrete Structures, FRAMCOS-2*, Edited by Wittmann F.H., Zurich, Switzerland, pp. 899-911.
- Lee Y-H. and Willam K. (1997): Mechanical Properties of Concrete in Uniaxial Compression. *ACI Materials Journal*, V. 94, No. 6, pp. 457-471.
- Leonhardt F., Walther R. and Dieterle H. (1973): Versuche zur Ermittlung der Tragfähigkeit von Zugschlaufstößen (In German). *Deutscher Ausschuss für Stahlbeton*, Heft 226, pp. 1-53.
- Limberger E., Brandes K. and Herter J. (1982): Influence of Mechanical Properties of Reinforcing Steel on the Ductility of Reinforced Concrete Beams with Respect to High Strain Rates. Presented in *Concrete Structures under Impact and Impulsive Loading*, BAM, Berlin, Germany, pp. 134-156.
- Lundgren K. (1999): Three-Dimensional Modelling of Bond in Reinforced Concrete: Theoretical Model, Experiments and Applications. Division of Concrete Structures, Chalmers University of Technology, Ph.D. Thesis, Publication 99:1, Göteborg, Sweden.
- Magnusson J. (2000): Bond and Anchorage of Ribbed Bars in High-Strength Concrete. Division of Concrete Structures, Chalmers University of Technology, Ph.D. Thesis, Publication 00:1, Göteborg, Sweden.
- Malvar L. J. (1998): Review of static and dynamic properties of steel reinforcing bars. *ACI Materials Journal*, Vol. 95, No. 5, pp. 609-616.
- Malvar L. J. and Ross C. A. (1998): Review of strain rate effects for concrete in tension. *ACI Materials Journal*, Vol. 95, No. 6, pp. 735-739.
- Malvar L. J., and Ross C. A. (1999). Discussion of Malvar and Ross (1998), *ACI Materials Journal*, Vol. 99, No. 6, pp. 614-616.
- Markeset G. (1993): Failure of Concrete under Compressive Strain Gradients. Department of Structural Engineering, The Norwegian Institute of Technology, Ph.D. Thesis, Trondheim, Norway.

- Martinez C. and Sanchez D. (2000): Nonlinear Finite Element Analysis of Continuous Deep Beams. Division of Concrete Structures, Chalmers University of Technology, Master Thesis 00:5, Göteborg, Sweden.
- Mattiasson K., Bernspång L., Honecker A., Schedin E., Hammam T. and Melander A. (1991): On the use of explicit time integration in finite element simulation of industrial sheet forming process. Department of Structural Mechanics, Chalmers University of Technology, Publication 91:2, Göteborg, Sweden.
- Mayfield B., Kong, F.K., Bennison, A. and Davies, J.C.D.T. (1971): Corner Joint Details in Structural Lightweight Concrete, ACI Journal, V. 68, No. 5, pp. 366-372.
- Mayfield B., Kong F.K., and Bennison A. (1972): Strength and Stiffness of Lightweight Concrete Corners, ACI Journal, V. 69, No. 7, pp. 420-427.
- Marx E.M. (1993): Analysis of Reinforced Concrete Wall to Slab Connections Subjected to Severe Impulse Loading. Department of Civil Engineering, The Pennsylvania State University.
- Mörnstad M. (1998): Cut-and-Cover Tunnels at the Arlanda Link. IABSE Conference, Tunnel Structures, Stockholm, Sweden, pp. 181-186.
- Mörnstad M. (2000): Personal Communication. Chief Engineer, NCC AB, Malmö, Sweden.
- Nilsson I.H.E. (1976): Undersökning av ramhörn med positivt moment (Reinforced Concrete Frame Joints Subjected to Positive Moment, Test Report 2. In Swedish). Division of Concrete Structures, Chalmers University of Technology, Report 67:1, Göteborg, Sweden.
- Nilsson I.H.E. (1973): Reinforced concrete corners and joints subjected to bending moment. National Swedish Institute for Building Research, Document D7:1973, Stockholm, Division of Concrete Structures, Chalmers University of Technology, Ph.D. Thesis, Publication 73:6, Göteborg, Sweden.
- Nilsson I.H.E. and Losberg, A. (1976): Reinforced Concrete Corners and Joints Subjected to Bending Moment, ASCE Journal of the Structural Division, Vol. 102, No. 6, pp. 1229-1254.

- Nilsson L. (1979): Impact Loading on Concrete Structures, A constitutive modelling, finite element analysis, and experimental study of nonlinear wave propagation. Department of Structural Mechanics, Chalmers University of Technology, Ph.D. Thesis, Publication 79:1, Göteborg, Sweden.
- Noor F.A. (1977): Ultimate Strength and Cracking of Wall Corners, Concrete, Cement and Concrete Association, London, July, pp. 31-35.
- Olofsson T., Ohlsson U. and Klisinski M. (1995): A Simple Fracture Mechanics Model for Mixed-mode Failure in Concrete. Fracture Mechanics of Concrete Structures, FRAMCOS-2, Edited by Wittmann F.H., Zurich, Switzerland, pp 473-494.
- Olsson M. (1996): Olinjär finit elementanalys av ramhörn i armerad betong (Non-linear Finite Element Analysis of Concrete Frame Corners. In Swedish). Division of Concrete Structures, Chalmers University of Technology, Master Thesis 96:6, Göteborg, Sweden.
- Otani R.K. and Krauthammerr T. (1997): Assessment of Reinforcement Details for Blast Containment Structures. ACI Structural Journal, Vol. 94, No. 2, pp. 124-132.
- Plos M. (1994a): Ny armeringsskarv för ramhörn i skyddsrum (New Reinforcement Splice for Frame Corners in Civil Defence Shelters. In Swedish). Division of Concrete Structures, Chalmers University of Technology, Report 94:2, Göteborg, Sweden.
- Plos M. (1994b): Splicing of Reinforcement in Frame Corners -Experimental Studies. Nordic Concrete Research, Publ. no. 14, The Nordic Concrete Federation, Oslo, Norway, pp 103-121.
- Plos M. (1995): Application of Fracture Mechanics to Concrete Bridges - Finite Element Analyses and Experiments. Division of Concrete Structures, Chalmers University of Technology, Ph.D. Thesis, Publication 95:3, Göteborg, Sweden.
- Reinhardt H.W. (1982): Concrete under Impact Loading, Tensile Strength and Bond. HERON, Vol. 27, No. 3, Delft, The Netherlands.
- Reinhardt H.W., Körmeling H.A., Zielinski A.J. (1985): The split Hopkinson bar, a versatile tool for the impact testing of concrete. Materials and Structures, Vol. 19, pp. 55-63.

- Reinhardt H.W., Rossi P., van Mier J.G.M. (1990): Joint investigation of concrete at high strain rates of loading. *Materials and Structures*, Vol. 23, pp. 213-216.
- RILEM 50-FMC (1985): Determination of the Fracture Energy of Mortar and Concrete by Means of Three-point Bend Tests on Notched Beams. *Materials and Structures*, Vol. 18, pp. 285-290.
- Ross C.A., Tedesco J.W., Kuennen S.T. (1995): Effects of Strain Rate on Concrete Strength. *ACI Materials Journal*, Vol. 92, No. 1, pp. 37-47.
- Ross C.A., Jerome D.M., Tedesco J.W., Hughes M.L. (1996): Moisture and Strain Rate Effects on Concrete Strength. *ACI Materials Journal*, Vol. 93, No. 3, pp. 293-300.
- Rossi P. (1991a): A physical phenomenon which can explain the mechanical behaviour of concrete under high strain rates. *Materials and Structures*, Vol. 24, pp. 422-424.
- Rossi P. (1991b): Influence of cracking in the presence of free water on the mechanical behaviour of concrete. *Magazine of Concrete Research*, Vol. 42, No. 154, pp. 53-57.
- Rossi P., van Mier J.G.M., Boulay C., Le Maou F. (1992): The dynamic behaviour of concrete: influence of free water. *Materials and Structures*, Vol. 25, pp. 509-514.
- Rossi P., van Mier G.M., Toutlemonde F., Le Maou F., Boulay C. (1994): Effect of loading rate on the strength of concrete subjected to uniaxial tension. *Materials and Structures*, Vol. 27, pp. 260-264.
- Rossi P. and Toutlemonde F. (1996): Effect of loading rate on the tensile behaviour of concrete: description of the physical mechanisms. *Materials and Structures*, Vol. 29, Mar., pp. 116-118.
- Rots J.G. (1988): *Computational Modelling of Concrete Fracture*. Department of Civil Engineering, Delft University of Technology, pp. 132.
- Rots J.G. (1989): *Fracture Mechanics of Concrete Structures: From theory to applications*. RILEM Technical Committee 90-FMA, Edited by Elfgrén L., Chapman and Hall, London, England, pp. 138-145.

- Schmidt-Hurtienne B., Häußler U. and Eibl J. (1998): Strain Rate Effects in Concrete – an Uniaxial Constitutive Law. Transient loading and response of structures, Edited by Langseth M. and Krauthammer T., Trondheim, Norway, pp. 41-61.
- Seabold R.B. (1970): Dynamic Shear Strength of Reinforced Concrete Beams, Part III. Technical Report No. R-695, U.S. Naval Civil Engineering Laboratory, Port Hueneme, USA.
- Serecombe J., Ulm F.-J. and Toutlemonde F. (1998): Viscous Hardening Plasticity for Concrete in High-Rate Dynamics. Journal of Engineering Mechanics, Vol. 124, No. 9, pp. 1050-1057.
- Skettrup E., Strabo J., Andersen N.H. and Brondum-Nielsen T. (1984): Concrete Frame Corners, ACI Journal, Vol. 81, No. 6, 1984, pp. 587-593.
- Soroushian P., Choi K.-B., Alhamad A. (1986): Dynamic Constitutive Behaviour of Concrete. ACI Journal, Mar.-Apr., pp. 251-259.
- Stroband J. and Kolpa J.J. (1981): The Behaviour of Reinforced Concrete Column-to-Beam joints, Part 2: Corners Subjected to Positive Moments, Stevin Laboratory, Delft University of Technology, Report 5-81-5, Delft, The Netherlands
- Stroband J. and Kolpa J.J. (1983): The behaviour of reinforced concrete column-to-beam joints, Part 1, Corners subjected to negative moments. Stevin Laboratory, Delft University of Technology, Report 5-83-9, Delft, The Netherlands.
- Suaris W. and Shah S.P. (1985): Constitutive Model for Dynamic Loading of Concrete. Journal of Structural Engineering. Vol. 111, No. 3, pp. 563-576.
- Sundquist H. (1977): Betongplatta på pelare vid dynamisk engångslast, Del 3 (Concrete Slab on Column Subjected to Impact Load, Part 3. In Swedish). Department of Building Statics and Structural Engineering, Royale Institute of Technology, Message No. 126, Stockholm, Sweden.



- Sundquist H. (1978): Betongplatta på pelare vid dynamisk engångslast, Del 2 (Concrete Slab on Column Subjected to Impact Load, Part 2. In Swedish). Department of Building Statics and Structural Engineering, Royale Institute of Technology, Message No. 125, Stockholm, Sweden.
- Sundquist H. (1979): Concrete Slabs Supported on Slender Columns under Short Duration Loads, Summary. Department of Building Statics and Structural Engineering, Royale Institute of Technology, Ph.D. Thesis, Message No. 134, Stockholm, Sweden.
- Swann R. A., (1969): Flexural Strength of Corners of Reinforced Concrete Portal Frames. Technical Report TRA 434, Cement and Concrete Association, London.
- Swedish Rescue Services Agency (1990): Skyddsrumregler SR – Första utgåvan (Shelter Regulations – First Edition. In Swedish). Swedish Rescue Services Agency, Publication B54-141/92, Karlstad, Sweden.
- Swedish Rescue Services Agency (1994): Shelter Regulations, SR - English edition. Swedish Rescue Services Agency, Publication B54-168/94, Karlstad, Sweden.
- Swedish Rescue Services Agency (1998): Skyddsrumregler SR – Produktion and vidmakthållande (Shelter Regulations – Production and Maintenance. In Swedish). Swedish Rescue Services Agency, Publication B54-141/98, Karlstad, Sweden.
- Taerwe L. (1993): Empirical Analysis of the Fracture Process in High Strength Concrete Loaded in Uniaxial Compression. Fracture and Damage of Concrete and Rock – FDCR-2, Vienna, Austria, Edited by Rassmanith H.P., E & FN Spon, pp. 122-134.
- Timm G. (1969): Untersuchungen zur Verbindung von Stahlbetonplatten mit hakenförmig gebogenen Stäben (Examination of Connections of Reinforced Concrete Slabs using Hook-formed Bars. In German.) Department of Civil Engineering, University of Karlsruhe, Ph.D. Thesis, Karlsruhe, Germany.
- Ulfkjaer J.P., Pilegaard Hansen L., Qvist S., Madsen S.H. (1996): Fracture Energy of Plain Concrete Beams at Different Rates of Loading. Fracture & Dynamics Paper No. 74, Department of Building Technology and Structural Engineering, Aalborg University, Aalborg, Denmark.

- van Mier J.G.M. (1984): Strain Softening of Concrete Under Multiaxial Loading Conditions. Eindhoven University of Technology, Ph.D. Thesis, Eindhoven, The Netherlands.
- van Mier J.G.M., Shah S.P., Arnaud M., Balayssac J.P., Bascoul A., Choi S., Dasenbrock D., Ferrara G., French C., Gobbi M.E., Karihaloo B.L., König G., Kotsovos M.D., Labuz J., Lange-Kornbak D., Markeset G., Pavlovic M.N., Simsch G., Thienel K-C. and Turatsinze A., (1997): Strain-softening of concrete in uniaxial compression. *Materials and Structures*, Vol. 30, May, pp. 195-209.
- Vos E. and Reinhardt H-W. (1980): Bond resistance of deformed bars, plain bars and strands under impact loading. Department of Civil Engineering, Delft University of Technology, Report 5-80-6, Delft, The Netherlands
- Vägverket (1994): BRO 94 - Allmän teknisk beskrivning för broar (Bridge 94 – General Technical Description for Bridges. In Swedish). Swedish Road Administration, Borlänge, Sweden.
- Weerheijm J. (1992): Concrete under impact tensile loading and lateral compression. TNO-Prins Maurits Laboratory, Ph.D. Thesis, Rijswijk, The Netherlands.
- Wästlund G. (1935): Om armering av vinkelformade betongkonstruktioner (Reinforcement of Angle-shaped Concrete Structures. In Swedish). *Betong*, No. 1, Stockholm, Sweden, pp. 22-35.
- Yan C. and Mindess S. (1998): Effect of Loading Rate on Bond Behaviour Under Dynamic Loading. *Concrete and Blast Effects*, ACI International SP-175, Edited by Bounds W., Michigan, USA, pp. 179-197.
- Zielinski A.J., Reinhardt H.W., Körmeling H.A. (1981): Experiments on concrete under uniaxial impact tensile loading. *Materials and Structures*, Vol. 14, No. 80, pp. 103-112.
- Zielinski A.J. (1982): Fracture of Concrete and Mortar under Uniaxial Impact Tensile Loading. Delft University of Technology, Ph.D. Thesis, Delft, The Netherlands.

Ågårdh L. and Laine L. (1997): Experiments and FE-Modelling of Fibre Reinforced Concrete Beams Exposed to Impact. Reprint from 2<sup>nd</sup> Asian Pacific Conference of Shock and Impact Loads on Structures, Melbourne, Australia.

Åkesson M. (1996): Implementation and Application of Fracture Mechanics Models for Concrete Structures. Division of Concrete Structures, Chalmers University of Technology, Ph.D. Thesis, Publication 96:2, Göteborg, Sweden.

Östlund L. (1963): Inverkan av böckningsradier and täckande betongskikt hos kamstål på spjälkningsrisken för armerade betongkonstruktioner (The Influence of Bending Radius and Concrete Cover for Deformed Bars on the Risk of Splitting Failure in Reinforced Concrete Structures. In Swedish). The Royal Institute of Technology, Stockholm, Sweden.

## Appendix A Summary of Frame Corner Tests

This Appendix summarises the test results of frame corners subjected to opening or closing moment that are presented in Chapter 2. In the original work, the cube strength was often used when referring to the compressive strength of the concrete. However, both the Swedish concrete handbook Code BBK 94, Boverket (1994), and Eurocode 2, CEN (1991), make use of the concrete cylinder strength in the design. Therefore, recalculations to such values were made where necessary. It is well known that the compressive strength depends on both the curing condition and the geometry of the specimen tested; see Betonghandboken Material (1994). But, there was often no clear information on what curing conditions had been used, and when such information was available, the method used often differed considerably from that prescribed in standards of today. Hence, it would not be an easy task to consistently recalculate the concrete used in the different tests. As a simplification, the cube strength  $f_{c,cube}$  was therefore related to the cylinder strength  $f_c$  as

$$f_{c,cube} = 1.35f_c \quad (\text{A.1})$$

which is the relation given in BST Byggstandardiseringen (1991) for dry cured concrete cubes (side 150 mm) and water cured concrete cylinders ( $\phi 150 \times 300$  mm). Further, no account was taken of the influence of different cube or cylinder sizes used. The approximation in equation (A.1) might lead to a slight underestimation of the concrete cylinder strength and the results obtained were therefore compared to the case if  $f_{c,cube} = 1.25f_c$  had been used instead. It was then found that the difference was quite negligible (see Figure A1) and it was concluded that the approximation made was appropriate. Due to this recalculation of the compressive strength, and the fact that all tests presented here were originally not evaluated in the same way, the theoretical strength  $M_{uc}$  of each frame corner was redetermined. Hence, the efficiencies presented herein may also differ somewhat from those reported by the original authors.

Several different reinforcement detailings were tested. Many of them, though, show such large resemblances to each other that the structural responses obtained were more or less the same. Accordingly, it was possible to divide them into three major types: *Type 1*, *Type 3* and *Type 4*; see Figure A.1. Of these types, the addition of radial bars in the *Type 1* detailing was considered so important that it was denoted detailing *Type 2*. The combination of radial stirrups and reinforcement loops (i.e. detailings *Type 3* and *Type 4*) did not have a very pronounced effect and they were therefore only regarded as variants of the original detailings.

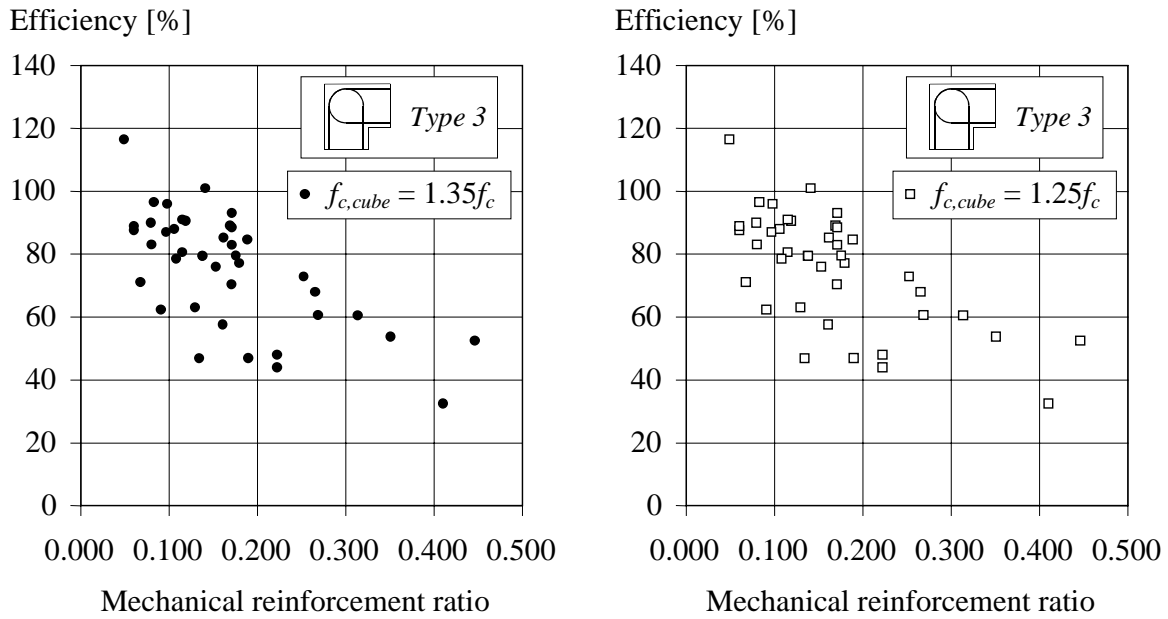


Figure A.1 Comparison of efficiency versus mechanical reinforcement ratio obtained when different relations between the compressive cube strength  $f_{c,cube}$  and the compressive cylinder strength  $f_c$  are used.

	<i>a</i>	<i>b</i>	<i>c</i>	<i>d</i>	<i>e</i>	<i>f</i>
<i>Type 1</i>						
<i>Type 2</i>						
<i>Type 3</i>						
<i>Type 4</i>						

Figure A.2 Reinforcement detailings tested. The denotations *a* to *e* shown here are also used in Tables A.1 to A.8 to clarify which detailing was used in the individual tests.

The test set-ups used by different researchers are shown in Figures A.3 and A.4 for tests on opening and closing corners, respectively. The tests by Mayfield et al. (1971,1972) were carried out using a lightweight concrete with a density of  $1762 \text{ kg/m}^3$ . Nevertheless, the relation between compressive and tensile concrete was assumed to be the same as that for

ordinary concrete, i.e. according to equation (2.15). All frame corners tested, except those by Nilsson, had the same dimensions for the adjoining members. Unless stated otherwise, the effective height of the larger member in his test series was  $d + 50$  mm.

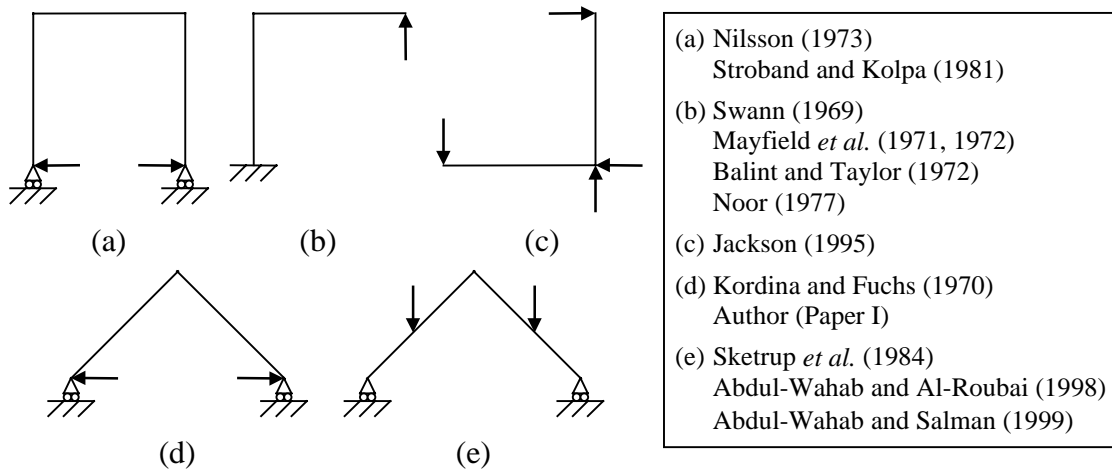


Figure A.3 Schematic views of the test set-ups used by different researchers in tests on opening moment.

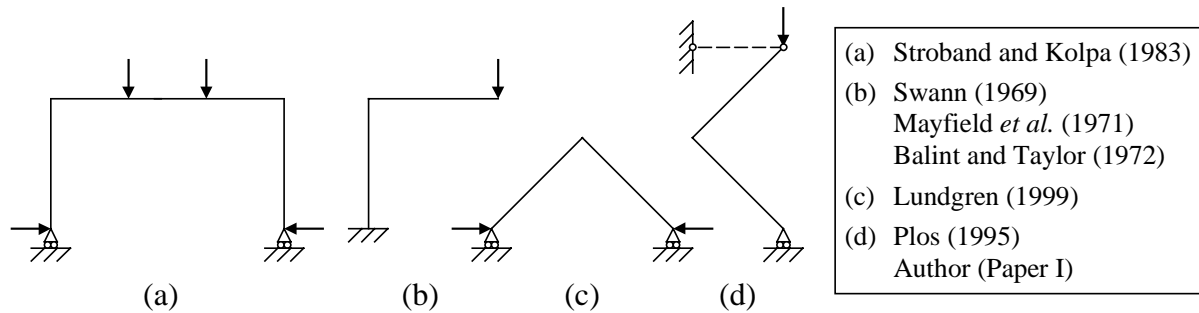
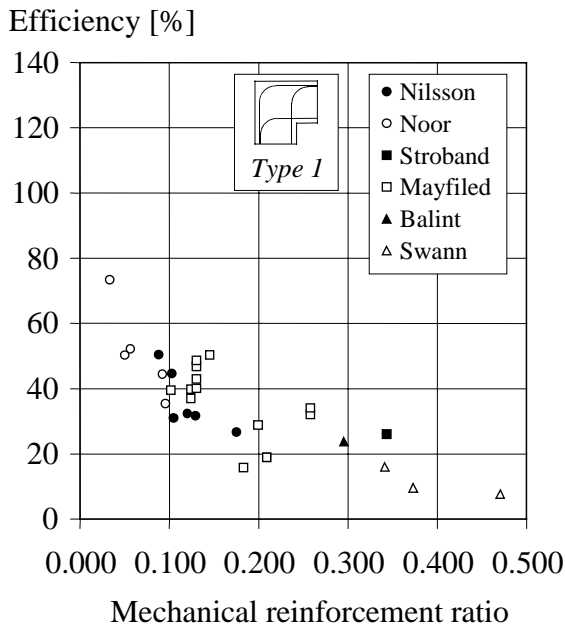
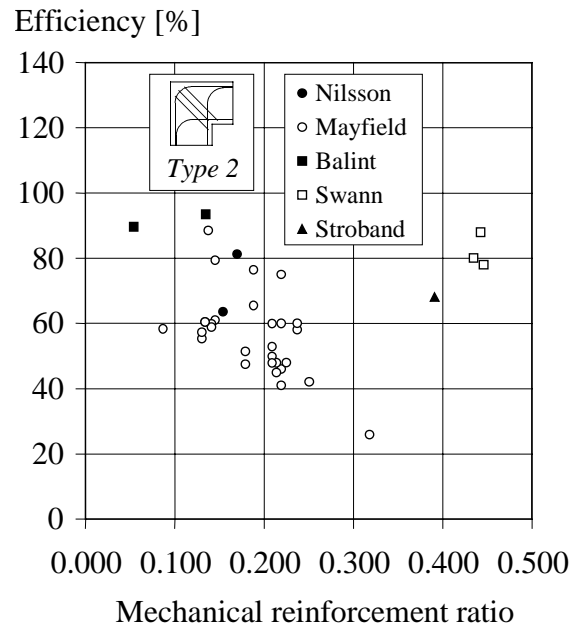


Figure A.4 Schematic views of the test set-ups used by different researchers in tests on closing moment.

Figures A.5 to A.7 summarises the efficiencies obtained by different researchers when the reinforcement detailing was varied. Figure A.8 shows what influence the ratio between the resisting force  $F_R$  and the tensile force  $R$  (see Sections 2.2.1 and 2.3.3.2) has on the *Type 2* detailing. Tables A.1 to A.8 summarises dimensions and results of the tests on opening and closing frame corners presented herein. In these Tables, the full reference is not given. Instead, only the first name in each reference is given. In the case of Mayfield *et al.* and Abdul-Wahab and co-workers, the year of publication is also given to distinguish between the references. In all tests, except those reported by Mayfield *et al.*, Lundgren, Plos and the Author, were the compressive strength originally determined on concrete cubes. Therefore, the compressive strength  $f_c$ , given below, for these references was recalculated according to equation (A.1).

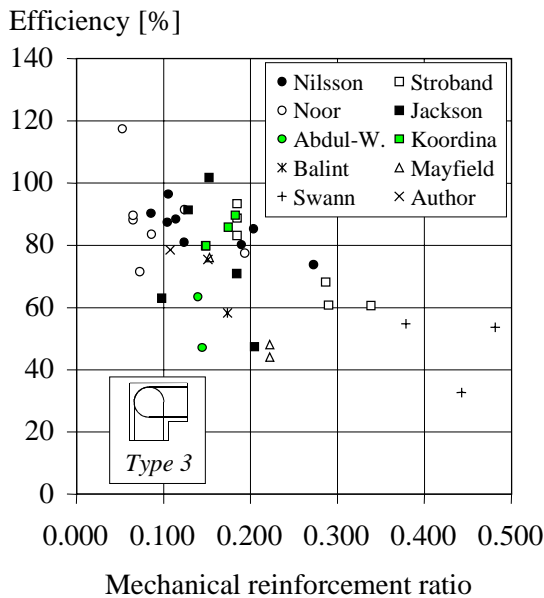


(a)

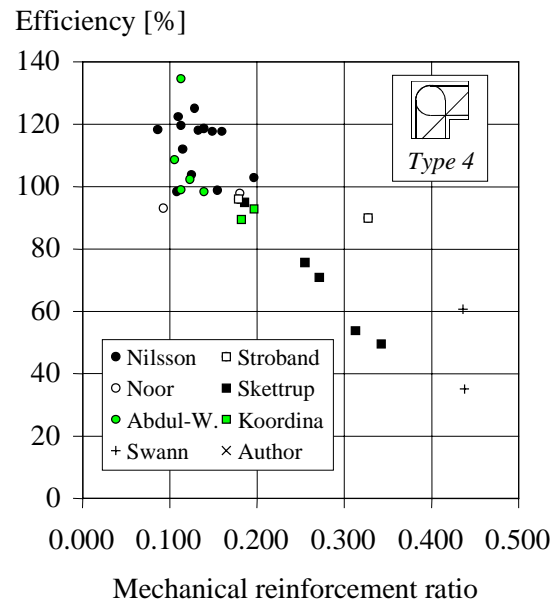


(b)

Figure A.5 Efficiencies of opening frame corners reinforced with (a) detailing *Type 1* and (b) detailing *Type 2*.



(a)



(b)

Figure A.6 Efficiencies of opening frame corners reinforced with (a) detailing *Type 3* and (b) detailing *Type 4*. The conventional evaluation method (see Section 2.1.3) has been used when determining the efficiencies for detailing *Type 4*.

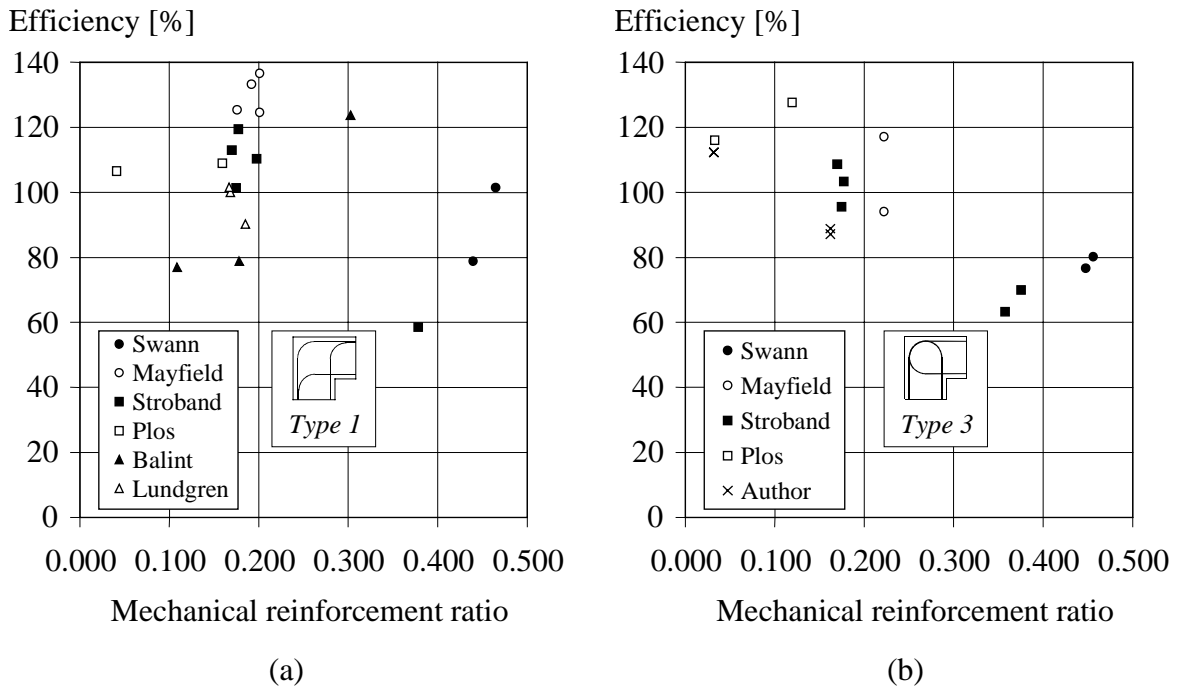


Figure A.7 Efficiencies of closing frame corners reinforced with (a) detailing *Type 1* and (b) detailing *Type 3*.

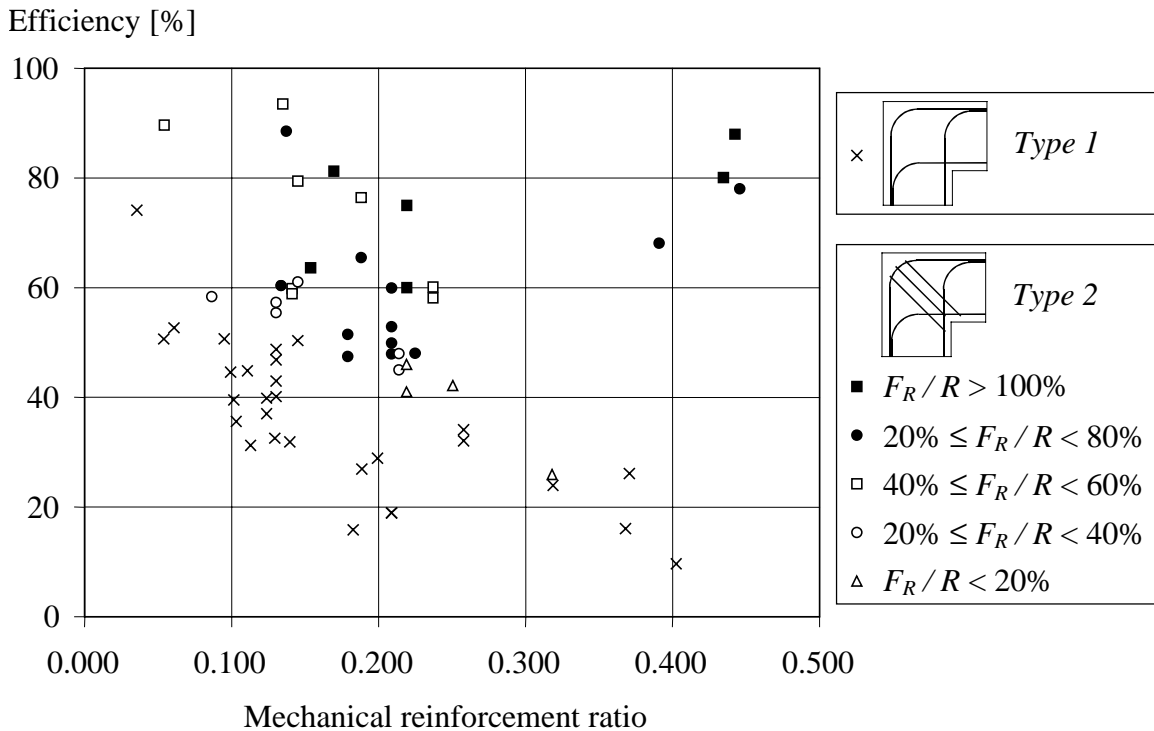


Figure A.8 Influence of radial stirrups within the corner for varying value on the ratio  $F_R/R$ .



Table A.1 Summary of test results for opening frame corner reinforced with detailing *Type 1*.



Type	Author	Specimen	$A_s$	$b$ [mm]	$d$ [mm]	$f_{sy}$ [MPa]	$f_c$ [MPa]	$\rho$ [%]	$\omega_s$	$M_{ut}$ [kNm]	$M_{ue}$ [kNm]	$M_{ue}/M_{uc}$ [%]	$M_{ut}/M_{uc}$ [%]
1a	Balint	NS014/3	2 $\phi$ 12	152	124	433	16.3	1.20	0.319	2.5	1.2	11	24
1a	Mayfield 71	1-1	2 $\phi$ 12	150	158	449	20.6	0.96	0.209	2.7	2.4	17	19
1a		1-2	2 $\phi$ 12	150	158	449	20.6	0.96	0.209	2.7	2.4	17	19
1c		3-1	2 $\phi$ 12	150	158	449	23.5	0.96	0.183	2.3	2.8	19	16
1c		4A-1	2 $\phi$ 12	150	158	449	21.6	0.96	0.199	4.2	2.6	18	29
1c		4B	2 $\phi$ 12	150	158	449	16.7	0.96	0.258	4.5	1.9	14	32
1c		4C	2 $\phi$ 12	150	158	449	16.7	0.96	0.258	4.7	1.9	14	34
1e	Mayfield 72	1-1	2 $\phi$ 10	150	158	375	20.1	0.66	0.124	3.7	2.4	26	40
1e		1-2	2 $\phi$ 10	150	158	375	20.1	0.66	0.124	3.4	2.4	26	37
1e		2-1	2 $\phi$ 10	150	158	375	19.1	0.66	0.130	3.9	2.3	25	43
1e		2-2	2 $\phi$ 10	150	158	375	19.1	0.66	0.130	4.2	2.3	25	47
1e		3	2 $\phi$ 10	150	158	375	24.5	0.66	0.102	3.8	3.0	31	40
1a		9	2 $\phi$ 10	150	158	375	17.2	0.66	0.145	4.5	2.0	23	50
1c		19-1	2 $\phi$ 10	150	158	375	19.1	0.66	0.130	3.6	2.3	25	40
1c		19-2	2 $\phi$ 10	150	158	375	19.1	0.66	0.130	4.4	2.3	25	49
1b	Nilsson	U1	5 $\phi$ 16	500	270 <sup>1</sup>	419	32.9	0.74	0.095	54.9	49.7	46	51
1b		U2	5 $\phi$ 16	500	270 <sup>1</sup>	410	27.0	0.74	0.113	32.8	31.9	30	31
1b		U3	3 $\phi$ 25	500	263 <sup>2</sup>	398	31.9	1.12	0.140	45.7	45.3	32	32
1b		U20	4 $\phi$ 10	350	175	432	20.0	0.51	0.111	10.1	8.7	39	45
1b		U21	4 $\phi$ 12	350	169	417	24.6	0.76	0.130	9.7	10.0	34	33
1b		U22	6 $\phi$ 12	350	169	426	25.9	1.15	0.189	11.9	10.3	23	27
1a	Noor	A1	8 $\phi$ 10	800	130	433	43.0	0.60	0.061	18.8	18.0	50	53
1a		A1R	8 $\phi$ 10	800	135	433	46.7	0.58	0.054	18.4	20.8	57	51
1a		A2	8 $\phi$ 12	800	137	455	37.8	0.83	0.099	23.9	17.8	33	45
1a		A3	8 $\phi$ 8	800	133	448	47.4	0.38	0.036	18.6	20.7	82	74
1a		A4	11 $\phi$ 10	800	133	433	34.1	0.81	0.103	16.8	15.3	32	36
1a	Stroband	B13	2 $\phi$ 6	70	109	504	10.1	0.74	0.371	0.7	0.2	6	26
1d	Swann	1	2 $\phi$ 19	152	123	295	17.6	3.02	0.508	1.2	1.2	8	8
1c		2	2 $\phi$ 19	152	123	295	22.2	3.02	0.403	1.7	1.6	9	10
1a		3	2 $\phi$ 19	152	123	295	24.2	3.02	0.368	2.8	1.7	10	16

<sup>1</sup>Unequal effective height in the members adjoining the corner, add 100 mm to larger member.

<sup>2</sup>Unequal effective height in the members adjoining the corner, add 200 mm to larger member.

Table A.2 Summary of test results for opening frame corner reinforced with detailing *Type 2*.



Type	Author	Specimen	$A_s$	$A_{s,r}$	$b$ [mm]	$d$ [mm]	$f_{sy}$ [MPa]	$f_c$ [MPa]	$\rho$ [%]	$\alpha_s$	$F_R/R$ [%]	$M_{ut}$ [kNm]	$M_{ue}$ [kNm]	$M_{ue}/M_{uc}$ [%]	$M_{ut}/M_{uc}$ [%]
2c	Balint	NS005	2 $\phi$ 8	3 $\phi$ 6	152	124	433	42.6	0.53	0.054	60	5.4	3.2	53	90
2c		NS014/5	2 $\phi$ 12	6 $\phi$ 6	152	124	433	38.5	1.20	0.135	53	10.8	5.7	49	93
2c	Mayfield 71	5A-1	2 $\phi$ 12	2 $\phi$ 12	150	158	449	24.0	0.96	0.179	71	7.6	11.2	76	51
2c		5A-2	2 $\phi$ 12	2 $\phi$ 12	150	158	449	24.0	0.96	0.179	71	7.0	11.2	76	47
2c		5B-1	2 $\phi$ 12	2 $\phi$ 6	150	158	449	19.6	0.96	0.219	18	5.8	2.5	18	41
2c		5B-2	2 $\phi$ 12	2 $\phi$ 6	150	158	449	19.6	0.96	0.219	18	6.6	2.5	18	46
2c		5C-1	2 $\phi$ 12	2 $\phi$ 12	150	158	449	19.1	0.96	0.225	71	6.8	10.7	75	48
2c		5D-1	2 $\phi$ 12	2 $\phi$ 6	150	158	449	17.2	0.96	0.251	18	5.9	2.5	18	42
2c		5E-1	2 $\phi$ 16	2 $\phi$ 6	150	158	449	24.0	1.70	0.318	10	6.2	2.8	12	26
2c		5F-1	2 $\phi$ 8	2 $\phi$ 6	150	158	449	22.1	0.43	0.087	40	4.4	2.8	37	58
2c		6A-1	2 $\phi$ 12	4 $\phi$ 6	150	158	449	20.1	0.96	0.214	35	6.4	5.1	35	45
2c		6A-2	2 $\phi$ 12	4 $\phi$ 6	150	158	449	20.1	0.96	0.214	35	6.9	5.1	35	48
2c		6B-1	2 $\phi$ 12	4 $\phi$ 8	150	158	449	20.6	0.96	0.209	63	8.6	9.9	69	60
2c		6B-2	2 $\phi$ 12	4 $\phi$ 8	150	158	449	20.6	0.96	0.209	63	7.6	9.9	69	53
2c		6C-1	2 $\phi$ 12	4 $\phi$ 12	150	158	449	19.6	0.96	0.219	141	8.6	18.4	100	60
2c		6C-2	2 $\phi$ 12	4 $\phi$ 12	150	158	449	19.6	0.96	0.219	141	10.7	18.4	100	75
2c		7-1	2 $\phi$ 12	6 $\phi$ 6	150	158	449	18.1	0.96	0.237	53	8.2	8.4	60	58
2c		7-2	2 $\phi$ 12	6 $\phi$ 6	150	158	449	18.1	0.96	0.237	53	8.5	8.4	60	60
2c	8-1	2 $\phi$ 12	8 $\phi$ 6	150	158	449	20.6	0.96	0.209	71	7.2	10.8	75	50	
2c	8-2	2 $\phi$ 12	8 $\phi$ 6	150	158	449	20.6	0.96	0.209	71	6.9	10.8	75	48	
2a	Mayfield 72	10	2 $\phi$ 10	2 $\phi$ 6	150	158	375	17.2	0.66	0.145	25	5.4	2.2	24	61
2a		11	2 $\phi$ 10	4 $\phi$ 6	150	158	375	17.2	0.66	0.145	51	7.1	4.3	49	79
2a		12	2 $\phi$ 10	6 $\phi$ 6	150	158	375	18.1	0.66	0.137	76	7.9	7.3	81	89
2c		20-1	2 $\phi$ 10	2 $\phi$ 6	150	158	375	19.1	0.66	0.130	25	5.0	2.3	26	55
2c		20-2	2 $\phi$ 10	2 $\phi$ 6	150	158	375	19.1	0.66	0.130	25	5.2	2.3	26	57
2c		21A-1	2 $\phi$ 10	4 $\phi$ 6	150	158	375	17.7	0.66	0.141	51	5.3	4.3	48	60
2c		21A-2	2 $\phi$ 10	4 $\phi$ 6	150	158	375	17.7	0.66	0.141	51	5.3	4.3	48	59
2c		21B	2 $\phi$ 10	4 $\phi$ 6	150	158	375	13.2	0.66	0.188	51	6.5	5.0	59	76
2c		22A-1	2 $\phi$ 10	6 $\phi$ 6	150	158	375	18.6	0.66	0.134	76	5.5	7.3	81	60
2c		22A-2	2 $\phi$ 10	6 $\phi$ 6	150	158	375	18.6	0.66	0.134	76	5.5	7.3	81	60
2c		22B	2 $\phi$ 10	6 $\phi$ 6	150	158	375	13.2	0.66	0.188	76	5.5	6.8	80	66
2b	Nilsson	U27	4 $\phi$ 12	8 $\phi$ 10	350	169	405	20.1	0.76	0.154	107	18.1	29.5	100	64
2a		U28	4 $\phi$ 12	24 $\phi$ 6	350	169	439	19.8	0.76	0.170	99	24.9	30.3	99	81
2a	Stroband	B14	2 $\phi$ 6	10 $\phi$ 2.8	70	109	504	9.6	0.74	0.391	77	1.9	2.2	77	68
2c	Swann	9	2 $\phi$ 19	4 $\phi$ 12.7	152	123	295	20.0	3.02	0.446	63	13.3	11.2	66	78
2c		9'	2 $\phi$ 19	4 $\phi$ 12.7	152	123	295	17.3	3.02	0.514	63	8.7	11.1	65	51
2c		10	2 $\phi$ 19	4 $\phi$ 19	152	123	295	20.2	3.02	0.442	141	15.1	23.3	100	88
2c		10'	2 $\phi$ 19	4 $\phi$ 19	152	123	295	20.5	3.02	0.435	141	13.7	23.3	100	80

Table A.3 Summary of test results for opening frame corner reinforced with detailing *Type 3*.



Type	Author	Specimen	$A_s$	$b$ [mm]	$d$ [mm]	$f_{sy}$ [MPa]	$f_c$ [MPa]	$\rho$ [%]	$\alpha_s$	$M_{ut}$ [kNm]	$M_{ue}$ [kNm]	$M_{ue}/M_{uc}$ [%]	$M_{ut}/M_{uc}$ [%]
3a	Abdul-98	E2	3 $\phi$ 10	300	115	491	23.2	0.68	0.145	5.8	3.0	24	47
3a		E7 <sup>1</sup>	3 $\phi$ 10	300	115	491	37.6	0.68	0.089	12.3	4.7	37	97
3a	Abdul-99	A3	3 $\phi$ 10	300	115	467	22.8	0.68	0.140	7.5	2.9	25	63
3a	Balint	NS014/4	2 $\phi$ 12	152	124	450	31.1	1.20	0.174	6.7	2.3	20	58
3c	Kordina	E1	6 $\phi$ 12	700	124	475	25.0	0.78	0.149	28.38	8.71	25	80
3c		E2	6 $\phi$ 12	700	124	475	24.9	0.78	0.149	28.4	8.7	24	80
3b		E3	6 $\phi$ 12	700	124	475	21.3	0.78	0.174	30.2	7.4	21	86
3b		E4	6 $\phi$ 12	700	124	475	20.4	0.78	0.182	31.4	7.0	20	90
3a	Jackson	A16-4	4 $\phi$ 16	400	167	542	31.9	1.20	0.205	30.9	11.2	17	47
3a		A10-10	10 $\phi$ 10	400	170	440	33.3	1.15	0.152	55.1	12.1	22	102
3a		A10-6	6 $\phi$ 10	400	170	440	23.7	0.69	0.128	30.2	9.0	27	91
3a		A12-6	6 $\phi$ 12	400	169	544	29.6	1.00	0.184	40.1	10.8	19	71
3a		A12-4	4 $\phi$ 12	400	169	499	34.1	0.67	0.098	23.3	12.4	34	63
3a	Mayfield	2-1	2 $\phi$ 12	150	158	449	19.4	0.96	0.222	6.3	2.3	16	44
3a		71	2-2	2 $\phi$ 12	150	158	449	19.4	0.96	0.222	6.8	2.3	16
3a	Mayf. 72	14	2 $\phi$ 10	150	158	375	16.3	0.66	0.153	6.7	1.9	21	76
3a	Nilsson	U23	4 $\phi$ 10	350	175	456	22.2	0.51	0.106	22.9	9.7	41	96
3a		U24	4 $\phi$ 12	350	169	432	28.9	0.76	0.114	27.5	11.7	37	88
3a		U25	6 $\phi$ 12	350	169	414	23.3	1.15	0.204	36.4	9.3	22	85
3a		U57	3 $\phi$ 10	350	175	588	26.4	0.38	0.086	20.9	11.7	50	90
3a		U59	4 $\phi$ 12	350	169	697	19.6	0.76	0.272	33.9	7.8	17	74
3b		U11	4 $\phi$ 10	350	175	441	21.7	0.51	0.104	20.1	9.5	41	87
3b		U12	4 $\phi$ 12	350	169	418	25.8	0.76	0.124	24.3	10.5	35	81
3b		U13	6 $\phi$ 12	350	169	408	24.7	1.15	0.189	34.0	9.8	23	80
3d		Noor	B1	8 $\phi$ 10	800	133	433	39.3	0.59	0.065	31.4	17.5	49
3d	B2		8 $\phi$ 12	800	136	455	51.9	0.83	0.073	39.0	22.1	41	72
3d	B3		8 $\phi$ 8	800	131	448	32.6	0.38	0.053	27.9	14.9	63	117
3d	B4R		11 $\phi$ 10	800	133	433	40.8	0.81	0.086	40.0	17.8	37	84
3d	B5		6 $\phi$ 10	800	129	433	30.4	0.46	0.065	23.3	13.7	53	90
3d	B6		19 $\phi$ 10	800	132	416	30.4	1.41	0.193	58.1	13.5	18	78
3d	B7R		11 $\phi$ 10	800	132	416	27.4	0.82	0.124	40.7	12.5	28	91
3a	Stroband	B4	2 $\phi$ 6	70	109	504	20.2	0.74	0.185	2.6	0.5	19	89
3a		B5	2 $\phi$ 6	70	109	504	20.2	0.74	0.185	2.7	0.5	19	93
3a		B10	2 $\phi$ 6	70	109	504	20.2	0.74	0.185	2.4	0.5	19	83
3a		B18	2 $\phi$ 6	70	109	504	13.0	0.74	0.286	1.9	0.3	11	68
3a		B19	2 $\phi$ 6	70	109	504	12.9	0.74	0.290	1.7	0.3	10	61
3a		B24	2 $\phi$ 6	70	109	504	11.0	0.74	0.338	1.7	0.2	8	61
3a	Swann	4	2 $\phi$ 19	152	123	295	20.2	3.02	0.442	5.6	1.4	8	33
3b		6	2 $\phi$ 19	152	123	295	23.6	3.02	0.378	9.2	1.6	10	55
3b		6'	2 $\phi$ 19	152	123	295	18.5	3.02	0.481	8.4	1.3	8	54
3a	Author	RV10	5 $\phi$ 16	600	268	570	33.0	0.63	0.108	106.6	45.8	34	79
3a		RV11	7 $\phi$ 16	600	268	570	33.0	0.88	0.151	140.9	45.2	24	75

<sup>1</sup>Fibre reinforced concrete used, and therefore not included in the presentations and comparisons given in Chapter 2.

Table A.4 Summary of test results for opening frame corner reinforced with detailing *Type 4*.



Type	Author	Specimen	$A_s$	$A_{s,i}$	b [mm]	d [mm]	$f_{sy}$ [MPa]	$f_c$ [MPa]	$\rho$ [%]	$\omega_s$	$\rho^*$ [%]	$\omega_s^*$	$M_{ut}$ [kNm]	$M_{ut}/M_{uc}$ [%]	$M_{ut}/M_{uc}^*$ [%]
4a	Abdul-W 98	A1	3 $\phi$ 10	3 $\phi$ 10	300	115	491	29.8	0.68	0.113	1.17	0.192	12.4	99	61
4a		A2 <sup>1</sup>	3 $\phi$ 10	3 $\phi$ 10	300	115	491	27.3	0.68	0.123	1.17	0.210	12.8	102	63
4a		A3 <sup>1</sup>	3 $\phi$ 10	3 $\phi$ 10	300	115	491	31.9	0.68	0.105	1.17	0.180	13.7	109	66
4a		A4 <sup>1</sup>	3 $\phi$ 10	3 $\phi$ 10	300	115	491	29.7	0.68	0.113	1.17	0.193	16.9	135	82
4a	Abdul-99	B3	3 $\phi$ 10	3 $\phi$ 10	300	115	467	22.9	0.68	0.139	1.17	0.238	11.6	98	61
4e	Kordina	E5	6 $\phi$ 12	6 $\phi$ 10	700	124	466	18.5	0.78	0.197	1.17	0.293	31.9	93	63
4e		E6	6 $\phi$ 12	6 $\phi$ 10	700	124	466	20.0	0.78	0.182	1.17	0.272	30.9	89	61
4a	Nilsson	UV5	4 $\phi$ 12	4 $\phi$ 12	350	169	422	24.4	0.76	0.133	1.31	0.226	35.6	118	73
4a		UV6	4 $\phi$ 12	4 $\phi$ 10	350	169	413	21.2	0.76	0.149	1.14	0.222	34.4	118	82
4a		UV7	4 $\phi$ 12	4 $\phi$ 8	350	169	413	24.6	0.76	0.128	1.01	0.169	37.0	125	97
4a		U50	4 $\phi$ 10	4 $\phi$ 8	350	175	662	24.4	0.51	0.139	0.75	0.202	40.2	119	85
4a		U50c	4 $\phi$ 10	4 $\phi$ 8	350	175	658	21.8	0.51	0.155	0.75	0.225	33.0	99	71
4a		U50d	4 $\phi$ 10	4 $\phi$ 8	350	175	679	27.9	0.51	0.125	0.75	0.181	36.3	104	74
4a		U51	4 $\phi$ 12	4 $\phi$ 10	350	169	657	25.6	0.76	0.196	1.14	0.293	46.6	103	73
4a		U52	3 $\phi$ 10	3 $\phi$ 8	350	175	605	27.0	0.38	0.086	0.56	0.125	28.3	118	83
4e		U53	3 $\phi$ 10	3 $\phi$ 8	350	175	646	21.7	0.38	0.115	0.56	0.167	28.2	112	79
4c		U54	3 $\phi$ 10	3 $\phi$ 8	350	175	652	22.9	0.38	0.110	0.56	0.159	31.1	123	87
4a		U56 <sup>2</sup>	3 $\phi$ 10	3 $\phi$ 8	350	175	598	20.4	0.38	0.113	0.56	0.164	27.9	120	85
4a	U61	4 $\phi$ 10	3 $\phi$ 8	350	175	625	20.1	0.51	0.160	0.69	0.214	37.2	118	91	
4d	Noor	BD1	11 $\phi$ 8	5 $\phi$ 8	800	132	498	28.2	0.52	0.093	0.69	0.122	32.4	93	71
4d		BD2	19 $\phi$ 10	9 $\phi$ 10	800	132	416	32.6	1.41	0.180	1.89	0.241	73.5	98	74
4a	Skettrup	7701	2 $\phi$ 25	1 $\phi$ 25	229	413	597	18.1	1.04	0.342	1.41	0.463	106.0	50	37
4a		7702	2 $\phi$ 20	1 $\phi$ 20	224	426	573	13.9	0.66	0.271	0.89	0.367	99.0	71	53
4a		7703	2 $\alpha$	1 $\alpha$	227	730	575	21.9	0.97	0.255	1.31	0.345	471.0	76	57
4a		7704	2 $\phi$ 25	1 $\phi$ 25	226	745	564	17.7	0.58	0.186	0.79	0.251	369.0	95	71
4a		8001	2 $\phi$ 16	1 $\phi$ 16	162	231	562	19.3	1.07	0.313	1.45	0.424	25.2	54	40
4a	Stroband	B9	2 $\phi$ 6	2 $\phi$ 6	70	109	504	20.9	0.74	0.179	1.27	0.305	2.8	96	57
4a		B23	2 $\phi$ 6	2 $\phi$ 6	70	109	504	11.4	0.74	0.327	1.27	0.559	2.6	90	54
4a	Swann	5	2 $\phi$ 19	2 $\phi$ 19	152	123	295	20.4	3.02	0.438	5.16	0.747	6.0	35	21
4b		7	2 $\phi$ 19	2 $\phi$ 19	152	123	295	20.5	3.02	0.436	5.16	0.744	9.8	61	44
4a	Author	RV9	5 $\phi$ 16	3 $\phi$ 16	600	268	570	33.0	0.63	0.108	0.89	0.154	133.5	98	70

<sup>1</sup>Fibre reinforced concrete used, and therefore not included in the presentations and comparisons given in Chapter 2.

<sup>2</sup>Unequal effective height in the members adjoining the corner, add 200 mm to larger member.

<sup>3</sup> $\alpha = \phi 20 + \phi 25$ .

Table A.5 Summary of test results for opening frame corner reinforced with detailing *Type 3* with stirrups.



Type	Author	Specimen	$A_s$	$A_{s,r}$	$b$ [mm]	$d$ [mm]	$f_{sy}$ [MPa]	$f_c$ [MPa]	$\rho$ [%]	$\omega_s$	$F_R/R$ [%]	$M_{ut}$ [kNm]	$M_{ue}$ [kNm]	$M_{ue}/M_{uc}$ [%]	$M_{ut}/M_{uc}$ [%]
3a	Mayfield 72	15	2 $\phi$ 10	2 $\phi$ 6	150	158	375	16.3	0.66	0.153	25	7.5	2.2	25	86
3a		16	2 $\phi$ 10	4 $\phi$ 6	150	158	375	16.3	0.66	0.153	51	7.1	4.3	49	81
3a		17	2 $\phi$ 10	6 $\phi$ 6	150	158	375	15.3	0.66	0.163	76	6.6	7.0	81	77
3a	Stroband	B6	2 $\phi$ 6	10 $\phi$ 2.8	70	109	504	20.2	0.74	0.185	77	2.8	2.2	78	99
3a		B20	2 $\phi$ 6	10 $\phi$ 2.8	70	109	504	9.6	0.74	0.391	77	1.2	2.2	77	43

Table A.6 Summary of test results for opening frame corner reinforced with detailing *Type 4* with stirrups.



Type	Author	Specimen	$A_s$	$A_{s,i}$	$A_{s,r}$	$b$ [mm]	$d$ [mm]	$f_{sy}$ [MPa]	$f_c$ [MPa]	$\rho$ [%]	$\omega_s$	$\rho^*$ [%]	$\omega_s^*$	$F/R$ [%]	$M_{ut}$ [kNm]	$M_{ue}$ [kNm]	$M_{ue}/M_{uc}$ [%]	$M_{ut}/M_{uc}$ [%]	$M_{ut}/M_{uc}^*$ [%]
4a	Mayfield 72	18-A	2 $\phi$ 10	2 $\phi$ 6	2 $\phi$ 6	150	158	375	17.8	0.66	0.140	1.14	0.175	25	8.1	2.2	24	91	74
4a		18-B	2 $\phi$ 10	2 $\phi$ 6	2 $\phi$ 6	150	158	375	17.8	0.66	0.140	1.14	0.175	25	8.8	2.2	24	98	80
4c	Skettrup	8002	2 $\phi$ 16	1 $\phi$ 16	$\beta$	162	231	589	17.2	1.07	0.368	0.76	0.130	95	38.2	45.9	100	86	69
4c		8003	2 $\phi$ 16	1 $\phi$ 16	$\beta$	162	232	605	17.8	1.07	0.364	0.76	0.129	95	45.3	47.5	100	98	79
4c		8201	2 $\phi$ 16	1 $\phi$ 16	$\beta$	162	231	645	16.3	1.07	0.425	0.76	0.150	95	48.5	50.2	100	103	84
4c		8203	2 $\phi$ 16	1 $\phi$ 16	$\beta$	162	228	650	17.2	1.09	0.411	0.77	0.145	95	49.1	49.5	100	104	84
4c		8205	2 $\phi$ 16	1 $\phi$ 16	$\beta$	162	228	644	15.6	1.09	0.449	0.77	0.159	95	44.1	48.9	100	96	79
4c		8207	2 $\phi$ 16	1 $\phi$ 16	2 $\phi$ 12	162	228	655	17.9	1.09	0.398	0.77	0.141	40	48.1	22.0	46	100	81
4a	Stroband	B8	2 $\phi$ 6	2 $\phi$ 6	4 $\phi$ 6	70	109	504	20.2	0.74	0.185	1.27	0.316	141	2.8	4.0	100	96	57
4a		B22	2 $\phi$ 6	2 $\phi$ 6	4 $\phi$ 6	70	109	504	10.7	0.74	0.350	1.27	0.598	141	2.3	4.0	100	82	50

<sup>1</sup> $\beta = 4\phi 10 + 2\phi 12$ .

Table A.7 Summary of test results for closing frame corner reinforced with detailing *Type 1*.



Type	Author	Specim.	$A_s$	$b$ [mm]	$d$ [mm]	$f_{sy}$ [MPa]	$f_c$ [MPa]	$\rho$ [%]	$\alpha_s$	$M_{ut}$ [kNm]	$M_{ut}/M_{uc}$ [%]
1e	Lundgren	1U	10 $\phi$ 16	600	307	570	37.0	1.09	0.168	349.7	100
1f		2L	10 $\phi$ 16	600	307	570	37.3	1.09	0.167	355.4	102
1f		4Ss	10 $\phi$ 16	600	307	570	33.6	1.09	0.185	312.1	90
1a	Mayfield 71	1-3	2 $\phi$ 12	150	158	449	21.4	0.96	0.201	18.0	125
1a		1-4	2 $\phi$ 12	150	158	449	21.4	0.96	0.201	19.7	137
1c		3-2	2 $\phi$ 12	150	158	449	24.5	0.96	0.176	18.5	126
1c		4A-2	2 $\phi$ 12	150	158	449	22.4	0.96	0.192	19.4	133
1e	Balint	NS004/2	3 $\phi$ 6	152	124	565	23.4	0.45	0.109	4.5	77
1e		NS008/2	2 $\phi$ 10	152	124	600	28.1	0.83	0.178	8.4	79
1e		NS014/1	2 $\phi$ 12	152	124	476	18.9	1.20	0.303	14.2	124
1a	Plos	RV1	8 $\phi$ 16	600	268	473	29.7	1.00	0.159	210.4	109
1a		RV3	5 $\phi$ 10	600	280	504	28.7	0.23	0.041	52.9	107
1e	Stroband	A1	2 $\phi$ 6	70	109	450	19.1	0.74	0.175	2.6	101
1e		A4	2 $\phi$ 6	70	109	450	18.8	0.74	0.177	3.1	119
1e		A7	2 $\phi$ 6	70	109	450	19.6	0.74	0.170	2.9	113
1e		A22	2 $\phi$ 6	70	109	450	16.9	0.74	0.197	2.8	110
1e		A28	2 $\phi$ 6	70	109	450	8.8	0.74	0.378	1.5	59
1a	Swann	103	2 $\phi$ 19	152	123	295	20.3	3.02	0.439	13.5	79
2c <sup>1</sup>		109	2 $\phi$ 19	152	123	295	17.3	3.02	0.515	14.8	87
2c <sup>1</sup>		110	2 $\phi$ 19	152	123	295	19.2	3.02	0.465	17.3	101

<sup>1</sup>Radial bars included.

Table A.8 Summary of test results for closing frame corner reinforced with detailing *Type 3*.



Type	Author	Specim.	$A_s$	$b$ [mm]	$d$ [mm]	$f_{sy}$ [MPa]	$f_c$ [MPa]	$\rho$ [%]	$\alpha_s$	$M_{ut}$ [kNm]	$M_{ut}/M_{uc}$ [%]
3a	Mayfield 71	2-3	2 $\phi$ 12	150	158	449	19.4	0.96	0.222	13.4	94
3a		2-4	2 $\phi$ 12	150	158	449	19.4	0.96	0.222	16.6	117
3a	Plos	RV2	6 $\phi$ 16	600	268	473	29.7	0.75	0.119	159.9	128
3a		RV4	4 $\phi$ 10	600	280	504	28.7	0.19	0.033	44.5	116
3a	Stroband	A10	2 $\phi$ 6	70	109	450	19.1	0.74	0.175	2.5	96
3a		A13	2 $\phi$ 6	70	109	450	18.8	0.74	0.177	2.7	103
3a		A16	2 $\phi$ 6	70	109	450	19.6	0.74	0.170	2.8	109
3a		A30	2 $\phi$ 6	70	109	450	9.3	0.74	0.357	1.6	63
3a		A32	2 $\phi$ 6	70	109	450	8.9	0.74	0.375	1.8	70
3a	Swann	104	2 $\phi$ 19	152	123	295	19.9	3.02	0.448	13.1	77
3b		106	2 $\phi$ 19	152	123	295	19.6	3.02	0.456	13.7	80
3a	Author	RV5	7 $\phi$ 16	600	268	567	30.6	0.88	0.162	176.7	87
3a		RV6	7 $\phi$ 16	600	268	567	30.6	0.88	0.162	180.3	89
3a		RV7	4 $\phi$ 10	600	280	573	33.8	0.19	0.032	50.5	112
3a		RV8	4 $\phi$ 10	600	280	573	33.8	0.19	0.032	50.5	112



## Appendix B Simply Supported Beams Reinforced with Spliced Reinforcement Loops

The following tests have been carried out as part of a Master Thesis work by Peter Grassl under supervision by the author. Below, only a very brief description of the test results is given; for further information about this work, see Grassl (1999).

Simply supported beams were tested to examine what influence the splice length of the reinforcement loops and width of the beam had on the structural response of the beam. The beam dimensions and reinforcement ratio were determined to be the same as in the frame corner tests presented in Paper I. Further, the concrete and reinforcement quality was similar with a compressive strength  $f_c = 28$  MPa and reinforcement yield strength  $f_{sy} = 543$  MPa. The beam dimensions and test set-up are shown in Figure B.1, while Table B.1 presents the parameters varied. To simplify the registration of the longitudinal cracks expected in the spliced zone, the beams were tested upside-down.

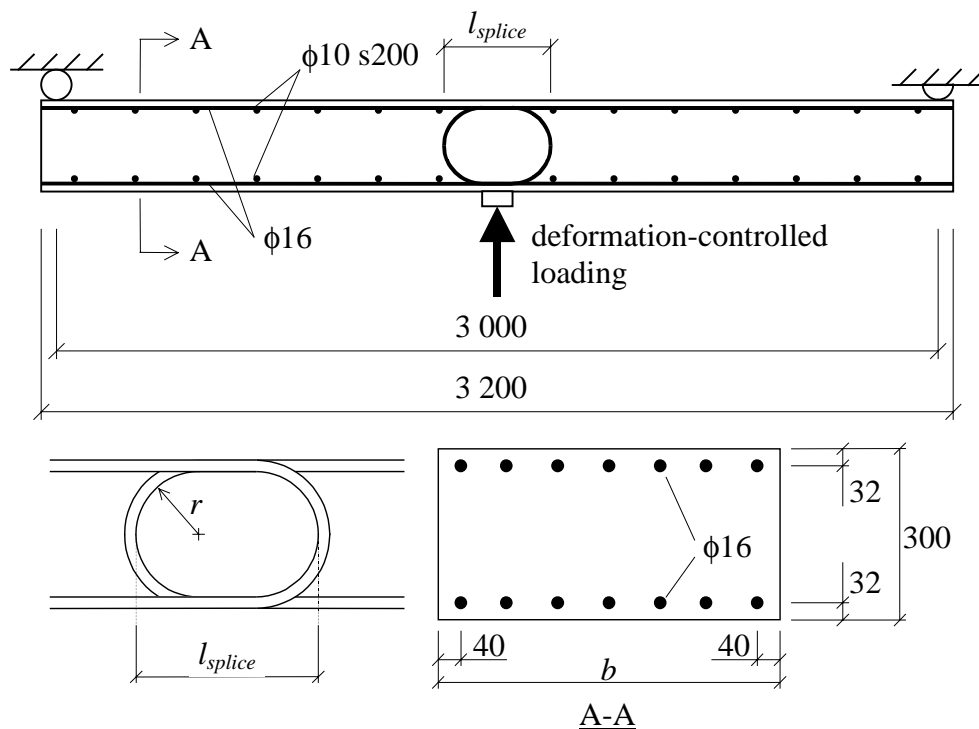


Figure B.1 Dimensions and test set-up of beams.



Table B.1 Parameters varied in the beam tests.

Specimen	$b$ [mm]	$l_{splice}$ [mm]	$r$ [mm]	$A_s$	$\rho$ [%]	$\omega_s$
RV12	600	220	110	7 $\phi$ 16	0.88	0.171
RV13	- " -	600	- " -	- " -	- " -	- " -
RV14	1200	- " -	- " -	14 $\phi$ 16	- " -	- " -
RV15 <sup>1</sup>	600	---	---	7 $\phi$ 16	- " -	- " -

<sup>1</sup>Unspliced beam used as reference beam.

The load-displacement relations obtained in tests are compared in Figure B.2; the maximum load and the corresponding displacement are summarised in Table B.2. Due to the larger beam width of RV14, the load values for this specimen were halved to ensure a direct comparison to the other beams. The reference beam RV15 obtained a ductile behaviour and failed due to shear at a rather large displacement. The behaviour in the beams provided with short splice length, though (i.e. specimens RV12 and RV14), was determined by spalling of the side concrete cover. This is also reflected in the load-displacement relation, where it can be seen that neither specimen reached the same load capacity as the reference beam RV15. Nevertheless, both specimens still obtained a rather ductile post-peak behaviour. In specimen RV13, where long splice lengths were provided, side concrete spalling was never initiated. However, splitting cracks at the straight part of the spliced loops were observed at a load of 260 kN. Shortly after this, the load suddenly dropped about by 50 kN and a distribution of internal forces took place, when the main anchorage of the loops changed from the straight to the bent part. The load then increased again until shear failure was obtained, hence resulting in a brittle failure at a rather small displacement. The beam crack patterns at end of test are shown in Figure B.3.

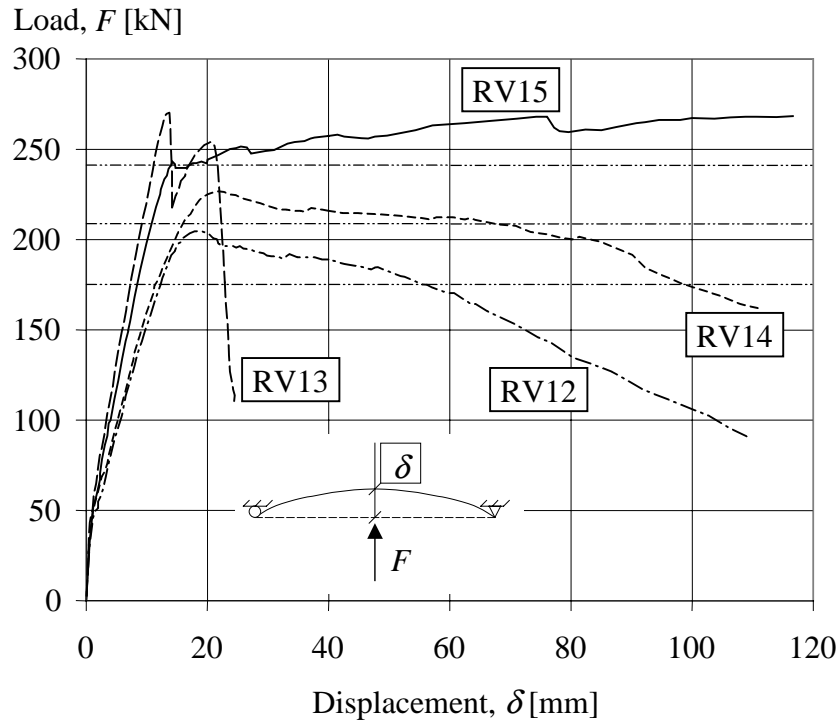


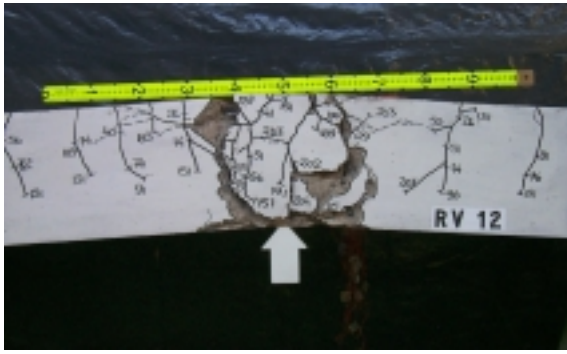
Figure B.2 Load-displacement relation of beams tested.

Table B.2 Summary of test results.

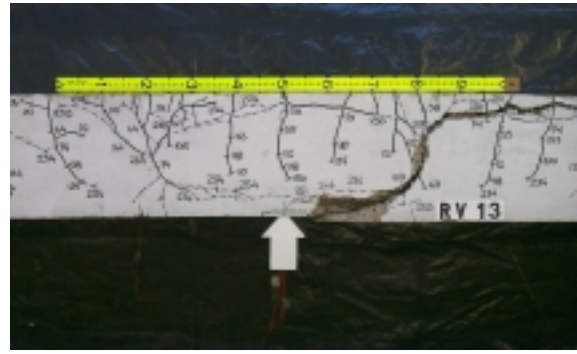
Specimen	Maximum load [kN]	Displacement at maximum load [mm]	Estimated load [kN]	Efficiency [%]
RV12	205	18	241	85
RV13	268	14	241	111
RV14	227 <sup>1</sup>	22	241 <sup>1</sup>	94
RV15	268	113	241	111

<sup>1</sup>Load halved to simplify comparison with the other tests.

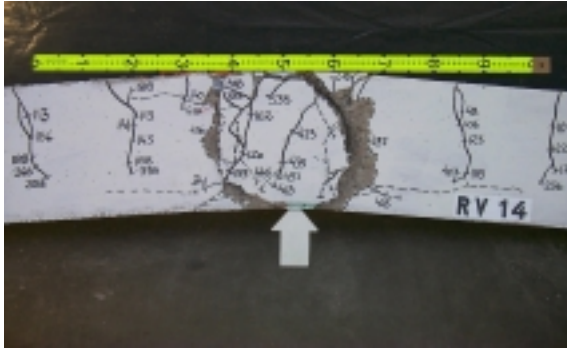
In specimen RV12 it was found that all but the outer loop pairs obtained yielding at a load of about 180 to 200 kN. The outer loops, though, never reached yielding; instead they started to unload shortly prior to the yielding of the inner loops. Hence, it can be concluded that the outer loop pairs were not fully active in this stage but that it still was possible to increase the load. However, after a while the influence of the side concrete spalling spreads to the inner



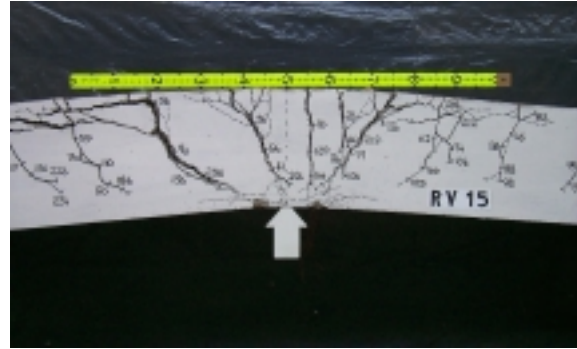
Specimen RV12



Specimen RV13



Specimen RV14



Specimen RV15

Figure B.3 Crack patterns at final failure.

loops so that they eventually unload too, thus limiting the maximum load capacity. From this, it seems reasonable that the structural response obtained is related to what percentage of the total reinforcement amount is affected by the initiation of the side concrete spalling; i.e. the number of internal bars compared to the total amount of reinforcement is important. This was also confirmed in the tests; the maximum load and post-peak ductility reached in specimen RV14 were higher than those of specimen RV12. In the former, two out of fourteen bars were affected; i.e. 86% of the reinforcement present was still fully available to balance the external load. The corresponding value for specimen RV12 was five out of seven bars or, differently put 71% of the original amount of reinforcement. Thus, it is also logical that the former obtains both higher load capacity and improved post-peak response compared to the latter.

Even though the load capacity reached in specimen RV13 was higher than that in the specimens using short splice length, it may be argued that its structural behaviour was less preferable due to its sudden load drop. The somewhat too low load capacity obtained, when short splice length was used, can be dealt with in a simplified way by not taking into account the outer reinforcement loops when determining the structure's load capacity; i.e. by basing the estimated moment capacity on a reduced reinforcement amount  $A_{s,red}$  as

$$A_{s,red} = (n-2) \cdot A_{\phi}$$

where  $n$  is the total number of reinforcement loops used and  $A_{\phi}$  is the cross-section of one bar. If using this approach for specimen RV12 and RV14, the estimated load and efficiency obtained would then be as shown in Table B.3.

Table B.3 Summary of test results; specimen RV15 is included for comparison.

Specimen	Maximum load [kN]	Estimated load [kN]	Efficiency [%]
RV12	205	175	117
RV14	227 <sup>1</sup>	209 <sup>1</sup>	109
RV15	268	241	111

<sup>1</sup>Load halved to simplify comparison with the other tests.



# Reinforcement Detailing in Concrete Frame Corners

by Morgan Johansson

*Results of an experimental study and a literature survey of the reinforcement detailing in concrete frame corners subjected to closing or opening moment are presented. A total of eleven full-scale specimens, eight for closing moment and three for opening moment, were tested to evaluate whether a new reinforcement detailing, using reinforcement loops spliced within the corner, is appropriate to use in Swedish civil defence shelters. In combination with non-linear finite element analyses (not presented here) it was found that the new detailing, even though resulting in a higher risk of side concrete spalling within the corner, was sufficient to be used. Further, it is shown that the use of inclined bars, commonly accepted in opening frame corners, may not be as effective as previously believed.*

**Keywords:** frame corners; reinforcement detailing; reinforced concrete; opening moment; closing moment; side concrete spalling.

## INTRODUCTION

From a safety point of view it is important that a concrete structure, apart from necessary load capacity, also is able to show ductile behaviour so that a local failure does not lead to total collapse of the structure. A structure's ability to exhibit such behaviour is highly dependent on the reinforcement detailing of the joint connections between its adjoining members. Ideally, the joint should resist a moment at least as large as the estimated failure moment of the structural members connected to it and ensure ductile behaviour in the ultimate limit state. The reinforcement detailings in frame corners previously described in the Swedish Shelter Regulations (1994) shown in Figs. 1a and 1b were regarded as difficult to carry out correctly at the construction site. Thus, even though they fulfilled the structural requirements for a joint connection mentioned above, there was a need for a simpler detailing. Therefore, a detailing in which all reinforcement bars are spliced within the corner region (see Fig. 1c) was proposed and evaluated in a project carried out at the Division of Concrete Structures at Chalmers University of Technology.

Concrete frame corners can be separated into two principal types: those that are subjected to a positive moment (opening of the corner) and those subjected to a negative moment (closing of the corner). By the use of a simple strut and tie model it can be seen that opening of the corner tries to

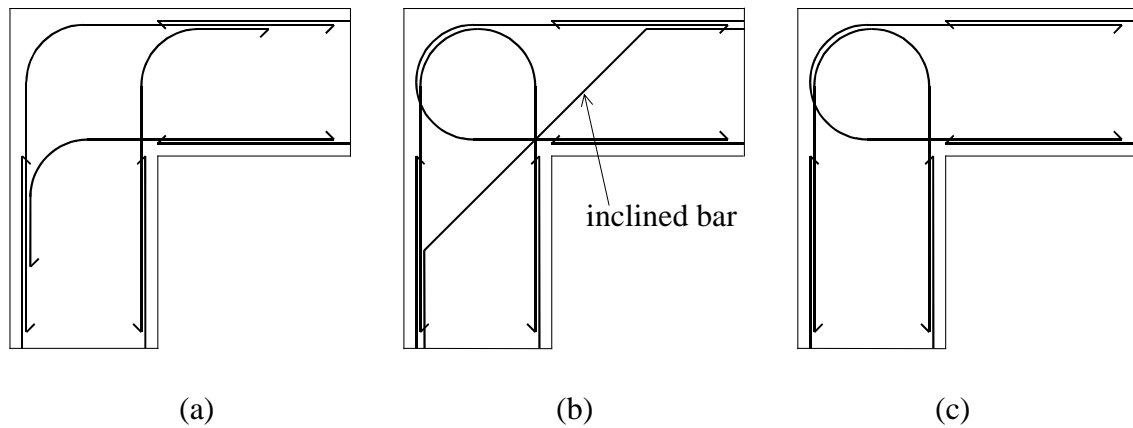


Fig. 1 Schematic figures of the detailings previously described in the Swedish Shelter Regulations for (a) closing moment; (b) opening moment; (c) the new proposal examined.

split the corner in two by pushing off the outside portion (Fig. 2). This is opposite to what happens when closing the corner; the tensile and compressive forces then interact in a way that instead confines the concrete between them. Accordingly, the two cases also present quite different difficulties in their respective reinforcement detailing. Generally speaking, it can be said that an opening moment is characterised by the concrete tensile failure, while a closing moment depends more on the compressive strength of the concrete. Consequently, in theoretical and experimental studies it has also been concluded that the reinforcement detailing of frame corners is more sensitive in the former case than the latter (Mayfield *et al.* 1971; Nilsson and Losberg 1976). Therefore, the main effort of experimental studies has also been concentrated on frame corners subjected to opening moments. Especially Mayfield *et al.* (1971, 1972) and Nilsson (1973) carried out extensive test series where many different reinforcement detailings were examined. Other valuable contributions to the knowledge of opening corners have been made by, for example: Swann (1969), Noor (1977), Stroband and Kolpa (1981), Jackson (1995), and Abdul-Wahab and Al-Roubai (1998). Of these, Swann, Mayfield *et al.* (1971), Stroband and Kolpa (1983) also studied the behaviour of closing frame corners; other researchers in this field are for instance Balint and Taylor (1972), Plos (1994) and Lundgren (1999).

The aim of this study was to investigate whether the proposed reinforcement detailing (detailing *c* in Fig. 1) is appropriate to use instead of the conventional ones (detailings *a* and *b* in Fig 1.). To do this, a combination of full-scale tests, comparison to previous research and non-linear finite element analyses was carried out. This paper, though, is limited to the two first parts; for information about the finite element analyses, see Johansson (1996), Karlsson and Johansson (1997), and Johansson (2000a).

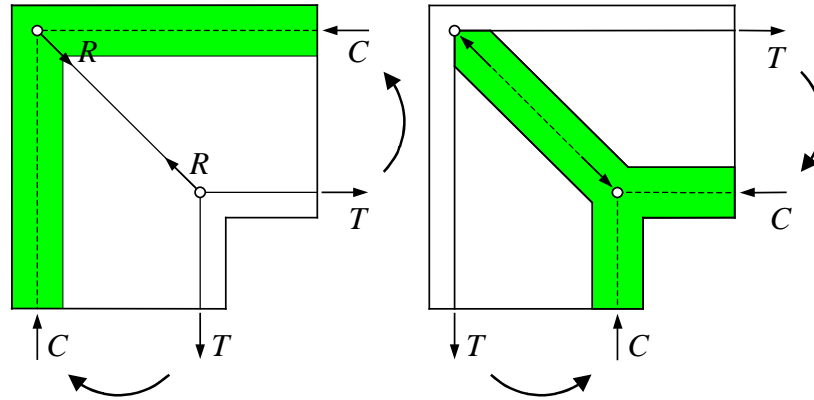


Fig. 2 Simple sketch of the principal forces in corner subjected to (a) positive (opening) moment; (b) negative (closing) moment.

### EXPERIMENTS

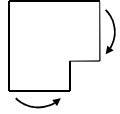
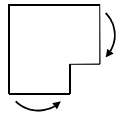
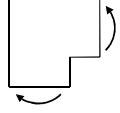
To examine the effectiveness of the new detailing when subjected to an opening or a closing moment, three test series were carried out. In the first two series, each consisting of four specimens, the effect of a closing moment was examined. Two specimens were reinforced with the conventional detailing and six with the new proposal. Opening of frame corners was studied in the third test series with one specimen using the conventional detailing and two using the new proposal (Table 1). This paper, though, emphasises the second and third test series; results obtained in the first one were previously reported in Plos (1994) but are briefly included here since it was part of the same project. Thus, unless otherwise stated, the descriptions of the closing moment tests refer to the specimens in the second test series. More information about the two latter test series can be found in Johansson (1996) and Johansson and Karlsson (1997), respectively.

The dimensions and test set-up of the frame corners used in the three test series are shown in Fig. 3. The amount of reinforcement (hot-rolled, deformed bars) used in the first two test series corresponded approximately to the maximum and minimum amount of reinforcement allowed in the Swedish Shelter Regulations. The reinforcement ratio used in the third test series were based on the high reinforcement ratio in the previous test series as further described below. In the first two test series the influence of a construction joint was also examined. According to the Swedish Shelter Regulations the reinforcement amount in such a joint should be increased by at least 25% compared to that in the adjoining members. However, in the first test series the specimens with new detailing (RV2 and RV4) had an unequal amount of reinforcement in the sections adjacent to the frame corner (Table 1). In the second test series, though, the adjoining sections of the frame corner were designed to be of equal strength. To obtain a construction joint, one adjoining member was cast first, and four days later the second adjoining member and corner joint were cast. The specimens were made



in pairs; the two specimens that would be directly compared with each other were cast with concrete from the same batch. The specimens in the third test series did not have a construction joint and were all cast at the same time. The distance from the centre of the outermost bar to the free concrete sides was 40 mm in the closing frame corners. In the opening frame corners this distance was doubled to 80 mm to avoid spalling failure of the side concrete cover. The concrete covers on the tensile and compressive side of the specimens were  $1.5\phi$  in all specimens, where  $\phi$  is the bar diameter used; the reinforcement bars were in all specimens positioned in one layer only. The strength of the concrete used was determined by tests on water-cured cylinders ( $\phi 150 \times 300$  mm) at day of testing according to Swedish standard, BST Byggstandardiseringen (1991).

Table 1 Reinforcement amount and detailing in tested frame corners.

Type of moment	Detailing <sup>1</sup>	Test specimen	Reinforcement		$f_{sy}$ [MPa]	$f_c$ [MPa]	$\rho$ [%]	$\omega_s$
			adjoining members	corner				
	a	RV1	6 $\phi$ 16	8 $\phi$ 16	473	29.7	1.00	0.159
	c	RV2	- - -	6 $\phi$ 16 <sup>2</sup>	- - -	- - -	0.75	0.119
	a	RV3	4 $\phi$ 10	5 $\phi$ 10	504	28.7	0.23	0.041
	c	RV4	- - -	4 $\phi$ 10 <sup>3</sup>	- - -	- - -	0.19	0.033
	c	RV5	5 $\phi$ 16	7 $\phi$ 16	567	30.6	0.88	0.162
	c	RV6	- - -	- - -	- - -	- - -	0.88	0.162
	c	RV7	3 $\phi$ 10	4 $\phi$ 10	573	33.8	0.19	0.032
	c	RV8	- - -	- - -	- - -	- - -	0.19	0.032
	b	RV9	5 $\phi$ 16	5 $\phi$ 16 <sup>4</sup>	570	32.2	0.63 <sup>5</sup>	0.110 <sup>5</sup>
	c	RV10	- - -	5 $\phi$ 16	- - -	- - -	0.63	0.110
	c	RV11	- - -	7 $\phi$ 16	- - -	- - -	0.88	0.155

<sup>1</sup> The notation refers to that used in Fig. 1.

<sup>2</sup> Unequal amount in adjacent sections; 8 $\phi$ 16 crossed the construction joint.

<sup>3</sup> Unequal amount in adjacent sections; 5 $\phi$ 10 crossed the construction joint.

<sup>4</sup> Also 3 $\phi$ 16 inclined bars.

<sup>5</sup>  $\rho = 0.89$  and  $\omega_s = 0.158$  if the inclined bars are taken into account as shown in Eq. (2).

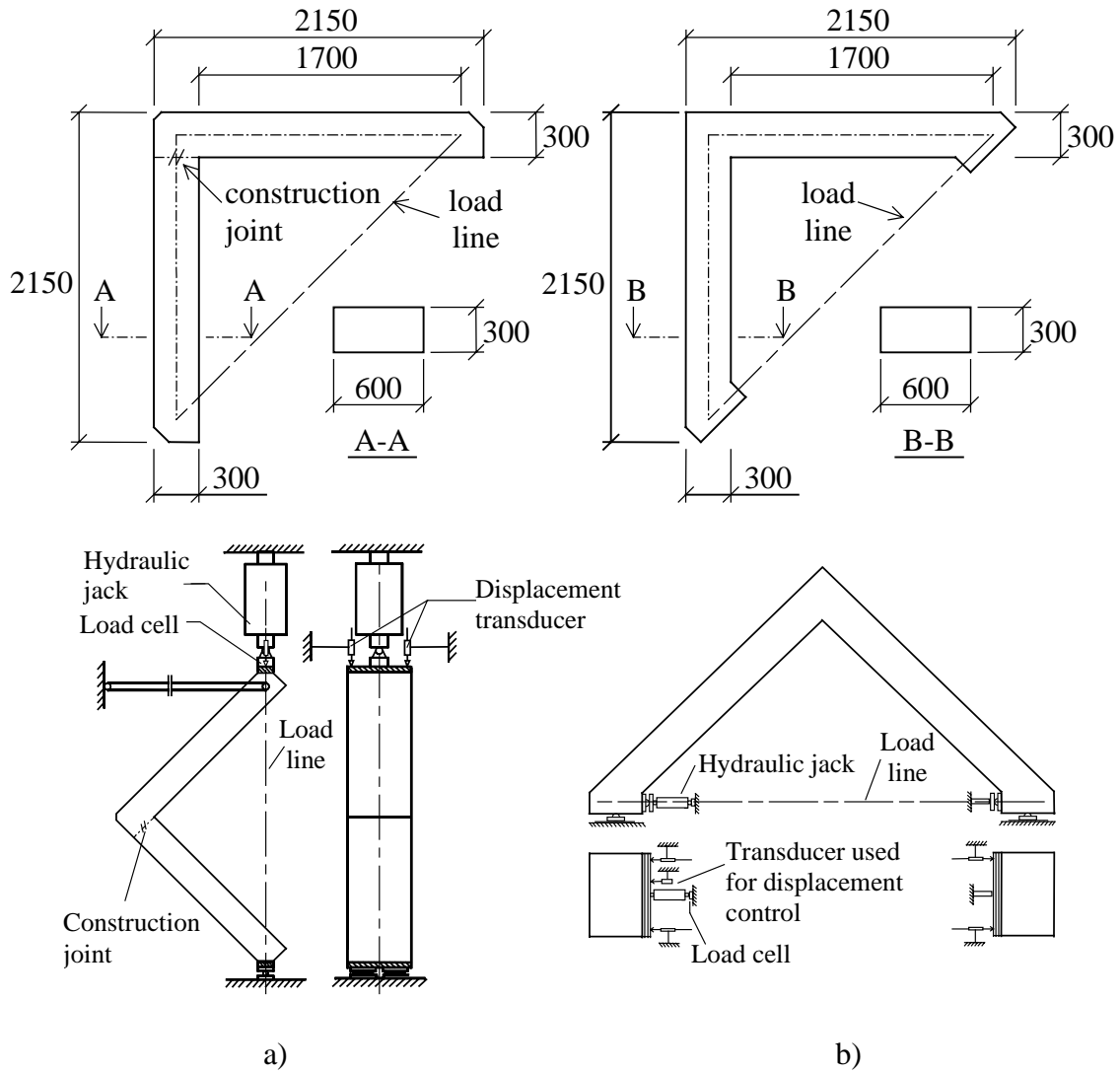


Fig. 3 Dimensions and test set-up of (a) first and second test series (closing moment); and (b) third test series (opening moment).

It is common to discuss in terms of reinforcement ratio  $\rho$  when determining the allowable amount of reinforcement in a frame corner. However, this measure is inadequate since it does not take into account the reinforcement quality or the strength of the concrete. This statement is especially true for frame corners subjected to opening moment, where the concrete behaviour in tension may have a very large influence on the overall response, but also in closing moments when there is risk of spalling of the concrete side cover or crushing of the compressive zone. However, a variable that takes these factors into consideration is the mechanical reinforcement ratio

$$\omega_s = \rho \frac{f_{sy}}{f_c} = \frac{A_s f_{sy}}{b d f_c} \quad (1)$$

where  $A_s$  is the amount of reinforcement,  $b$  is the specimen width,  $d$  is the effective height,  $f_{sy}$  is the reinforcement yield strength and  $f_c$  is the compressive strength of the concrete. Accordingly, this term is also used in the present paper while the reinforcement ratio  $\rho$  is only shown for reference.

The critical sections used in the frame corners when determining the expected load capacity were defined as shown in Fig. 4a. Thus, the critical crack in the closing frame corners was assumed to appear just outside the corner; the critical crack in the opening frame corners was assumed to form at the inside of the corner and then develop along the reinforcement loops. When determining the amount of reinforcement loops in specimen RV11 the idea was that the amount of reinforcement crossing the initial crack at the inside of the corner should be approximately the same as that used in the specimen reinforced with inclined bars (i.e. specimen RV9). This can be achieved as shown in Fig. 4b. Hence, the necessary amount of reinforcement in the loops can be determined as

$$A_s^* = A_s + \frac{1}{\sqrt{2}} A_{s,i} \quad (2)$$

where  $A_s^*$  is the loop reinforcement area in detail  $c$  and  $A_s$  and  $A_{s,i}$  are the loop reinforcement area and area of the inclined bars, respectively, in detail  $b$ .

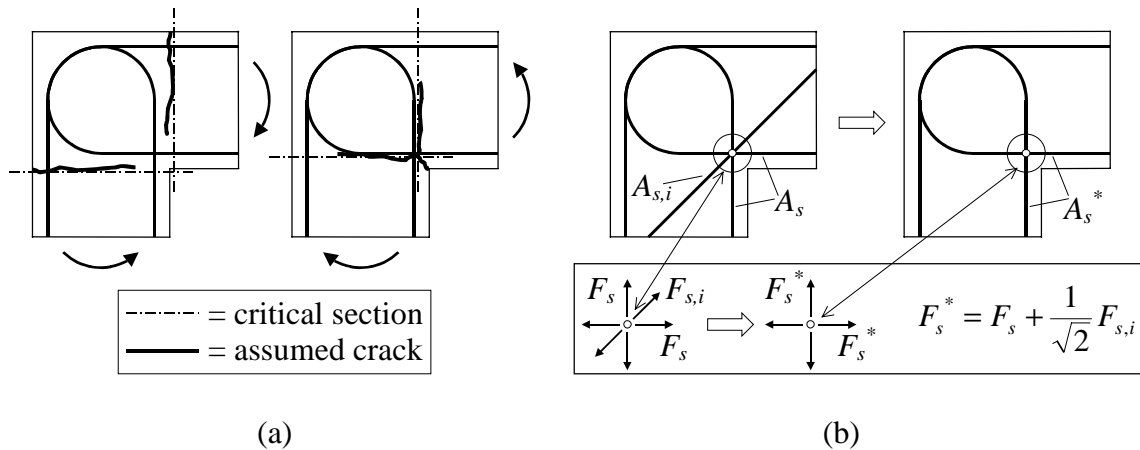


Fig. 4 (a) Definition of critical section in closing and opening corner; (b) determination of equivalent amount of reinforcement loops when the inclined bars are replaced.

## RESULTS

### Closing moment

The load on the frame corners in the first and second test series was controlled manually so that it could be adjusted to the response of the specimen. Thus, it was also possible to register the post-peak behaviour in a relatively controlled manner. The load was initially applied in load increments of 5 or 10 kN for the specimens with low and high amount of reinforcement, respectively. At each increment the load was held constant while the propagation of cracks was marked. To make it easier to follow the behaviour of the frame corners near the maximum load, the load increments were halved when a non-linear response was observed. The total time of testing for each specimen was about two hours.

The load-displacement relations for the closing frame corners are shown in Fig. 5; the efficiency of the tests, i.e. the ratio between the moment obtained in each test,  $M_{ut}$ , and the estimated theoretical moment capacity,  $M_{uc}$ , are presented in Table 2. During the initial loading of the frame corners in the two first test series, two primary cracks were observed close to the corner in all the specimens, one in each section adjacent to the corner. However, as mentioned above, the frame corners reinforced with the new detailing in the first test series (specimens RV2 and RV4) had an unequal amount of reinforcement in the sections adjacent to the frame corner. This caused the deformations to concentrate in just one plastic hinge in these specimens, and was also the reason for the lower load capacity obtained for specimens RV2 and RV4 compared to that of specimens RV1 and RV3, respectively. The other six specimens, though, developed plastic hinges on either side of the corner.

For specimens RV5 and RV6, very few cracks were observed outside the immediate vicinity of the frame corner. The behaviour of the two specimens was similar, and the maximum load was determined for both of them by spalling of the concrete side cover in the frame corner. Even so, strain gauges glued on the two reinforcement loops next to the centre bar registered a strain of about 5‰, thus indicating that the reinforcement yielded at maximum load. Before the spalling occurred, the largest cracks were observed in the section between the corner and the upper adjoining member. In the tests of the specimens with low reinforcement ratio, cracks were formed with a spacing of approximately 0.20 m between them in both adjoining members. The cracks that led to failure for specimen RV7 appeared in the upper adjoining member close to the corner; for specimen RV8, the decisive crack appeared along the construction joint. For both specimens, the first crack was observed in the construction joint at a load level lower than expected. However, apart from the lower crack load the construction joint did not appear to have any effect on the overall behaviour, a statement also confirmed in the non-linear finite element analyses carried out; see Johansson (2000a).

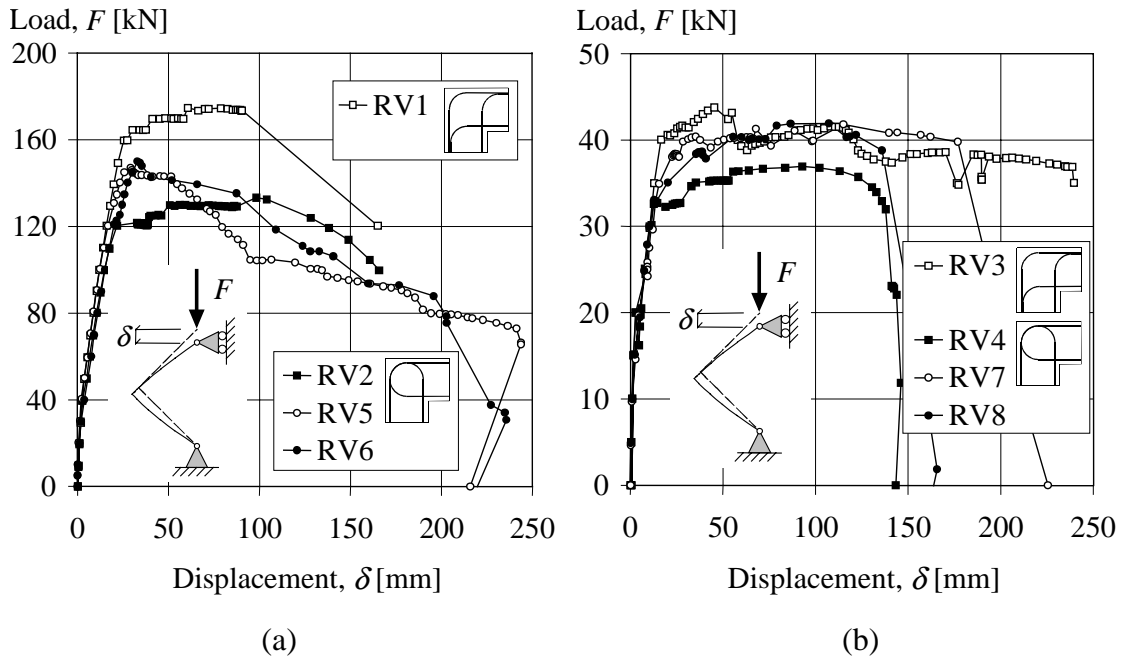


Fig. 5 Load-displacement relations for the frame corners subjected to closing moment: (a) high reinforcement ratio; (b) low reinforcement ratio. Specimens RV1 to RV4 were tested by Plos (1994).

The maximum displacements in specimens RV1 to RV3 were governed by limitations in the test rig; specimen RV4, though, was loaded until failure when two reinforcement bars were torn off. Specimen RV5 still showed ductile behaviour when the test had to be stopped because of the obliquity of the hydraulic jack, while specimens RV6 to RV8 were deformed until rupture of two (RV6) or three (RV7 and RV8) reinforcement bars was obtained. The crack patterns obtained in the specimens of the second test series were very similar when using high or low reinforcement ratio, respectively. Therefore, photos only of specimens RV6 and RV7 are shown (Fig. 6).

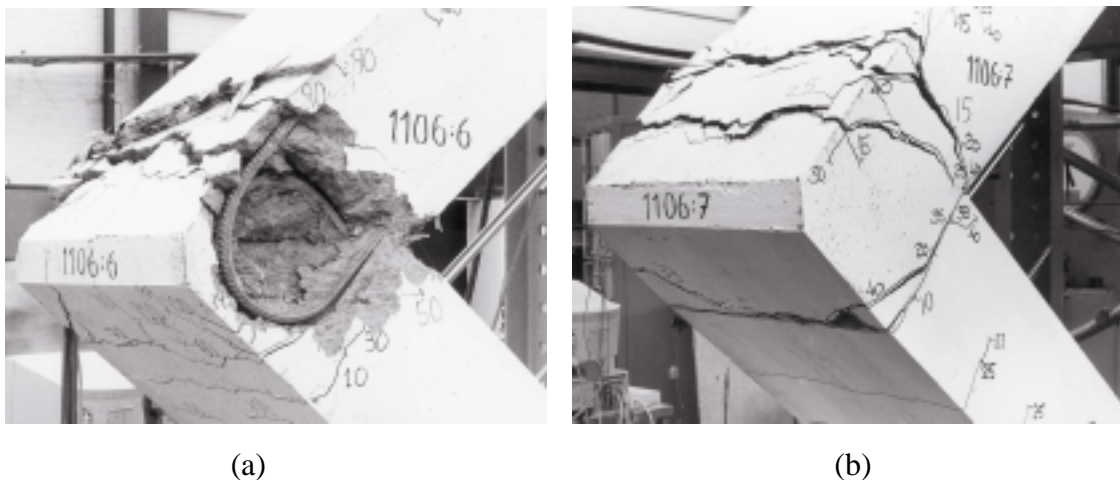
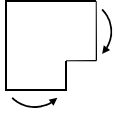
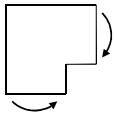
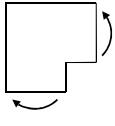


Fig. 6 Crack patterns at end of test in: (a) specimen RV6; and (b) specimen RV7.

Table 2 Summary of test results in the three test series.

Type of moment	Detailing <sup>1</sup>	Test specimen	$\omega_s$	Load in test, $F$ [kN]	Moment in test, $M_{ut}$ [kNm]	Estimated capacity, $M_{uc}$ [kNm]	$\frac{M_{ut}}{M_{uc}}$ [%]
	a	RV1	0.159	175	210	193	109
	c	RV2	0.119	133	161	145	128
	a	RV3	0.041	44	53	50	107
	c	RV4	0.033	37	45	38	116
	c	RV5	0.162	147	178	203	87
	c	RV6	0.162	150	180	203	89
	c	RV7	0.032	42	50	45	112
	c	RV8	0.032	42	50	45	112
	b	RV9	0.110 <sup>2</sup>	109	133	136 / 192 <sup>3</sup>	98 / 70 <sup>3</sup>
	c	RV10	0.110	87	107	136	79
	c	RV11	0.155	115	141	187	75

<sup>1</sup> The notation refers to that used in Fig. 1.

<sup>2</sup>  $\omega_s = 0.158$  if the inclined bars are taken into account.

<sup>3</sup> Inclined bars not accounted for / inclined bars accounted for.

### Opening moment

The testing of the opening frame corners in the third test series was controlled by means of displacement control as shown in Fig. 3b. Initially the load was applied with a deformation speed of 0.15 mm/min. However, to limit the total time needed for one test, the speed was doubled to 0.3 mm/min about 10 minutes after reaching the maximum load. Due to an error in the initial loading of RV9 this specimen was deformed with a speed of about 3 mm/min until reaching a load of 33 kN at which time it was unloaded; it was then loaded again, this time using the correct deformation speed. Even though it is unlikely that this had any significant effect on the maximum load capacity, the initial crack pattern might have been somewhat influenced. The load-displacement relations for the opening frame corners are compared in Fig. 7; for a summary of the obtained load capacities and efficiencies of the detailings, see Table 2. The small irregularities in the curves are due to stops made during loading to mark the crack propagation in the specimen. The loading was stopped when reaching a post-peak load of about 80% of the maximum load (RV9 and RV10) or when the large deformations of the frame corners caused problems in the test set-up (RV11).

Fig. 8a shows a schematic crack propagation similar to that obtained in all tests. The first crack appeared at the inside of the corner (1) and then followed the reinforcement loops until it approached the compressive reinforcement (2). At this stage the load was still quite low, only about 30 to 40 kN, and the forming of new cracks in the corner came to a standstill while the existing ones inside the corner increased in size. It was not until a load of about 80% of the final maximum load that any serious crack propagation within the corner started again. The cracks then deviated in the direction of the adjoining members (3) and eventually, just prior to the maximum load, the cracks closed around the reinforcement loops (4), hence limiting the corner capacity when the concrete part outside the reinforcement spalled off. The crack patterns for the three specimens at end of test are shown in Fig. 8. Further, longitudinal cracks were observed on the tensile side about 8 to 10 cm from the free concrete sides (i.e. approximately at the location of the outer reinforcement loops) in both specimens RV9 and RV11 shortly before the maximum loads were reached. In RV10 such cracks were observed after maximum load was reached. The mean crack spacing of the bending cracks observed outside the corner region was about 0.21 m.

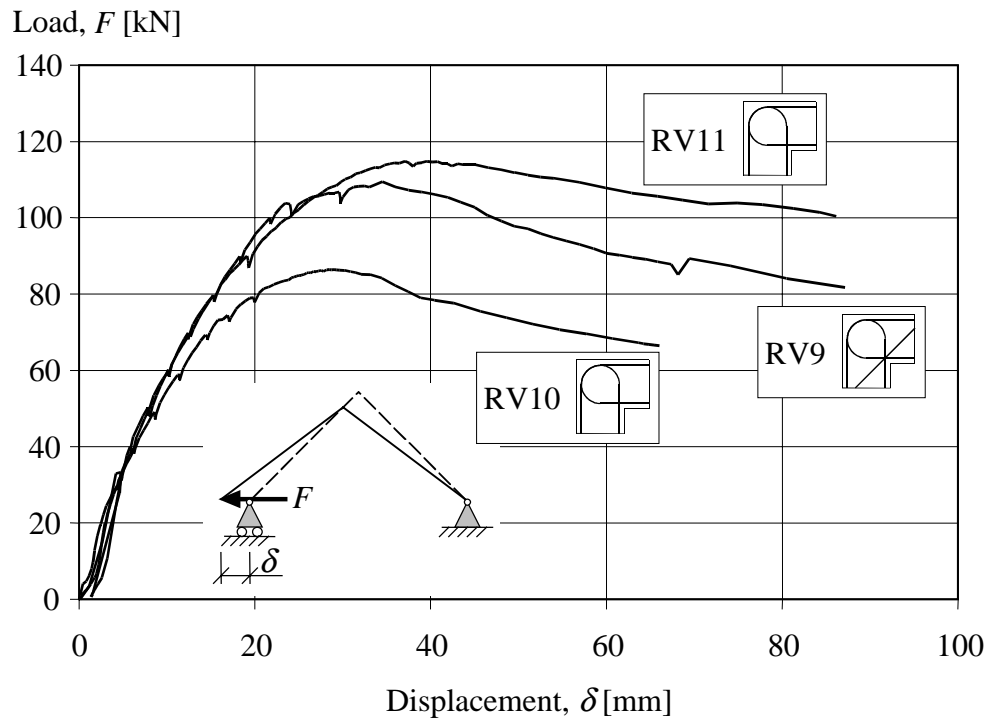


Fig. 7 Load-displacement relations of frame corners subjected to opening moment.

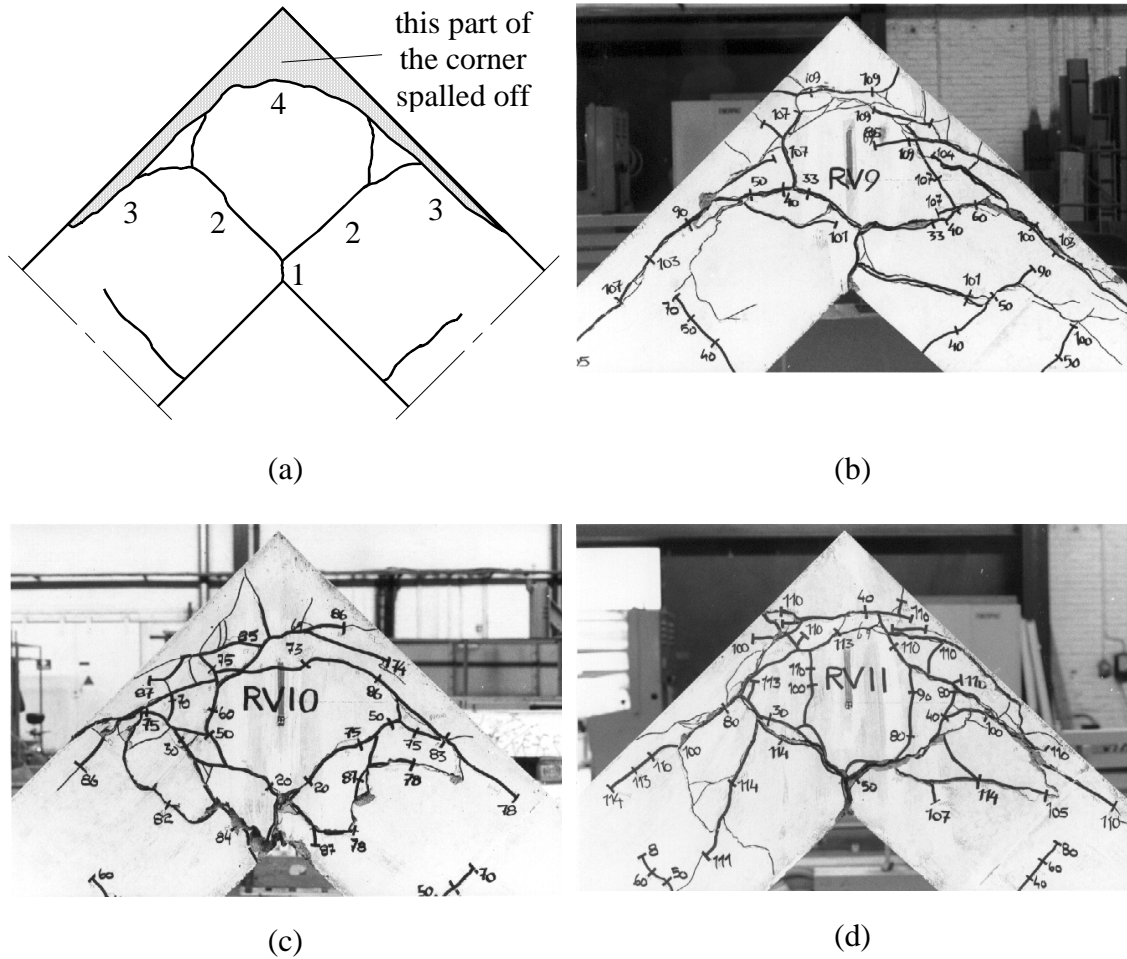


Fig. 8 Crack patterns in frame corner subjected to opening moment: (a) schematic sketch of crack propagation; (b) specimen RV9; (c) specimen RV10 ; and (d) specimen RV11.

## DISCUSSION OF TEST RESULTS

### Estimation of theoretical load capacity

The theoretical strength of each specimen was determined by using a concrete stress block as described in, for example, Eurocode 2. The effect of normal force due to the external load and the reinforcement on the compressive side was accounted for. Further, due to the test set-up used for the closing frame corners, the dead weight had a relatively large influence on the theoretical load capacity in these specimens, especially for the frame corners with low reinforcement ratio. Therefore, the dead weight was considered for these specimens and thus, the estimated moment capacity  $M_{uc}$  given in Table 2 is not the moment capacity in the critical section but the product of the estimated maximum point load and its lever arm of 1.202 m to this section. In the specimens subjected to opening moment, though, the dead weight had only a small effect and was therefore neglected. The same method was also used in the re-evaluation made below of test results reported in the literature.



## Closing moment

Due to uneven capacities in the adjoining member, it is not possible to make a direct comparison of the specimens in the first test series. However, the efficiencies were all above 100% and the ductility similar, thus indicating that the examined detailings are comparable. The unusually high efficiency obtained in specimen RV2 was due to substantial hardening in the reinforcement; as can be seen in Fig. 5, though, yielding of the reinforcement first occurred at a load of about 121 kN which corresponds well to the estimated load capacity of 120 kN. Because of the spalling of the concrete side cover in specimens RV5 and RV6 in the second test series, a somewhat lower maximum load capacity than expected was obtained. Also, the plateau in the load-displacement relation, observed for RV1 and RV2, did not appear. The differences between the estimated and observed maximum load capacities for the specimens with low reinforcement ratios, though, were similar and the large plateau in the load-displacement relation was observed in all tests.

Based on experience gained in tests on simply supported beams of identical concrete cross sections and spliced with the same type and amount of reinforcement loops as used here, according to Grassl (1999), it can be assumed that the efficiency of the outermost bars, due to the spalling of the concrete cover, probably was only about 50% when the maximum load was reached. On this assumption, the estimated load capacity obtained would be 144 kN, a value that corresponds quite well with the loads of 147 kN and 150 kN reached in the tests of the specimens that spalled (i.e. RV5 and RV6). Because of the spalling, the strain in the inner reinforcement bars increased more rapidly near the maximum load in an attempt to compensate for the loss of the outermost bars. Eventually, though, depending for example on the bar spacing, the loss of concrete cover may influence the bars further from the free side too and cause them to lose their anchorage capacity as well, something that probably also happened here. However, the fact that two reinforcement bars in RV6 were torn off before the end of the tests shows that the innermost bars were still fully active. Hence, contrary to what is said in Stroband and Kolpa (1983), the spalling did not give rise to a sudden failure. The reason for this was that even though the contribution of the outer bars in specimens RV5 and RV6, due to loss of anchorage, largely disappeared close to the maximum load, the inner bars were still able to balance a large part of the load. The specimen width and number of reinforcement bars used by Stroband and Kolpa in their tests were 70 mm and  $2\phi 6$ , respectively. Thus, when the reinforcement loops started to fail in anchorage due to the spalling, there were no extra bars to assist in balancing the internal section force.

Accordingly, if a large percentage of the total reinforcement amount is affected by spalling, as may be the case in beam-column joints, there is a risk of brittle behaviour. From the tests it can be concluded that there is higher risk of spalling of the side concrete cover when using the

new proposal than is the case when using the conventional detailing shown in Fig. 1a, an observation that is in agreement with those made by Stroband and Kolpa. However, if the corner is laterally restrained or if only a small percentage of the total number of reinforcement bars are affected, this type of failure has a very limited, if any, effect on the total load-carrying capacity or ductility of the corner. Thus, the risk of a spalling failure in a civil defence shelter is small and, even if such a failure were initiated, its effect would be quite negligible due to the large width used in a wall-slab connection. Hence, the test results together with these observations support the idea that it would be appropriate to use the new detailing in corners subjected to closing moment. However, special care still has to be taken when using reinforcement loops in beam-column connections where the effect of spalling can have a large influence.

### **Opening moment**

According to previous research, the detailings used in RV10 and RV11 (i.e. reinforcement loops without inclined bars) are inferior to that used in RV9 (inclined bars included). However, this was not clearly the case in the tests carried out here. Even though the inclined bars supplied in RV9 resulted in an increased load capacity compared to that of RV10, the structural response was quite similar for all three specimens. It is especially interesting to note that RV9 and RV11 showed almost exactly the same stiffness until maximum capacity was reached, a value that was also more or less the same in the two tests. According to Nilsson, diagonal cracks within the loops or along the inclined bars are the cause of failure in the detailings tested. In an attempt to register the development of the cracks within the reinforcement loops, strain gauges were glued on the concrete. However, such cracks did not form as described by Nilsson; in fact, it was not until after maximum load that the strain gauges even indicated tensile stresses in this region. Instead, maximum load was governed by spalling of the concrete outside the reinforcement loops. When this occurred, the anchorage decreased and the reinforcement loops started to slide around the concrete sprint in the corner. Hence, the failure obtained in these tests can probably best be characterised as an anchorage failure, an observation also made by Jackson (1995) in his tests. The photos in Fig. 8 also show that the final crack patterns were more or less the same independently of whether inclined bars were used or not.

The reinforcement loops in both RV9 and RV11 yielded in the direct vicinity of the initial crack at the inside of the corner; the strains measured as high as 12‰. Nevertheless, the load level at this stage was still considerably smaller than the theoretical one. The strain gauges used to register the strain in the reinforcement, though, were glued on the two bars next to the centre bar and are thus not necessarily representative for the bars next to the free concrete

side. Hence, based on the observations made by Grassl discussed in the previous section, this strongly indicates that the load capacity of the opening frame corners was affected by spalling of the side concrete cover. This statement is also strengthened by the appearance of the longitudinal cracks observed close to the free concrete sides in both specimens before reaching maximum load. Accordingly, it is the author's belief that if spalling of the side concrete cover had been prevented, a higher load capacity would also have been obtained in the tests. Whether the efficiency would have reached 100%, though, is unclear but not probable since the forming of the critical crack around the reinforcement loops (crack 4 in Fig. 8a) at a later stage would still have affected the anchorage capacity and thus decreased the force taken by the reinforcement loops. Further, the post-peak behaviour in specimens RV9 and RV10 was more or less the same; a somewhat more ductile behaviour was obtained in RV11. Based on the amount of reinforcement loops used in each specimen, this indicates that the response in this stage to a large degree depends on the amount of reinforcement loops, while the presence of inclined bars seems to have a quite negligible effect in this stage.

### **COMPARISON WITH OTHER RESEARCH**

As mentioned in the introduction, various researchers have been working with the behaviour of frame corners subjected to closing and/or opening moment and several detailings have been tested and evaluated. Hence, an attempt is made here to summarise the test results known by the author using the detailings shown in Fig. 1 and detailings similar to those as shown in Johansson (2000b). Different combinations, using various amounts and types of secondary reinforcement, are not considered. Due to this, the work by Luo *et al.* (1994) was not included; further, the tests reported by Östlund (1963) was not taken into account since no information about the steel strength was available.

The load-displacement relations after maximum load are rarely shown in the literature. This is due to the use of pure load-controlled testing by which it is not possible to register the post-peak behaviour. Accordingly, this makes it hard to know anything about the post-peak ductility obtained when using different detailings; many results are instead reported only as the ratio of the maximum moment obtained in test and the theoretical estimated ultimate moment. Such results reported by various researchers on frame corners subjected to closing and opening moment, respectively, are illustrated in Figs. 9 and 10; a thorough summary of the results can be found in Johansson (2000b). Due to limited space, the sources of the test results in these figures are only identified by the use of the author's name first mentioned in the reference list. Most of these reports originally refer to the concrete compressive strength as the cube strength. However, since the compressive strength used for design in both Eurocode

2, CEN (1991) and the Swedish regulations BBK 94, Boverket (1994), is related to the cylinder strength a recalculation was done in those cases. The relation used was taken from Swedish Standard SS 13 72 07, BST Byggstandardiseringen (1991), which states that the relation between the compressive strength for normal strength concrete obtained from water-cured cylinders ( $\phi 150 \times 300$  mm) and cubes (side 150 mm) cured dry can be approximated as

$$f_{c,cyl} = \frac{f_{c,cube}}{1.35} \quad (3)$$

where  $f_{c,cyl}$  and  $f_{c,cube}$  are cylinder and cubic compressive strengths of the concrete, respectively. Even though the curing conditions of the cubes and cylinders used to determine the concrete strength differed a lot between different researchers, just this one expression was used, the difference obtained in the results shown below being quite negligible regardless of whether another expression is used. Due to this recalculation of the concrete compressive strength and the fact that all results were not evaluated in an identical manner by the original authors (e.g. some considered the compressive reinforcement, some did not), the theoretical strength,  $M_{uc}$ , of each specimen was re-determined. As mentioned in the Discussion section, this was done by using the method given in Eurocode 2, i.e. neglecting the influence of the dead weight but taking into account the effect of any compressive reinforcement and normal force from the external load. Hereby, all results were evaluated in the same way and consequently, the efficiencies shown here may differ from those reported by the original authors.

When comparing the efficiencies of the different detailings, no consideration has been given to those which had a considerably higher mechanical reinforcement ratio  $\omega_s$  than that allowed in the design of civil defence Shelters in Sweden. The allowed reinforcement ratio in the present Swedish Shelter Regulations (1998) is 1.1%. Together with the mean strength of about  $f_c = 27$  MPa for the lowest concrete quality allowed, and the mean reinforcement yield strength of approximately  $f_{sy} = 550$  MPa, it is possible to determine an upper limit to  $\omega_s = 0.224$  by using Eq. (1). This upper limit of  $\omega_s$  is also marked in Figs. 9 and 10.

From Fig. 9 it can be seen that most tests on closing frame corners with a mechanical reinforcement ratio lower than 0.224 obtained an efficiency of at least 100% or more, independently of what detailing was used. Of the results below full efficiency, it can be mentioned that at least three were due to spalling failure (Stroband and Kolpa, and this author) and one was because the maximum moment was limited due to shear failure (Lundgren). The reason for the low efficiencies obtained in the tests by Balint and Taylor, though, are not known to the author. Nevertheless, this comparison supports the statement made by Mayfield *et al.* (1971) that the detailing is not very important in closing frame corners. However, as can

be seen in Fig. 10, such is not the case with opening frame corners. Due to this, the further discussion focuses on the opening of frame corners.

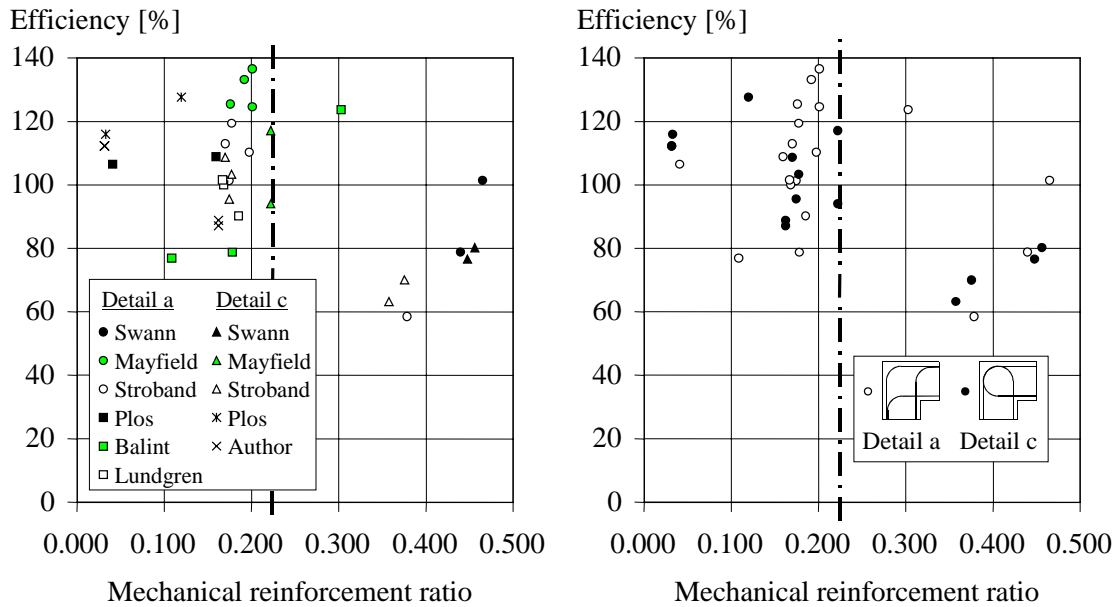


Fig. 9 Efficiency of frame corners subjected to closing moment when the reinforcement detailing varies. The dashed line marks the maximum mechanical reinforcement ratio allowed in the Swedish Shelter Regulations.

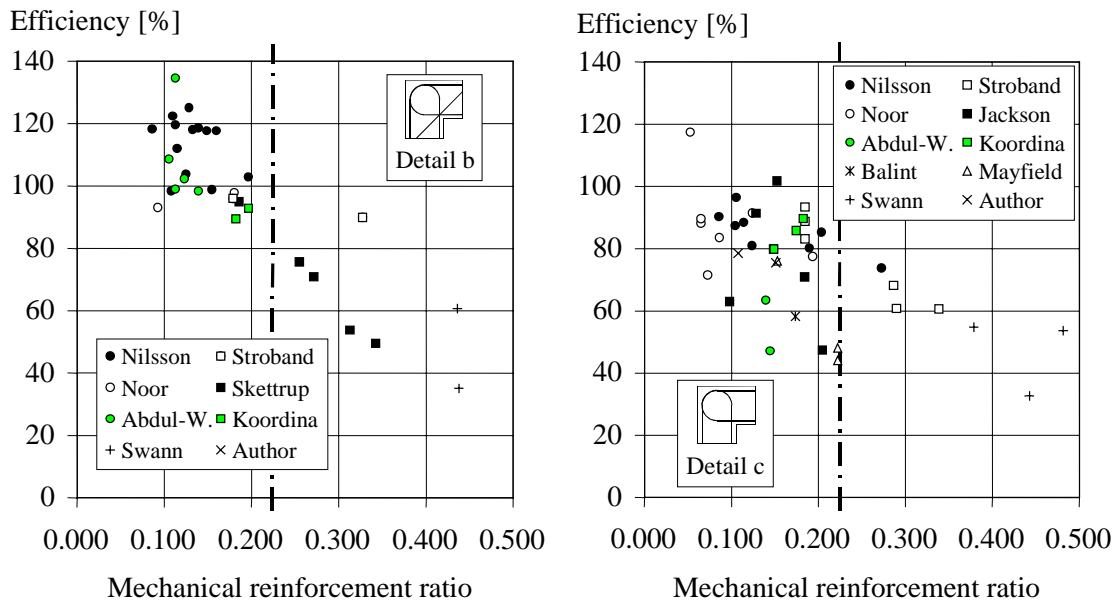


Fig. 10 Efficiency of frame corners subjected to opening moment when different detailings are used. The dashed line marks the maximum mechanical reinforcement ratio allowed in the Swedish Shelter Regulations.

When comparing the efficiencies of detailings *b* and *c* in opening frame corners shown in Fig. 10, it may first appear that the former is superior to the latter. However, a comment about these results should first be made. When Nilsson and other researchers determined the efficiency of detail *b* they did not include the contribution to the moment capacity from the inclined bars; neither did they take this extra reinforcement into account when determining the reinforcement ratio of the detailing. If this is done as described in Eq. (2), the result will also be quite different (Fig. 11). Accordingly, even though it is important to be aware that the specimens with inclined bars often failed in an adjoining member, hence making the maximum moment obtained in these tests dependent on its capacity, these results still indicate that the efficiencies of both detailings are quite similar.

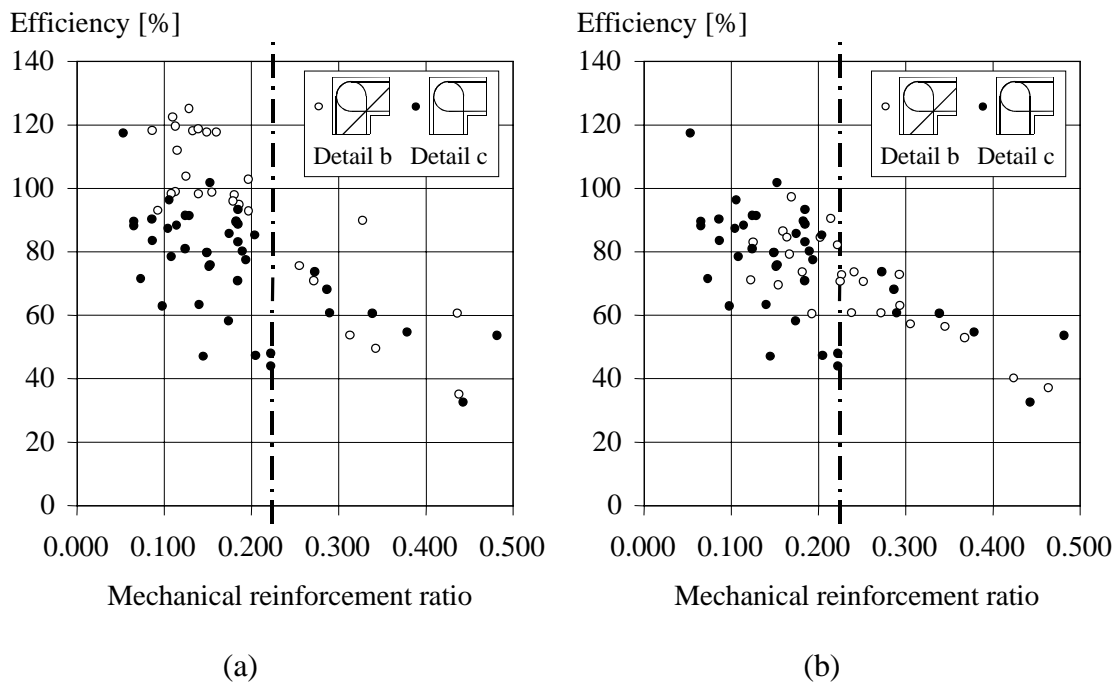


Fig. 11 Comparison of efficiencies for detail *b* and detail *c* in tests on opening moment when: (a) inclined bars are not taken into account; and (b) inclined bars are taken into account.

In most tests carried out on frame corners subjected to opening moment, the test set-up has been arranged so that at least one of the adjoining members has had a constant moment acting on it (Fig. 12). This is not on the safe side, though, since such a member may then fail in any section independently of the distance from the corner (this is, for instance, what happened in many of Nilsson's tests). Accordingly, if the external moment decreases with increasing distance to the corner, the possibility for a critical crack to develop outside the corner also decreases. Further, the author is not aware of any tests but those presented in this paper where

the reinforcement loops were spliced to straight bars just outside the corner region. Still, such a procedure is frequently used and, for instance, is even given as an example in ACI (1999) of how such a detailing should be carried out. Provided that such a splice is carried out correctly, it usually produces a stronger section due to the higher amount of reinforcement, thus effectively hindering the development of a plastic hinge in the adjoining member close to the corner.

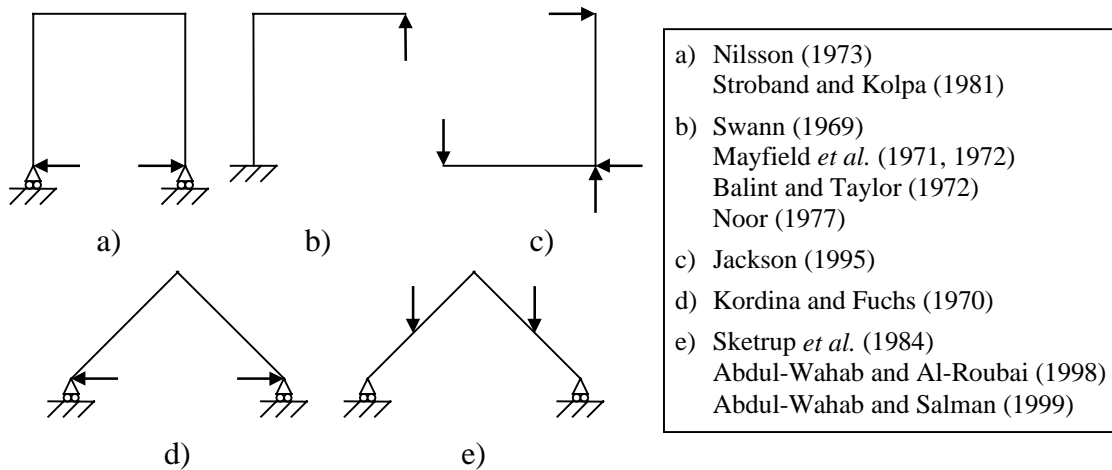


Fig. 12 Schematic figures of the test set-ups used by different researchers in tests on opening moment.

The test set-up used for the tests presented in this paper was arranged so that the moment varied along the adjoining members. Consequently, a more dangerous load case was obtained. Further, as shown in Fig. 1, the reinforcement loops were spliced to straight bars in the adjoining members just outside the corner, thus strengthening those parts close to the corner. The result from the test was also that the usage of inclined bars in specimen RV9 did not prevent the critical cracks from forming within the corner, something that to a large degree contradicts previous observations reported in the literature. Hence, the combination of varying moment and extra amount of reinforcement was sufficient to prevent the development of a critical crack in the adjoining members before the corner failed. Of the results summarised here only Kordina and Fuchs, and Jackson, used a test set-up in which the applied moment varied in both members adjoining the corner. Based on this, it is interesting to note that the tests of Kordina and Fuchs did not reach full efficiency; unfortunately Jackson did not carry out any tests with inclined bars. When increasing the number of reinforcement loops in specimen RV10 so that the effective amount of reinforcement area which crossed the critical crack at the inside of the corner was similar to that used in specimen RV9, the structural behaviour and final load capacity were also more or less the same.

Accordingly, it can be concluded that the usage of inclined bars is not more effective in strengthening the corner region than is the use of extra reinforcement loops; the test results presented here even indicate the opposite. Instead, it is the lower amount of reinforcement in the adjoining member compared to that in the corner that causes the failure to occur outside the corner. Hence, the reliability of the inclined bars depends on the external moment distribution and whether the reinforcement loops are spliced to straight bars just outside the corner. When using only reinforcement loops it is unlikely that the final failure will occur outside the corner. This is because the loops increase the load capacity in the adjoining member just as much as in the corner. Thus, since the external moment probably reaches its maximum within the corner and the theoretical moment capacity is the same in both cases, it is inevitable that the critical section also will be positioned at the inside of the corner. Even so, as has been shown in the tests presented here, quite a ductile behaviour might very well still be the case. Consequently, the inclined bars could, if it seems proper, equally well be replaced by extra reinforcement loops. If a response similar to that obtained when using inclined bars is wanted, Eq. (1) can be used to determine the necessary amount of extra reinforcement loops in the connection. The amount of inclined bars previously prescribed in the Swedish Shelter Regulations was based on the recommendations given in Nilsson (1973) and thus required this amount to be at least half that of the reinforcement loops used. Hence, using Eq. (1) it can be concluded that, if detail *c* is to be used the total amount of reinforcement loops shall be about  $1.35A_s$ , where  $A_s$  is the amount of reinforcement needed if the efficiency of the detailing had been 100%. This value is also what is prescribed in the present regulations, Swedish Rescue Services Agency (1998).

## CONCLUSIONS

A combination of full-scale tests and a literature survey of concrete frame corners subjected to closing or opening moment has been carried out to evaluate the usage of a new reinforcement proposal, using reinforcement loops spliced within the corner, in Swedish civil defence shelters.

Although there is a greater risk of spalling of the side concrete cover, it was concluded that it is suitable to replace the conventional detailing previously used in closing frame corners with the new one. However, special care still has to be taken when using this kind of detailing in beam-column connections where the effect of spalling can have large influences on the final capacity.

It was found that the commonly accepted reinforcement detailing in opening corners, using inclined bars at the inside of the corner, may not be as effective as previously believed; its efficiency largely depends on the applied moment distribution and the detailing of the



reinforcement just outside the corner area. A similar effect can instead be obtained by the presence of extra reinforcement loops, thus making the detailing easier to carry out. Further, it was found that even though full efficiency of such a corner detailing may not be achieved, ductile behaviour may very well still be obtained. While the test series is quite limited, it still indicates that the post-peak response of opening frame corners depends to a large degree on the amount of reinforcement loops, whereas the influence of any inclined bars seems to be small.

The work presented has, in combination with non-linear finite element analyses resulted, in a change of the previous Shelter Regulations so that the detailing evaluated here now is also valid for use in the design of civil defence shelters in Sweden.

### ACKNOWLEDGEMENTS

The research presented in this paper was financed by the Swedish Rescue Services Agency. The author would like to thank Professor Kent Gylltoft, head of the Division of Concrete Structures, for his support and advice. Special thanks are due to Björn Ekengren at the Swedish Rescue Services Agency and Dr. Mario Plos at Reinertsen Engineering for their much appreciated and encouraging support in the project. The author would also like to express his gratitude to Stefan Karlsson and Mathias Johansson for their valuable contributions in the testing and evaluation of the opening frame corners. Thanks also to the staff of the Structural Engineering Laboratory, for their invaluable assistance in the experimental part of this work.

### NOTATIONS

$A_s$	reinforcement area
$A_s^*$	effective reinforcement area when inclined bars are considered
$A_{s,i}$	reinforcement area of inclined bars
$b$	width
$C$	compressive force
$d$	effective height
$F$	load
$F_s$	force in reinforcement loops
$F_s^*$	effective force when inclined bars are considered
$F_{s,i}$	force in inclined bars
$f_c$	concrete
$f_{c,cube}$	compressive cube strength of concrete
$f_{c,cyl}$	compressive cylinder strength of concrete

$f_{sy}$	reinforcement yield strength
$M_{uc}$	estimated moment capacity
$M_{ut}$	maximum moment obtained in test
$R$	resultant force
$T$	tensile force
$\delta$	displacement
$\rho$	reinforcement ratio
$\phi$	diameter
$\omega_s$	mechanical reinforcement ratio

## REFERENCES

Abdul-Wahab, H. M. S., and Al-Roubai, A. A. M., "Strength and behaviour of steel fibre reinforced concrete corners under opening bending moment," *Magazine of Concrete Research*, V. 50, No. 4, Dec. 1998, pp. 305-318.

Abdul-Wahab, H. M. S., and Salman, S.A.R., "Effect of Corner Angle on Efficiency of Reinforced Concrete Joints under Opening Bending Moment," *ACI Structural Journal* V. 96, No. 1, Jan-Feb. 1999, pp. 115-121.

ACI Committee 315, "Details and Detailing of Concrete Reinforcement (ACI 315-92)," American Concrete Institute, Farmington Hills, Mich., 1999.

Balint, P. S., and Taylor, H. P. J., "Reinforcement Detailing of Frame Corner Joints with Particular Reference to Opening Corners," *Technical Report 42.462*, Cement and Concrete Association, London, 1972, 16 pp.

Boverket, "Boverkets handbok för Betongkonstruktioner BBK 94, Band 1, Konstruktion (Boverket's Handbook for Concrete Structures, BBK 94, Vol. 1, Design)," Boverket, Byggavdelningen, Karlskrona, Sweden, 1994, 185 pp. (in Swedish)

BST Byggstandardiseringen, "Betongprovning med Svensk Standard, BST handbok 12, utgåva 6 (Concrete Testing according to Swedish Standard, BST Handbook 12, sixth edition)," SIS – standardiserings-kommisionen i Sverige och Svensk Byggtjänst, Stockholm, Sweden, 1991, 285 pp. (in Swedish)

Eurocode 2, "Design of concrete structures Part 1: General rules and rules for buildings," European Committee for Standardisation, 1991, 253 pp.

Grassl, P., "Splicing of Reinforcement Loops in Beams: Experiments and Non-linear Finite Element Analyses," Division of Concrete Structures, Chalmers University of Technology, *Master Thesis* 99:4, Göteborg, Sweden, 1999.

Jackson, N., "Design of reinforced concrete opening corners," *The Structural Engineer*, Vol. 73, No. 13, July 1995, pp. 209-213.

Johansson, J. P. M., and Karlsson, S., “Nytt armeringsutförande i betongramhörn utsatta för positivt moment (New Reinforcement Detailing in Concrete Frame Corners Subjected to Positive Moment),” Division of Concrete Structures, Chalmers University of Technology, *Master Thesis 97:5*, Göteborg, Sweden, 1997. (in Swedish)

Johansson, M., “New Reinforcement Detailing in Concrete Frame Corners of Civil Defence Shelters: Non-linear Finite Element Analyses and Experiments,” Division of Concrete Structures, Chalmers University of Technology, *Licentiate Thesis 96:1*, Göteborg, Sweden, 1996.

Johansson M., “Non-linear Finite Element Analyses of Concrete Frame Corners,” *ASCE Journal on Structural Engineering* in Feb. V. 126, No. 2, Feb. 2000a, pp. 190-199.

Johansson M., “Structural Behaviour in Concrete Frame Corners of Civil Defence Shelters: Non-linear Finite Element Analyses and Experiments”, Division of Concrete Structures, Chalmers University of Technology, Ph.D. Thesis, Göteborg, Sweden. To be published in Mar. 2000b.

Kordina, K., and Fuchs, G., “Untersuchungen zur Anwendung von hakenförmigen Übergreifungsstößen in Rahmenecken (Examination of the use of Reinforcement Loops in Frame Corners),” Institut für Baustoffkunde und Stahlbetonbau, Der Technischen Universität Braunschweig, Braunschweig, Germany, 1970. (in German)

Lundgren, K., “Static Tests of Frame Corners Subjected to Closing Moments,” Division of Concrete Structures, Chalmers University of Technology, *Report 99:2*, Göteborg, Sweden, 1999.

Luo, Y. H.; Durrani, A. J.; Bai, S.; and Yuan, J., “Study of Reinforcing Detail of Tension Bars in Frame Corner Connections,” *ACI Structural Journal*, V. 91, No. 4, July-Aug. 1994, pp. 486-496.

Mayfield, B.; Kong, F. K.; Bennison, A.; and Davies, J. C. D. T., “Corner Joint Details in Structural Lightweight Concrete,” *ACI Journal*, V. 68, No. 5, May 1971, pp. 366-372.

Mayfield, B.; Kong, F. K.; and Bennison, A., “Strength and Stiffness of Lightweight Concrete Corners,” *ACI Journal*, V. 69, No. 7, July 1972, pp. 420-427.

Nilsson, I. H. E., “Reinforced concrete corners and joints subjected to bending moment.” National Swedish Institute for Building Research, *Document D7:1973*, Stockholm, Sweden, 1973.

Nilsson, I. H. E., and Losberg, A., “Reinforced Concrete Corners and Joints Subjected to Bending Moment,” *ASCE Journal of the Structural Division*, V. 102, No. 6, June 1976, pp. 1229-1254.

Noor, F.A., “Ultimate Strength and Cracking of Wall Corners,” *Concrete*, Cement and Concrete Association, London, July 1977, pp. 31-35.

Plos, M., "Splicing of Reinforcement in Frame Corners -Experimental Studies," *Nordic Concrete Research, Publ. No. 14*, The Nordic Concrete Federation, Norsk Betongforening, Oslo, Norway, 1994, pp. 103-121.

Skettrup, E.; Strabo, J.; Andersen, N. H.; and Brondum-Nielsen T., "Concrete Frame Corners," *ACI Journal*, V. 81, No. 6, Nov-Dec. 1984, pp. 587-593.

Stroband, J., and Kolpa, J. J., "The behaviour of reinforced concrete column-to-beam joints, Part 1: Corners Subjected to Negative Moments," Stevin Laboratory, Delft University of Technology, *Report 5-83-9*, Delft, The Netherlands, 1983, 105 pp.

Stroband, J.; and Kolpa, J. J., "The Behaviour of Reinforced Concrete Column-to-Beam joints, Part 2: Corners Subjected to Positive Moments," Stevin Laboratory, Delft University of Technology, *Report 5-81-5*, Delft, The Netherlands, 1981, 103 pp.

Swann, R. A., "Flexural Strength of Corners of Reinforced Concrete Portal Frames," *Technical Report TRA 434*, Cement and Concrete Association, London, 1969.

Shelter Regulations, "Shelter Regulations, SR English edition," Swedish Rescue Services Agency, *Publication B54-168/94*, Karlstad, Sweden, 1994, 94 pp.

Shelter Regulations, "Skyddsrumregler SR – Produktion och vidmakthållande (Shelter Regulations – Production and Maintenance)," Swedish Rescue Services Agency, *Publication B54-141/98*, Karlstad, Sweden, 1998, 167 pp. (in Swedish)

Östlund, L., "Inverkan av böckningsradier och täckande betongskikt hos kamstål på spjälkningsrisken för armerade betongkonstruktioner (The Influence of Bending Radius and Concrete Cover for Deformed Bars on the Risk of Splitting Failure in Reinforced Concrete Structures)," The Royal Institute of Technology, Stockholm, Sweden, 1963. (in Swedish)

# NONLINEAR FINITE-ELEMENT ANALYSES OF CONCRETE FRAME CORNERS

By Morgan Johansson<sup>1</sup>

**ABSTRACT:** A research project is currently being conducted to evaluate a new reinforcement detailing in frame corners in civil defense shelters where all reinforcement bars are spliced within the frame corner. As part of this, full-scale frame corners subjected to negative bending moment were tested and analyzed using the nonlinear finite-element program DIANA. A concrete material model based on nonlinear fracture mechanics to take cracking into account and plasticity models for concrete in compression and reinforcement steel were used. An interface model accounted for the bond-slip relation between reinforcement and surrounding concrete. Parameters that varied in the study were reinforcement detailing, reinforcement ratio, the effects of the weakness of the construction joint, and the interaction between reinforcement and concrete. Tests and finite-element analyses support the idea that the new reinforcement detailing is appropriate to use. Furthermore, it was found that the effect on the maximum load capacity of different bond-slip relations, the weakness of the construction joint, and incorrect positioning of the reinforcement bars in the corner were negligible.

## INTRODUCTION

A concrete frame structure's bearing capacity and ability to exhibit ductile behavior are highly dependent on the reinforcement detailing of the joint connections between its independent members, such as beams and columns. Accordingly, to obtain a sound structural behavior, the joints must be constructed to be at least as strong as the structural members connected to them and show ductile behavior in the ultimate limit state. Even though the reinforcement detailing required for such joint behavior is not obvious, only a few experimental studies on different reinforcement detailings for frame corners subjected to positive (opening of the corner) or negative moment (closing of the corner) have been reported (Swann 1969; Mayfield et al. 1971, 1972; Balint and Taylor 1972; Nilsson 1973; Stroband and Kolpa 1983; Skettrup et al. 1984; Luo et al. 1994; Plos 1995; and Abdul-Wahab and Al-Roubai 1998), and of these, only Plos and Gylltoft (1998) combined the experimental work with the use of nonlinear finite-element (FE) analyses.

In the present Swedish shelter regulations (*Shelter* 1994), the reinforcement detailing allowed for the design of frame corners in civil defense shelters, which are subjected to negative moment, is time consuming and quite difficult to carry out correctly. Consequently, there is a need for a simpler reinforcement detailing to be used. Therefore, a new design proposal, in which all the reinforcement bars are spliced within the corner area, was worked out (Fig. 1). This detailing is similar to that proposed by Nilsson for corners subjected to positive moment; the difference is that the inclined bars at the inside of the corner used by Nilsson are removed. However, this is justified since the presence of inclined reinforcement at the inside of a corner subjected to negative moment will only have a negligible effect on the moment capacity of the structure. Furthermore, tests on opening corners by Johansson and Karlsson (1997) showed that inclined bars could be replaced by a corresponding amount of reinforcement loops, and the structural behavior would still remain approximately the same. The aim of this study is to evaluate the new design proposal

and to determine whether it is appropriate to replace the conventional reinforcement detailing with the new kind. The service criterion set is that the new reinforcement detailing must withstand loading at least as well as the conventional detailing so that a safe and ductile structure is obtained. To examine the effectiveness of the new detailing, a combination of experiments and nonlinear FE analyses were carried out. The parameters that varied in the tests were the reinforcement detailing, the reinforcement ratio, the reinforcement type, and the configuration of the reinforcement bars. FE analyses were used to compare the new and conventional reinforcement detailing. Furthermore, the effects of different interactions between reinforcement and concrete, the weakness of the construction joint, and the consequence of incorrect positioning of the reinforcement loops in the new detailing were examined using this method.

## EXPERIMENTS

The emphasis of this paper is on nonlinear FE analyses; therefore, the tests are only briefly described. [More detailed information about the tests can be found in Plos (1995) and Johansson (1996)].

To gain a better understanding of the behavior of frame corners under loading to failure, two test series, each consisting of four full-scale specimens, were carried out. Two specimens were reinforced with the conventional reinforcement detailing and six with the new proposal (Table 1). The amount of reinforcement used (hot-rolled, deformed bars) corresponded approximately to the maximum and minimum amount of reinforcement allowed in the Swedish shelter regulations (*Shelter* 1994). Concrete quality with a target cylinder compressive strength of 30 MPa was used in all specimens. Fig. 2 shows the dimensions of the specimens and the test setup.

The load-displacement relations for the tests are shown in Fig. 3. Specimens RV1–RV4 were tested by Plos in the first test series. In this series, the specimens with new detailing (RV2 and RV4) had an unequal amount of reinforcement in the sections adjacent to the frame corner (Table 1). This was the reason for the somewhat lower load capacity obtained for these specimens compared with that of the specimens with the conventional detailing. In the second test series, the specimens with a high reinforcement ratio (RV5 and RV6) did not reach the load capacity expected due to spalling of the side concrete cover; this was also the reason the plateau in the load-displacement relation observed for the other specimens did not appear.

<sup>1</sup>Grad. Student, Div. of Concrete Struct., Chalmers Univ. of Technol., S-412 96 Göteborg, Sweden.

Note. Associate Editor: David J. Stevens. Discussion open until July 1, 2000. To extend the closing date one month, a written request must be filed with the ASCE Manager of Journals. The manuscript for this paper was submitted for review and possible publication on April 7, 1998. This paper is part of the *Journal of Structural Engineering*, Vol. 126, No. 2, February, 2000. ©ASCE, ISSN 0733-9445/00/0002-0190-0199/\$8.00 + \$.50 per page. Paper No. 18062.

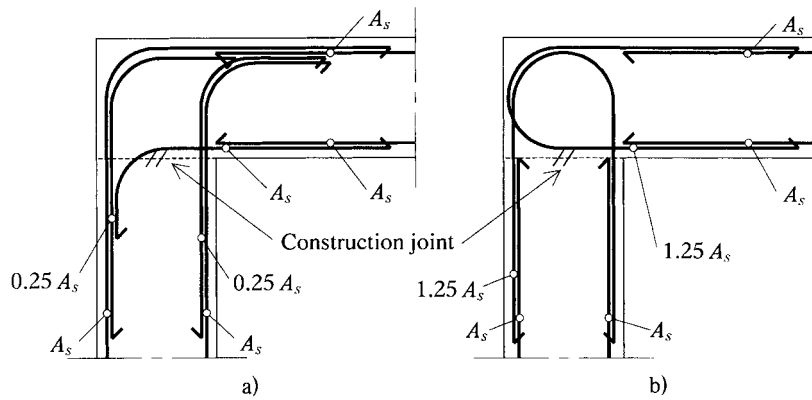


FIG. 1. Detailing of Reinforcement According to: (a) Conventional Method; (b) New Alternative. Extra 25% of Reinforcement at Corner Area Is Only Necessary If There Is Construction Joint Present

TABLE 1. Reinforcement Amount and Configurations for Test Specimens<sup>a</sup>

Test specimen (1)	Bar diameter (mm) (2)	Number of Reinforcement Bars		Reinforcement detailing (5)	Tensile strength (MPa) (6)
		Beam and column (3)	Frame corner (loops) (4)		
RV1 <sup>b</sup>	16	2 × 6	2 × 8	Conventional	473
RV2 <sup>b</sup>	16	2 × 6	2 × 6/2 × 8 <sup>d</sup>	New	473
RV3 <sup>b</sup>	10	2 × 4	2 × 5	Conventional	504
RV4 <sup>b</sup>	10	2 × 4	2 × 4/2 × 5 <sup>d</sup>	New	504
RV5 <sup>c</sup>	16	2 × 5	2 × 7	New	567
RV6 <sup>c</sup>	16	2 × 5	2 × 7	New	567
RV7 <sup>c</sup>	10	2 × 3	2 × 4	New	573
RV8 <sup>c</sup>	10	2 × 3	2 × 4	New	573

<sup>a</sup>Same number of reinforcement bars was placed on both compressive and tensile sides of beam and column.

<sup>b</sup>Reinforcement type Ks 40 S used— $f_{yk} = 400$  MPa, tested by Plos (1995).

<sup>c</sup>Reinforcement type K500 used— $f_{yk} = 500$  MPa.

<sup>d</sup>Number of bars were higher in column than in beam.

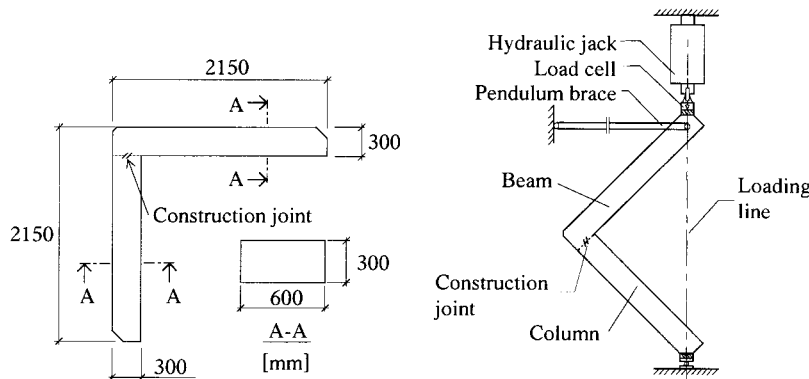


FIG. 2. Dimensions of Specimens and Test Setup. Concrete Cover Was Equal to  $1.5\phi$ , Where  $\phi$  Is Bar Diameter Used, in All Specimens

## NONLINEAR FE ANALYSES

### General

To study the structural behavior of the frame corner more thoroughly, the FE method was used. In this method, the concrete material models are based on nonlinear fracture mechanics (Hillerborg et al. 1976), to account for cracking, and plasticity models are used for the concrete in compression and the steel reinforcement. Hereby, it is possible to evaluate the stresses and deformations of a structure more thoroughly than can be done experimentally. Accordingly, the use of nonlinear FE analyses will result in a better understanding of the mechanical behavior in a structure during loading to failure.

The specimens of the second test series were analyzed using the FE program DIANA (DIANA 1993). The 2D plane stress

models were used to simulate the concrete. The cracking of the concrete was modeled using the smeared crack concept with nonorthogonal fixed cracks. Plasticity models accounted for the nonlinearity of concrete in compression and the steel reinforcement. The specimens were modeled at two different levels of detail. A relatively coarse mesh, with the assumption of a perfect bond between the reinforcement bars and the concrete, was used to simulate the general response of the specimens. To compare the new and the conventional reinforcement detailings, a refined element model with a finer mesh was used, taking into account the interaction between reinforcement and concrete. In the tests of specimens with high reinforcement ratio, the side concrete cover in the corner area spalled off. As this behavior could not be simulated in the FE models used, these specimens were analyzed using only the

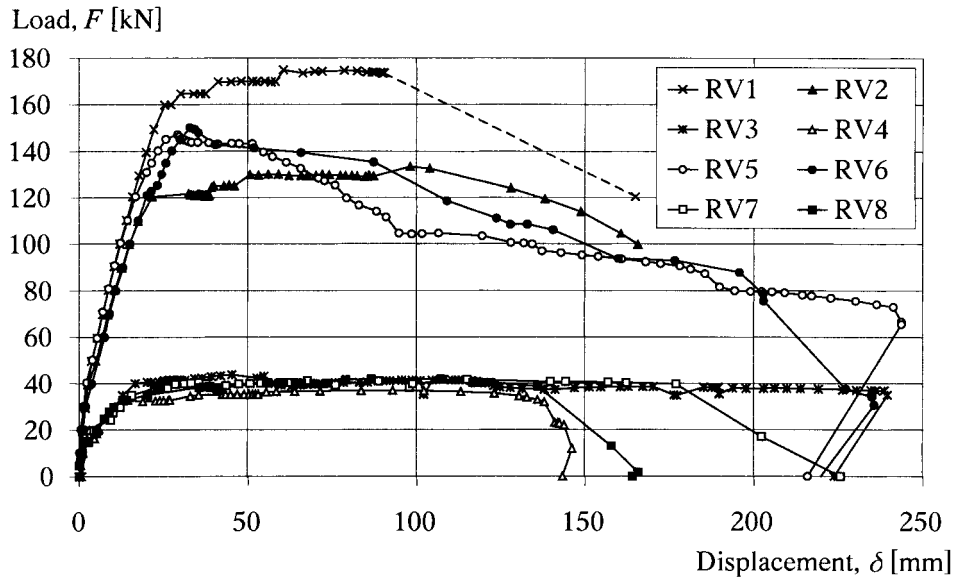


FIG. 3. Load-Displacement Relations for Test Specimens. Specimens RV1–RV4 Were Tested by Plos (1995)

less detailed model. In this paper only the more detailed analyses of specimens with low reinforcement ratio are presented. [A more thorough description of the analyses can be found in Johansson (1996).]

### Modeling of Concrete

In the analyses used here, cracking is taken into consideration by using a constant stress cutoff criterion. This means that once the maximum principal tensile stress reaches the tensile strength, independent of the other principal stresses, a crack is initiated perpendicular to the principal stress. The orientation of the crack is then stored and the material response perpendicular to the crack is determined by a stress-strain relation for the cracked material volume. Additional cracks may appear at the same location, but their formation is restricted to a minimum angle (here, set at  $60^\circ$ ) to previous cracks.

To simulate the softening curve of the concrete, a bilinear stress-crack opening relation according to recommendations given in Gylltoft (1983) was used. The fracture energy  $G_f$  and the tensile strength  $f_t$  were used to calculate the value of the ultimate crack opening  $w_u$ . A three-point bending test according to the recommendations of RILEM 50-FMC (1985) determined the fracture energy of the concrete. The tensile strength  $f_t$  used in the analyses was determined from the compressive strength  $f_c$  according to CEB-FIP Model Code (CEB-FIP 1993)

$$f_t = 0.30(f_c)^{2/3} \quad (1)$$

In the refined model the analyses took into account the interaction between the reinforcement and the concrete in the region close to the corner where cracking of the concrete was expected. Hereby, the crack distribution was given by the analysis, and since the smeared cracking of each element represents the development of one real crack, the stress-strain relation of the cracked concrete depends on the length of the FE. Therefore, in this region, the crack width was divided by the element lengths to determine the softening stress-strain relation used in the analyses. This length  $l_{\text{element}}$  was approximated as the length perpendicular to an assumed crack direction as shown in Fig. 4. Outside the corner area, this direction was set to be perpendicular to the direction of the beam and column, respectively. Within the corner the cracks were assumed to be “pointing” at the inside of the corner.

In the regions where perfect bonding between the reinforcement

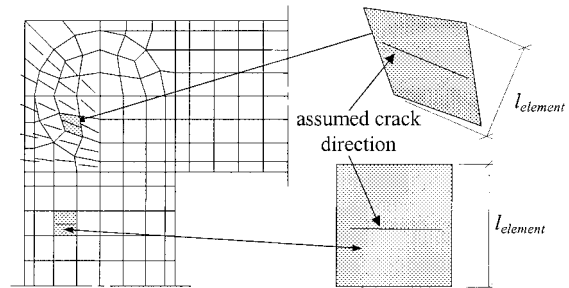


FIG. 4. Definition of Element Length  $l_{\text{element}}$

and concrete was assumed, the stress-strain relation for the concrete was determined by dividing the ultimate crack opening by the mean crack distance  $s_m$  (0.2 m) observed in the tests. However, as an approximation to consider the higher stiffness in the structure due to the effects of tension stiffening (Plos 1995), the gradient of the descending part of the stress-strain curve was halved for the concrete where perfect bond was assumed.

In compression, the response of the concrete was taken into account by an elastic-plastic model. The elastic stress-state was limited by a Drucker-Prager yield surface. Once yielding had occurred, an associated flow rule with isotropic hardening was used. In DIANA, this yield surface is evaluated from the current stress state, the angle of internal friction  $\phi$ , and the cohesion  $c$ . In accordance with recommendations given in the DIANA manual, the angle of internal friction in concrete was approximated to be  $\phi = 30^\circ$ . The cohesion  $c$  used in the analyses was calculated as

$$c = f_c(\epsilon_{\text{uniaxial}}^p) \frac{1 - \sin \phi}{2 \cos \phi} \quad (2)$$

where  $f_c(\epsilon_{\text{uniaxial}}^p)$  was the compressive strength as a function of the plastic strain in the direction of the uniaxial stress. The stress-strain relations up to the peak stress were determined on standard uniaxial tests on cylinders in which concrete from the same batch as the test specimens was used. In these tests the stress-strain relation could only be registered up to the maximum strength. Therefore, the postpeak behavior of the concrete was evaluated using the cylinder compression strength according to recommendations in CEB-FIP Model Code. Poisson's ratio was approximated to be 0.20.

In Fig. 5, the stiffness used in the analyses for unloaded

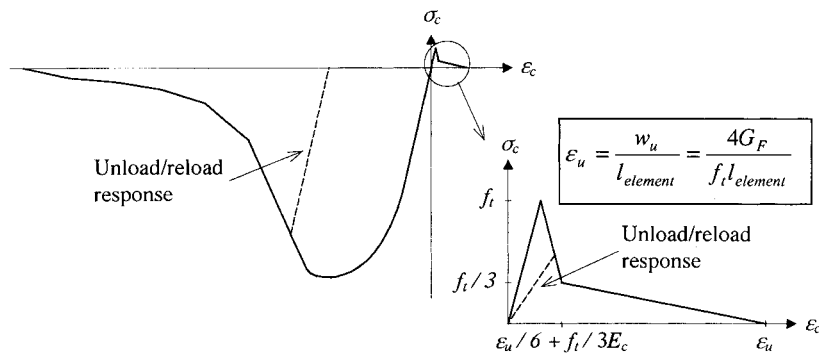


FIG. 5. Stiffness Used in Analyses for Unloaded Concrete in Compression and Tension ( $l_{\text{element}} = s_m/2$  When Perfect Bond Is Assumed)

TABLE 2. Material Properties for Concrete Used in Analyses

Object (1)	$E_c$ (GPa) (2)	$f_c$ (MPa) (3)	$f_t$ (MPa) (4)	$G_f$ (N/m) (5)
Column	24.6	27.8	2.7	108
Beam	23.5	33.8	3.1	66

concrete in tension and compression is shown. When the cracked concrete is unloaded, the secant unloading modulus is used as tangent stiffness so that the strain across the crack is reduced linearly to zero as the stress approaches zero. When concrete in compression is unloaded, the initial elastic stiffness is used. The material properties of the concrete used in the analyses are shown in Table 2.

### Modeling of Reinforcement

The von Mises yield criterion with associated flow and isotropic strain hardening was used to describe the constitutive behavior of the reinforcement bars. These were modeled with either the DIANA option “embedded reinforcements” or, according to recommendations given in the DIANA-manual, separate steel elements using truss elements. In the embedded reinforcement option, the reinforcement does not have separate degrees of freedom; instead, the strength and stiffness of the concrete elements are increased in the direction of the embedded reinforcement. With this model, perfect bonding is assumed between the reinforcement and the surrounding material. When the interaction between the reinforcement and the concrete was taken into consideration, the reinforcement bars

were modeled by separate elements, using truss elements in combination with interface elements. The mechanical properties of the reinforcement were Young’s modulus  $E_s = 191$  GPa; yield strength  $f_{sy} = 573$  MPa; ultimate strength  $f_{su} = 675$  MPa, strain at hardening  $\epsilon_{sh} = 2.8\%$ ; and strain at maximum stress  $\epsilon_{su} = 12.0\%$ .

In DIANA, the bond-slip relation between the reinforcement and the concrete is modeled using interface elements. In these elements, the bond stresses only depend on the longitudinal slip; the stresses normal to the bar are described with a stiff linear relation to the deformations in this direction. Consequently, splitting failures cannot be modeled. Instead, the effect of splitting has to be included in the nonlinear bond-slip relation. The bond-slip relation between the reinforcement and the concrete was approximated according to the CEB-FIP Model Code (CEB-FIP 1993). Here, the effect of splitting cracks is taken into account by giving different bond-slip relations for confined and unconfined concrete. Furthermore, the code differs between two different bond qualities: “good” and “other.” Because no splitting cracks were observed in the test specimens with low reinforcement ratio, “confined concrete” was assumed in the analyses. However, according to Engström (1992), the bond stress decreases considerably when the reinforcement steel yields. In the bond-slip relation proposed by Engström, the bond stress is not given explicitly but depends on when the steel reinforcement yields. The principal bond-slip relation for this yield case is similar to the relation given when “unconfined concrete” is assumed; therefore, as an approximation, “unconfined concrete” was assumed for the reinforcement bars positioned close to the corner where yielding of the reinforcing steel was likely to occur. To study the effect

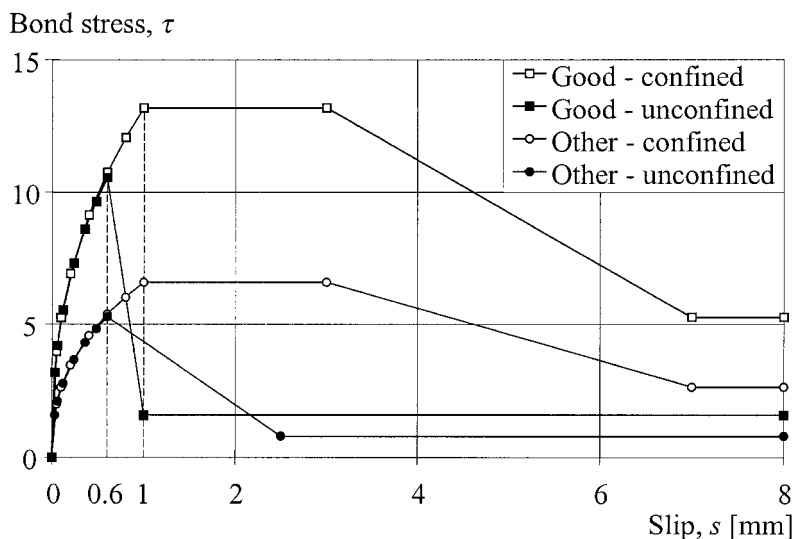


FIG. 6. Bond-Slip Relations Used in Analyses for Interaction in Column



of the structural behavior of various bond-slip relations, both good and other bond conditions were used in the analyses. To illustrate the essential difference of the bond qualities and bond conditions mentioned above, the bond-slip relations used within the column are shown in Fig. 6.

### FE Models

In the FE analyses, 2D plane-stress first-order elements were used to model the concrete. A Gauss integration scheme with  $2 \times 2$  integration points were used. To enhance the bending behavior of the elements, selective reduced integration (Hughes 1987) was used when evaluating the shear. Hereby, the shear strains are evaluated in the element midpoint only, and the shear locking, usually encountered when using fully integrated elements of the first order, can be avoided. To compare the effect of the new and the conventional reinforcement detailing, two different models, with a total of 322 and 336 elements, respectively, were used (Fig. 7). Two-node truss elements in combination with four-node interface elements, a total of 137 and 203 each, for the new and conventional detailing, respectively, were used to model more accurately the reinforcement bars within 1.0 m of the corner. Outside this area, the reinforcement bars were modeled with embedded reinforcement. The material parameters for concrete and reinforcing steel were identical in both models.

Furthermore, the effect of the weakness in the construction joint on the structural behavior of the frame corner was examined. The test specimens were cast with a construction joint (Fig. 2). The test results indicated that this joint exhibited a zone of weakness in the material in which cracking first occurred. This was modeled by reducing the tensile strength and the fracture energy of the concrete modeling the construction joint. Thus, the first crack was made to form at the same place as in the tests, and because this crack was observed at a load level approximately half of that expected, the tensile strength and fracture energy of the concrete modeling the construction joint were reduced to 50%. Furthermore, to study the effect of the weakness in the construction joint, an FE analysis with tensile strength and fracture energy reduced to 90%, compared with that used in the rest of the model, was also carried out for both reinforcement detailings. By using this slight weakness, the first crack was still made to form at the same place as in the tests.

Unless otherwise stated, good bond condition and a construction joint strength of 50%, compared with that in the rest of the model, were used in the FE analyses.

### Numerical Procedure

A displacement-controlled incremental loading was applied in the FE analyses to model the load of the structure. Two

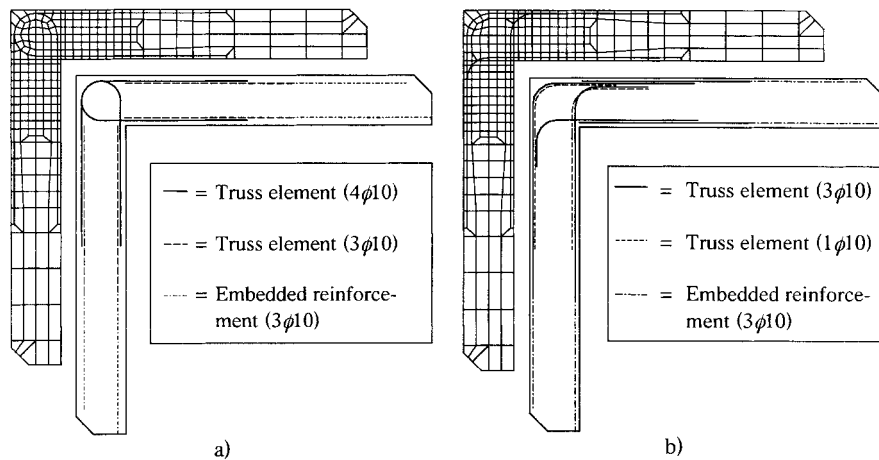


FIG. 7. FE Mesh and Modeling of Reinforcement Bars of Frame Corner with: (a) New Reinforcement Detailing; (b) Conventional Detailing

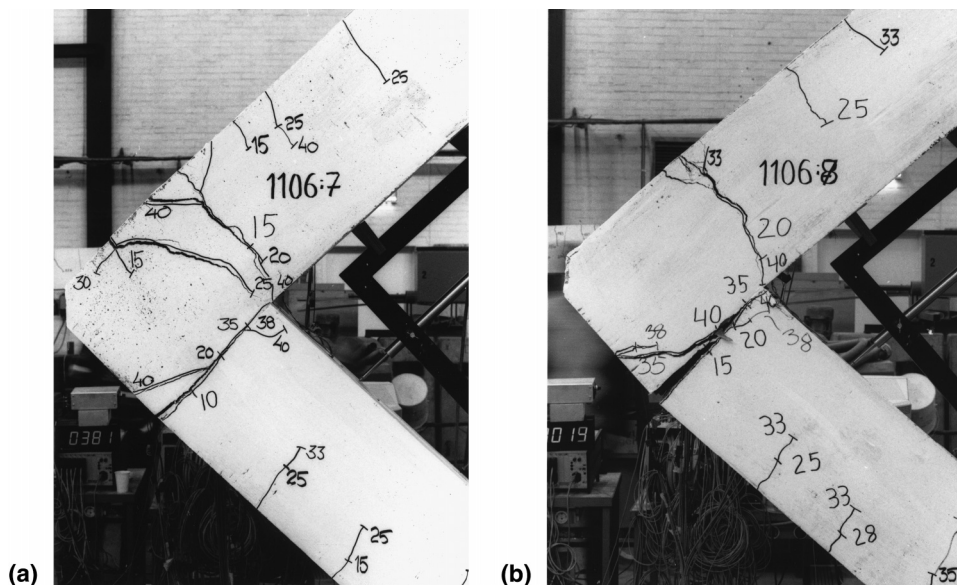


FIG. 8. Crack Patterns Obtained for Test Specimens: (a) RV7; (b) RV8

different iteration methods, the modified Newton-Raphson method and the BFGS (Broyden-Fletcher-Goldfarb-Shanno) secant stiffness method [e.g., Bathe (1996)], were tested. It was found in the more detailed analyses that the former method gave a somewhat smoother load-displacement relation than that achieved with the latter. However, the difference in the results obtained when using these methods was negligible, and because fewer numerical problems were encountered with

the BFGS method, this was the iteration method mainly used. To check the quality of the solution within each increment, a tolerance given as a percentage (usually 0.01%) of the energy norm was used as the convergence criterion.

### Results

In the first stage of the analyses, the bond condition corresponding to that of the test specimens was to be determined.

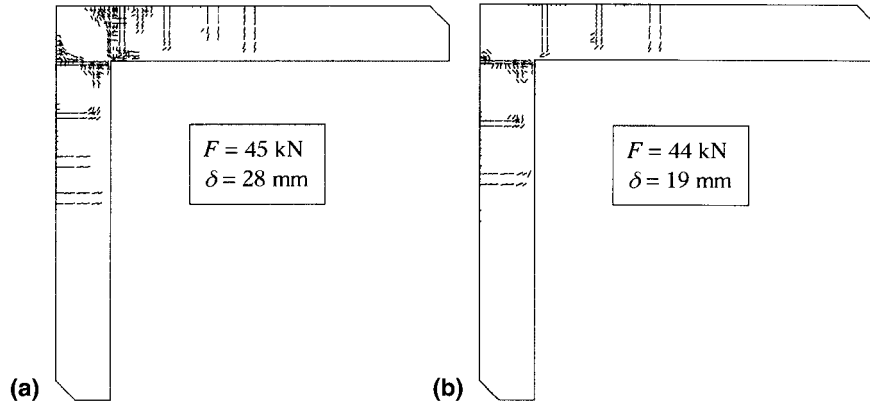


FIG. 9. Crack Pattern at End of Analyses for Frame Corner with New Reinforcement Detailing When Assuming Two Bond Conditions: (a) Good; (b) Other

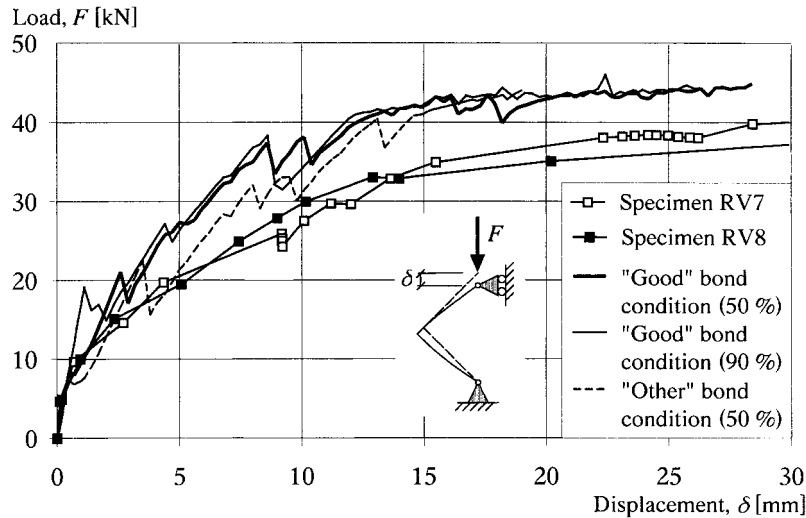


FIG. 10. Load-Displacement Relations for Tests and FE Analyses with New Reinforcement Detailing. Values between Brackets Show Strength of Concrete Modeling Construction Joint

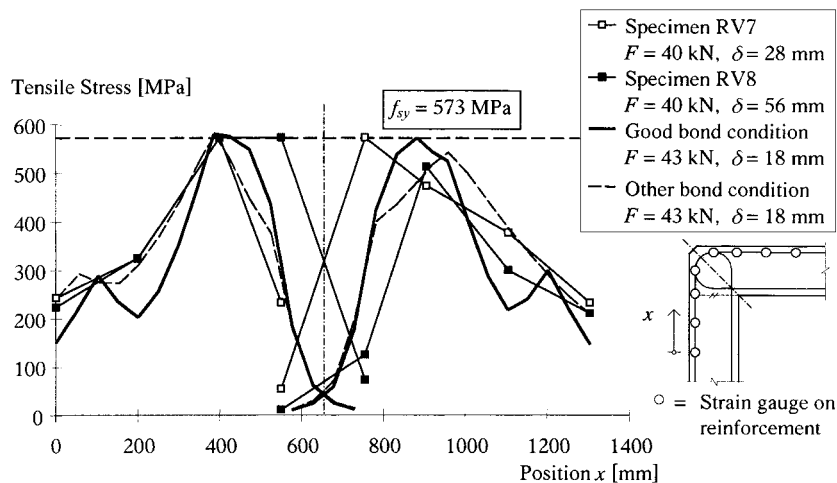


FIG. 11. Distribution of Tensile Stresses in Reinforcement Bars in Frame Corner for Tests and FE Analyses (New Reinforcement Detailing)

Two criteria can be used for this determination: (1) The mean spacing of the major cracks observed in the test specimens; and (2) the load-displacement relation obtained in the tests. The former criterion was assumed to be the better one to use because some factors of uncertainty, such as the fracture energy and the generally stiffer behavior of the FE analysis, have less effect on it. The crack pattern and load-displacement relations of the analyses were compared with those obtained in the tests (Figs. 8 to 10). The FE analysis assuming good bond condition showed the best agreement with the mean crack spacing of 0.2 m observed in the tests. Therefore, a bond-slip relation corresponding to this one was assumed to be the closest to that of the test specimens even though the load-displacement relation was somewhat stiff in comparison with the tests.

The distribution of the tensile stresses along the reinforcement loops, when yielding of the steel reinforcement has just occurred is presented in Fig. 11. The difference in the distributed tensile stresses observed for the different bond-slip rela-

tions was due to the different appearance of major cracks in the column and the beam near the corner area.

In Fig. 12, the load-displacement relation of the FE analyses for the frame corner with the new reinforcement detailing is compared with that of the frame corner with the conventional reinforcement detailing. The crack propagation and the distribution of tensile stresses along the reinforcement bars at the corner are shown in Figs. 13 and 14 for the frame corner with conventional detailing at displacements between 26 and 32 mm.

### Discussion of Results

The results of the FE analyses corresponded quite well with the results from the experiments; the behavior was similar for both the maximum load capacity obtained and the stiffness of the structure. Furthermore, the crack pattern and positioning of the plastic hinges in the detailed analyses corresponded very

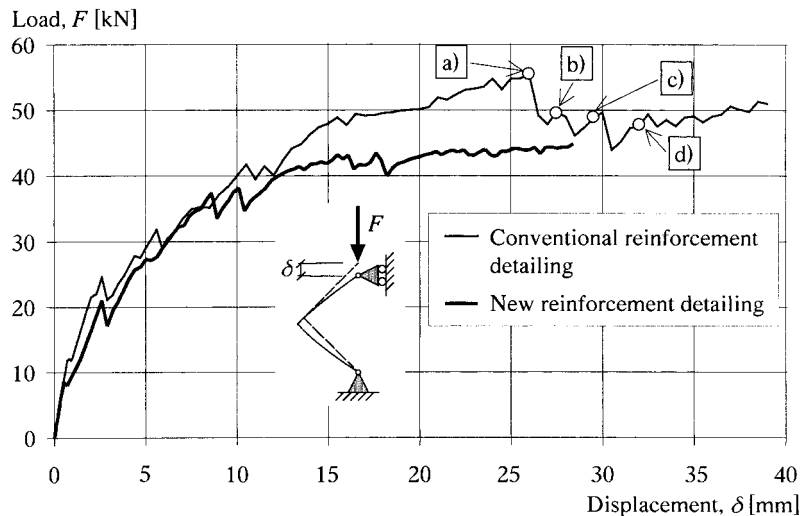


FIG. 12. Comparison of Load-Displacement Relations for Frame Corners Carried Out with New and Conventional Reinforcement Detailing. Crack Propagation in Corner at Marked Points, (a) to (d), Is Shown in Fig. 13.

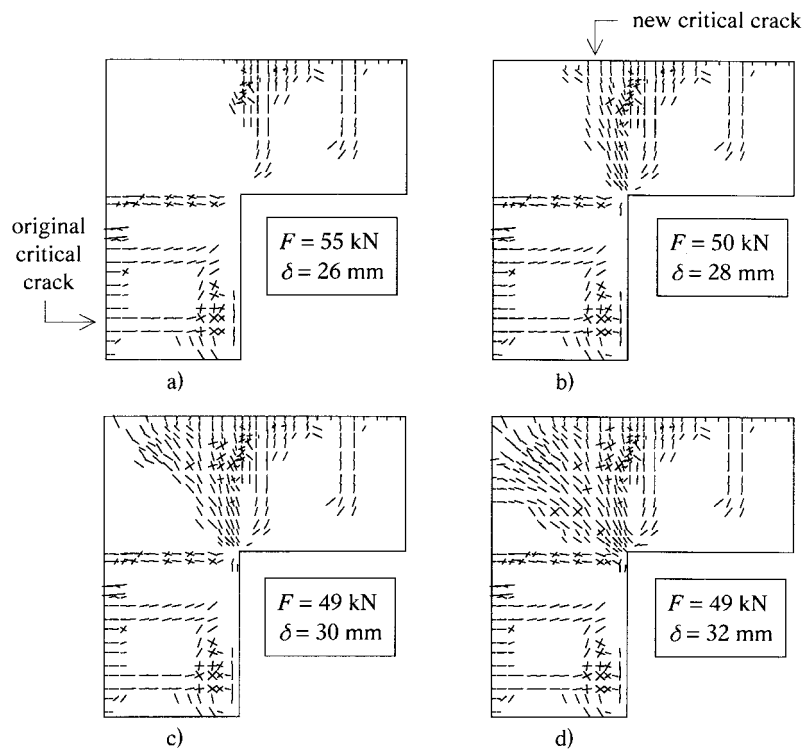
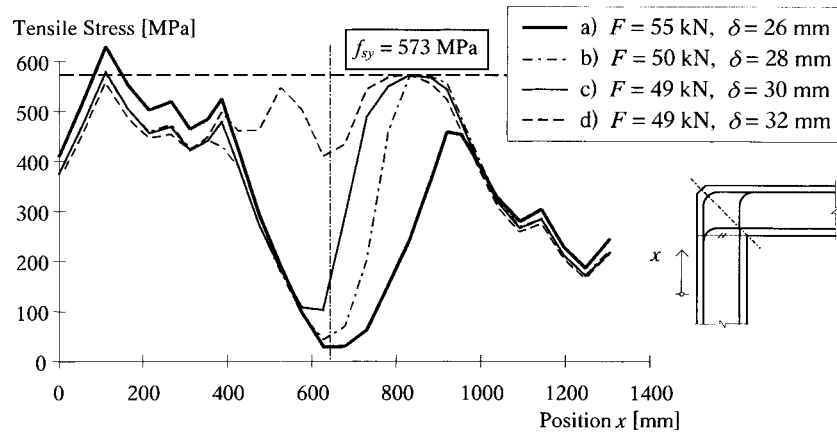


FIG. 13. Crack Propagation in Corner Area for Conventional Reinforcement Detailing at Load Levels Marked in Fig. 12



**FIG. 14. Distribution of Tensile Stresses in Reinforcement Bars in Frame Corner Carried Out with Conventional Reinforcement Detailing. Tensile Forces Are Shown at Same Load Levels Marked in Fig. 12**

well with those observed in the test specimens with both the new and conventional reinforcement detailings. However, it was not possible to predict the behavior of the frame corner throughout total failure. This was because all analyses of the frame corner were disrupted due to numerical problems when the compression strength of the concrete was reached at one integration point in the corner area. At this stage, yielding of the reinforcement bars had occurred and, in some cases, also started to harden.

In Fig. 10 it can be seen that the stiffness of the structure is affected by the bond-slip relation up to the point at which the steel reinforcement yields: the higher the stiffness of the bond-slip relation, the higher the stiffness of the structure. However, the effect of the bond-slip relation on the load capacity was negligible. Furthermore, the FE analyses indicate that, if rupture of the reinforcement bars is the cause of failure, then the deformation capacity of the frame corner would be lower for a stiffer bond-slip relation. The influence of the weakness of the construction joint in the frame corner was limited to the initial cracking stage and had a negligible effect on the general behavior of the structure. In Johansson (1996) it is shown that these statements also hold true for a frame corner made with the conventional reinforcement detailing.

In Fig. 12 it can be seen that the structural behavior of the frame corners with the new and conventional detailing was similar up to a load of about 40 kN, at which point the reinforcement bars in the frame corner with new reinforcement detailing started to yield. Due to a greater amount of reinforcement in the sections adjacent to the corner [compare Figs. 7(a) and b)], the load capacity of the frame corner with conventional reinforcement detailing continued to increase until yielding was reached at a load level just below 50 kN. The sudden loss of load capacity at a displacement of about 26 mm was caused by a redistribution of forces. The critical crack section moved from a region about 300 mm below the construction joint (the section where the bent reinforcement bars, extending from the beam, ended) into the corner (Fig. 13). This crack behavior corresponded well with that observed in the test of the frame corner with low reinforcement ratio and conventional detailing (Plos 1995).

The frame corner with new reinforcement detailing showed a similar symmetrical distribution of the tensile forces, with yielding of the reinforcement bars in the sections adjacent to the corner. This was not the case for the frame corner with the conventional detailing. Due to the different amount of reinforcement used in the sections adjacent to the corner [Fig. 7(b)] the tensile forces were shifted into the leg below the construction joint. However, the propagation of new cracks in the corner caused the tensile forces in the reinforcement bars to increase considerably (Fig. 14) and, thereby, obtain a force

distribution more similar to that observed in the frame corner with the new detailing.

Accordingly, the FE analyses showed that a frame corner with the conventional reinforcement detailing may have a somewhat higher load capacity than a frame corner with the new reinforcement detailing. However, this is only temporary since a redistribution of forces soon occurs which reduces the load capacity to a level similar to that obtained when using the new reinforcement detailing. Thus, the load capacity is approximately the same, independent of which of the two reinforcement detailings are used.

On the construction site, it sometimes happens that the reinforcement bars are not positioned according to the designers' drawings. Therefore, an analysis of a frame corner with the reinforcement loops in the column "mistakenly" positioned approximately 90 mm below that shown in Fig. 7(a) was carried out (Johansson 1996). It was found that this incorrect positioning of the reinforcement loops in the new detailing had a limited effect on the behavior of the frame corner, and that the load capacity obtained from the analyses was found to be approximately the same. Even though these results are not verified by tests, the analyses give an indication of the structural behavior.

In the analyses of the test specimens, a state of plane stress was assumed. However, in a real civil defense shelter structure, a state of plane strain is possibly a more accurate assumption. Therefore, to examine the behavior of a frame corner when plane strain is assumed, a detailed analysis of a frame corner with the new detailing was carried out. It was found that the load capacity and structural behavior were similar for the frame corner whether a state of plane stress or plane strain was assumed. Consequently, because the state in a real structure is somewhere between plane stress and plane strain, the analyses assuming plane stress presented here should be valid for a frame corner in a real structure.

### Suggestions for Improvements of Analyses

The results from the FE analyses showed a somewhat stiffer behavior with a higher (approximately 10%) load capacity than that observed in the tests. A possible reason for this might be that the mesh is too coarse in the compressive zone at the inside of the corner. By using a finer mesh and/or a different integration rule [Newton-Cotes; e.g., see Bathe (1996)] in this area, it might have been possible to better catch the response of the concrete in compression, thus resulting in a less stiff load-displacement behavior. Furthermore, a decrease of the size of the load increments in the initial cracking stage or of the allowable angle between cracks might have had a similar positive effect.

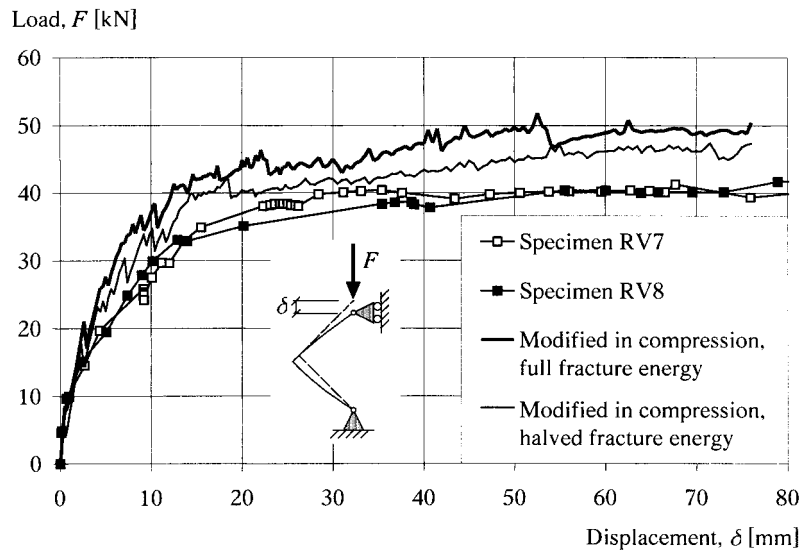


FIG. 15. Comparison of Load-Displacement When Stress-Strain Relations in Compression Are Modified to Take into Account Length of Elements. Different Values of Fracture Energy (Full and Halved) Were Used

The major problem encountered in the analyses was the crushing of the concrete in one integration point. This caused the analyses to stop at a displacement far lower than that observed in the tests. A probable explanation for this is the brittleness in the postpeak behavior of the concrete in compression. The essential stress-strain relation used for the concrete in compression is shown in Fig. 5. However, van Mier (1984) showed that the postpeak behavior of concrete is due to a localization in the material. Consequently, the stress-strain relations used in the analyses for concrete in compression should, as is the case when dealing with cracking, also be a function of the element length. This was not considered in the analyses, which means that the postpeak stress-strain relations used in compression are too brittle. The length of the standard cylinders, used to evaluate the recommendations given in the CEB-FIP Model Code, is 300 mm. This indicates that the stress-strain relation given in the CEB-FIP Model Code should be valid when the elements used in an analysis are 300 mm. However, the length of the elements near the corner in these analyses is 50 mm. Therefore, an analysis where this was taken into consideration was carried out. The postpeak stress-strain relation in compression was modified by a factor of  $300/50 = 6$  (i.e., after the peak the plastic strain was multiplied by 6). However, this modification presumed that, when the compressive strength is reached in one element, a localization will occur and the adjacent elements unload elastically. This was not the case in the analysis, which meant that a stiffer behavior with an increasing load capacity (due to the hardening of the reinforcement) was obtained (Fig. 15). Thus the analysis was stopped (even though it could have been driven further) at a displacement of about 75 mm. Even though these second stress-strain relations were too ductile, the results from the analyses indicate that a similar modification of the postpeak behavior is correct. In what way this modification should have been done instead has not been further studied within the scope of the work presented here.

In Fig. 15, the importance of the fracture energy is also shown (the stress-strain relations in compression are still modified as described above). It was found that the behavior of the frame corner was approximately the same independent of the fracture energy used in the analyses. However, when using a lower value (halved) on the fracture energy a better correspondence in the load-displacement relation was obtained, thus indicating that the tensile stress-strain relation used in the analyses was somewhat too ductile. This can be due to several reasons such as different sizes and curing conditions of the

specimens used in the tests and those used to measure the fracture energy. It can also be due to the method used when determining the element length  $l_{\text{element}}$  as described in Fig. 4.

## CONCLUSIONS

A new design proposal in concrete frame corners in civil defense shelters has been studied using full-scale tests in combination with nonlinear FE analyses. The parameters studied were the reinforcement detailing, the reinforcement ratio, the effects of the weakness of the construction joint, and the interaction between reinforcement and concrete.

The tests and the FE analyses conducted have shown that the conventional and the new reinforcement detailings for practical purposes are equivalent for a frame corner structure with a low amount of reinforcement. Comparisons of tests and FE analyses indicate that this is also the case for a frame corner with a high amount of reinforcement. Thus, the tests and analyses support the idea that the new alternative is suitable to use instead of the conventional reinforcement detailing.

The FE analyses have shown that the stiffness of the structure is affected by the bond-slip relation up to the point at which the steel reinforcement starts to yield: the higher the stiffness of the bond-slip relation, the higher the stiffness of the structure. When rupture of the reinforcement bars is the cause of final failure, a weak bond-slip relation has a positive effect on the deformation capacity of the structure. However, the maximum load capacity is relatively unaffected by the bond-slip relation.

The weakness of the construction joint affects the structural behavior of the frame corner only in the initial cracking stage; its effect on the maximum load capacity is negligible. The FE analyses showed that an incorrect positioning of the reinforcement loops in one of the legs adjacent to the corner has a limited effect on the maximum load capacity.

Due to localization in the postpeak region, the element length should be considered when determining the concrete stress-strain relations used in compression. However, there does not seem to be a direct connection between what modification should be made and the length of the independent element.

## ACKNOWLEDGMENTS

The work presented was carried out at the Division of Concrete Structures, Chalmers University of Technology, Göteborg, Sweden, and was financed by the Swedish Rescue Services Agency, Karlstad, Sweden. The

writer would like to thank his supervisor Prof. Kent Gylltoft for his guidance and support. Special thanks are due to Björn Ekengren and Magnus Kjellman from the Swedish Rescue Services Agency and Mario Plos for their enthusiastic encouragement and valuable help in the project.

## APPENDIX I. REFERENCES

- Abdul-Wahab, H. M. S., and Al-Roubai, A. A. M. (1998). "Strength and behaviour of steel fibre reinforced concrete corners under opening bending moment." *Mag. of Concrete Res.*, 50(4), 305–318.
- Balint, P. S., and Taylor, H. P. J. (1972). "Reinforcement detailing of frame corner joints with particular reference to opening corners." *Tech. Rep. 42.462*, Cement and Concrete Association, London.
- Bathe, K. J. (1996). *Finite element procedures*. Prentice-Hall, Englewood Cliffs, N.J.
- CEB-FIP model code 1990, design code. (1993). Thomas Telford, Lausanne, Switzerland.
- DIANA, version 6.1 (1996). Dept. of Engrg. Mech. and Information Technol., TNO Building and Construction Research, Delft, The Netherlands.
- Engström, B. (1992). "Ductility of tie connections in precast structures," PhD thesis, Div. of Concrete Struct., Chalmers University of Technology, Göteborg, Sweden.
- Gylltoft, K. (1983). "Fracture mechanics models for fatigue in concrete structures." PhD thesis, Div. of Struct. Engrg., Luleå University of Technology, Luleå, Sweden.
- Hillerborg, A., Modéer, M., and Petersson, P.-E. (1976). "Analysis of crack formation and crack growth in concrete by means of fracture mechanics and finite elements." *Cement and Concrete Res.*, 6(6), 773–782.
- Hughes, T. J. R. (1987). *The finite element method—Linear static and dynamic finite element analyses*. Prentice-Hall, Englewood Cliffs, N.J.
- Johansson, M. (1996). "New reinforcement detailing in concrete frame corners of civil defence shelters: Non-linear finite element analyses and experiments," Licentiate thesis, Div. of Concrete Struct., Chalmers University of Technology, Göteborg, Sweden.
- Johansson, M., and Karlsson, S. (1997). "New reinforcement detailing in concrete frame corners subjected to positive moment." *Rep. 97:5*, Div. of Concrete Struct., Chalmers University of Technology, Göteborg, Sweden (in Swedish).
- Luo, Y. H., Durrani, A. J., Bai, S., and Yuan, J. (1994). "Study of reinforcing detail of tension bars in frame corner connections." *ACI Struct. J.*, 91(4), 486–496.
- Mayfield, B., Kong, F. K., and Bennison, A., and Davies, J. C. D. T. (1971). "Corner joint details in structural lightweight concrete." *ACI J.*, 68(5), 366–372.
- Mayfield, B., Kong, F. K., and Bennison, A. (1972). "Strength and stiffness of lightweight concrete corners." *ACI J.*, 69(7), 420–427.
- Nilsson, I. H. E. (1973). "Reinforced concrete corners and joints subjected to bending moment." *Document D7:1973*, National Swedish Institute for Building Research, Stockholm, Sweden.
- Plos, M. (1995). "Application of fracture mechanics to concrete bridges

- Finite element analyses and experiments," PhD thesis, Div. of Concrete Struct., Chalmers University of Technology, Göteborg, Sweden.
- Plos, M., and Gylltoft, K. (1998). "Nonlinear FE analyses of RC bridge frame corners, based on fracture mechanics." *J. Bridge Engrg.*, ASCE, 3(4), 204–210.
- RILEM 50-FMC Committee. (1985). "Determination of the fracture energy of mortar and concrete by means of three-point bend tests on notched beams." *Mat. and Struct.*, 18(106), 285–290.
- Shelter regulations, SR*. (1994). English Ed., *Publ. B54-168/94*, Swedish Rescue Services Agency, Karlstad, Sweden.
- Skettrup, E., Strabo, J., Andersen, N. H., and Brondum-Nielsen, T. (1984). "Concrete frame corners." *ACI J.*, 81(6), 587–593.
- Stroband, J., and Kolpa, J. J. (1983). "The behaviour of reinforced concrete column-to-beam joints, Part 1, Corners subjected to negative moments." *Rep. 5-83-9*, Stevin Lab., Delft University of Technology, Delft, The Netherlands.
- Swann, R. A. (1969). "Flexural strength of corners of reinforced concrete portal frames." *Tech. Rep. TRA 434*, Cement and Concrete Association, London.
- van Mier, J. G. M. (1984). "Strain softening of concrete under multiaxial loading conditions," PhD thesis, Eindhoven University of Technology, Eindhoven, The Netherlands.

## APPENDIX II. NOTATION

The following symbols are used in this paper:

- $c$  = cohesion;  
 $E_c$  = Young's modulus for concrete;  
 $E_s$  = Young's modulus for steel;  
 $F$  = load;  
 $f_c$  = compressive strength of concrete;  
 $f_{su}$  = ultimate strength of reinforcement;  
 $f_{sy}$  = yield strength of reinforcement;  
 $f_t$  = tensile strength of concrete;  
 $f_{yk}$  = characteristic yield strength of reinforcement;  
 $G_F$  = fracture energy;  
 $l_{\text{element}}$  = length of FE as defined in Fig. 4;  
 $s$  = slip;  
 $s_m$  = mean crack spacing;  
 $w_u$  = ultimate crack opening;  
 $x$  = coordinate along reinforcement bars in corner region;  
 $\delta$  = displacement;  
 $\epsilon_c$  = concrete strain;  
 $\epsilon_{sh}$  = strain at steel hardening;  
 $\epsilon_{su}$  = strain at maximum steel stress;  
 $\epsilon_u$  = ultimate strain;  
 $\epsilon_{\text{uniaxial}}^p$  = plastic strain in direction of uniaxial stress;  
 $\sigma_c$  = concrete stress;  
 $\tau$  = bond stress; and  
 $\phi$  = bar diameter, angle of internal friction.

# FE ANALYSES OF CONCRETE CIVIL DEFENCE SHELTERS SUBJECTED TO TRANSIENT LOADING

By Morgan Johansson

**ABSTRACT:** Civil defence shelters subjected to a blast load from a nearby explosion or the impact due to falling masses from a collapsing building were studied using the non-linear finite element programme ABAQUS/Explicit. It was found that the most critical stage in the shelter subjected to a blast load was during the first 10 ms. Further, it was observed that the deformations obtained in the shelter subjected to falling masses largely depend on the time it takes for the whole mass to hit the structure but, more importantly, also the mass of each independent part hitting the structure. Nevertheless, in none of the analyses did any critical cracks form within the corners, so it seems reasonable to believe that the response within a transiently loaded corner will be similar to that obtained in a statically loaded structure. It was concluded that even though the structural behaviour can differ a lot when subjected to transient loads, locally there are still large similarities to that in static loading.

Keywords: Transient loading, blast load, impact load, civil defence shelter, non-linear finite element analysis, dynamic, reinforcement detailings in corner

## INTRODUCTION

From a safety point of view it is important that a concrete structure, apart from necessary load capacity, also is able to show ductile behaviour that allows redistribution of forces so that a total collapse of the structure can be avoided if local failure is obtained. The ability of a concrete frame structure to meet these requirements depends much on the reinforcement detailing of the joint connections between its independent members. In co-operation between the Swedish Rescue Services Agency and the Division of Concrete Structures at Chalmers University of Technology, such a reinforcement detailing, using reinforcement loops spliced within the corner, has previously been evaluated for frame corners in civil defence shelters; see Plos (1995), Johansson (1996, 2000a, 2000b) and Johansson and Karlsson (1997). Static tests and non-linear finite element analyses have shown that it is feasible to replace the conventional detailing with a new one. However, since a civil defence shelter is designed to withstand transient loading, such as blast waves from an explosion and falling debris from collapsing buildings, this has to be taken into consideration.

When designing a civil defence shelter according to the present Swedish Shelter Regulations (1998), it is considered as a statically loaded structure. But, whether this approximation is appropriate has not been sufficiently examined. Therefore, the main aim of the study was to gain more knowledge of how a civil defence shelter behaves when subjected to transient loads such as those mentioned above. This was made possible by the use of non-linear finite element analyses (FE analyses) in which cracking of the concrete and yielding of the reinforcement were taken into account. Based on these analyses, another important question was also to be answered: whether the conclusions drawn from the static tests and analyses carried out in previous studies is correct also for such transient load cases?

Due to the shortage of space available, this paper just presents the major results and findings in the study carried out; more information about the material presented herein may be found in Johansson (1999).

## **SHELTERS STUDIED**

In this paper, a study of two different load cases is presented: blast load (i.e. a weapon load) from a nearby explosion, and impact load due to falling debris from a collapsing building. The effect of the blast load is studied for a building with a low-weight (i.e. timber) building on top, and the effect of the impact load is examined for the case when the shelter has a three-story concrete building, of height 9.0 m and a mass  $2,930 \text{ kg/m}^2$ , standing on top of it. The purpose of the timber building is mainly to motivate the lack of diffraction effects at the top of the shelter roof (Baker 1973) and its dead weight is therefore neglected in the analyses.

When designing a civil defence shelter in Sweden, equivalent static load cases are used. For the weapon load this is represented by the long-term pressures (both positive and negative) due to a nuclear detonation at long range and for the impact load an equivalent static load based on the work by Hallgren and Granström (1977) is used; see Fig. 1. The magnitudes of the static loads shown in Fig. 1, and used in the design for the cases studied here are  $q_{\text{weapon}} = 50 \text{ kN/m}^2$  and  $q_{\text{impact}} = 86 \text{ kN/m}^2$ . The dimensions of the civil defence shelter and the reinforcement amount required in a 1.0 m wide strip are shown in Fig. 2. These dimensions fulfil the requirements set up in the Swedish Shelter Regulations that the minimum reinforcement ratio shall be 0.14% and that the concrete wall and roof thickness shall be at least 350 mm. The design values used were  $f_{cd} = 21.5 \text{ MPa}$  and  $f_{syd} = 450 \text{ MPa}$  for concrete in compression and reinforcement yield strength, respectively.



These static loads, though, are just simplifications used to make it easier to design the shelter; the real loads acting on the shelter will be more similar to those shown in Fig. 3a. The pressure, due to a nearby explosion, acting on the front shelter wall is highly transient and will present a very large peak pressure but a short duration. On the other hand, the impact load will be composed of falling debris hitting the shelter roof with a certain velocity.

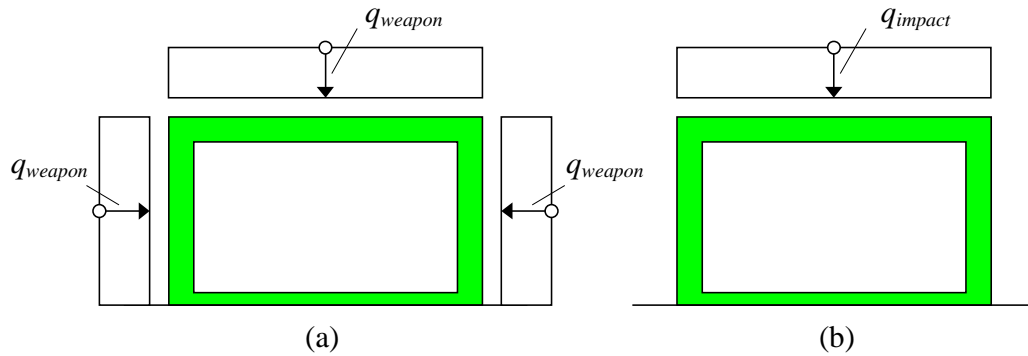


Fig. 1 Equivalent static loads used in the design of a shelter: (a) weapon load; (b) impact load.

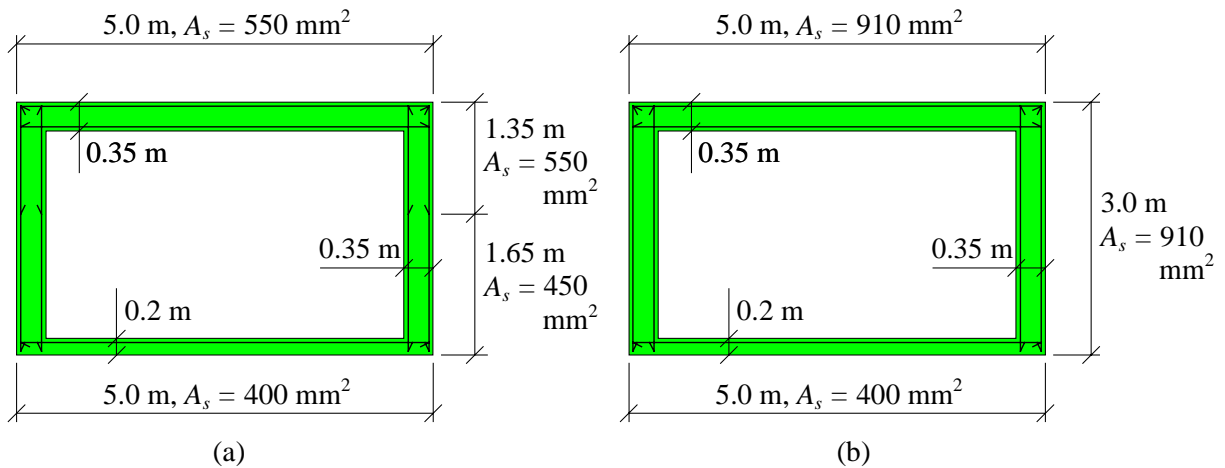


Fig. 2 Dimensions and reinforcement detailing for civil defence shelter subjected to: (a) weapon load; (b) impact load. The reinforcement centre is positioned 30 mm from the concrete edge.

According to the Swedish Shelter Regulations (1998) a civil defence shelter shall be able to withstand the effect of a pressure wave corresponding to that produced by 125 kg TNT which bursts freely outside at a distance of 5.0 metres from the outside of the shelter during free pressure release. From this description the blast load's pressure-time relation can be approximated as shown in Fig. 3b, ConWep (1992). In the FE analyses the impact load is simulated by letting falling masses hit the shelter roof with a certain velocity. Assuming that

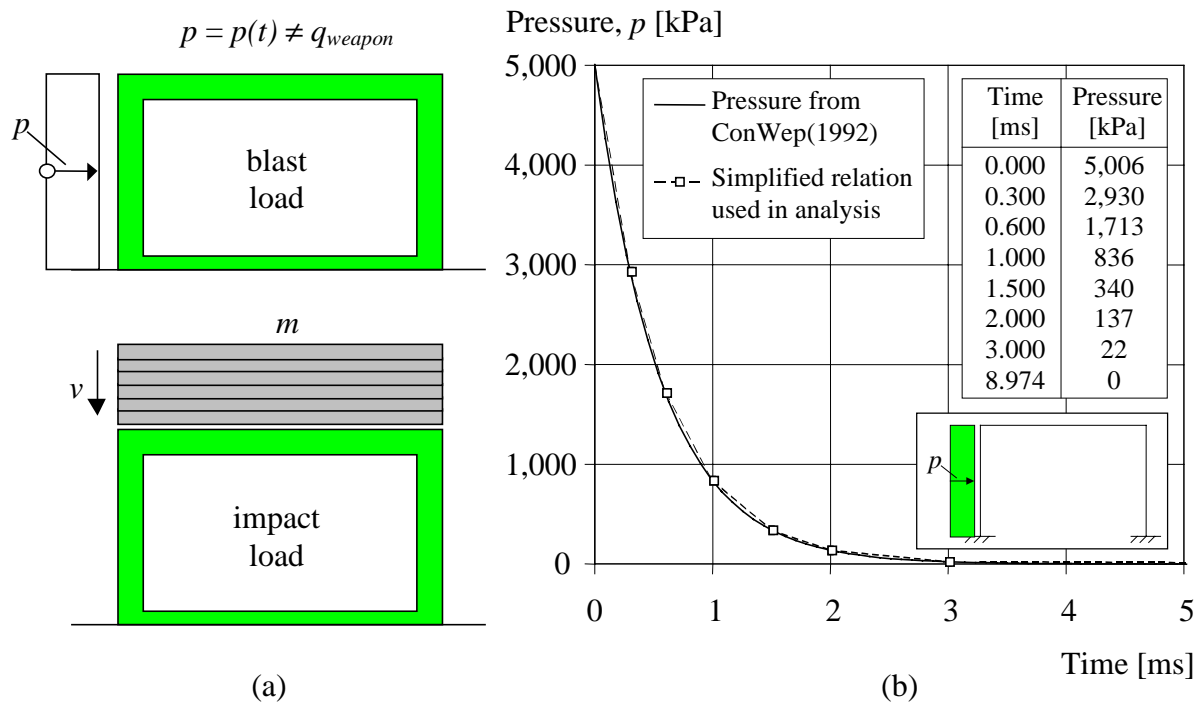


Fig. 3 (a) Transient loads carried out in the FE analyses presented herein; (b) pressure-time relation used in the blast load analyses.

the collapse of the concrete building standing on top of the shelter starts at the top floor, and assuming plastic impact, the velocity of the falling mass can be determined to be 9.6 m/s just before reaching the shelter roof; see Johansson (1999, 2000b).

## NON-LINEAR FE ANALYSES

### Modelling of concrete and reinforcement

The analyses presented herein were carried out using the finite element programme ABAQUS/Explicit, HKS (1998). The programme uses the explicit integration method and is therefore a suitable tool to study structures subjected to transient loading. Here it is possible to model the cracking of concrete by the use of the *brittle cracking* model, which is a smeared crack model with fixed, orthogonal cracks. Unfortunately, this model was developed for cases where concrete cracking dominates and is therefore limited to linear elastic behaviour in compression. To consider the non-linear response of concrete in compression a plastic model, such as that of von Mises or Drucker-Prager, can be used. However, it is not possible to combine these models with the crack model in the same element. Therefore, in the analyses presented in this paper, linear elastic material behaviour was used for concrete in compression.

A crack is initiated perpendicular to the maximum principal stress when this, independent of the other principal stresses, reaches the tensile strength of the material. Once initiated the orientation of the crack is fixed for the duration of the analysis and a stress-strain relation, as shown in Fig. 4a, determines the material response perpendicular to the crack. Hence, stresses can be transferred across the crack until it reaches its ultimate strain,  $\epsilon_u$ , in which case it is said to be fully open. When the cracked concrete is unloaded and reloaded, the secant stiffness is used, and thus a crack closes completely when the stress reaches zero. Additional cracks may form at the same location but must be perpendicular to the present crack (i.e. orthogonal cracks). This limitation of the formation of a second or third crack is still valid even if the first crack closes completely. Consequently, once a crack has formed it will also affect the crack formation at later stages of the load history. Accordingly, stress locking may occur and the ability of the cracked concrete to take shear forces along the crack is therefore reduced with increasing crack openings. In ABAQUS/Explicit this is treated by the use of a shear retention model in which the cracked shear stiffness  $G_{crack}$  can be described as

$$G_{crack} = \beta(\epsilon_{crack})G_c \quad (1)$$

where  $\beta(\epsilon_{crack})$  is a function (given by the user) of the crack strain  $\epsilon_{crack}$  in the studied crack and  $G_c$  is the shear stiffness of the uncracked material. This means that when the crack opening is large enough the shear stiffness reaches zero.

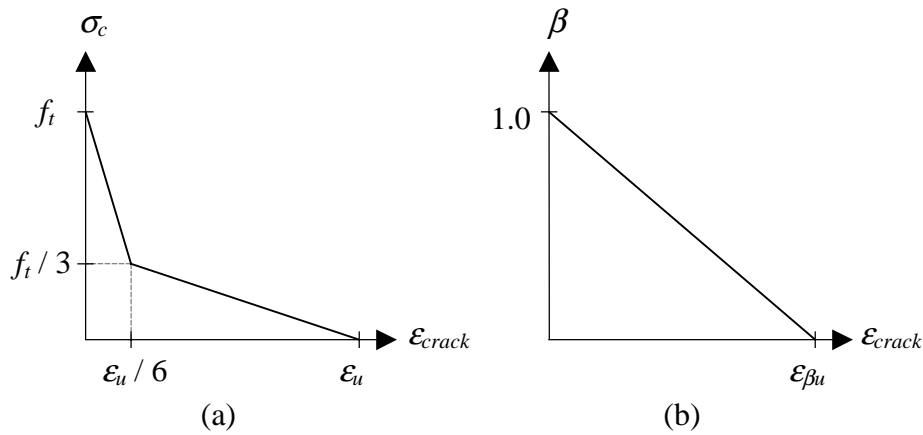


Fig. 4 Modelling of concrete in: (a) tension; (b) shear retention.

To simulate the softening curve of the cracked concrete, a bilinear stress-crack opening relation according to recommendations given in Gylltoft (1983) was used as shown in Fig. 4a. The fracture energy  $G_F$  was used together with the tensile strength  $f_t$ , to calculate the ultimate crack opening  $w_u$  where the post-peak stress reaches zero. However, the input data to the

crack model is given by a stress-crack strain curve, and thus the stress-crack opening relation has to be translated to this by dividing the crack opening by an appropriate crack extension  $l$ . Thereby, the ultimate crack strain  $\varepsilon_u$  can be calculated as

$$\varepsilon_u = \frac{w_u}{l} = \frac{4G_F}{f_t l} \quad (2)$$

From this expression it is obvious that the value of the crack extension  $l$  is just as important as the fracture energy  $G_F$  when determining the ultimate strain  $\varepsilon_u$ . If there is no reinforcement in the concrete,  $l$  is usually set to the length of the element perpendicular to the crack; see Johansson (2000a, 2000b). In a reinforced concrete structure, though, it is more complicated to determine  $l$ . If the interaction between reinforcement and concrete is taken into account properly, the method described above can be used. However, when modelling a reinforced structure where perfect bond is assumed, it is probably more correct to use the mean crack spacing as a value for the crack extension  $l$ ; see de Borst (1995), Plos (1995) and Johansson (2000b). In the analyses carried out here, perfect bond was assumed, and the crack extension  $l$  used in Eq. (2) was therefore approximated to be equal to a mean crack spacing of 0.2 m. The material properties used in the FE analyses were based on mean values: tensile strength  $f_t = 2.36$  MPa, fracture energy  $G_F = 100$  N/m, Young's modulus  $E_c = 30$  GPa and Poisson's ratio  $\nu = 0.2$ . Hence, the ultimate crack strain used was  $\varepsilon_u = 0.847\%$ .

In these analyses the linear relation shown in Fig. 4b was used to model the shear retention;  $\varepsilon_{\beta u}$  was set to  $10\varepsilon_u$  and  $47.2\varepsilon_u$  for the blast load and impact load, respectively. The former value was not based on a physical interpretation, but on a previous study in Johansson (1998) which showed that it had negligible effect on the structural behaviour of a frame corner. Therefore, the use of a "reasonable" value was assumed to be accurate enough. However, in the impact load analyses, the concrete failed in a way that was interpreted to be due to large shear forces. The shear retention was then determined more thoroughly. Such a physical interpretation is possible by considering the maximum aggregate size used in the analysed structure. It seems reasonable to assume that the shear capacity perpendicular to a crack is exhausted when the crack opening exceeds a value larger than half the aggregate size. Hereby, it is possible to determine a relation between  $\varepsilon_{\beta u}$  and  $\varepsilon_u$  as

$$\frac{\varepsilon_{\beta u}}{\varepsilon_u} = \frac{d_\phi f_t}{8G_F} \quad (3)$$

and  $\varepsilon_{\beta u} = 47.2\varepsilon_u$  was obtained by assuming a maximum aggregate size  $d_\phi = 16$  mm.

The steel reinforcement was modelled using von Mises yield criterion with associated flow and isotropic hardening. As for the concrete, mean material properties were used for the reinforcement: yield strength  $f_{sy} = 550$  MPa, ultimate strength  $f_{su} = 605$  MPa, Young's modulus  $E_s = 200$  GPa, strain at hardening  $\varepsilon_{sh} = 2.75\%$  and strain at ultimate strength  $\varepsilon_{su} = 100\%$ .

However, since ABAQUS/Explicit takes into account the theory of large deformations, these values were recalculated into true stresses  $\sigma_{s,true}$  and logarithmic strains  $\varepsilon_{ln,s}$ , using

$$\sigma_{s,true} \approx \sigma_s(1 + \varepsilon_s) \quad (4)$$

$$\varepsilon_{ln,s} = \ln(1 + \varepsilon_s) \quad (5)$$

where  $\sigma_s$  and  $\varepsilon_s$  are the engineer stress and engineer strain of the steel, respectively; see HKS (1998).

### Strain rate effects

It is commonly accepted that the material properties of both concrete and steel are affected by what strain rate effect they are subjected to. From the test summaries provided by, for example, Bischoff and Perry (1991), and Malvar and Ross (1998) it is evident that the load-carrying capacity of concrete in compression and tension can be substantially increased at high strain rates. This is especially true for strain rates that exceed the value of the so-called transition zone which appears at a strain rate of approximately  $3 \text{ s}^{-1}$  and  $30 \text{ s}^{-1}$  for concrete in tension and compression, respectively. Below such strain rates, though, the dynamic increase factor (DIF) for a concrete of a compressive strength  $f_c = 30 \text{ MPa}$  is, according to the CEB-FIP Model Code, CEB (1993), less than 1.6 and 1.7 in compression and tension, respectively. Reinforcement is less strain rate sensitive than concrete and does not seem to have a transition zone like that observed for concrete, Malvar (1998).

In ABAQUS/Explicit it is not possible to consider the effect of the strain rate in the constitutive equations for concrete. Consequently, this effect is neglected in the analyses carried out here. For the steel reinforcement it is possible to take the strain rate effect into account but since the magnitude of its strain rate will be mesh-dependent (see Johansson 2000b), it was decided not to include it in the analyses.

### FE models

The concrete, the ground and the simulated falling masses were modelled using four-node plane stress elements with reduced gauss integration; the reinforcement was modelled using two-node truss elements. Since non-linear material behaviour was used, no material damping was included; the default value of 0.06 for the bulk viscosity, though, was kept to reduce the “noise” in the solution.

Many factors can affect the final result in a FE analysis and, since there are always some uncertainties in the choices made, it is important to examine the sensitivity of the results due to different parameters. The shelter subjected to blast load was exposed to such a sensitivity study where the main parameters varied were: element mesh, assumed crack extension, and the coefficient of friction between ground and floor slab. Further, the influence of different shear retention  $\varepsilon_{\beta u}$ , the use of non-linear behaviour of concrete in compression, and modelling the concrete using plain strain elements, were also examined. However, the space available in this paper does not permit these comparisons to be dealt with herein, and therefore only the results of one of the blast load analyses are presented here. Nevertheless, it should be mentioned that even though these parameters did affect the structural response of the shelter, the initial behaviour, which is of most interest for such a structure, was found to be approximately the same. For more information on the other analyses, see Johansson (1999).

The element mesh used for the shelter in both the blast and impact analyses is shown in Fig. 5. To get a proper picture of the behaviour of the shelter it was modelled so that it could lift from, and/or slide along, the ground when subjected to a blast load. This was made possible by modelling the contact between the shelter floor slab and the ground. In the analyses presented herein the frictional coefficient was set to 0.75. Initially the ground was modelled as a rigid surface but it was found that this caused the shelter to lift from the ground and then bounce, instead of slide, along it. Hence, the influence of the frictional coefficient was considerably reduced in a very unrealistic way. By modelling the ground as a linear elastic material (6 x 0.3 m modelled by 50 x 6 elements), though, the bouncing vanished and a more realistic behaviour was obtained.

The blast load was modelled with the pressure-time relation shown in Fig. 3b, the same pressure being applied on the whole shelter front wall. The impact load was simulated by modelling falling mass parts and their impact with the shelter roof. Since a sensitivity study was carried out for the blast load it was not done here. According to the theoretical background of the design method used in the Swedish Shelter Regulations, the falling debris is assumed to hit the shelter roof with a constant mass per second. This was modelled by activating different amounts of the total mass within a constant time interval. The time interval chosen was 1/5, 1/10 and 1/20 of the total time, hereafter denoted as the active time, which it took for all of the falling debris to reach the shelter; i.e. the mass was modelled as 6, 11 and 21 individual parts, respectively, see Fig. 6a. Thus, the average amount of mass hitting the shelter was about the same as that assumed when the equivalent static load was derived (Fig. 6b). Further, to examine the influence of the active time, it was also varied to be 0.50, 0.25 or 0.10 s.

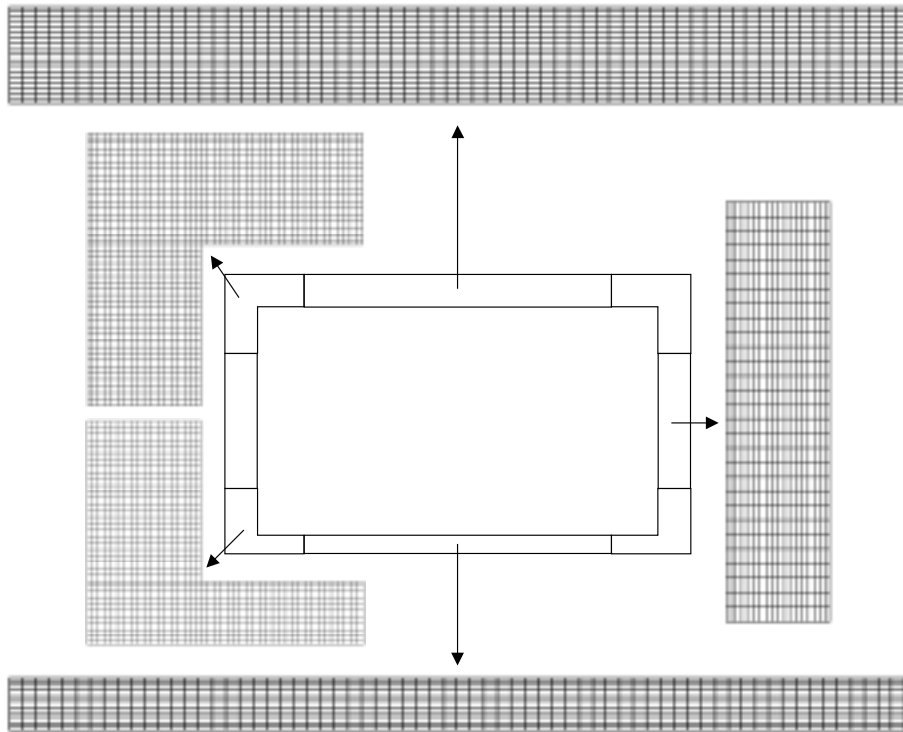


Fig. 5 Element mesh of the civil defence shelter used in the analyses presented here.

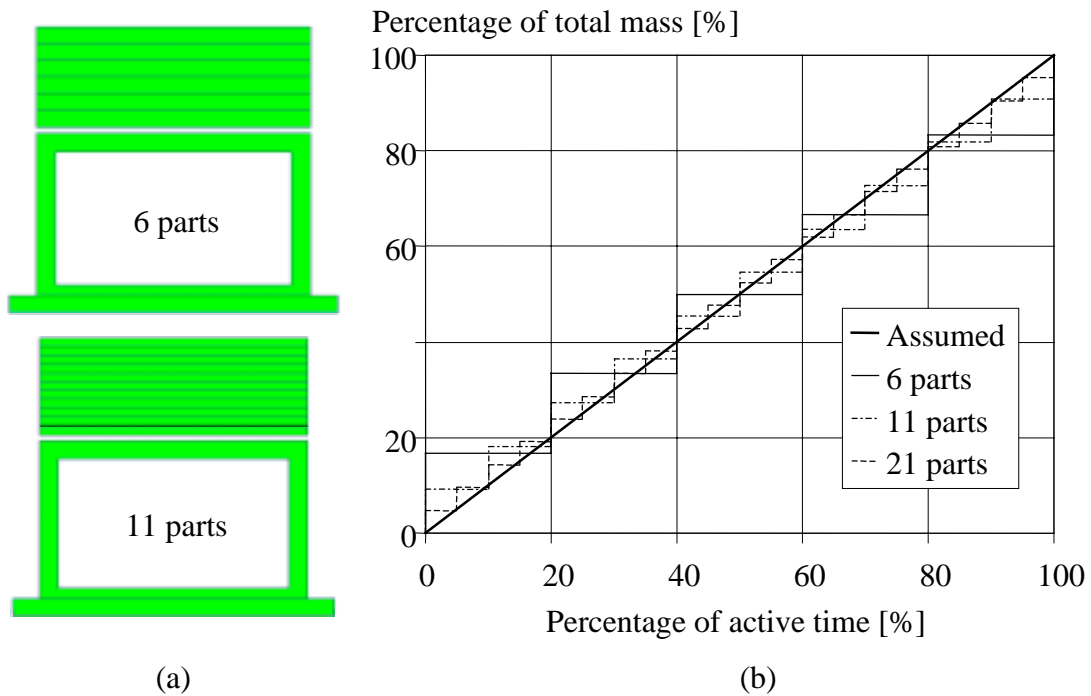


Fig. 6 (a) Modelling of falling masses using 6 and 11 individual parts; (b) mass-time relation used in the analyses.

When modelling the impact load, the intention was to simulate a falling mass of debris with a very low stiffness. The Young's modulus and strength of the falling debris were therefore approximated as one tenth of those of concrete in tension, i.e.  $E_{debris} = 3 \text{ GPa}$  and  $f_{debris} = 0.236 \text{ MPa}$ . Von Mises plasticity was used and a bilinear stress-strain relation with zero hardening was assumed. The falling masses were modelled as individual parts, each part built up of  $50 \times 3$  (6 and 11 parts) or  $50 \times 2$  (21 parts) elements, where the interaction of adjacent parts was modelled with contact assuming a coefficient of friction equal to 0.10. Further, the density of the rubble was assumed to be  $2/3$  of that of the concrete, i.e.  $1600 \text{ kg/m}^3$ .

## RESULTS

### Blast load analysis

The blast load acts during a very short but intense period of time. As can be seen in Fig. 3b, it starts with a pressure just above 5 MPa, decreases rapidly to about 20 kPa after 3 ms and reaches zero pressure just prior to 9 ms. The wave velocity,  $c$ , in the material can be determined as

$$c = \sqrt{\frac{E}{\rho}} \quad (6)$$

where  $E$  is Young's modulus and  $\rho$  is the density of the material. With a Young's modulus of 30 GPa and a density of  $2400 \text{ kg/m}^3$  the wave velocity in the concrete becomes about 3500 m/s. This means that it will take about 1.4 ms before the compressive stress wave reaches the right wall "informing" it that the structure has been hit by an external pressure. It will then take a further 0.3 ms before the whole structure (the midsection of the right wall is farthest away) "knows" what has happened. Consequently, when the reflection of this stress wave reaches the left wall again, the external overpressure has all but vanished. This will also greatly affect the behaviour of the structure, especially in the left wall. In Fig. 7a the propagation of the stress wave in the shelter is shown for the first 0.4 ms. After this time the compressive wave has reached about 1.4 m into the floor and roof slabs. It is also possible to see how a stress wave reflects back and forth in the front wall, changing sign at each reflection.



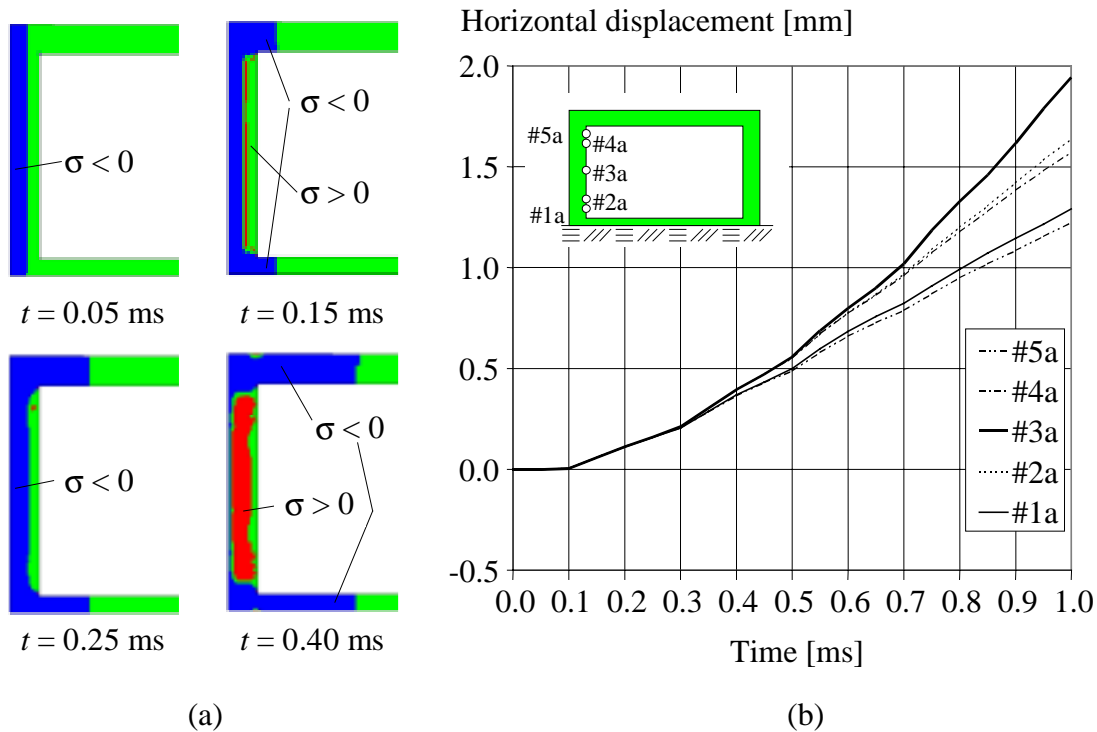


Fig. 7 (a) Initial stress wave propagation in shelter; (b) horizontal displacement at the inside of the left wall when subjected to a blast load from the left.

Since the load condition changes fast in relation to the wave velocity, it can be said that the boundary conditions of the front wall change with time. Initially, the wall does not “know” that it is connected to the rest of the structure. This is why, for instance, the back of the left wall does not start to move until after 0.1 ms, which is the time it takes for the stress wave to travel through the 0.35 m thick shelter wall. The displacements are then the same in about 0.2 ms, at which time points #1a and #5a start to differ. This also results in a behaviour that differs from what may be expected, and the largest initial tensile stresses do not appear in the middle of the wall but in a section close to the floor and roof slabs. Hence, the first cracks arise after 0.30 ms at a distance of about 0.4 m from the floor and roof slabs respectively (Fig. 8). It can be noted that points #2a, #3a and #4a have the same displacement until 0.5 ms and that point #3a at a time of 1.0 ms still hardly seems to be affected by the support conditions. Consequently, bending cracks will not dominate the crack pattern in the middle of the wall until after about 1.5 ms.

The maximum strain rate obtained in the blast load analysis was about  $1.2 \text{ s}^{-1}$  for uncracked concrete and about  $15 \text{ s}^{-1}$  in the reinforcement. The latter value was higher because the reinforcement obtains its maximum values when a localisation occurs in a cracked concrete element and, as previously mentioned, this strain rate will therefore be mesh-dependent. Hence, if the strain rate effect had been taken into account for the reinforcement, its dynamic

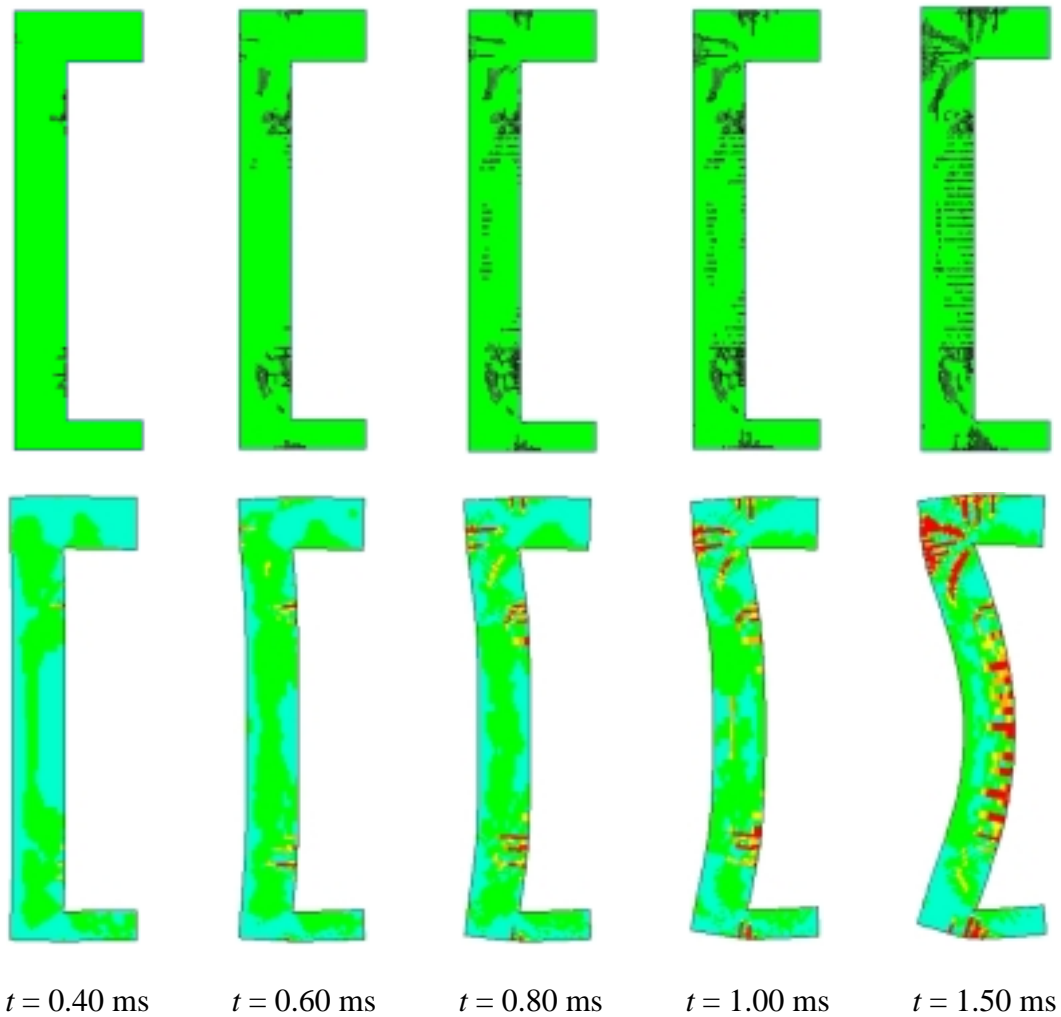


Fig. 8 Initial crack propagation in left wall. The upper part shows where the tensile strength has been exceeded and the lower part (magnified 100 times) where the cracks localise. Dark areas indicate where the principal strain has exceeded the ultimate crack strain  $\epsilon_u$ .

yield strength would also have become mesh-dependent. Using a strain rate of  $1.2 \text{ s}^{-1}$  the DIF should according to the CEB-FIP Model Code, CEB (1993), be about 1.6 for concrete in tension. The increase in reinforcement yield strength should at this strain rate, according to CEB Bulletin d'Information No 187, CEB (1988), be about 1.1. To take these effects into account in a very approximate way, another analysis where the concrete tensile strength and reinforcement yield strength were increased to  $f_t = 1.6 \cdot 2.36 = 3.8 \text{ MPa}$  and  $f_{sy} = 1.1 \cdot 550 = 605 \text{ MPa}$ , respectively. Nevertheless, the structural response in the critical initial stage was still more or less the same, the effects observed being only positive in either case, and the results presented here should therefore still be valid.

During the first 0.2 s the left wall in the shelter obtains large horizontal displacements (Fig. 9a). During the same time, the vertical displacement-time relations in Fig. 9b show that

all but point #9 in the shelter also lift from the ground. After about 0.4 s the sliding along the ground stops; thus the shelter receives a permanent movement to the right of about 50 mm.

To better understand the behaviour of the shelter during the first second, the horizontal displacements, relative to point #1, and some corresponding deformation plots are shown in Figs. 10a and 11, respectively. Hereby, it is easier to see how the shelter sways back and forth during the initial loading. It can be noted that the crack patterns obtained at these stages are similar to what would have been caused by an external static load acting on the front wall in the same direction as the shelter sways. Thus, the initial time-dependent change in boundary conditions, mentioned above, now has a negligible effect.

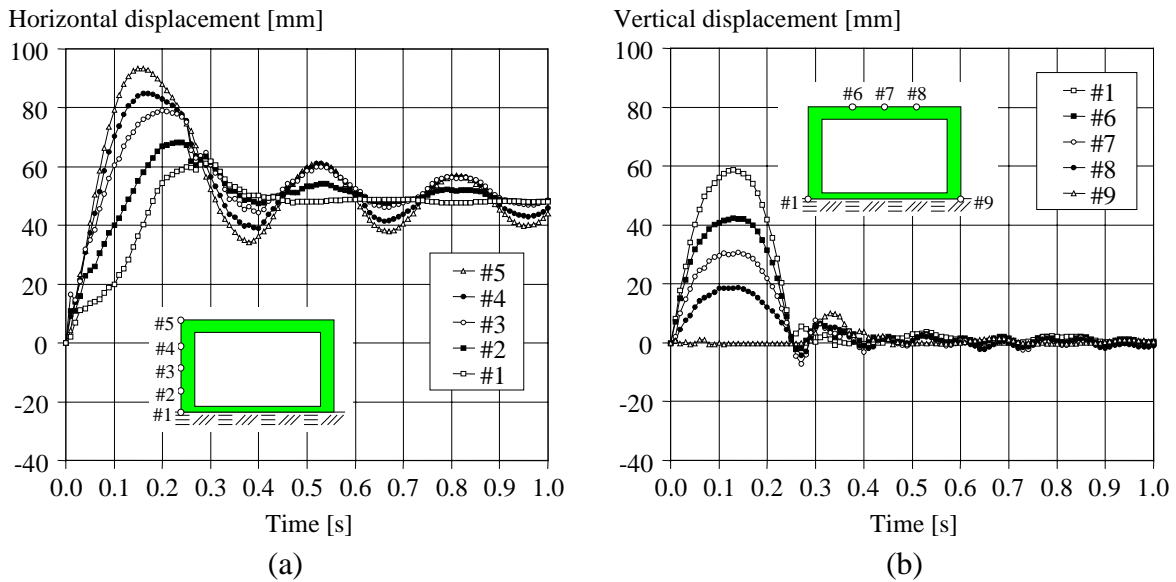


Fig. 9 (a) Horizontal, and (b) vertical displacement in the blast load analysis.

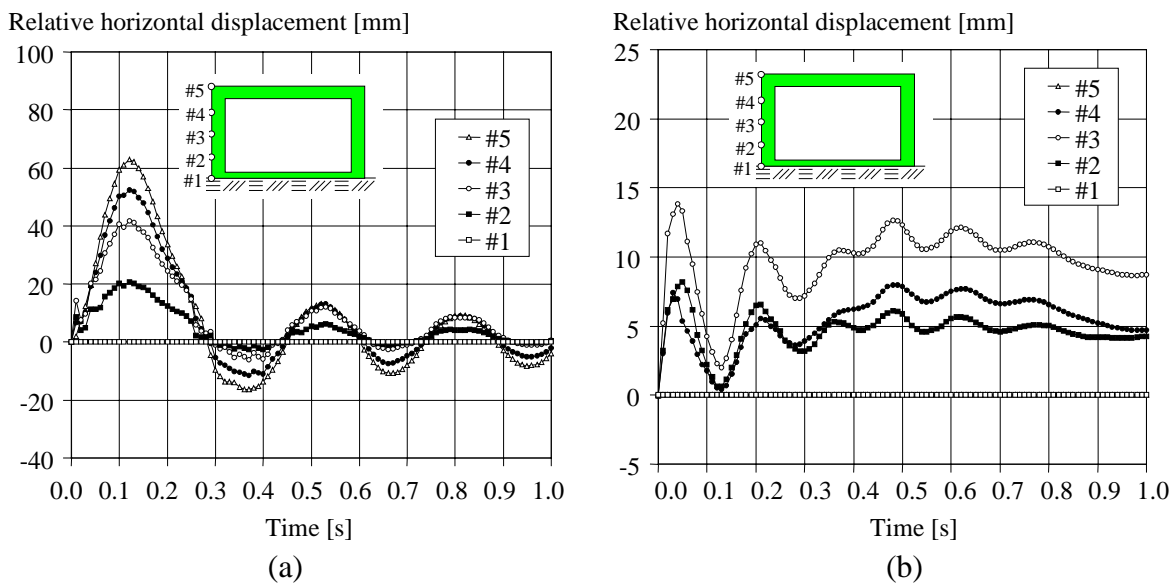


Fig. 10 Relative horizontal displacement in blast load analysis when: (a) related to point #1; (b) related to points #1 and #5 according to Eq. (7).

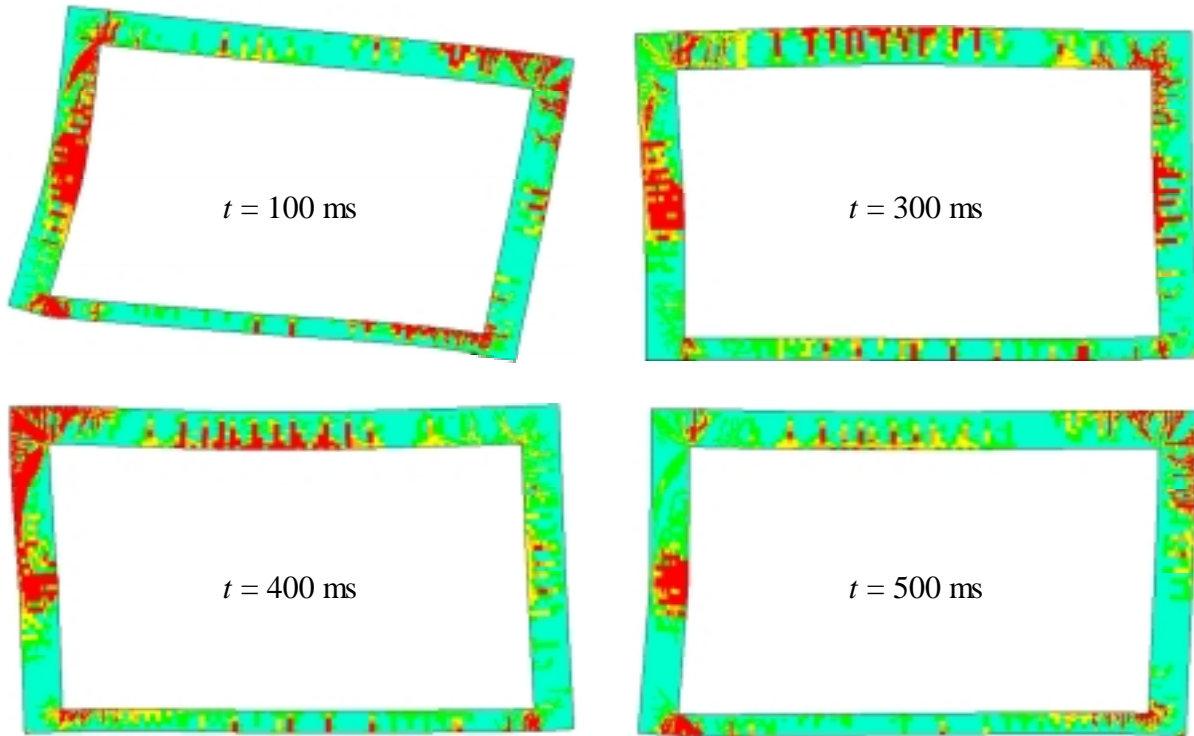


Fig. 11 Deformation and crack propagation in shelter during the first 0.5 s after loading. Dark areas show where the principal strain in the concrete is higher than that of a fully opened crack. Magnification factor = 10.

From Fig. 10a it can be seen that the largest displacements relative to point #1 are obtained after about 120 ms, but also that a local maximum of the displacements in points #2, #3 and #4 occurs after about 10 ms. A large relative displacement in point #5 indicates that the top left corner is subjected to an opening moment. However, it does not say much about the response in the left wall itself. To get an opinion of this it is necessary to determine the relative displacement of the shelter wall when related to both points #1 and #5. By using the expression

$$u_{i,relative} = (u_i - u_1) - \frac{u_5 - u_1}{h} y \quad (7)$$

where  $u_i$  is the displacement in point # $i$ ,  $h$  is the height of the shelter and  $y$  is the vertical distance from the ground to point # $i$ , it is found that the relative displacements in points #2, #3 and #4 obtain their largest values after about 10 ms; see Fig. 10b. Since these relative displacements are more important than the global displacements when looking at the response in the left shelter wall, this indicates that the most critical stage for the structure may occur shortly after initial loading. This is also confirmed when comparing the critical reinforcement stresses in the structure; see Fig. 12. From this it is clear that the most strained part in the structure is the shelter wall closest to the explosion and that this occurs during the initial 10 ms after loading. However, the relative displacements in points #2 to #4 at  $t \approx 100$  ms are

almost as large as in the initial stage. Nevertheless, as shown in Fig. 12 the maximum reinforcement stresses in different parts of the structure are still far below the steel yield strength at this time. The upper left corner is not even subjected to a closing moment any more; instead, it is at about this time that the maximum reinforcement stresses is obtained at the inside of this corner (point #4). Thus, it may be somewhat illusory to look only at the displacements to find the critical stage in the structural behaviour.

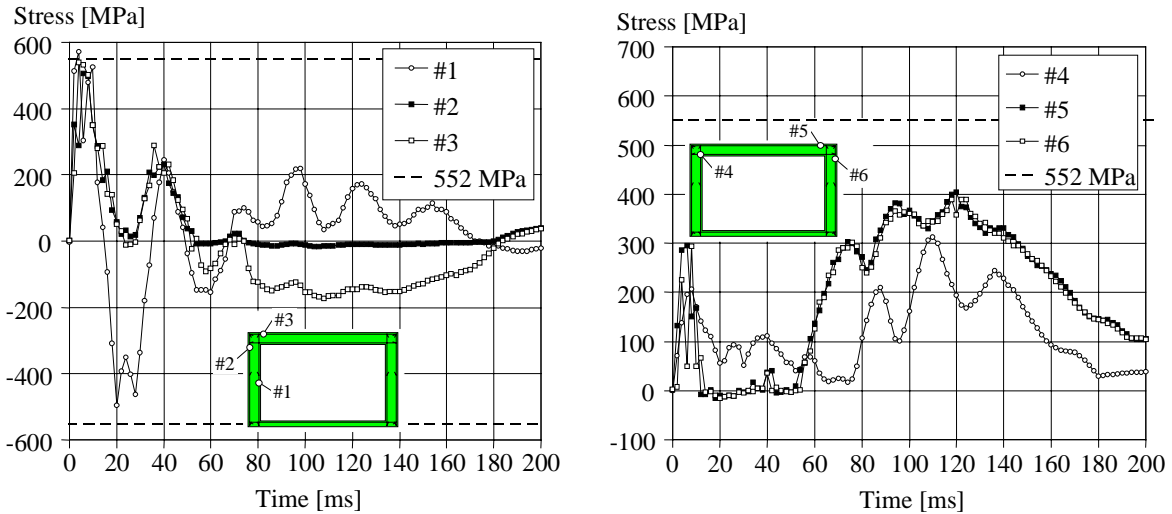


Fig. 12 Stress-time relation for the most critical reinforcement elements during the first 200 ms. The dashed lines marked “552 MPa” represent the reinforcement yield strength when the influence of large deformations (Eq. 4) has been taken into account.

The largest reinforcement stresses are obtained in the middle of the left wall (point #1) and in the corner area between the left wall and the roof (point #3); no other regions in the structure obtained reinforcement yielding. A further magnification in time shows that the reinforcement starts to yield in these sections after about 2 and 3 ms, respectively (Fig. 13). Thus, it is also of interest to further study the behaviour of the shelter during the initial 10 ms. The crack propagation during this time period is shown in Fig. 14 and reveals that the structural behaviour differs considerably from that in Fig. 11. It is of special interest to note that the left wall initially behaves in a way similar to a slab fixed at both ends. This is because in the initial stage the left wall is not “aware” of the rest of the structure. As previously mentioned it will take a certain time before the information about the external load has reached all parts of the structure and then returned to the front wall, “informing” it about its surroundings.

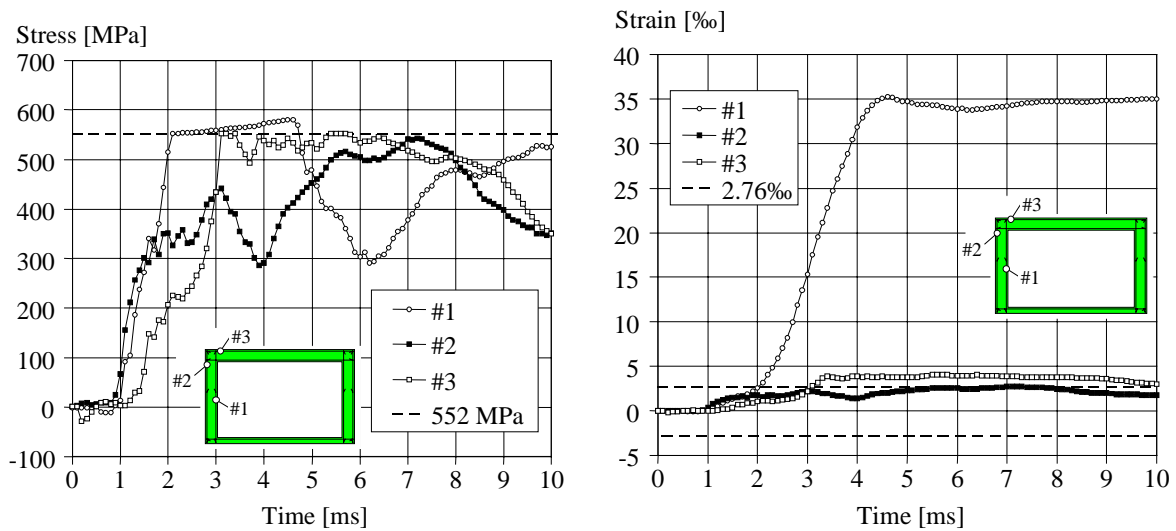


Fig. 13 Stress-time and strain-time relations in points #1 to #3 for the most critical reinforcement elements during the first 10 ms.

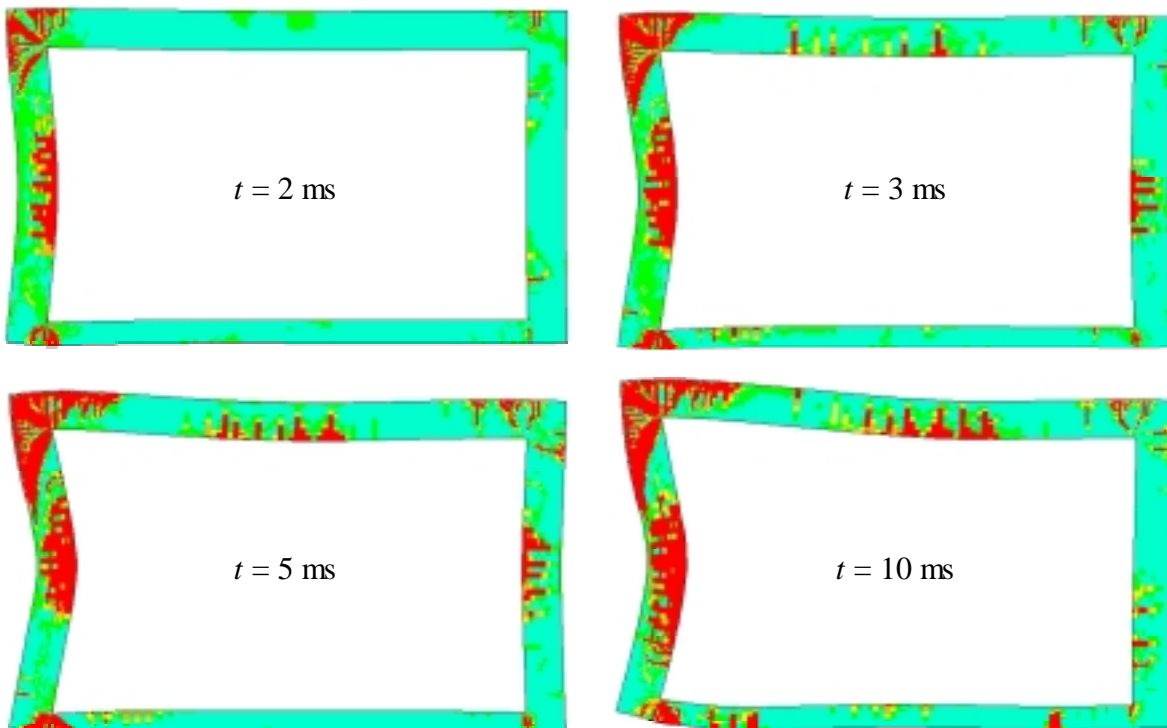


Fig. 14 Crack propagation in shelter during the first 10 ms after loading. Dark areas show where the principal strain in the concrete is higher than that of a fully opened crack. The deformations are magnified with a factor of 20.

To further investigate the initial behaviour of the shelter, moment and normal forces were calculated in different sections; the moment was determined as acting around the normal force, which in turn was positioned in the neutral layer of the uncracked cross section. Fig. 15

shows the resulting moment and normal force distributions during the first 10 ms for two such sections in the shelter. Hereby it can be seen that the maximum sectional forces in these two sections are obtained after about 1 to 2 ms. However, when comparing this to the time when the maximum reinforcement stresses are obtained it is clear that the times do not necessarily coincide. The reason is that the large normal force in compression has a very positive effect on the section's capacity. This is especially apparent when comparing the maximum moments obtained in the analysis with the estimated moment capacities when assuming pure bending. These were determined as prescribed in Eurocode 2, CEN (1991), to be 82 kNm and 98 kNm for the mid-wall and roof corner, respectively, values that can be compared to the maximum moments of 214 kNm and 195 kNm obtained in the analysis.

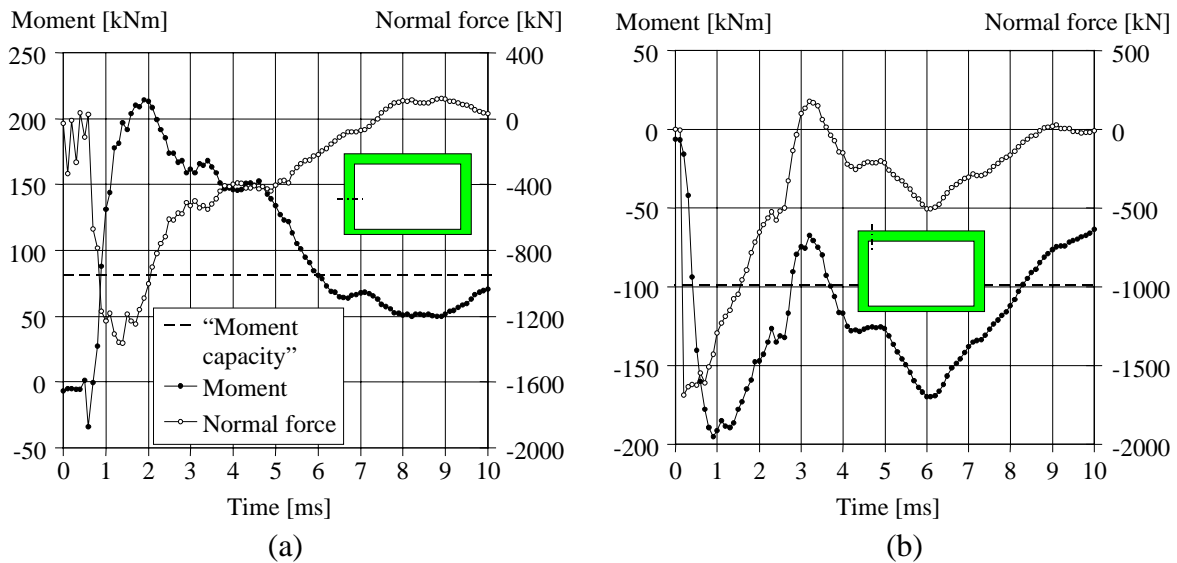


Fig. 15 Sectional forces in (a) midsection in left wall, and (b) roof slab close to left corner, during the first 10 ms after loading.

It is not surprising that the moment capacity increases when the compressive normal force assists the reinforcement to keep the section together. Neither is it strange that such a compressive force appears in the roof section, since a compressive stress wave travels through the roof slab; compare Fig. 7a. However, the peculiarity is that such large compressive forces also appear in the wall. In Fig. 16a it can be seen that the compressive force varies between about 0 and 350 kN during the first 0.6 ms. This force is caused by the restrained elongation obtained due to a combination of a stress wave travelling forth and back in the wall (see Fig. 7a) and the Poisson's ratio. But, at 0.7 ms the compressive force increases rapidly and reaches its maximum of 1364 kN after 1.4 ms, and becoming 1092 kN after 1.9 ms when the maximum moment is obtained. This sudden increase is due to the cracking in the wall (Fig. 8). When the wall cracks it elongates and, if this elongation is restrained, large

compressive forces arise. A similar behaviour is obtained in a statically loaded slab that is fixed in both ends. It can be argued that the short ends of the left wall are not fixed but are relatively free to elongate. This would be true if the load had been applied slowly enough; here however, the cracking occurs so fast that there is no time for the wall to respond as in such a case. Consequently, the wall experiences its boundary conditions to be fixed, which in turn produces large normal forces that help the section withstand the external load. Accordingly, it seems appropriate to regard the boundary conditions of the left wall as fixed in the initial stage of the loading. The duration of these large compressive forces, though, is quite short; after about 7 ms the compressive force has disappeared all along the wall (shown in Johansson 1999). This return of the compressive force to about zero is coupled to the vertical movement of the roof slab and thus the removal of the initial restraining caused by the time-dependent boundary conditions. Thereafter, the compressive forces are comparatively low, never reaching a value higher than 100 kN again. Hence, this observation supports the statement made above that the boundary conditions change with time.

If the compressive force of 1092 kN had been taken into consideration when determining the moment capacity in the wall, it would have increased to 242 kNm, a value that is about three times as high as the “ordinary” moment capacity of 82 kNm. Thus, the appearance of such large compressive forces offers the wall considerable help to withstand the blast load. When checking other sections in the left wall they show a similar presence of compressive forces, even though these seem to decrease at increasing distance from the wall midsection. Accordingly, a possible reason for the increased moment capacity in a dynamically loaded structure might be that large compressive forces appear in the critical sections. Hence, if these normal forces are not considered when evaluating the test results, the increase in load capacity might be interpreted as just a cause of high strain rate effects in the concrete and reinforcement. Even though part of the increase in load capacity can be explained due to this, the results presented here suggest that a substantial part of such an increase may be a pure structural effect.

### **Impact load analyses**

The falling mass was modelled as 6, 11 or 21 individual parts. Further, three different values (0.50 s, 0.25 s and 0.10 s) of the active time, i.e. the time during which the falling mass was activated, were used to study its effect on the shelter behaviour. The displacement and velocity in the midsection of the roof slab, in the case when six mass parts are used and the active time used was 0.50 s, are shown in Fig. 16a. The sudden increase in velocity at regular



time intervals of about 100 ms corresponds to the impact obtained when a falling mass part reaches the shelter. The last falling part affects the shelter after about 540 ms and after this the slab velocity approaches zero. Hence, the displacement observed after 700 ms of about 180 mm corresponds to the final displacement of the roof slab. The crack patterns obtained in the shelter during the impact of the falling masses are shown in Fig. 16b and it can be seen that both the roof slab and the upper parts of the walls are cracked to a large extent. The reinforcement yielded at several places both in the slab midsection and on either side in both corners ( $\varepsilon_s \approx 70\%$ ) and was even torn off in the wall about 100 mm below the right corner.

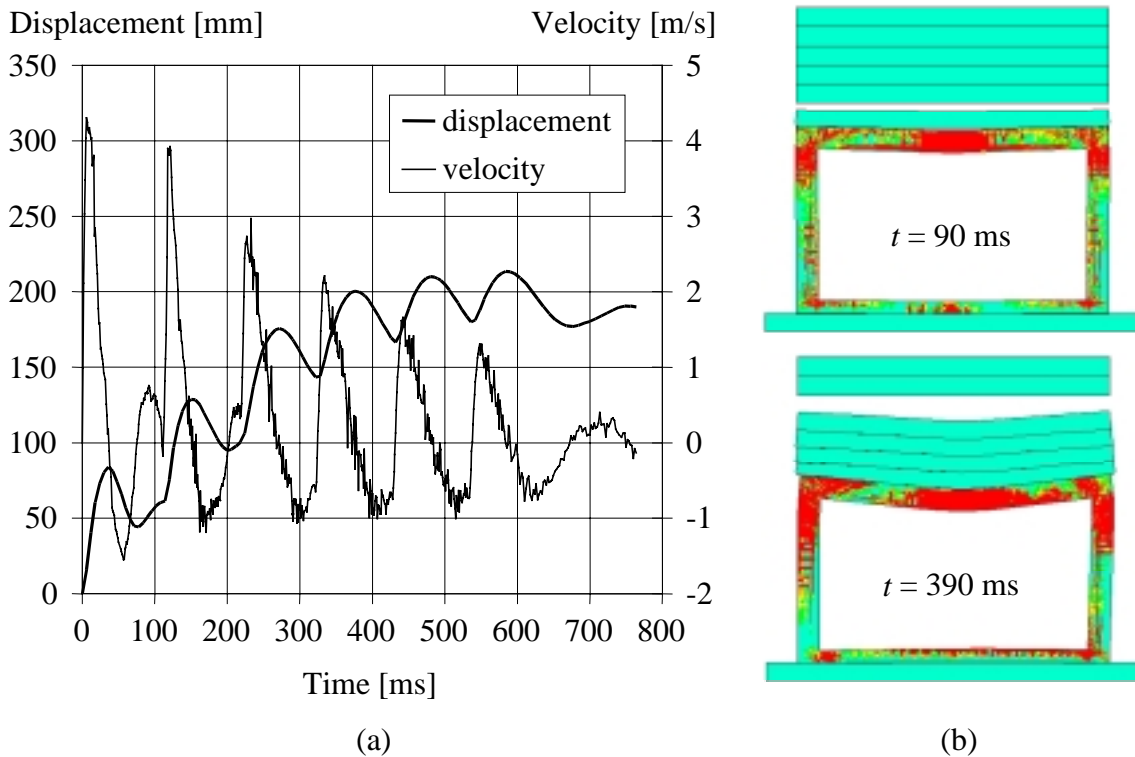


Fig. 16 (a) Displacement and velocity in midsection of shelter roof slab, and (b) crack pattern in shelter, when the falling mass is modelled by using 6 parts activated during 0.5 s.

Normally, the deformation of the shelter should increase with decreasing active time. However, this was not the case in the analyses carried out here when using 6 mass parts. Instead, the displacement in the roof midsection was more or less halved when the active time was set to 0.25 s. The reason for this, though, was that the frequency of the falling mass parts in this case did not correspond as well to the eigenfrequency of the shelter roof and the already activated mass, as it did when the active time was 0.50 s. Thus, when a falling part reached an already activated mass below, this was moving in the direction opposite to the falling part, and hence much of the kinetic energy was consumed in the plastic impact

between the two parts. If the mass fell within a period of 0.10 s, though, the shelter could not withstand the impact but failed in several locations.

It was found that the maximum displacement obtained in the shelter depended greatly on how many load parts were used to simulate the falling debris. Thus, the decrease in mass for each of the parts was not compensated by their increased falling frequency. Accordingly, even though the essential behaviour was similar it is evident that the displacement becomes considerably smaller when using more but lighter falling mass parts. Hence, the strain in the reinforcement also became substantially lower, reaching a maximum value of about 35‰ when using 11 falling mass parts. Nevertheless, the analyses using 11 and 21 parts to simulate the collapsing mass confirmed the idea that a decrease in the active time also results in an increase in the total displacement of the shelter (Fig. 17).

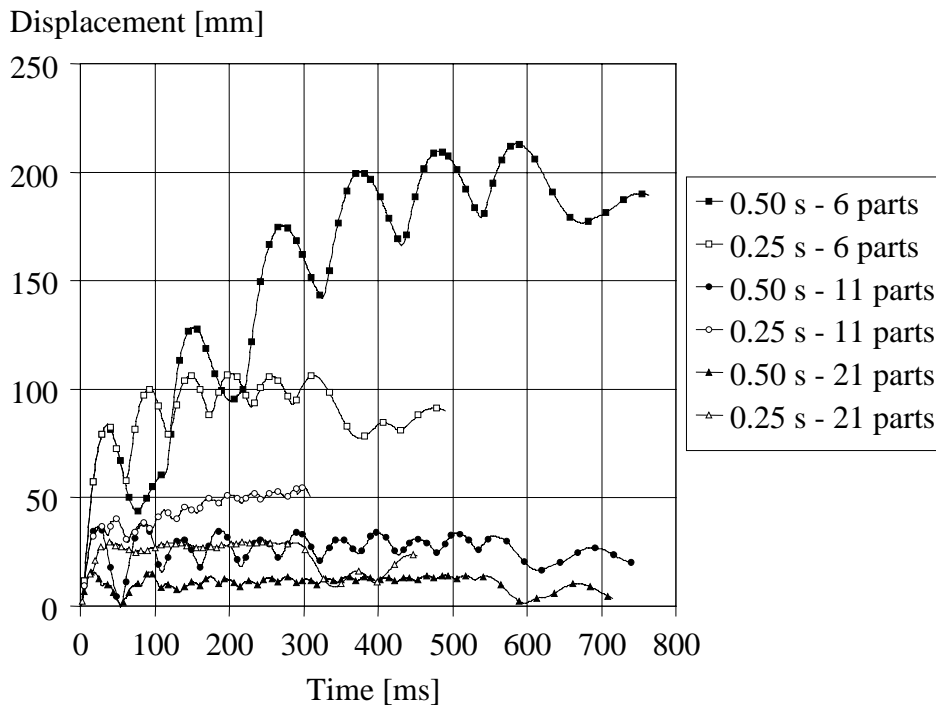


Fig. 17 Comparison of shelter roof displacement when the active time and the number of falling mass parts were varied.

### Comparison with static loading

This section makes a brief comparison of the static behaviour of the shelter to that obtained when subjected to the transient loads examined above. These analyses are not “truly” static since ABAQUS/Explicit was used. However, as shown in for instance Johansson (1998) it is possible to simulate a statically loaded structure in an explicit programme as long as it is

made sure that the material models used are strain rate independent and the load velocity used is so low that inertia effects can be neglected. The static load cases used are shown in Fig. 1 and the load velocity chosen was an external pressure of  $50 \text{ kN/m}^2\text{s}$ . Due to the large difference between the transient and static load cases, though, it is not meaningful to compare load-displacement relations between them. Nevertheless, it is still of interest to compare the critical crack patterns and differences or similarities in the general behaviour.

When applying the static load shown in Fig. 1a it was concluded that the load capacity of the shelter was much higher than designed for. This is partly due to the use of mean values in the analysis (the reinforcement amount was determined using design values) but mostly because of the positive effect caused by the high normal forces, obtained in the structure for this load case. At a load twice as high as the static design load, the reinforcement had just reached yielding in the roof midsection but the reinforcement was still to yield in the corners. Nevertheless, this load level was considered adequate to compare the crack patterns within the corner with that obtained in the blast load analysis. Fig. 18a shows the crack pattern in the upper left corner region for two different load levels, and it can be seen that they are rather similar to those obtained in the blast load analysis at 1 ms and 3 ms, respectively; compare Fig. 14. The major difference is perhaps that the inclined shear crack seems to be more pronounced in the blast load analysis. On the other hand, the responses within the corner region are approximately the same. It is also worth recalling that the maximum reinforcement stresses in the corner region obtained in the blast load analysis were located in the roof slab outside the corner, hence suggesting that the corner will not be very critical in such a load case.

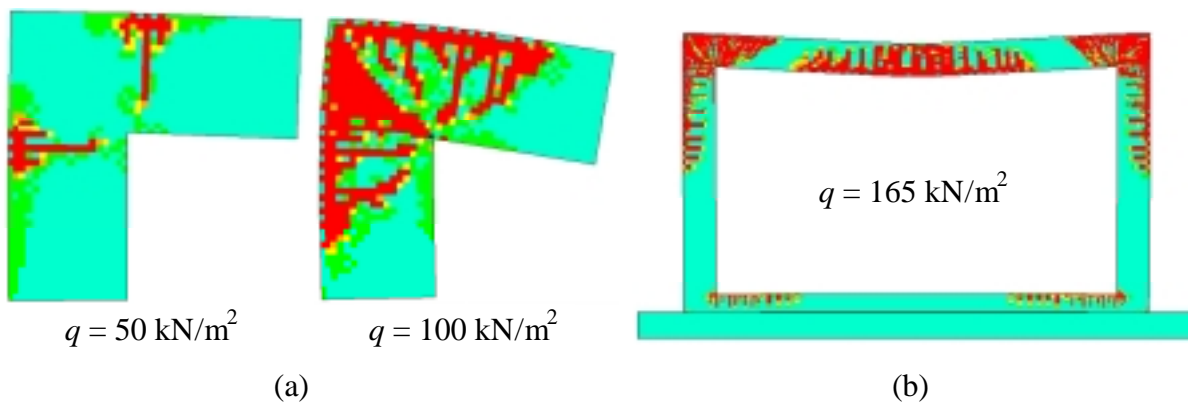


Fig. 18 Crack pattern in (a) corner region when the shelter is subjected to the static weapon load case used in the design (Fig. 1a), and (b) shelter at failure when subjected to a static pressure from above (Fig.1b).

Fig. 18b shows the shelter crack pattern at failure when it is subjected to a static load as shown in Fig. 1b. This may be compared to that shown in Fig. 16b, and despite the fact that the cracking seems to be more intense when subjected to the impact load, it can be concluded that the general crack behaviour is still approximately the same. It is also interesting to note that the critical sections at the corner are not located on the same sides of the corner in the static and dynamic load analyses. In the former, the reinforcement is torn off in the roof slab about 50 mm from the corner, while in the latter they appear in the wall approximately 100 mm below the corner. Above all, though, in neither case is cracking within the corner critical; this implies that a reinforcement corner detailing sufficient to use in a static load case is also adequate in a shelter subjected to impact load.

## CONCLUSIONS

A civil defence shelter subjected to a blast load from an explosion or falling mass from a collapsing building has been studied using the non-linear finite element programme ABAQUS/Explicit. It was found that the global response of a structure subjected to a blast load in the initial stage may be very different from that of a static load, an important reason being that the boundary conditions initially can be said to vary with time. The most critical stage for the shelter studied here was during the initial 10 ms. It is during this period that yielding of the reinforcement occurs in the most strained sections: the midsection of the front wall and the section between corner and roof slab. The corner itself, though, does not seem to be very critical.

An impact load of falling debris from a collapsing building was simulated and it was found that the results depend greatly much on how much time it takes for the total mass to reach the structure, but more importantly on what mass each independent part has that hits the structure. The impact of few but heavy masses is more dangerous than that obtained by the same amount of mass distributed more evenly during the same time period. Further, the FE analyses strongly imply that no critical cracks will form within the corner region, and hence it seems reasonable to believe that the response within a corner will be similar to that obtained in a statically loaded structure. Accordingly, even though the structural behaviour may be completely different in static and transient loaded structures, the results presented herein indicate that the local behaviour still may be quite alike. This also suggests that the conclusions made in Johansson (1996, 2000a, 2000b) and Johansson and Karlsson (1997), that it is appropriate to use spliced reinforcement loops within the corner, should be valid for a transient loaded structure as well.

## ACKNOWLEDGEMENT

The research presented in this paper was financed by the Swedish Rescue Services Agency. The author would like to thank the head of the Division of Concrete Structures, Professor Kent Gylltoft, for his support and advice. Thanks also to Björn Ekengren at the Swedish Rescue Services Agency and Dr. Mario Plos at Reinertsen Engineering for their much appreciated support in the project.

## APPENDIX I      REFERENCES

- Baker, W. E. (1973). *Explosions in air*. University of Texas Press, Austin, USA.
- Bischoff, P.H., and Perry, S.H. (1991). "Compressive behaviour of concrete at high strain rates". *Materials and Structures*, 24, 425-450.
- CEB (1988). CEB Bulletin d'Information No 187, Lausanne, Switzerland.
- CEB (1993). CEB-FIP Model Code 1990, Design Code. Thomas Telford, Lausanne, Switzerland.
- CEN (1991). Eurocode 2: Design of concrete structures, Part 1: General rules and rules for buildings. European Committee for Standardisation.
- ConWep (1992): ConWep – Collection of Conventional Weapons Effects Calculations based on TM 5-855-1, Fundamentals of Protective Design for Conventional Weapons, U.S. Army Engineer Waterways Experiment Station, Vicksburg, MS.
- de Borst R. (1995). "Analyses of reinforced concrete in a historical perspective". Nordic Symposium on Modern Design of Concrete Structures, Aalborg University, Denmark, 261-299.
- Gylltoft, K. (1983). "Fracture mechanics models for fatigue in concrete Structures." Division of Structural Engineering, Luleå University of Technology, Ph.D. Thesis, 1983:25D, Luleå, Sweden.
- Hallgren, P., and Granström, S. (1977). "Ras mot skyddsrumstak – beräkningsmodell (Impact of falling masses on shelter roof – calculation method.)" Tyréns, Stockholm, Sweden. (In Swedish)
- HKS (1998): *ABAQUS/Explicit Version 5.7*. Hibbit, Karlsson and Sorensen Inc. Pawtucket, RI.

- Johansson, J. P. M., and Karlsson, S. (1997). "Nytt armeringsutförande i betongramhörn utsatta för positivt moment (New reinforcement detailing in concrete frame corners subjected to positive moment)." Division of Concrete Structures, Chalmers University of Technology, Report 97:5, Göteborg, Sweden. (in Swedish)
- Johansson, M. (1996). "New reinforcement detailing in concrete frame corners of civil defence shelters: non-linear finite element analyses and experiments." Division of Concrete Structures, Chalmers University of Technology, Licentiate Thesis, Publication 96:1, Göteborg, Sweden.
- Johansson M. (1998): "Betongens töjningshastighetsberoende och explicit lösnings-metodik (Strain rate effects in concrete and explicit solution methods)." Division of Concrete Structures, Chalmers University of Technology, Report 98:2, Göteborg, Sweden. (In Swedish)
- Johansson M. (1999). "Non-linear finite element analyses of civil defence shelters subjected to explosion load or impact load." Division of Concrete Structures, Chalmers University of Technology, Report 99:8, Göteborg, Sweden.
- Johansson M. (2000a): "Nonlinear finite-element analyses of concrete frame corners." *ASCE Journal on Structural Engineering*, 126(2), 190-199.
- Johansson M. (2000b). "Structural behaviour of concrete frame corners in civil defence shelters: non-linear finite element analyses and experiments." Division of Concrete Structures, Chalmers University of Technology, Ph.D. Thesis, Publication 00:2, Göteborg, Sweden.
- Malvar L. J., and Ross C. A. (1998). "Review of strain rate effects for concrete in tension." *ACI Materials Journal*, 95(6), 735-739.
- Malvar L. J. (1998). "Review of static and dynamic properties of steel reinforcing bars." *ACI Material Journal*, 95(5), 609-616.
- Plos, M. (1995). "Application of fracture mechanics to concrete bridges - finite element analyses and experiments." Division of Concrete Structures, Chalmers University of Technology, Ph.D. Thesis, Publication 95:3, Göteborg, Sweden.
- Swedish Shelter Regulations (1998). *Skyddsrumregler SR – Produktion och vidmakthållande* (Shelter Regulations – production and maintenance.) Statens Räddningsverk, Publication B54-141/98, Karlstad, Sweden. (In Swedish)

## APPENDIX II NOTATIONS

The following symbols are used in this paper:

$A_s$	=	reinforcement area;
$c$	=	wave speed velocity;
$d_\phi$	=	maximum aggregate size;
$E_c$	=	Young's modulus for concrete;
$f_{cd}$	=	concrete design compressive strength;
$f_{su}$	=	ultimate strength of reinforcement;
$f_{sy}$	=	yield strength of reinforcement;
$f_{syd}$	=	design yield strength of reinforcement;
$f_t$	=	concrete tensile strength;
$G_c$	=	shear modulus for uncracked concrete;
$G_{crack}$	=	shear modulus for cracked concrete;
$G_F$	=	fracture energy;
$E_s$	=	Young's modulus of reinforcement;
$E$	=	Young's modulus;
$E_{debris}$	=	Young's modulus of falling mass material;
$f_{debris}$	=	strength of falling mass material;
$h$	=	height of shelter;
$l$	=	crack extension;
$m$	=	mass;
$p$	=	pressure;
$q_{impact}$	=	equivalent static impact load;
$q_{weapon}$	=	equivalent static weapon load;
$t$	=	time;
$u$	=	displacement;
$v$	=	velocity;
$w_u$	=	crack opening;
$y$	=	vertical position in shelter;
$\beta$	=	shear retention factor;
$\epsilon_{crack}$	=	crack strain;
$\epsilon_{ln,s}$	=	logarithmic strain in reinforcement;
$\epsilon_s$	=	reinforcement strain;
$\epsilon_{sh}$	=	strain at reinforcement hardening;

$\epsilon_{su}$	=	strain at ultimate strength of reinforcement;
$\epsilon_u$	=	ultimate strain;
$\epsilon_{\beta u}$	=	ultimate strain for shear retention;
$\sigma_c$	=	concrete stress;
$\sigma_s$	=	reinforcement stress;
$\sigma_{s,true}$	=	true reinforcement stress;
$\nu$	=	Poisson's ratio; and
$\rho$	=	density.



## **Doctoral Theses and Licentiate Theses, Division of Concrete Structures, Chalmers University of Technology, 1990-2000**

- 90:1 Stig Öberg: Post Tensioned Shear Reinforcement in Rectangular RC Beams. Publication 90:1. Göteborg, April, 1990. 603 pp. (No 1021). Doctoral Thesis.
- 90:2 Johan Hedin: Långtidsegenskaper hos samverkanskonstruktioner av stål och betong (Long Time Behaviour of Composite Steel Concrete Structures). Publication 90:2. Göteborg, August, 1990. 53 pp. (No 1079). Licentiate Thesis.
- 92:1 Björn Engström: Ductility of Tie Connections in Precast Structures. Publication 92:1. Göteborg, October, 1992. 368 pp. (Nos 936, 999, 1023, 1052). Doctoral Thesis.
- 93:1 Mario Plos: Shear Behaviour in Concrete Bridges - Full Scale Shear Test. Fracture Mechanics Analyses and Evaluation of Code Model. Publication 93:1. Göteborg, April, 1993. 70 pp. (Nos 1088, 1084). Licentiate Thesis.
- 93:2 Marianne Grauers: Composite Columns of Hollow Steel Sections Filled with High Strength Concrete. Publication 93:2. Göteborg, June, 1993. 140 pp. (No 1077). Doctoral Thesis.
- 93:4 Li An: Load Bearing Capacity and Behaviour of Composite Slabs with Profiled Steel Sheet. Publication 93:4. Göteborg, September, 1993. 134 pp. (No 1075). Doctoral Thesis.
- 93:5 Magnus Åkesson: Fracture Mechanics Analysis of the Transmission in Zone in Prestressed Hollow Core Slabs. Publication 93:5. Göteborg, November, 1993. 64 pp. (No 1112). Licentiate Thesis.
- 95:1 Christina Claeson: Behavior of Reinforced High Strength Concrete Columns. Publication 95:1. Göteborg, June, 1995. 54 pp. (No 1105). Licentiate Thesis.
- 95:2 Karin Lundgren: Slender Precast Systems with Load-Bearing Facades. Publication 95:2. Göteborg, November, 1995. 60 pp. (No 1098). Licentiate Thesis.

- 95:3 Mario Plos: Application of Fracture Mechanics to Concrete Bridges. Finite Element Analysis and Experiments. Publication 95:3. Göteborg, November, 1995. 127 pp. (Nos 1067, 1084, 1088, 1106). Doctoral Thesis.
- 96:1 Morgan Johansson: New Reinforcement Detailing in Concrete Frame Corners of Civil Shelters. Non-linear Finite Element Analyses and Experiments. Publication 96:1. Göteborg, November, 1996. 77 pp. (No 1106). Licentiate Thesis.
- 96:2 Magnus Åkesson: Implementation and Application of Fracture Mechanics Models for Concrete Structures. Publication 96:2. Göteborg, November, 1996. 159 pp. (No 1112). Doctoral Thesis.
- 97:1 Jonas Magnusson: Bond and Anchorage of Deformed Bars in High-Strength Concrete. Publication 97:1. Göteborg, November, 1997. 234 pp. (No 1113). Licentiate Thesis.
- 98:1 Christina Claeson: Structural Behavior of Reinforced High-Strength Concrete Columns. Publication 98:1. Göteborg 1998. 92 pp + I-IV, 75 pp. (No 1105.) Doctoral Thesis.
- 99:1 Karin Lundgren: Three-Dimensional Modelling of Bond in Reinforced Concrete. Theoretical Model, Experiments and Applications. Publication 99:1. Göteborg, November, 1999. 129 pp. (No 37). Doctoral Thesis.
- 00:1 Jonas Magnusson: Bond and Anchorage of Ribbed Bars in High-Strength Concrete. Publication 00:1. Göteborg, February, 2000. 300 pp. (No 1113). Doctoral Thesis.